

Kristoffer Smedal Olsen
Sara Linnea Larsson Grayston

Experimental Assessment of the Compression Strength of Conventional Ceramic Foam Filters, at Room Temperature and 730°C

Eksperimentell Vurdering av Kompresjonsstyrken til
Konvensjonelle Keramiske Filtre (CFF), i
Romtemperatur og ved 730°C

Bachelor's project in Material Sciences
Supervisor: PhD candidate Are Bergin, Dr. Robert Fritzsich and Prof.
Ragnhild E. Aune



NTNU – Trondheim
Norwegian University of
Science and Technology

Project number: IMA-B-14

Availability: Open

Experimental Assessment of the Compression Strength of Conventional Ceramic Foam Filters, at Room Temperature and 730°C

Eksperimentell Vurdering av Kompresjonsstyrken til
Konvensjonelle Keramiske Filtre (CFF), i Romtemperatur og
ved 730°C

Authors

Sara Linnea Larsson Grayston
Kristoffer Smedal Olsen

Supervisors

PhD candidate Are Bergin
Dr. Robert Fritsch
Prof. Ragnhild E. Aune

May 29, 2020

Abstract

Ceramic foam filters (CFFs) play an important part when recycling aluminium due to an often high amount of non-metallic inclusions in secondary aluminium, which will decrease the mechanical properties of the product. CFFs are designed to filter out the unwanted particles resulting in a better end product. While the mechanical properties of ceramic foams are well documented at room temperature, there has been done, at the time of writing, little to no research on the mechanical strength at working temperatures. This thesis will focus on the compressive strength of different manufacturers at room and working temperatures (730 °C) with different holding times.

Several analytical methods were used to get a broader understanding of the structural properties of the CFFs. Included methods were: geometric measurements of samples, light microscopy, scanning electron microscopy (SEM), energy dispersive spectroscopy (EDS), and mercury intrusion porosimetry. Of special interest was how structural properties affected the strut strength, which is an important parameter when testing compressive strength.

The compressive strength of conventional CFFs from four different manufacturers with varying pore density and composition was measured at room temperature and at 730 °C. While the procedures for room temperature testing is well established, the method for compressive testing at high temperatures had to be established. When testing at room temperatures the filter properties closely resembled established models dependent on relative density and strut thickness. The Sivex non-phosphorous filter was found to have the highest strength, and the Selee filter had the lowest strength.

When testing the compressive strength at working temperatures, there is generally a decrease in strength for longer holding times at working temperature. Since the methods for compression testing at high temperatures was under development, some inconsistencies were found where the filters from Lanik and Selee diverted from the trend.

Sammendrag

Keramiske filtre (CFF) spiller en viktig rolle når aluminium resirkuleres på grunn av at sekundært aluminium ofte inneholder en stor mengde ikke-metalliske partikler som vil redusere de mekaniske egenskapene til produktet. CFF-er er designet for å filtrere ut uønskede partikler, noe som resulterer i et bedre sluttprodukt. Mens de mekaniske egenskapene til keramisk porøse strukturer er godt dokumentert ved romtemperatur, har det i skrivende stund blitt gjort lite til ingen undersøkelser om den mekaniske styrken ved arbeidstemperaturer. Denne oppgaven vil fokusere på den kompressible styrken til forskjellige produsenter ved rom- og arbeidstemperaturer (730 °C) med forskjellige holdetider.

Flere analytiske metoder ble brukt for å få en bredere forståelse av de strukturelle egenskapene til CFF-ene. Inkluderte metoder var: geometriske målinger av prøver, lysmikroskopi, skanning elektronmikroskop (SEM), energidispersiv spektroskopi (EDS) og porosimetri med kvikksølv. Av spesiell interesse var hvordan strukturelle egenskaper påvirker styrken i strukturen, som er en viktig parameter når man tester kompresjonsstyrken.

Kompresjonstyrken til konvensjonelle CFF-er fra fire forskjellige produsenter med varierende poretetthet og sammensetning ble målt ved romtemperatur og ved 730 °C. Mens prosedyrene for testing av romtemperatur er godt etablert, måtte metoden for kompresjonstesting ved høye temperaturer etableres. Under testing ved romtemperatur lignet filteregenskapene godt på etablerte modeller avhengig av relativ tetthet og tykkelsen til strukturen. Sivex filter uten fosfor ble målt til å ha den høyeste styrken i kompresjon, og Selee hadde den laveste styrken i kompresjon.

Ved testing av kompresjonstyrken ved arbeidstemperaturer, er det generelt en reduksjon i styrke for lengre holdetid. Siden metodene for kompresjonstesting ved høye temperaturer var under utvikling, ble det funnet noen uoverensstemmelser der Lanik og Selee filterne divergerte fra normen.

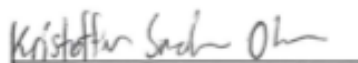
Preface

This bachelor thesis is assigned and funded by the Institute of Material Sciences at NTNU, and is a part of the doctorate degree by PhD candidate Are Bergin. The purpose of this thesis is to test the mechanical properties of ceramic foam filters at different temperatures and holding times.


The experimental work was conducted at the Department of Material Sciences and Engineering at Gløshaugen spring 2020.

Due to the current global situation the work was affected by the Covid-19 virus. This has impacted the range of work that was originally planned and affected communication to some extent.

We want to thank our supervisors PhD candidate Are Bergin, Dr. Robert Fritsch, and Prof. Ragnhild E. Aune in addition to Dr.-ing. Claudia Voigt for guidance and assistance with both theoretical and experimental work. We would also like to thank Pål Christian Skare for excellent help and guidance during the experimental work. We would like to express our sincere thanks to those who proof-read and endured us during this project.



Kristoffer Smedal Olsen



Sara Linnea Larsson Grayston

Contents

List of Figures	vii
List of Tables	viii
1 Introduction	1
2 Objective	2
3 Background	3
3.1 Structural Properties	3
3.2 Uniaxial Compression of Brittle Foams	5
3.2.1 Gibson and Ashbys Model	5
3.2.2 Damage Accumulation Model	6
3.2.3 Anisotropy of Cells	7
3.2.4 Failure of Ceramic Foam Filters	7
3.3 Filter Priming in Advance of Aluminium Filtration	8
3.4 Phosphate Bonded Filters	8
3.5 High Temperature Behavior of Ceramics	9
4 Experimental Procedures and Analysis	12
4.1 Analytical Methods	13
4.1.1 Microscopic Analysis	13
4.1.2 SEM- and EDS- Analysis	13
4.1.3 Porosimetry Measurement	14
4.2 Mechanical Testing at Room Temperature	14
4.2.1 Preparation of Samples	15
4.3 Mechanical Testing at 730 °C	16
4.3.1 Different Holding Times	16
5 Results and Discussion	19
5.1 Analytical Methods	19
5.1.1 Microscope Pictures	19
5.1.2 Scanning Electron Microscopy-Analysis (SEM)	22
5.1.3 Energy Dispersive Spectroscopy (EDS)	24
5.1.4 Mercury Intrusion Porosimetry	24
5.2 Compression Testing	27
5.2.1 The Effect of Sample Shape	27
5.2.2 Room Temperature Testing	28
5.2.3 Temperature Drop Test	30
5.2.4 Compression Strength Measurements at 730 °C	31
6 Conclusion	34
6.1 Further Work	34

Bibliography	35
7 Appendix	37
A The results from the compressive strength testing of all the filter types, filter porosities and experimental parameters	38
B Raw data from room temperature compressive tests	40
C Raw data from working temperatures compressive tests	47
D Microscopic photos with strut thickness displayed of the filters	54
E EDS RawData Sivex 30	67
F EDS RawData Sivex 65	75
G EDS RawData Sivex 80	79
H EDS RawData SivexNP 30	89
I EDS RawData Drache 30	99
J EDS RawData Drache 60	105
K EDS RawData Lanik 30	116
L EDS RawData Lanik 60	122
M EDS RawData Selee 30	131
N Risk Assessment Cold Testing	141
O Risk Assessment Hot Testing	144
P Project Plan	147
Q Popular Science Article	149

List of Figures

1.1	(a) Illustrates the inside of a filter, (b) illustrates how the molten metal flow through the filter and impurities is left behind.	1
3.1	Microscope picture of a ceramic foam filter.	3
3.2	A SEM image of a strut at 200x and 800x magnification.	4
3.3	The pentagonal dodecahedron structure.	5
3.4	The structure of a unit cell from Gibson and Ashbys model [6] where: (a) shows a cubic model of an open-cell foam, (b) shows fracture under compression, and (c) shows the cross-section of a hollow strut.	6
3.5	An axisymmetric unit cell [6].	7
3.6	Illustration of the placement of a filter in the filter bowl at a foundry. . . .	8
3.7	Temperature dependence of bending strength (inert strength) of alumina [23].	9
3.8	The crushing strength of porous open-cell alumina dependent on temperature [12].	10
3.9	Alumina-silica phase diagram [25].	11
4.1	The MTS 880 Hydraulic Tensile Testing Machine 100 kN.	13
4.2	The SEM Ultra 55 LE machine from Zeiss [26].	14
4.3	The equipment used for the preparation of the samples.	15
4.4	A sample with a thermocouple wire attached.	16
5.1	Microscopic photos of the 30 ppi samples at 30x magnification.	20
5.2	Microscopic photos of the other sample ppis at 30x magnification.	21
5.3	SEM photos of the Drache 30 ppi filter at 200x magnification.	22
5.4	SEM photos of different 30 ppi filters at 800x magnification.	23
5.5	Cumulative pore volume dependent of pore size.	26
5.6	Compressive strength of cylindrical and cubic samples at room temperature.	27
5.7	Compressive strength at room temperature of varying ppi filters.	28
5.8	A sample of Sivex 80. Note the ridges around the middle.	29
5.9	Pictures of Lanik samples.	29
5.10	Compressive strength of 30 ppi filters dependent on relative density.	30
5.11	The temperature drop when the filter is moved from the oven into room temperature. The increment to the trendline shows the average drop in temperature per second.	31
5.12	Compression tests of 30 ppi filters at working temperatures with varying holding times compared with room temperature tests.	32

List of Tables

4.1	The different manufacturers, ppi's, and the number of filters tested at the different holding times in the heated oven.	12
4.2	The different tests performed to analyse the effect of sample shape.	12
4.3	Ten-minute holding time at 800 °C.	17
4.4	One-hour holding time at 800 °C.	18
4.5	Two-hour holding time at 800 °C.	18
5.1	Average strut/wall thickness.	21
5.2	Elements found in the EDS-analysis from the different filters.	24
5.3	Results from porosimetry.	25

1 Introduction

When producing and recycling aluminium there are several stages and methods of cleaning the metal of impurities. These methods are split into two groups; furnace processes and in-line processes. The furnace processes are used while the metal is still in the furnace and includes fluxing, temperature control, settling, and skimming. After the furnace, inclusions can still form in transit to the casting table, for example by oxidation. The in-line processes include degassing and filtration [1].

There are mainly two types of filters used when filtering aluminium, not counting experimental filters such as the advanced compact filter from Rio Tinto Alcan [2]. For more critical and demanding products, deep bed filters (DBF) are used due to a high efficiency, but they are however more expensive and less flexible when changing alloys in a cast-house [1]. Ceramic foam filters (CFF) have a lower efficiency but are cheaper and more flexible. This study will focus on CFFs.

CFFs are manufactured in two ways: by replication and foaming. However, for metal melt filters the replication technique is mainly used as they yield an open-cell structure while foaming tends to yield a more closed cell structure. The replication technique consists of coating a polymer foam with a ceramic slurry, drying, and then burning out the remaining polymer. The used polymer foam, normally polyurethane, specifies the porosity as the resulting ceramic foam will copy the structural characteristics. While this process results in a structure well suited for filtration, it also results in a multitude of flaws and hollow struts and therefore low mechanical properties compared to foaming techniques, due to burning out the polymer [3].

The micro structure of these CFFs that comes from the replication process, is engineered to accumulate impurities in the multiple cavities [4]. How the filter looks like inside is illustrated in Figure 1.1. The priming process of the filter is an important step in filtration of aluminium, explained further in Chapter 3.3.

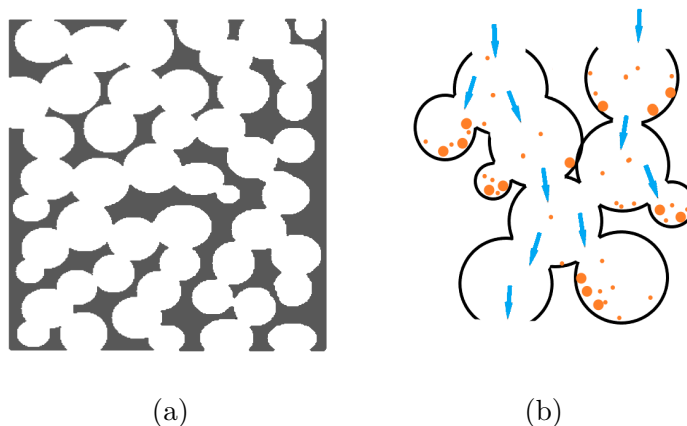


Figure 1.1: (a) Illustrates the inside of a filter, (b) illustrates how the molten metal flow through the filter and impurities is left behind.

2 Objective

The objective of this thesis is to determine the compressive strength of ceramic foam filters from various manufacturers with varied porosities. The experimental work is defined in two parts, the first being compressive testing at room temperatures, to determine the geometry of the samples and what ppi to go forward with. The second part is testing the compressive strength at working temperatures, 730 °C, while varying the holding time at working temperature. Various analytical methods will be used to compare the results from compression testing with the structural properties of the filters.

3 Background

3.1 Structural Properties

Ceramic foams are comprised of two structural components, struts and cell-walls, as seen in Figure 3.1. The distribution and ratio of struts and cell-walls is dependent on whether the foam is closed- or open-celled, whereby highly porous open-celled foams consist mostly of struts while closed-celled foams will have more filled cell-walls. Due to the manufacturing process, specifically incomplete sintering, macro and micro flaws can arise, such as micro cracks, pores in the struts, and triangular strut cavities, as seen in Figure 3.2. Upon compression, such flaws will facilitate crack propagation, leading to a decreased strength [5].

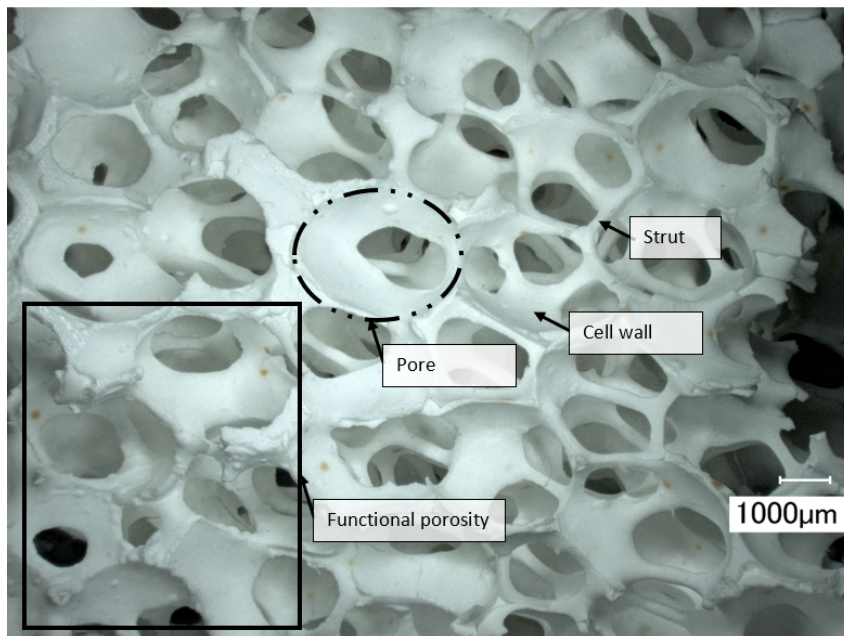


Figure 3.1: Microscope picture of a ceramic foam filter.

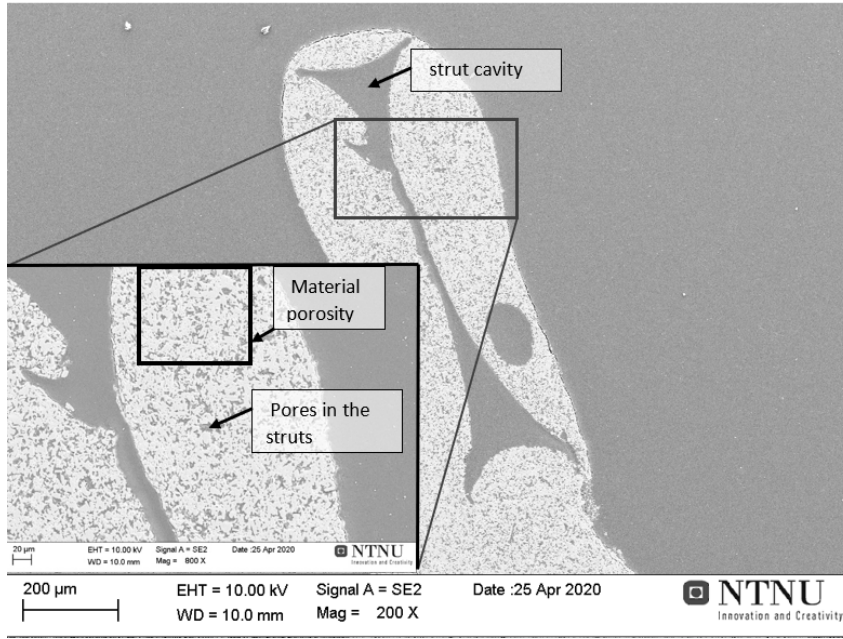


Figure 3.2: A SEM image of a strut at 200x and 800x magnification.

There are four types of densities used when characterizing foams; pore density, foam density, strut density and relative density. The pore density is the number of pores in a certain area, measured in pores per inch (ppi), and is used as a reference to different porosities from the manufacturer. For example Sivex 30 and Sivex 65 refers to different pore densities from the same manufacturer. The foam density (ρ^*) is the density of the entire foam, calculated by the total weight and volume of the foam (measured in g/cm^3). The strut density (ρ_s) is the density (g/cm^3) of the struts composing the foam. The strut density is measured by mercury intrusion porosimetry, see Chapter 4.1.3. The strut density can be calculated into material porosity (p_s) by Equation 3.1.

$$p_s = 1 - \rho_s \quad (3.1)$$

Relative density (ρ^*/ρ_s) describes the ratio between foam density and pore density. Gibson and Ashby [6] detail two ways to calculate relative density, depending on the porosity of the foams. An open cell foam with a relative density less than 0.1 will have the relative density [7]:

$$(\rho^*/\rho_s) = (t/l)^2 \quad (3.2)$$

When the relative density is higher than 0.1, greater consideration must be taken with regards to cell corners and the shape of the cell. If approximating the shape of the cell to a pentagonal dodecahedron as seen in Figure 3.3, Equation 3.3 is better suited to model relative density [7]. The pentagonal dodecahedron shape of unit cells is further supported by Lacroix et al. [8]. If the unit cell can be better approximated to a different structure Equation 3.3 would not apply as it is specific to the pentagonal dodecahedron. The relative density can also be given as functional porosity, as seen in Equation 3.4.

$$(\rho^*/\rho_s) = \frac{(t/l)^2 + 0.766(t/l)^3}{0.766(1 + t/l)^3} \quad (3.3)$$

$$p = 1 - (\rho^*/\rho_s) \quad (3.4)$$

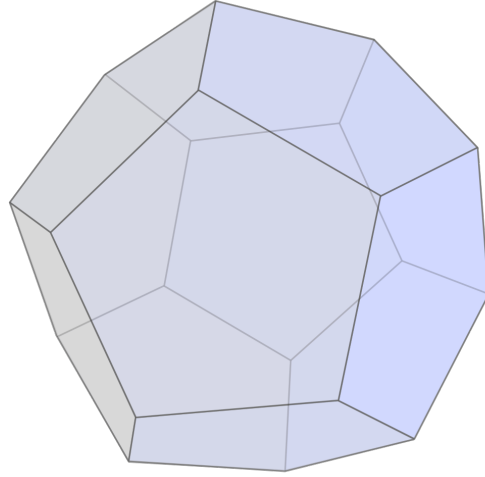


Figure 3.3: The pentagonal dodecahedron structure.

3.2 Uniaxial Compression of Brittle Foams

When characterizing ceramic foams various properties are used, such as porosity, density, permeability and mechanical strength. For the description of mechanical strength, the compressive and bending strength are taken into consideration. This thesis will focus on the compressive strength. Compressive strength is measured by compressing the sample between two loading plates with a constant loading rate. The force used to maintain the loading rate is recorded. Often a compliant loading pad is used, which is a rubber pad placed between the loading plates and the sample, used to distribute the pressure more evenly across the sample. The compressive strength (σ_{cr}) is defined as:

$$\sigma_{cr} = \frac{F_{max}}{A} \quad (3.5)$$

Where F_{max} is the maximum force recorded and A is the area of applied load. The measurement apparatus and method is according to NS-EN-993-5:2018 [9]. Voigt et al. [10] looked at how changing various parameters could alter the compressive strength. They found that the size of the sample and loading plate has a significant impact on the compressive strength, while the loading rate has less of an impact.

3.2.1 Gibson and Ashbys Model

A frequently used model for prediction of the mechanical properties of cellular materials was developed by Gibson and Ashby [6]. They detailed a simplified unit cell with rectangular struts as seen in Figure 3.4a. When the unit cell is placed in compression, individual struts will break as seen in Figure 3.4b. This model suggests that failure occurs at a certain critical load, where numerous cells break at the same time leading to catastrophic failure.

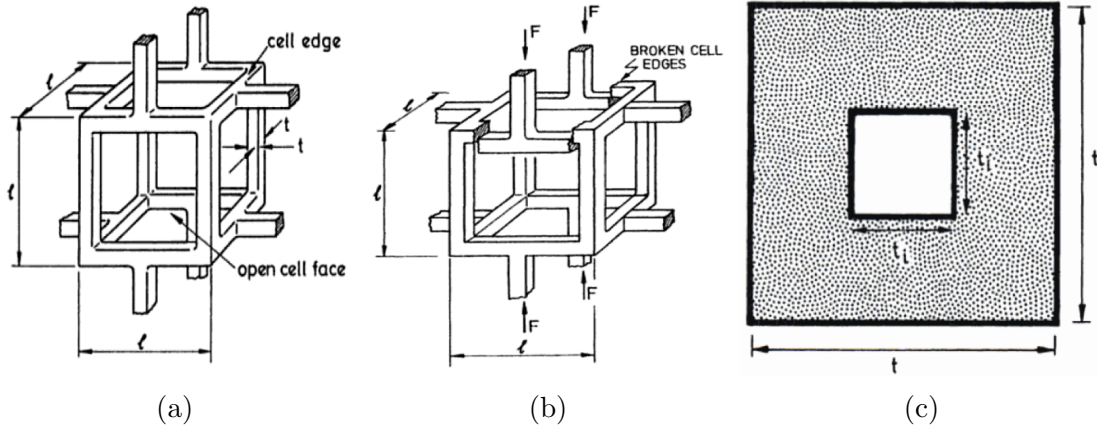


Figure 3.4: The structure of a unit cell from Gibson and Ashby's model [6] where: (a) shows a cubic model of an open-cell foam, (b) shows fracture under compression, and (c) shows the cross-section of a hollow strut.

Gibson and Ashby proposed that the compression strength is dependent on the bending strength of the struts. This is due to how individual struts break, as seen in Figure 3.4b. Based on the bending strength, the following equation is proposed [6]:

$$\sigma_{cr} = C\sigma_{fs}(\rho^*/\rho_s)^{3/2} \frac{1 + (t_i/t)^2}{\sqrt{1 - (t_i/t)^2}} \quad (3.6)$$

Where σ_{fs} is the strength of the struts, (ρ^*/ρ_s) is the relative density, t is the length of the struts, and t_i is the length of holes in the struts often created due to the manufacturing process (see Figure 3.4c). C is a constant found to be 0.65 by Gibson and Ashby [6]. If one assumes that the struts are not hollow, the equation can be simplified to:

$$\sigma_{cr} = C\sigma_{fs}(\rho^*/\rho_s)^{3/2} \quad (3.7)$$

As seen in Equation 3.6, the compressive strength of a foam is dependent on the strength and geometry of the struts and the relative density of the material. The strut strength is further dependent on strut diameter, or thickness, and cell size. The compressive strength increases with increased strut diameter, while the affect of cell size is disputed [11].

Equation 3.7 has however been found inaccurate with regards to the constant C . Brezny et al. [11] found C to be between 0.13 - 0.23, while Goretta et al. [12] found C to be 0.08. This discrepancy could be due to the cell structure. Most ceramic foams below a certain foam porosity will distribute the material in the cell faces resembling a closed cell. Since the constant is dependent on the geometry of the cell, this could have a significant impact. In addition, Gibson and Ashby does not take into account the variation in strut strength that arises from variations in strut thickness and material porosity [12].

3.2.2 Damage Accumulation Model

The other model for compressive failure is the damage accumulation model. This model suggests that failure occurs after a certain number of struts have failed. The struts will not fail simultaneously as in the Gibson and Ashby model, but propagate from cell to cell, often starting at a pre-existing flaw [11]. This model is quite similar to failure of brittle materials, where failure propagates from cracks or other inhomogenities [13].

3.2.3 Anisotropy of Cells

Most polymer foams are anisotropic, which means that the structure and properties vary with spatial direction. The anisotropy is commonly seen as an elongation of the cells, usually axisymmetric, which comes from the production of the polymer foam used in the replication process. Figure 3.5 shows an axisymmetric cell. An axisymmetric cell is symmetric around its axis, implying that the length and width are equal.

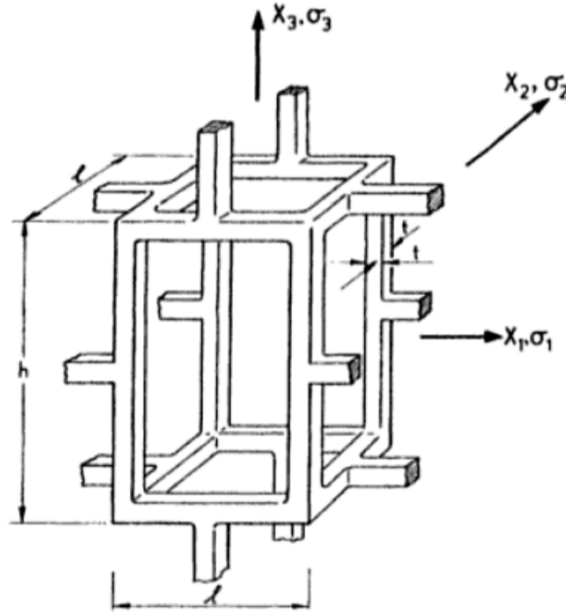


Figure 3.5: An axisymmetric unit cell [6].

$$R = \frac{h}{l} \quad (3.8)$$

A fundamental parameter characterizing an axisymmetric cell is the ratio (R) between the height and length of the cell (Equation 3.8). The relation between the compression strength in the different directions X_1 and X_3 , as seen in Figure 3.5, will then be [6]:

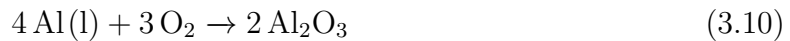
$$\frac{\sigma_3}{\sigma_1} = \frac{2R}{1 + (\frac{1}{R})} \quad (3.9)$$

3.2.4 Failure of Ceramic Foam Filters

Brezny and Green [14] found that different ceramic foams follow different fracture models. A vitreous carbon foam followed Gibson and Ashbys model, while an alumina-mullite foam followed the damage accumulation model. They proposed that the cause could be a greater amount of flaws (such as strut cavities or cracks) in the structure, mostly due to the replication manufacturing process. This could result in a greater variation in strut strength, causing the struts to break at different times. Failure would then happen after a certain amount of the weaker struts have broken. Since the ceramic foam filters studied in this paper are made using replication, similar results are expected.

3.3 Filter Priming in Advance of Aluminium Filtration

The priming of a CFF is the last step before the filtration process in the cast house. The priming allows molten metal, like aluminium, to flow through the filter and leave impurities behind in the numerous pores inside the filter, as illustrated in Figure 1.1. The greatest challenge when filtering aluminium is the reaction in Equation 3.10, where $2 \text{Al}_2\text{O}_3$ is an oxide layer that instantly forms when in contact with oxygen. This problem is further complicated with increased ppi. To fully submerge the filter, the oxide layer must therefore be broken [15] [16].



In Figure 3.6 the filter bowl setup in the foundry is illustrated, and the filter placement is represented. To properly prime the filters, it is necessary to place it in the filter bowl tightly. The filter box is tilted with a 3° to the horizontal plane, so that air can get out during the priming [17]. Then the filter bowl and the filter is preheated to 750°C . After the preheat, the metal is heated up and used to prime the filter. When the filter is thoroughly primed and the molten aluminium flows through, the filtration of aluminium begins. There are different ways to prime a filter other than using gravity only; Drain Free Filtration (DFF) explained by Tundal et al. [17], Advanced Compact Filter (ACF) explained by Breton et al. [4], and Electro Magnetic Field (EM) explained by Fritzsche et al. [15].

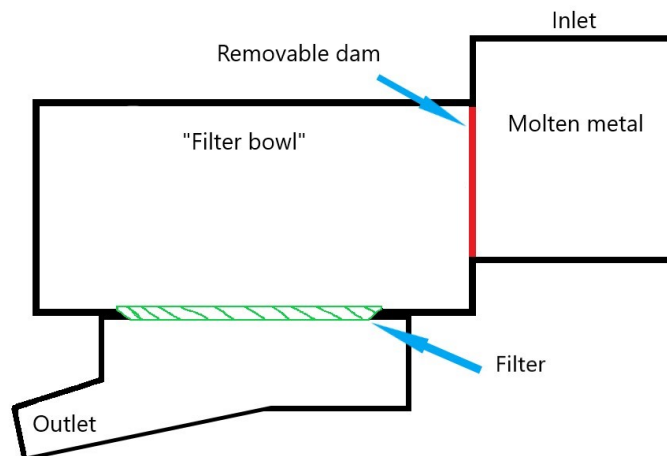
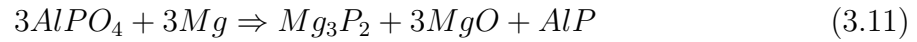


Figure 3.6: Illustration of the placement of a filter in the filter bowl at a foundry.

3.4 Phosphate Bonded Filters

Ceramic foam filters for continuous aluminium casting mainly consist of alumina, Al_2O_3 , and use different kinds of binder material. Inorganic binders, like phosphate or silica, are used to lower the sintering temperature of alumina as to decrease energy usage. Phosphate binders will lower the sintering temperature from 1600°C to 1300°C and result in a relatively high bending and compressive strength [18][19]. However, phosphate bonded filters have been found to be chemically unstable at higher temperatures, especially in

contact with aluminium. When the filters are used with aluminium alloys containing magnesium, the following reaction results [20][21]:



Aubrey et al. [21] shows that the magnesium reaction in Equation 3.11 will cause corrosion and reduce the compressive strength of the filter. Additionally, phosphate bonded filters will produce phosphine after being immersed in aluminium and in contact with water which represents a health risk.

Alternative filters have been developed that do not use phosphate binders. Pyrotek uses colloidal silica and boric oxide as a binder [22]. Non-phosphate filters will thereby reduce the degradation from contact with magnesium and potentially increase compressive strength.

3.5 High Temperature Behavior of Ceramics

Little research has been done on the mechanical properties of cellular ceramics with relation to temperature dependence. Since compression of cellular ceramics dependence on the bending strength, it is of interest to investigate the dependence of bending strength with temperature. In Figure 3.7 the bending strength of alumina is shown plotted against temperature. This graph shows a significant drop in strength at working temperatures (730 °C). This indicates that the compressive strength should exhibit a similar reduction. Goretta et al. [12] performed compressive strength tests at different temperatures of open cell alumina, consisting of 99 % alumina and relative densities between 0.09 and 0.24. As seen in Figure 3.8 there was little change to the crushing strength at 800 °C. Per the authors knowledge there has been done little to no research into the effect of longer holding times at working temperatures.

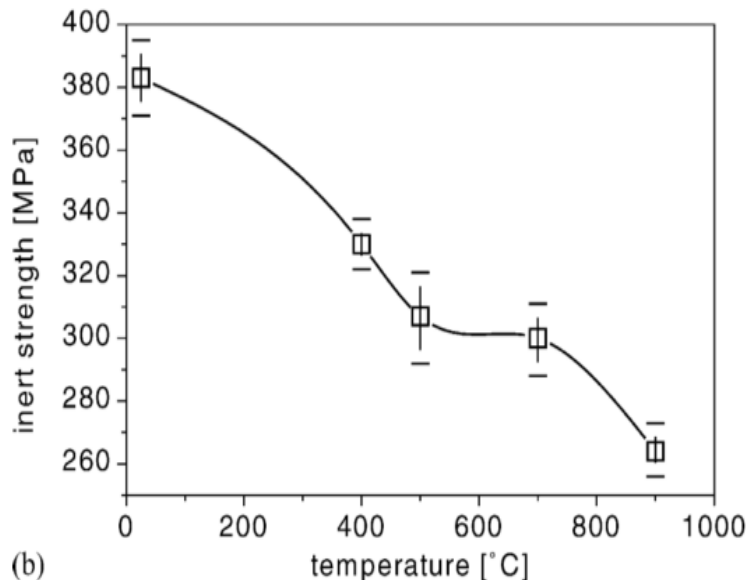


Figure 3.7: Temperature dependence of bending strength (inert strength) of alumina [23].

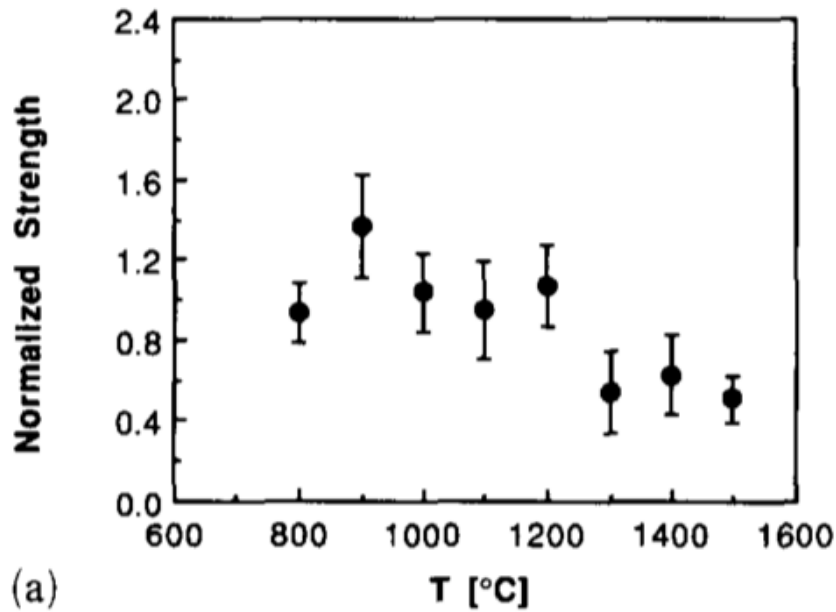


Figure 3.8: The crushing strength of porous open-cell alumina dependent on temperature [12].

CFFs are susceptible to thermal shock. When a ceramic material is non-homogeneous or anisotropic (as CFFs are) and exposed to temperature change, different components of the material will expand differently. This could occur even if the temperature change is constant through the material. However, a rapid change from room temperature to working temperatures will introduce a temperature gradient. This results in different expansion rates across the structure, leading to further thermal strain [24].

As silica is a common component in many CFFs, the phase diagram between alumina and silica (Figure 3.9) becomes relevant. As seen, silica has a lower melting point than alumina. Although the experiments forthwith do not reach 1600 °C, ceramics can transition into a glassy phase at lower temperatures.

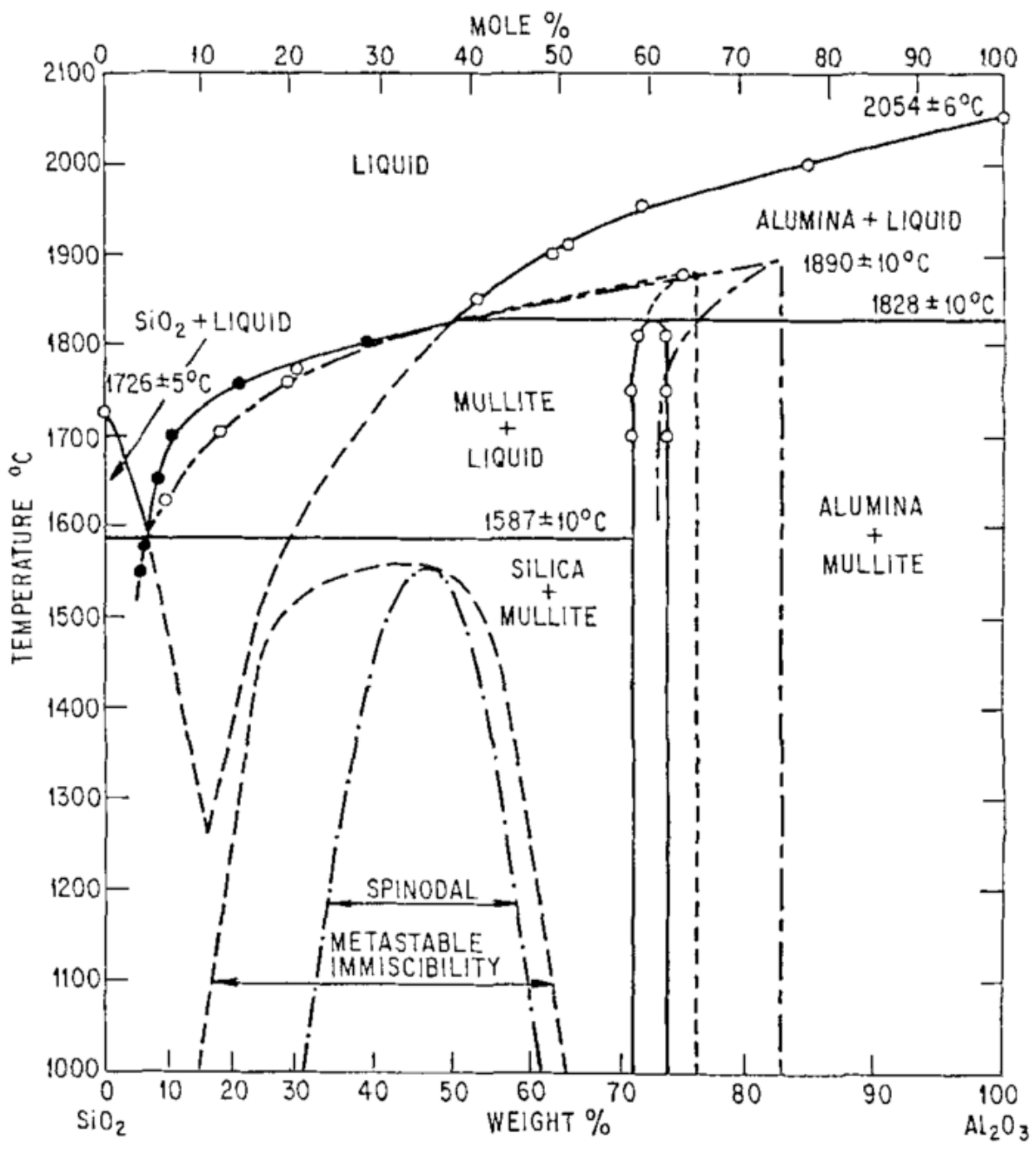


Figure 3.9: Alumina-silica phase diagram [25].

4 Experimental Procedures and Analysis

The compression tests that were performed on the CFFs included: testing of the effect of sample shapes (circular and square), testing at room temperature, testing the effect of thermal shock with a ten-minute oven holding time at 800 °C, and testing the effect in compression with different oven holding times at one-hour and two-hour at 800 °C. The testing was performed on CFFs from four different manufacturers: Sivex (Pyrotek, Czech Republic), Ceralu Al₂O₃ (Drache, Germany), VUKOPOR ®A (Lanik, Czech Republic) and SELEE® CS-X (Selee, United States). These are hereby referred to as Sivex, Drache, Lanik and Selee respectively. The various filter samples tested is summarized in Table 4.1. Samples with both cylindrical and cubic shapes were also tested, shown in Table 4.2.

Table 4.1: The different manufacturers, ppi's, and the number of filters tested at the different holding times in the heated oven.

Filter manufacturer	ppi	Cold tests	730°C 10 min	730°C 1 h	730°C 2 h
Sivex	30	22	10	10	10
	65	22	10	-	-
	80	22	10	-	-
Sivex NP	30	22	10	10	10
Drache	30	22	10	10	10
	60	22	10	-	-
Lanik	30	22	10	10	10
	60	22	-	-	-
Selee	30	22	10	10	10

Table 4.2: The different tests performed to analyse the effect of sample shape.

Filter manufacturer	ppi	Cold tests
Sivex cylinder	30	22
	65	22
	80	22
Sivex cubic	30	22
	65	22
	80	22

As detailed by Voigt et al. [10] it is important to use identical measurements and procedures. Sample size and the size of the loading plate can affect the results. The method for compression testing is based on NS-EN-993-5:2018 Methods of test for dense shaped refractory products. Determination of cold churning strength [9]. A compliant

loading pad was considered, but due to the high temperatures it could not be used.

All compression testing was performed with "MTS 880 Hydraulic Tensile Testing Machine 100 kN", as shown in Figure 4.1. The compression speed was constant at 2 mm/min with a circular loading plate with 50 mm diameter. The compression was done perpendicular to the elongation of the pores.



Figure 4.1: The MTS 880 Hydraulic Tensile Testing Machine 100 kN.

4.1 Analytical Methods

Several analytical tests were performed on the filters from the different manufacturers were made prior to mechanical testing. Microscopic pictures were taken to determine the wall thickness of the different filters. Additionally, a Scanning Electron Microscopy-analysis (SEM) was used to analyze the surface of the filter-walls. Based on the SEM-analysis, an Energy Dispersive Spectroscopy (EDS) was performed on different areas of the surface to determine the various elements present in the filters. Lastly, a mercury intrusion porosimetry test of the filters was performed to find the material- and the relative- density of the samples.

4.1.1 Microscopic Analysis

The light microscopic images were taken with the Keyence VHX-2000 with lens VHZ20R, to look at the pores in the filters and measure the strut thickness of the different filters from the different manufacturers.

4.1.2 SEM- and EDS- Analysis

Samples were cut out of different filters and prepared to be analyzed. The SEM apparatus used was an Ultra 55 LE (Zeiss) shown in Figure 4.2, which had the EDS apparatus XFlash Detector 4010 energy-dispersive X-ray microanalysis attached. The samples were put in an epoxy-resin (Epofix, manufactured by Struers) and then honed to a smooth surface.

Before the SEM analyze, the samples were carbon sputtered to make them conductive, since ceramic materials are a non-conductiv material.

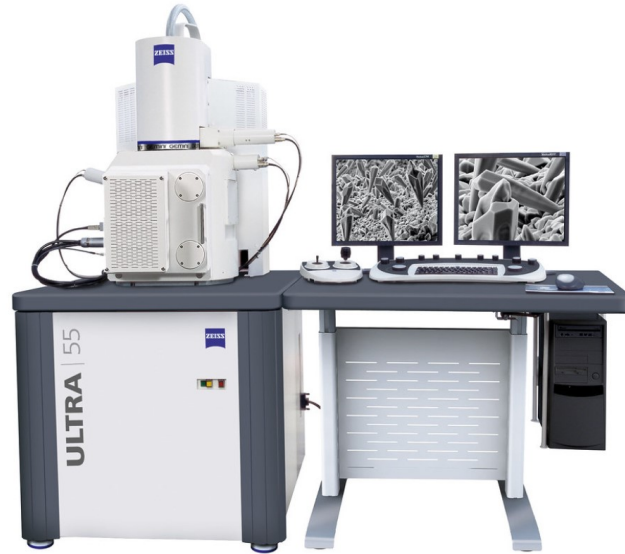


Figure 4.2: The SEM Ultra 55 LE machine from Zeiss [26].

4.1.3 Porosimetry Measurement

Additionally, mercury intrusion porosimetry measurements at the ceramic foam filters were conducted using an Autopore 5 (Micromeritics, USA). A penetrometer with 15 cm^3 cup volume and 0.392 cm^3 stem volume were used which allow the measurement of relatively large samples ($10 \times 10 \times 10 \text{ mm}^3$). The measurements consisted of 295 measuring points between 0.15 MPa and 420 MPa and the equilibrium time was five seconds. The pressure p was converted into the corresponding pore radius r with the help of the Washburn equation, see Equation 4.1:

$$p = 2\gamma \cos\theta / r \quad (4.1)$$

whereas θ (140° was used) is the contact angle and γ the surface tension (0.485 Nm^{-1} was used) of mercury.

4.2 Mechanical Testing at Room Temperature

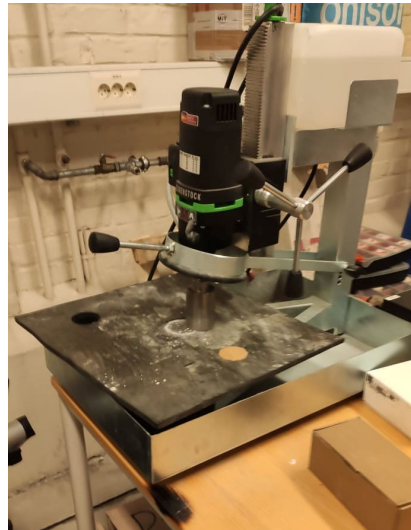
The cold compression strength tests were conducted at room temperature and 22 samples were tested per CFF type. The tested CFF samples were taken from filters for continuous casting ($600 \text{ mm} \times 600 \text{ mm} \times 50 \text{ mm}$). There were two possibilities for cutting the samples: usage of a band saw for the cubic samples and usage of a hollow drill which result in cylindrical samples. As mention in Chapter 3.2; the size and shape of the filter sample and of the loading plate influence the compression strength, and for that reason the first task was to investigate the influence of the samples form. The influence of sample form was tested using Sivex filters with functional pore sizes of 30 ppi, 65 ppi and 80 ppi. The circumference of the loading plate and the cylindrical filters was identical. The same loading plate were used for the cubic formed filters, resulting in samples surface area larger than the loading plate.

4.2.1 Preparation of Samples

Filters were cut into smaller samples, as shown in Figure 4.3a, from the 50 mm x 600 mm x 600 mm square filters. The cylindrical samples were cut by using the core drill "Eibenstock EFB152PX Tile Drilling Machine Wet 120.0 mm" as seen in Figure 4.3b, dressed with a diamond bit and water cooling attached. The cubic samples were cut with a band saw into 50 mm x 50 mm x 50 mm cubes, while the cylindrical samples had a height and diameter of 50 mm x 50 mm. Some of the filters were dried in oven shown in Figure 4.3c overnight at approximately 100 °C. The filters that were not dried in the oven, were dried on a cardboard box at room temperature. After the drying all the filters, they were weighted and its height and diameter was measured before performing the compression testing. The balance used was "Mettler Toledo SB32001 DeltaRange Balance" shown in Figure 4.3d, with an accuracy of ± 0.1 g.



(a) Example of the filter samples used.



(b) Eibenstock EFB152PX Tile Drilling Machine Wet 120.0 mm.



(c) Oven used for drying the samples after cutting and prior to compression test.



(d) The Mettler Toledo SB32001 Delta Range Balance used.

Figure 4.3: The equipment used for the preparation of the samples.

4.3 Mechanical Testing at 730 °C

Compression strength measurement at room temperature is an important part for the development of new compositions and quality control, but has limited value, since the compressive strength at the much higher operating temperature could be expected to be significantly different. Therefore, mechanical testing of CFF samples was also performed at temperatures between 650 °C to 750 °C in order to document the effect temperature has on the samples compressive strength.

To reach the chosen test temperature of 730 °C, the oven was preheated to 800 °C. The development of the sample temperature was monitored and controlled by using a temperature drop test. A thermocouple wire were attached to a sample as shown in Figure 4.4, while the oven preheated to 800 °C. When the oven reached the desired temperature of 800 °C, the sample with the thermocouple wire attached was put into the oven. The temperature of the sample was measured continuously. When the sample reached the desired temperature, the samples were transferred with great caution from the oven to the compression test machine. By doing this, the filters got minimal time exposed to the room temperature air. This procedure was done four times with cylindrical Sivex 30 ppi samples, and once using cylindrical Sivex 80 ppi, to get a more statistical precise result.



Figure 4.4: A sample with a thermocouple wire attached.

4.3.1 Different Holding Times

The mechanical tests at 730 °C were performed with three different holding times in the oven to determine the influence of this parameter. Particular attention was on the heating/testing procedure to reach optimal testing conditions. For every holding time this procedure was adapted to the time the samples were in the oven.

Ten samples of each CFF type were tested at the different oven holding times. Due to capacity limitations of the oven, samples were heated in batches of six. The samples were places in a systematic order to avoid mixing them.

Ten - Minute Holding Time at 800 °C

Ten samples per filter type were tested with ten minutes holding time in the oven at 800 °C. The first filter went into the oven, and after ten minutes, the second filter were put in the oven while the first was taken out of the oven and transferred to the compression machine for the compression test. When the second filter were ready to be compressed, the third filter was put in the oven as the second filter were taken out. This system continued with the remaining filters, with the time for the take out and put in as shown in Table 4.3.

Table 4.3: Ten-minute holding time at 800 °C.

Sample No.	Time going in the oven [min]	Time out of oven [min]
1	0	10
2	10	20
3	20	30
4	30	40
5	40	50
6	50	60
7	60	70
8	70	80
9	80	90
10	90	100

One - Hour Holding Time at 800 °C

Ten samples per filter type were tested with one-hour holding time at 800 °C, to document whether the high temperature and holding time affects the ceramic bonding in the filters. The heating schedule (sample number, when it was put in to and taken out of the oven) is summarized in Table 4.4.

The first sample was put in the oven at 800 °C, after ten minutes, sample number two was put in the oven. Taking care with placing the samples in the oven, the process was repeated until all six filters were in the oven. Once the first sample had been in the oven for one hour it was quickly transferred to the compression test machine and tested. It was crucial to use as little time as possible to move the sample out of the oven to the testing machine, as tested in temperature drop testing. When the second sample was tested, the seventh sample was put in the oven in sample number one's place. This system continued through the remaining samples, this way all the samples had a one hour holding time in the oven at 800 °C.

Table 4.4: One-hour holding time at 800 °C.

Sample No.	Time going in the oven [min]	Time out of oven [min]
1	0	60
2	10	70
3	20	80
4	30	90
5	40	100
6	50	110
7	70	130
8	80	140
9	90	150
10	100	160

Two - Hour Holding Time at 800 °C

Ten samples per filter type were tested with a two-hour holding time at 800 °C, to see if the high temperature and holding time affects the ceramic bonding strength in the filter material. The heating schedule is summarized in Table 4.5.

The procedure to the two-hour holding time was similar to the one hour holding time in the oven. The difference was a longer wait between putting samples number six in the oven and the start of compression testing of sample number one. This wait was 70 minutes long due to the oven limitations. When sample one had been in the oven for the two-hours, it was removed from the oven for compression strength testing. After putting sample number ten in the oven, there were a new waiting period of 90 minutes due to oven limitations. When the sixth sample had been in the oven for two hours, the second round of testing began with ten minutes in between each test.

Table 4.5: Two-hour holding time at 800 °C.

Sample No.	Time going in the oven [min]	Time out of oven [min]
1	0	120
2	10	130
3	20	140
4	30	150
5	40	160
6	50	170
7	130	250
8	140	260
9	150	270
10	160	280

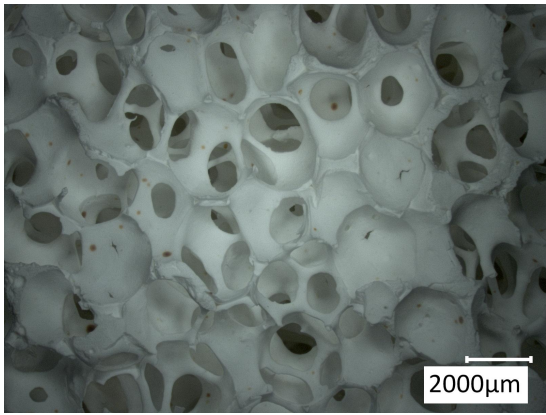
5 Results and Discussion

5.1 Analytical Methods

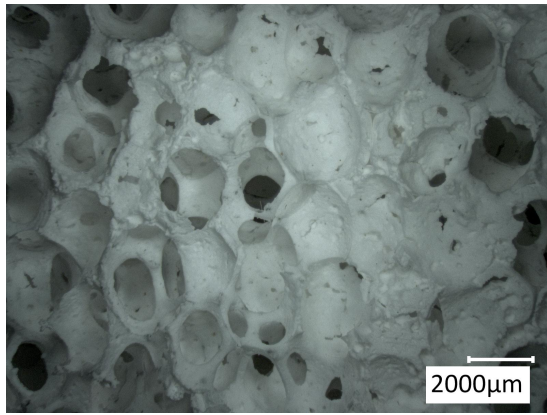
The following analytical methods were conducted on the different filter samples before cold and warm compression testing. Geometric and weight measurements of individual samples are shown as foam density in Appendix A.

5.1.1 Microscope Pictures

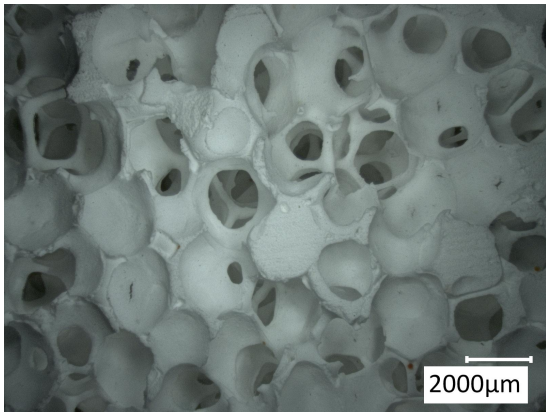
All sample were studied under the light microscope, as seen in Figure 5.1 for the 30 ppi samples, and Figure 5.2 for the 60 - 80 ppis samples. Although these foams are classified as open-celled structures, the microscope images shows a significant amount of closed cells. The images indicates that decreasing cell/pore size correlates with increasing pore density and increasing presence of closed cells. As discussed in Chapter 3.1, it is common that foams with a relative density over 0.1 will have more filled wall faces than struts, which further increases with increasing relative density. Struts and cell walls will subsequently be collectively referred to as struts.



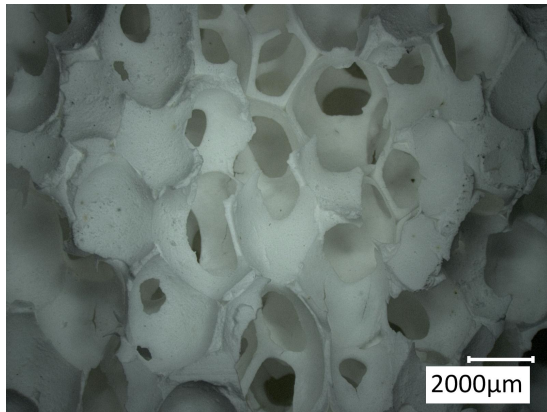
(a) Sivex 30.



(b) SivexNP 30.



(c) Drache 30.



(d) Lanik 30.



(e) Selee 30.

Figure 5.1: Microscopic photos of the 30 ppi samples at 30x magnification.

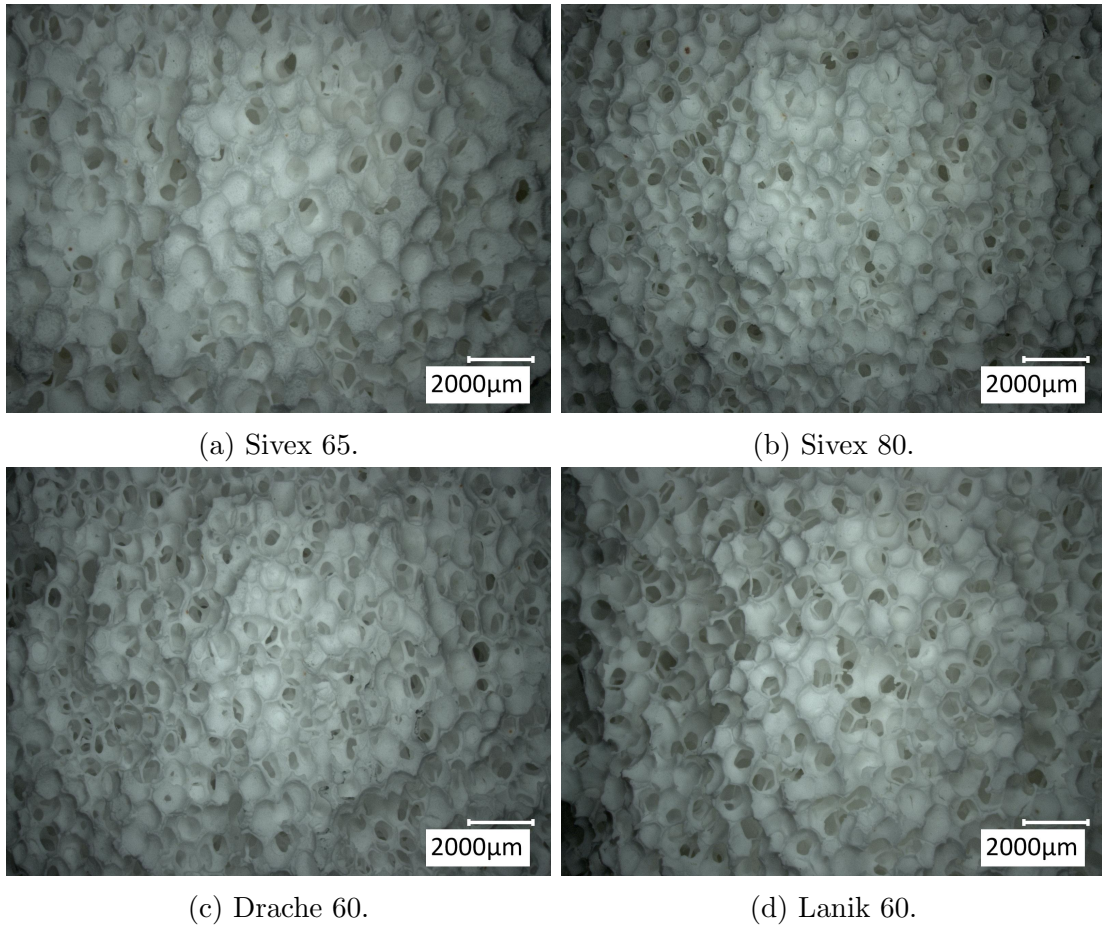


Figure 5.2: Microscopic photos of the other sample ppis at 30x magnification.

Strut Thickness

Table 5.1 shows the average strut thickness found by measuring the struts under the light microscope. As seen the strut thickness seems to be half as large with 60 and 80 ppi filters compared to 30 ppi filters. While this is positive for the function of the filters (as it results in greater permeability), it would result in weaker struts and potentially lower compressive strength. While SivexNP and Lanik 30 appear to have thicker struts, the sizeable standard deviation indicates large inaccuracies. However, a large standard deviation was expected due to the substantial variation in the structure of the foams.

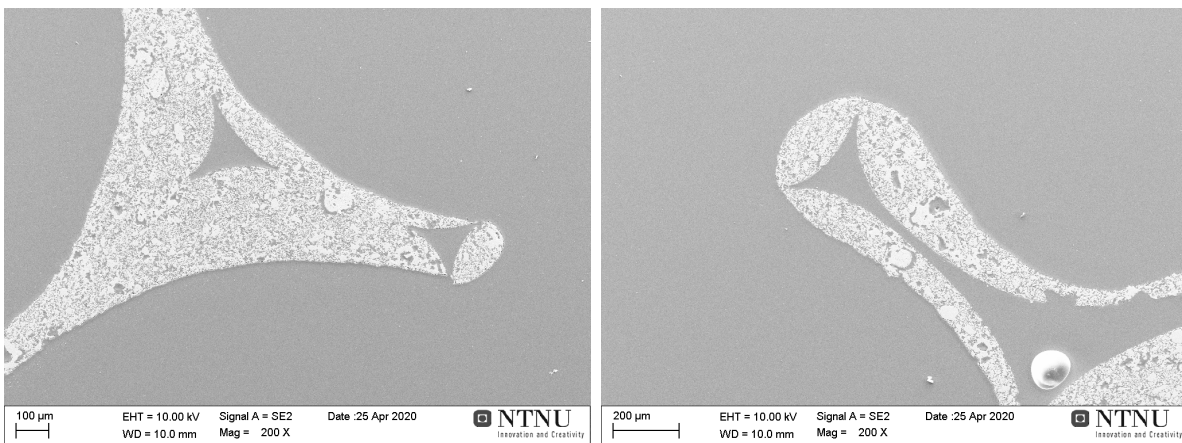
Table 5.1: Average strut/wall thickness.

Filter	Average Thickness (μm)	St. Dev. (μm)
Sivex 30	291	73
Sivex 65	162	53
Sivex 80	147	43
Sivex NP 30	341	74
Drache 30	319	111
Drache 60	130	37
Lanik 30	337	54
Lanik 60	130	51
Selee 30	295	62

5.1.2 Scanning Electron Microscopy-Analysis (SEM)

A SEM-analysis was conducted on samples from the different manufacturers prior to compression testing. SEM-analysis shows the surface of the filter, and how the different elements sintered together in the filter walls. The analysis also show pores in the structure, which can affect the mechanical strength in the material. One of these that is frequent in all of the filters are the triangular hole left in the structure after the melt out process.

Figure 5.3a and 5.3b shows two different struts from the same sample. Visible is the large variation in the strut cavities left from the production process. The large difference in strut structure is evident, as Figure 5.3a has two small triangular cavities while Figure 5.3b has one large cavity, almost comprising the entire width of the strut in some areas. This large variation was common in all filter samples. Note that Figure 5.3 are two-dimensional images of a three-dimensional structure. According to Equation 3.6 the size of the cavities has a significant impact on the compressive strength, as an increase of (t_i/t) will decrease the strength. The average size of the strut cavities can be seen from Figure 5.5, where Sivex has significantly smaller strut cavities, possibly increasing the compressive strength.



(a) Small strut cavity.

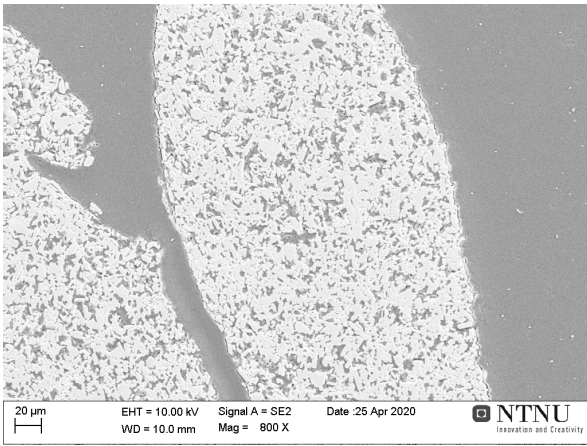
(b) Large strut cavity.

Figure 5.3: SEM photos of the Drache 30 ppi filter at 200x magnification.

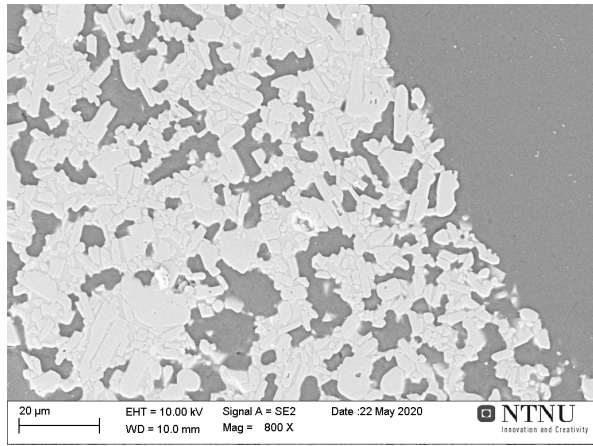
Figure 5.4 shows the SEM photos at 800x magnification of all the 30 ppi filters. While all the filters have material pores ranging in diameter from a couple μm to 20 μm , the average size and distribution varies.

As shown in Figures 5.4a, 5.4c, and 5.4d Sivex, Drache, and Lanik seem to have a similar average pore size, where most of the pores are smaller than 10 μm . However, the distribution is quite different where Drache has the largest areas with dense material, while in the Lanik sample the pores are finely distributed. Denser material lends to a higher compression strength. However, there are many pores with sharp edges, which could result in weaker struts leading to decreased strut strength.

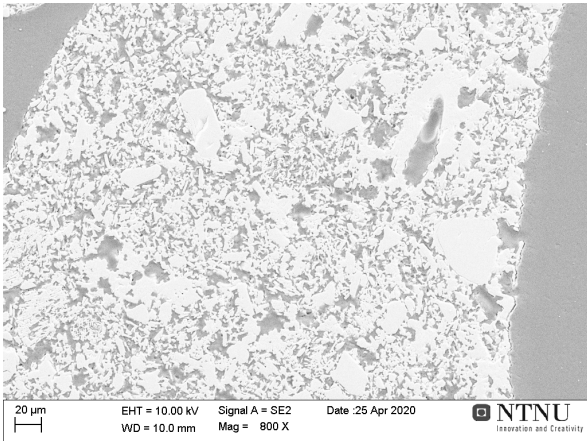
Figures 5.4b and 5.4e indicate that SivexNP and Selee have larger pores, with several pores exceeding 20 μm . However, Selee has fewer, but larger pores, which could lead to decreased compressive strength, as discussed in Chapter 3.1.



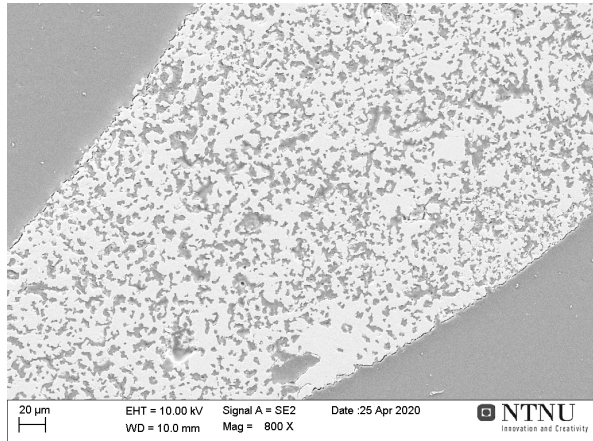
(a) Sivex.



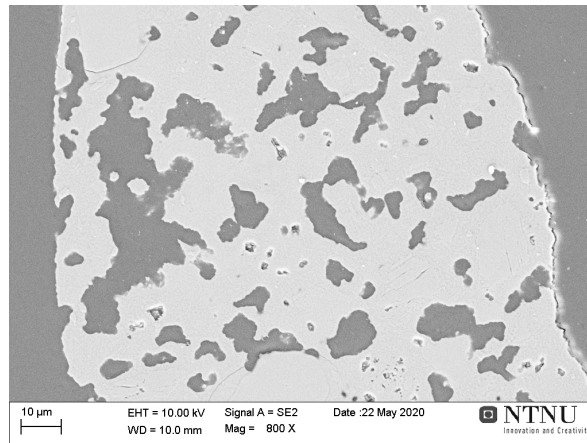
(b) SivexNP.



(c) Drache.



(d) Lanik.



(e) Selee.

Figure 5.4: SEM photos of different 30 ppi filters at 800x magnification.

5.1.3 Energy Dispersive Spectroscopy (EDS)

The EDS-analyses picks up the energy of X-ray photons from the different elements, with different constraints. These constraints involve a limit of detection and energy-resolution, and no indication of elements lighter than beryllium. This can cause a misinterpretation of the elements present in a filter. Elements as boron may not show, due to the similar output energy as neighboring elements. This indicates that boron may show as carbon, and because of the carbon sputtering prior to the EDS-analysis, it will not show. Here, the elements with an atomic % (at.%) less than 1 will be excluded from the results. The results from the EDS-analysis is listed in Table 5.2.

Table 5.2: Elements found in the EDS-analysis from the different filters.

Sample	Average at. %						St. Dev. at. %					
	O	Al	Si	P	Mg	Ca	O	Al	Si	P	Mg	Ca
Sivex 30	48.06	46.38	-	4.51	-	-	0.43	1.05	-	0.53	-	-
Sivex 65	47.63	47.28	-	3.99	-	-	0.33	0.64	-	0.52	-	-
Sivex 80	49.27	43.98	-	6.23	-	-	0.32	0.63	-	0.21	-	-
Sivex NP 30	49.15	43.93	5.48	-	-	-	0.66	1.95	1.09	-	-	-
Drache 30	48.35	45.01	3.53	1.98	-	-	0.50	1.07	0.67	0.51	-	-
Drache 60	47.42	46.53	3.426	1.44	-	-	0.45	2.09	1.40	0.49	-	-
Lanik 30	47.73	43.40	7.84	-	1.08	-	0.40	1.18	0.88	-	0.11	-
Lanik 60	47.85	44.38	6.65	-	1.07	-	0.23	0.44	0.34	-	0.12	-
Selee 30	53.24	26.51	18.15	-	-	1.56	0.36	1.14	1.02	-	-	0.25

As shown, all the samples except Selee seem to be alumina based, where Sivex appears to have a higher content of phosphorus. SivexNP 30, Lanik 30 and Selee 30 appear to be phosphorus free, and instead having higher content of silicon. Selee further diverges from the others with an apparently high ratio of oxygen and silicon compared to aluminium. The high content of silica could be explained by the presence of a mullite phase. XRD analysis could be used to determine the phase composition. According to the patent for SivexNP, the filter could also include boron, which an EDS analysis would not detect [22].

5.1.4 Mercury Intrusion Porosimetry

Density

Table 5.3 shows the material and relative densities. Relative density was calculated from the material density and the foam density in Appendix A. As supported by the SEM pictures in Figure 5.4, the Drache, Sivex and Lanik 30 filters seem to have a high material density and low relative density. While SivexNP and Selee exhibit a lower material density. While Sivex and Drache 30 have a similar material density, Sivex 30 has a significantly higher relative density, possibly due to smaller pores. SivexNP has a relatively high relative density compared to the other 30 ppi filters, indicating less empty space in the filter. This could be impacted by the thicker struts leading to more material per cell. Otherwise the order of relative density is well matched to the material density, as a lower material density yields a higher relative density.

Table 5.3: Results from porosimetry.

Sample	Material Density \pm St. Dev. (g/cm^3)	Relative Density
Sivex 30	2.145 ± 0.015	0.192
Sivex 65	2.249 ± 0.012	0.217
Sivex 80	2.088 ± 0.040	0.245
Sivex NP 30	1.738 ± 0.047	0.226
Drache 30	2.281 ± 0.224	0.182
Drache 60	2.157 ± 0.033	0.214
Lanik 30	2.029 ± 0.024	0.199
Lanik 60	2.076 ± 0.006	0.204
Selee 30	1.687	0.193

Pore Size

Figure 5.5 presents the cumulative pore volume in dependence on the pore size of the different filter types. Each measurement possesses two main increases of the cumulative pore volume. The first increase at mean pore sizes between 30 μm and 150 μm is the filling of the strut cavities resulted from the decomposition of the polyurethane foam [27]. There are significant differences between the filter types whereby the repeat measurement (two measurements per filter type) show a good agreement. It is notable that within one producer the mean pore size decreases with increasing pore density (ppi-number). A comparison between the producer gives no correlation which can be explained by the usage of polyurethane from different producers and different shrinkages during sintering caused by the slurry composition. The second main increase is caused by the mercury filling of the material porosity. It should be pointed out that the amount of intruded pore volume will not be considered due to sample taking issues discussed in Voigt et al. [27]. The mean pore size of the second increase of the intruded pore volume of the phosphate bonded Sivex filters (30, 65 and 80 ppi) show a pore size of around 1.5 μm and are in good agreement. This indicated the usage of the same slurry for the different pore densities (ppi-numbers). The Lanik filters possess a mean pore size of the second increase in the intruded pore volume of around 2.2 μm and are in good agreement. The Drache filter show a comparable mean pore size at the beginning of the second increase in the intruded pore volume of around 2.8 μm but then the 60 ppi measurement shows a smaller gradient. The SivexNP and Selee filter (both are non phosphate compositions) presents significant larger pore size for the material pores which is consistent with the SEM images. The main pore size of the second increase is for the SivexNP around 4.1 μm and for the Selee a main pore size is difficult to define.

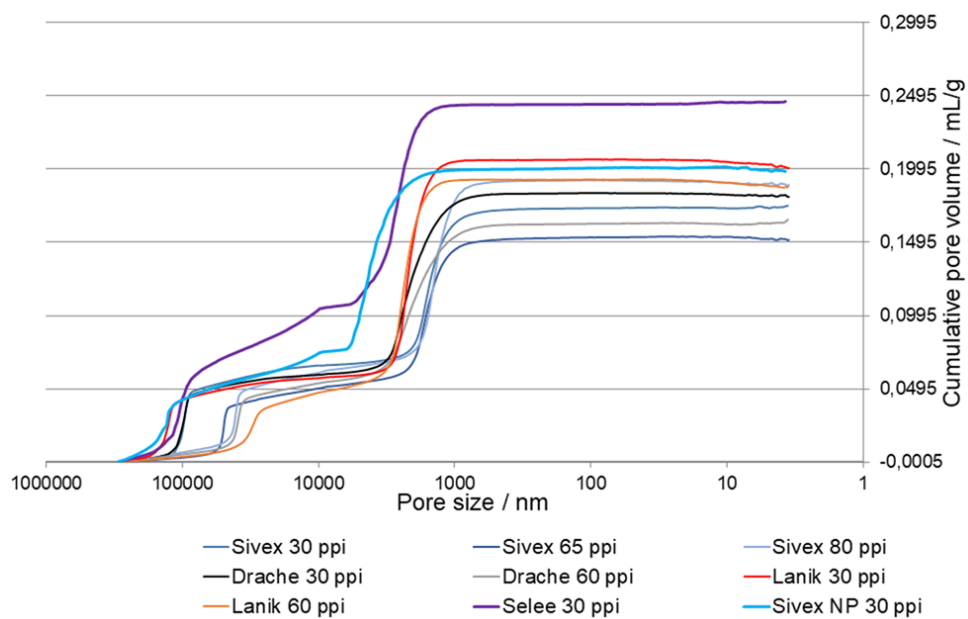


Figure 5.5: Cumulative pore volume dependent of pore size.

5.2 Compression Testing

The compression tests were performed in accordance with the procedures detailed in the method section. The results are summarized in Appendix A, and represent the peak values recorded for compression strength. Due to time constrictions and availability of the 30 ppi filters, they were prioritised for the different tests at a working temperature of 730 °C.

5.2.1 The Effect of Sample Shape

Figure 5.6 shows the compressive strength of cylindrical and cubic samples from the Sivex filters. The cubic samples exhibit a higher compressive strength, which was expected due to the rise in sample size [10]. The compression strength is comparable for the 30 ppi filters, while the difference increases with higher pore density where the cubic samples have the higher compressive strength. A statistical analysis using p-value was done, with a null hypothesis of a strong correlation between the compressive strengths of the cylindrical and cubic samples, meaning a significant resemblance between the values. The p-values for 30, 65 and 80 ppi respectively were 0.26, 0.04 and 5.39e-7. While the p-value suggests a correlation for the 30 ppi samples, there is little correlation between the 65 and 80 ppi filters, suggesting that the compressive strength is not sufficiently similar between the cylindrical and cubic samples. Therefore, cylindrical and cubic samples cannot be used interchangeably. While both shapes can be used according to the standard [9], the cylindrical tests exhibit a smaller standard deviation, see Appendix A. This could be due to the fact that the loading plates cover the entirety of the cylindrical sample surface, while the cubic samples had corners that were not being compressed, causing stress anisotropy in the sample. It was therefore decided to proceed with cylindrical samples.

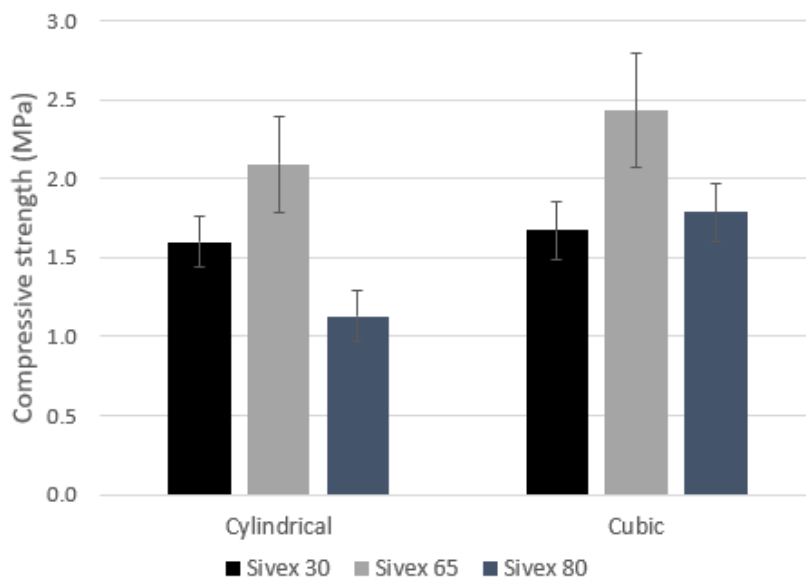


Figure 5.6: Compressive strength of cylindrical and cubic samples at room temperature.

5.2.2 Room Temperature Testing

Pore Density

Figure 5.7 shows the compressive strength plotted against pore density, showing three different responses to increased pore density. Sivex 65 shows an increase from 30 ppi, as could be expected from the higher relative density and material density. While both Sivex 65 and Sivex 80 have similar strut thickness (around half of Sivex 30), Sivex 80 exhibits a decreased strength compared to 30 ppi. This could potentially be due to the lower material density or impacted by a lesser phosphorus content. There could be a fault with the filter used in the test. As shown in Figure 5.8, there was a ring around the middle indicating a possible production fault. In addition, there was significantly more "snowing" from Sivex 80, snowing being loose particles emanating from the sample when moved or shaken. The Drache filters appear to have no noticeable change from 30 to 60 ppi, while Lanik exhibits a significant decrease in strength from 30 to 60 ppi, however due to the decrease in size of the Lanik 60 it is not comparative. The results suggests that compressive strength isn't necessarily directly dependent on pore density, but rather a combination of relative density and strut thickness.

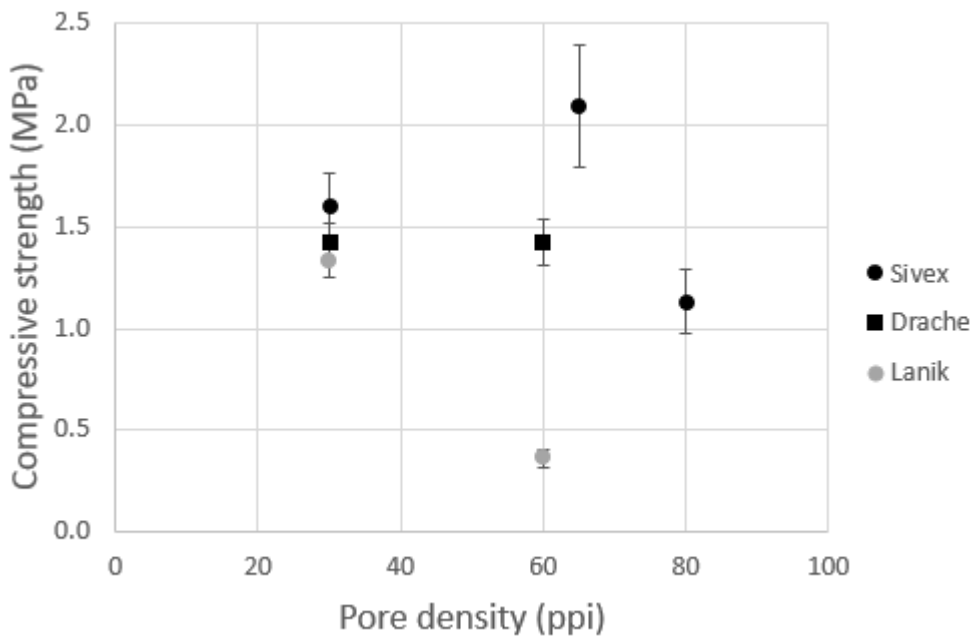


Figure 5.7: Compressive strength at room temperature of varying ppi filters.



Figure 5.8: A sample of Sivex 80. Note the ridges around the middle.

The method of shaping the filter samples, by cutting them with a diamond bit, could yield variable results. The Lanik filters had a tendency to crumble, which resulted in cavities in the samples, especially around the middle, see Figure 5.9. The Lanik 60 filter had a diameter of 43 mm compared to the standard 50 mm, and as detailed by Voigt et al. [10] the sample size has a significant impact on compressive strength. This could explain the low compressive strength of the Lanik 60 filters.



(a) Lanik 30.

(b) Lanik 60.

Figure 5.9: Pictures of Lanik samples.

Comparison With Established Models

Equation 3.6 suggests that the crushing strength increases with an increased strut strength, relative density, and t_i/t . Relative density is given in Table 5.3, and although strut strength was not measured, it can be discussed by examining the material porosity, composition and strut thickness. When looking at the lowest and highest strength filters they fit Gibson and Ashbys model well. Sivex NP had a high strength combined with the highest relative density and strut thickness. Although, the material porosity does also

seem to be quite high. Meanwhile, the Selee filter has the lowest strength, moderately low relative density and strut thickness as well as a seemingly high material porosity. Selee also has a different composition than the other filters, using mullite instead of pure alumina.

Figure 5.10 shows the compressive strength plotted against relative density, with a trendline (Equation 5.1):

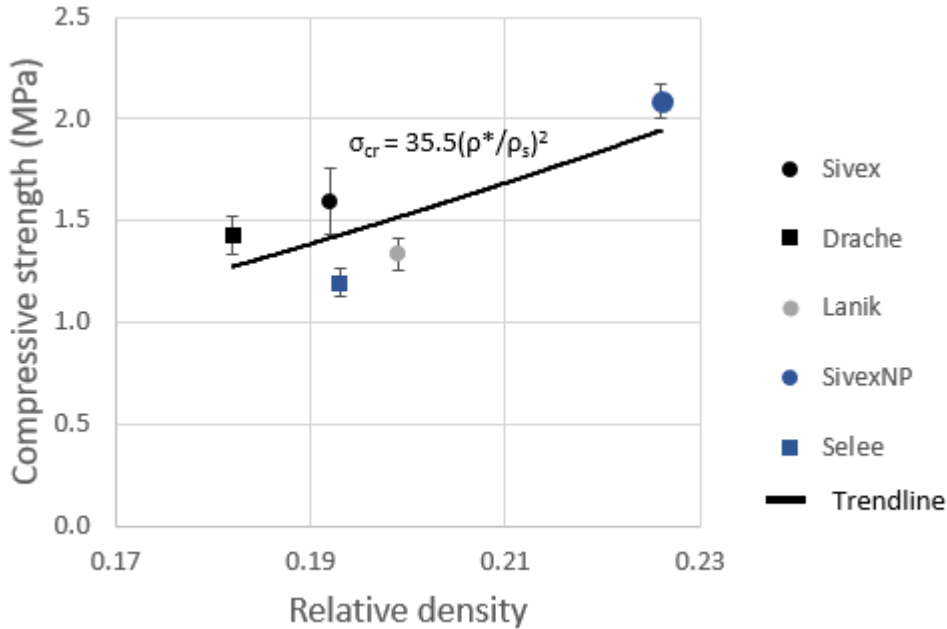


Figure 5.10: Compressive strength of 30 ppi filters dependent on relative density.

$$\sigma_{cr} = 35.5(\rho^*/\rho_s)^2 \quad (5.1)$$

This trend is quite similar to that found by Goretta et al. [12], with a slightly higher exponent than the one proposed by Gibson and Ashby's model in Equation 3.6 and 3.7. A higher exponent would indicate a higher dependence on relative density. However, the trend from Figure 5.10 was made from five data-points and does not fit perfectly and, unlike Goretta et al. and Brezny et al. [11], Equation 5.1 does not factor in the strut strength. This can for example be seen for Drache and Sivex, where the compressive strength is high compared to the trend. This could be due to the slightly higher material density, less porous struts, and in Sivex's case smaller strut cavities. These factors would comparatively increase the strut strength.

5.2.3 Temperature Drop Test

Figure 5.11 shows the measured temperature rate and the temperature drop of five samples, where test one - four are Sivex 30 ppi filters while test five is a Sivex 80 ppi sample. As seen in the graph demonstrated by the trendline, the average temperature drop is 2.07 °C/second. The time it took between the sample exiting the oven and completing the compression test was determined to be 35 ± 5 seconds. In this time the temperature of the sample will be approximately 730 °C based on the average temperature drop rate and the time used by moving the sample. The time it takes a sample to reach 800 °C is

approximately 480 seconds, around eighth minutes. This implies that a ten minute heating time in the oven will be sufficient for heating the samples to the given temperature. This gives the filters a temperature around 730 - 740 °C at the time of the compression test. It is assumed that the filters made from the different manufacturers does have a relative similar temperature drop rate. The exception being the difference in the ppi.

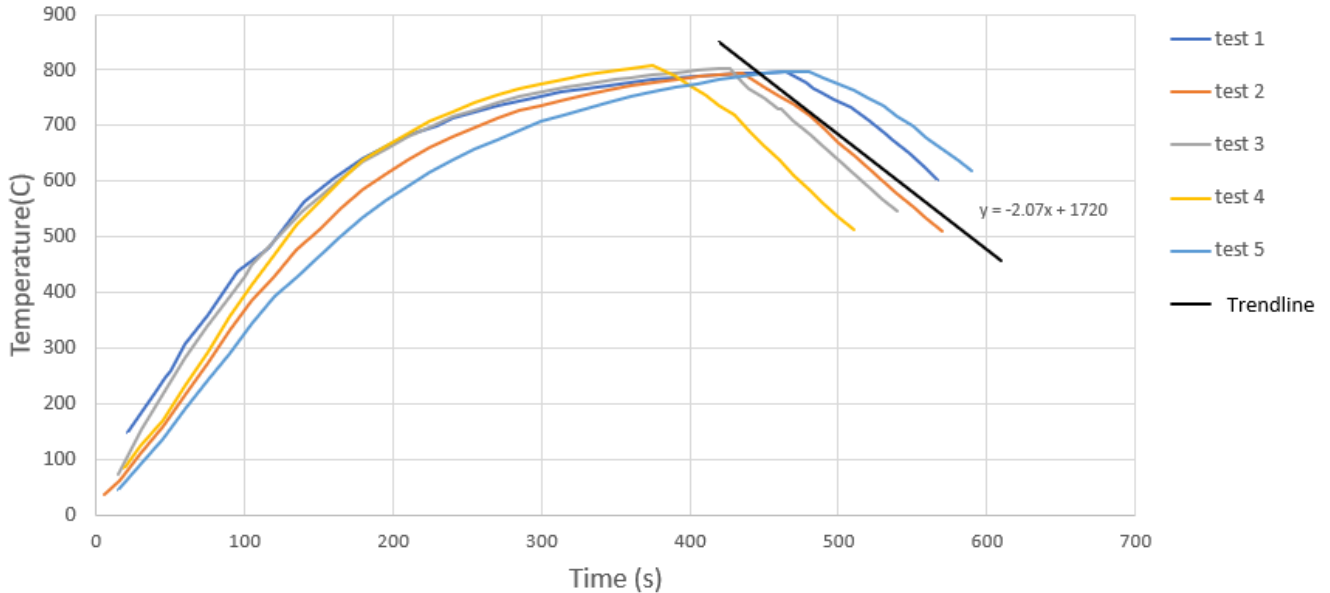


Figure 5.11: The temperature drop when the filter is moved from the oven into room temperature. The increment to the trendline shows the average drop in temperature per second.

5.2.4 Compression Strength Measurements at 730 °C

Figure 5.12 shows the results from compressive tests while the samples are hot after different holding times (ref. Appendix A). The compressive strength of the samples generally decrease with higher temperature and longer holding times. The two exceptions are Selee and Lanik. Lanik decreases significantly after ten-minutes, followed by an increase after one-hour, and decreases again after two-hours. The nearly opposite happens with Selee, where the compressive strength is higher at two-hours than at one-hour. In both these cases two separate filters were used, where room temperature and one-hour samples were taken from one filter and ten-minute and two-hour samples were taken from another filter. As previously seen with the Sivex 80 filter see Figure 5.8, flaws can arise in individual samples, which could result in the different results. In addition, the one-hour tests were done by the supervisor, so slight changes in method could arise. The Lanik filter was tested a second time by the supervisor with a ten-minute holding, yielding an average compressive strength of 0.915 MPa. While there were only tested four samples and the loading plate was different, the difference is significant indicating that there could be some variation in how the tests were performed. Alternatively, Selee has a different composition than the other filters, containing a high amount of silica. This could result in the Selee filters transitioning into a more glassy phase after two-hours, thereby softening pores and cracks, possibly regaining some strength and explaining the high compressive strength observed at the two hour holding time.

Not counting Selee and Lanik the average temperature drop was 18 %, 27 %, and 26 % respectively for ten-minutes, one-hour, and two-hours.

Note that while the averages of SivexNP resemble the pattern of Lanik, the standard deviation is sufficiently high as to overlap. However, SivexNP shows a large decrease in compressive strength at increased temperature indicating that while it is the strongest at room temperature, it is comparable with Sivex and Drache at higher temperatures.

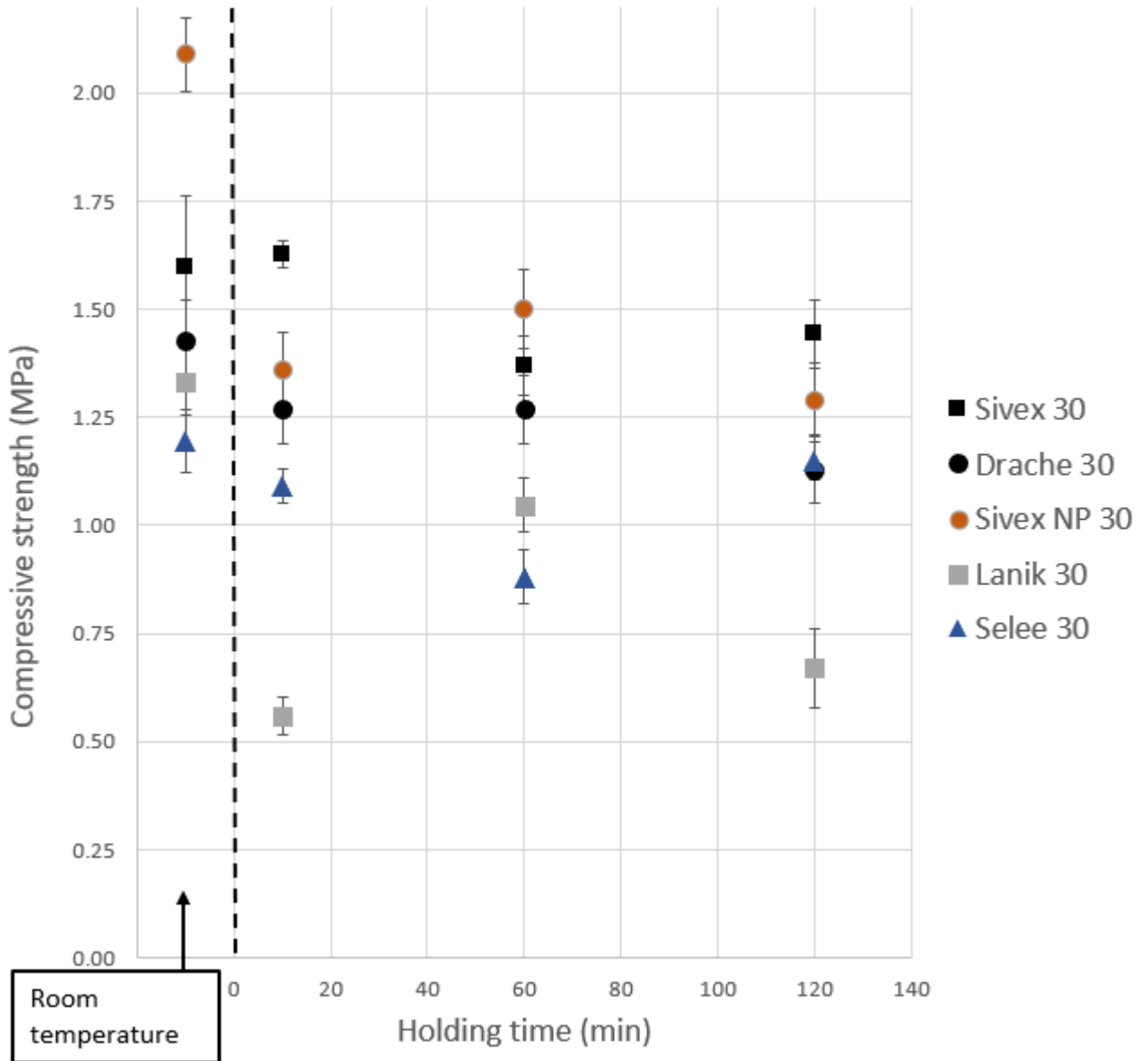


Figure 5.12: Compression tests of 30 ppi filters at working temperatures with varying holding times compared with room temperature tests.

Furthermore, The method used for heating the samples could have an affect on the measured compressive strength. Each time a new sample was placed in the oven or taken out, there was a 30 °C temperature drop in the oven. Therefore, there were fluctuations in the temperature, especially during one- and two-hour holding times. In addition, there would be a temperature shock whenever placing and removing the sample from the oven. An ideal test environment would be to have the compression test machine inside an oven,

so that the samples could be heated from room temperature without large fluctuations. However, this would significantly increase the time for each test. Additionally for future testing, it is recommended to take samples from one filter, as the mechanical properties vary greatly between different filters.

6 Conclusion

Compression tests of various filters were performed, from different manufacturers and pore densities, at room and working temperatures. The results resembled previous studies and models, where the compression strength had a significant dependence on relative density, where SivexNP exhibited the highest compressive strength at 2.09 MPa, and the Selee filter had the lowest compressive strength at 1.20 MPa. While the strut strength was not measured, it was discussed through various analytical methods such as; microscopy, mercury intrusion porosimetry, SEM, and EDS analysis, to characterize the structural properties of the CFFs. A significant match between structural properties and the compressive strength was found.

For the compressive testing at working temperatures, the compressive strength generally decreased with increased holding time with 18 %, 27 %, and 26 % respectively for ten-minutes, one-hour, and two-hours. While the Lanik and Selee filters exhibited a different pattern, it was attributed to flaws in the testing procedure and variations in quality between individual filters.

6.1 Further Work

This thesis may be used as a groundwork for future work in compression testing ceramic foam filters. Based on the procedures that have been created in coordination with this test, it is possible to conduct a larger scale test. It would be interesting to study the structure of the filters after holding time in the oven. If it has changed, and if this affects the compressive strength, particularly with regards to the material porosity.

It would be interesting to test the repeatability of the results, as there were some inconsistencies, in particular with regards to different holding times. Future refinement of the methods and possibly a different setup for compressive tests at working temperatures would be of interest to achieve more accurate results.

Measuring the strut strength of the different manufacturers at different temperatures could be of interest, as it is an important factor when characterizing the compressive strength of brittle foams. This could also give a better indication as to the affect of various structural parameters.

At the time of writing preliminary tests have been done on samples primed with molten aluminium at working temperatures. The progress of these tests will be interesting, as it closely resembles working conditions in the cast house.

Bibliography

- [1] D.C Chesonis. A holistic approach to molten metal cleanliness. *Light Metals 2017*, pages 1411–1417, 2017.
- [2] F. Breton, P. Waite, and P. Robichaud. Advanced compact filtration(acf): an efficient and flexible filtration process. *Light Metals 2013*, pages 967–972, 2013.
- [3] M. Scheffler and P. Colombo. *Cellular Ceramics: Structure, Manufacturing, Properties, and Applications*. Wiley-VCH, 2005.
- [4] F. Breton, P. Waite, and P. Robichaud. Advanced compact filtration (acf): an efficient and flexible filtration process. *Sadler B.A. (eds) Light Metals 2013. The Minerals, Metals & Materials Series. Springer, Cham*, pages 967 – 972, 2016.
- [5] E.G. Ramalho W.L. Torquato W. Acchar, F.B.M. Souza. Mechanical characterization of cellular ceramics. *Materials science and engineering A*, 513 - 514:340–343, 2009.
- [6] L. J. Gibson and M. F. Ashby. *Cellular Solids: Structure and Properties*. Cambridge University Press, 2. edition, 1997.
- [7] L. J. Gibson and M. F. Ashby. The mechanics of three-dimensional cellular materials. *proceedings of the royal society of London. Series A: mathematical and physical science*, 32:3959–3967, 1982.
- [8] T. T. Huu, M. Lacroix, C. P. Huu, D. Schewich, and D. Edouard. Towards a more realistic modeling of solid foam: use of the pentagonal dodecahedron geometry. *Chemical engineering science*, 64:5131–5142, 2009.
- [9] Methods of test for dense shaped refractory products-part 5: Determination of cold crushing strength, standard ns-en 993-5. 2018.
- [10] C. Voigt, J. Storm, M. Abendroth, C. G. Aneziris, M. Kuna, and J. Hubralkova. The influence of the measurement parameters on the crushing strength of reticulated ceramic foams. *Materials Research Society*, 28:2288–2299, 2013.
- [11] R. Brezny and D. J. Green. Fracture behaviour of open-cell ceramics. *Journal of the American Ceramic Society*, 72:1145–52, 1989.
- [12] K. C. Goretta, R. Brezny, C. Q. Dam, D. J. Green, A. R. de Arellano-Lopez, and A. Dominguez-Rodriguez. High temperature mechanical behaviour of porous open-cell al_2o_3 . *Materials science and engineering*, 24:151–158, 1990.
- [13] G. Heness, N. Booth, and B. Ben-Nissan. Does size matter? - the effect of volume on the compressive strength of open cell brittle ceramics. *Advanced Materials Research*, 41-42:221–226, 2008.

- [14] R. Brezny and D. J. Green. Uniaxial strength behavior of brittle cellular materials. *Journal of the American Ceramic Society*, 76:2185–2192, 1993.
- [15] R. Fritzsche, M. W. Kennedy, J. A. Bakken, and R. E. Aune. Electromagnetic priming of ceramic foam filters (cff) for liquid aluminum filtration. *Sadler B.A. (eds) Light Metals 2013. The Minerals, Metals & Materials Series. Springer, Cham*, pages 973 – 979, 2016.
- [16] S. Bao, M. Syvertsen, A. Kvithyld, and T. Engh. Wetting behavior of aluminium and filtration with Al_2O_3 and sic ceramic foam filters. *Transactions of Nonferrous Metals Society of China*, 24:3922 – 3928, 2014.
- [17] U. Tundal, I. Steen, Å. Strømsvåg, T. Haugen, J. O. Fagerlie, and A. Håkonsen. Drain free filtration (dff) — a new cff technology. *Chesonis C. (eds) Light Metals 2019. The Minerals, Metals & Materials Series. Springer, Cham*, pages 1097 – 1104, 2019.
- [18] A. Nishiwara. *Technology of monolithic refractories*. 1984.
- [19] J. A. Fernando and D. D. L. Chung. Improving an alumina fiber filter membrane for hot gas filtration using an acid phosphate binder. *Journal of materials science*, 36:5079–5085, 2001.
- [20] C. K. Solem, R. Fritzsche, and R. E. Aune. Preliminary experimental study of the thermal stability and chemical reactivity of the phosphate-based binder used in Al_2O_3 -based ceramic foam filters(cffs). 2018.
- [21] L. S. Aubrey, R. Olson, and D. D. Smith. Development of a phosphate-free reticulated foam filter material for aluminium cast houses. *Materials science forum*, 630:137–146, 2009.
- [22] Milton Keynes. Pyrotek engineering materials limited, 2019. US patent 2019/0240605.
- [23] R. Nejma, K. H. Lang, and D. Lohe. Influence of the temperature on the strength and the subcritical crack growth rate of alumina. *Materials Science and Engineering A*, 387-389:832–836, 2004.
- [24] W. D. Kingery. Factors affecting thermal stress resistance of ceramic materials. *American ceramic society*, 38:3–15, 1955.
- [25] F. J. Klug, S. Prochazka, and R. H. Doremus. Alumina-silica phase diagram in the mullite region. *Ceramic int.*, 44:22963–22975, 2018.
- [26] ZEISS.com. Ultra 55 le (zeiss), 2020. Retrieved: 17.05.2020.
- [27] C. Voigt, J. Hubáľková, L. Ditscherlein, R. Ditscherlein, U. Peuker, H. Giesche, and C.G. Aneziris. Characterization of reticulated ceramic foams with mercury intrusion porosimetry and mercury probe atomic force microscopy. *Ceramic int.*, 44:22963–22975, 2018.

7 Appendix

A The results from the compressive strength testing of all the filter types, filter porosities and experimental parameters

Table 0.1: Results from compression testing of all combinations of filter type, filter porosity and experimental parameters.

Sample	Foam Density(g/cm ³)		Compressive Strength(MPa)				
	Average	St. Dev.	Average	St. Dev.	Min	Max	Diff. from cold
Room temperature							
Sivex 30	0.412	0.024	1.60	0.33	1.06	2.19	–
Sivex 30 (cubic)	0.371	0.027	1.67	0.37	0.82	2.21	–
Sivex 65	0.489	0.023	2.09	0.60	1.17	3.43	–
Sivex 65 (cubic)	0.493	0.030	2.43	0.72	1.31	4.25	–
Sivex 80	0.511	0.031	1.04	0.30	0.46	1.54	–
Sivex 80 (cubic)	0.441	0.031	1.79	0.37	0.83	2.39	–
Sivex Np 30	0.391	0.011	2.09	0.17	1.65	2.48	–
Drache 30	0.415	0.016	1.43	0.19	1.11	1.79	–
Drache 60	0.460	0.017	1.43	0.22	0.98	1.79	–
Lanik 30	0.404	0.011	1.33	0.15	1.07	1.62	–
Lanik 60	0.423	0.028	0.36	0.08	0.21	0.53	–
Selee 30	0.325	0.011	1.20	0.14	0.90	1.50	–
10 min holding time at 800°C							
Sivex 30	0.416	0.008	1.63	0.06	1.50	1.71	+0.03
Sivex 65	0.478	0.017	1.30	0.44	0.36	1.88	-0.79
Sivex NP 30	0.363	0.014	1.36	0.17	1.07	1.60	-0.73
Drache 30	0.384	0.019	1.27	0.19	0.88	1.50	-0.16
Drache 60	0.547	0.002	1.11	0.27	0.56	1.58	-0.32
Lanik 30	0.391	0.017	0.56	0.09	0.36	0.73	-0.77
Selee 30	0.344	0.006	1.09	0.08	1.01	1.26	-0.11
1 hour holding time at 800°C							
Sivex 30	0.382	0.017	1.37	0.13	1.21	1.59	-0.23
Sivex NP 30	0.392	0.011	1.50	0.18	1.20	1.70	-0.59
Drache 30	0.423	0.014	1.27	0.16	0.97	1.56	-0.16
Lanik 30	0.398	0.010	1.05	0.12	0.83	1.21	-0.29
Selee 30	0.320	0.011	0.88	0.13	0.62	1.08	-0.31
2 hours holding time at 800°C							
Sivex 30	0.401	0.022	1.44	0.16	1.14	1.69	-0.16
Sivex NP 30	0.391	0.003	1.29	0.17	1.00	1.50	-0.80
Drache 30	0.404	0.020	1.13	0.16	0.88	1.39	-0.30
Lanik 30	0.375	0.037	0.67	0.18	0.54	1.16	-0.66
Selee 30	0.342	0.009	1.15	0.09	0.97	1.31	-0.05

B Raw data from room temperature compressive tests

Sivex cylindrical:

navn på filter		ppi	g	mm	mm	dm3	kg/m3	kN	Mpa
produsent	sys navn		Weight	Height	Diameter		density	max force	Crushing strength
Sivex	Sivexcy30_1	30	48.80	50.12	50.72	0.101	481.904	4.152	2.115
sylander	Sivexcy30_2	30	45.40	50.20	50.79	0.102	446.381	3.674	1.871
	Sivexcy30_3	30	43.90	50.12	50.70	0.101	433.858	4.300	2.190
	Sivexcy30_4	30	43.80	50.27	50.73	0.102	431.068	3.969	2.021
	Sivexcy30_5	30	42.90	50.05	50.94	0.102	420.577	3.659	1.864
	Sivexcy30_6	30	44.80	50.06	50.72	0.101	442.934	3.489	1.777
	Sivexcy30_7	30	43.20	50.17	50.83	0.102	424.336	3.398	1.731
	Sivexcy30_8	30	43.80	50.00	50.65	0.101	434.766	3.397	1.730
	Sivexcy30_9	30	42.00	50.05	50.77	0.101	414.516	3.386	1.724
	Sivexcy30_10	30	41.70	50.32	50.79	0.102	409.024	2.851	1.452
	Sivexcy30_11	30	42.60	50.01	50.30	0.099	428.674	3.585	1.826
	Sivexcy30_12	30	41.90	49.90	50.68	0.101	416.246	3.045	1.551
	Sivexcy30_13	30	41.60	50.03	50.51	0.100	414.971	3.284	1.673
	Sivexcy30_14	30	40.50	50.14	50.75	0.101	399.309	3.210	1.635
	Sivexcy30_15	30	42.00	49.94	50.70	0.101	416.577	3.228	1.644
	Sivexcy30_16	30	41.20	50.07	50.78	0.101	406.298	2.925	1.490
	Sivexcy30_17	30	38.60	50.01	50.26	0.099	389.041	2.520	1.283
	Sivexcy30_18	30	38.40	50.24	50.33	0.100	384.183	2.170	1.105
	Sivexcy30_19	30	38.20	50.14	50.72	0.101	377.078	2.274	1.158
	Sivexcy30_20	30	37.10	50.46	50.69	0.102	364.328	2.233	1.137
	Sivexcy30_21	30	36.90	50.19	50.62	0.101	365.321	2.076	1.057
	Sivexcy30_22	30	37.40	50.17	50.74	0.101	368.669	2.263	1.153
Average			41.67	50.12	50.67	0.101	412.275	3.140	1.599
Standard deviation							24.238		0.327
Max. value			48.80	50.46	50.94	0.102	481.904	4.300	2.190
Min. value			36.90	49.90	50.26	0.099	364.328	2.076	1.057
Max. Min. difference			11.900	0.560	0.680	0.003	117.576	2.224	1.133

navn på filter		ppi	g	mm	mm	dm3	kg/m3	kN	Mpa	
produsent	sys navn		Weight	Height	Diameter		density	max force	Crushing strength	
sivex65	sivexcy65_1		47.3	50.41	47.90	0.091	520.695	3.983	2.029	
	sivexcy65_2		49.5	50.33	50.31	0.100	494.743	3.985	2.030	
	sivexcy65_3		48.1	50.40	50.43	0.101	477.801	3.983	2.029	
	sivexcy65_4		48.9	50.51	49.15	0.096	510.264	5.160	2.628	
	sivexcy65_5		50.0	50.36	49.80	0.098	509.725	4.219	2.149	
	sivexcy65_6		51.6	50.67	50.76	0.103	503.229	5.772	2.940	
	sivexcy65_7		48.5	50.94	47.87	0.092	529.013	4.544	2.314	
	sivexcy65_8		51.8	50.66	50.77	0.103	505.080	5.965	3.038	
	sivexcy65_9		55.0	51.06	50.73	0.103	532.920	5.264	2.681	
	sivexcy65_10		47.9	50.86	50.69	0.103	466.686	4.487	2.285	
	sivexcy65_11		51.2	50.62	50.83	0.103	498.446	6.734	3.430	
	sivexcy65_12		47.6	50.87	49.66	0.099	483.105	4.228	2.153	
	sivexcy65_13		49.4	50.61	49.90	0.099	499.114	3.801	1.936	
	sivexcy65_14		49.3	50.44	50.80	0.102	482.230	3.890	1.981	
	sivexcy65_15		47.9	50.81	50.01	0.100	479.935	2.755	1.403	
	sivexcy65_16		48.0	50.56	50.48	0.101	474.357	3.883	1.978	
	sivexcy65_17		47.3	50.57	50.56	0.102	465.869	3.288	1.675	
	sivexcy65_18		47.8	49.37	50.61	0.099	481.285	2.562	1.305	
	sivexcy65_19		44.9	50.56	48.71	0.094	476.555	2.188	1.114	
	sivexcy65_20		45.7	51.01	50.80	0.103	442.022	2.693	1.372	
	sivexcy65_21		43.4	50.88	49.33	0.097	446.304	2.918	1.486	
	sivexcy65_22		43.6	51.02	47.68	0.091	478.612	2.463	1.254	
Average			48.4	50.6	49.9	#DIV/0!	0.1	489.0	4.0	2.1
standard deviation							23.345		0.602	
Max. value			55.0	51.1	50.8	0.0	0.1	532.9	6.7	3.4
Min. value			43.4	49.4	47.7	0.0	0.1	442.0	2.2	1.1
Max. Min. Difference			11.6	1.69	3.15		0.01	90.899	4.546	2.315

navn på filter			g	mm	mm		dm3	kg/m3	kN	Mpa
produsent	sys navn	ppi	Weight	Height	Diameter		volume	density	max force	Crushing strength
sivex	sivexcy80_1	80	50.30	49.43	48.61		0.092	548.323	2.546	1.297
sylander	sivexcy80_2	80	51.30	49.58	48.26		0.091	565.648	2.263	1.153
	sivexcy80_3	80	50.70	49.59	48.71		0.092	548.640	1.322	0.673
	sivexcy80_4	80	50.90	49.35	48.30		0.090	562.920	3.018	1.537
	sivexcy80_5	80	41.50	49.69	47.48		0.088	471.702	2.087	1.063
	sivexcy80_6	80	49.30	49.76	48.95		0.094	526.467	2.414	1.229
	sivexcy80_7	80	49.00	49.35	47.71		0.088	555.393	2.441	1.243
	sivexcy80_8	80	42.30	49.56	47.45		0.088	482.666	2.363	1.203
	sivexcy80_9	80	44.40	49.75	47.67		0.089	500.046	2.469	1.257
	sivexcy80_10	80	43.70	49.49	47.31		0.087	502.306	2.076	1.057
	sivexcy80_11	80	45.30	49.66	47.80		0.089	508.330	1.509	0.769
	sivexcy80_12	80	45.00	49.54	47.90		0.089	504.076	2.452	1.249
	sivexcy80_13	80	46.40	49.69	47.60		0.088	524.741	2.834	1.443
	sivexcy80_14	80	48.70	49.71	48.81		0.093	523.574	2.451	1.248
	sivexcy80_15	80	47.60	49.38	48.19		0.090	528.509	1.135	0.578
	sivexcy80_16	80	43.30	49.62	48.12		0.090	479.833	1.888	0.962
	sivexcy80_17	80	42.80	49.56	48.05		0.090	476.251	1.322	0.673
	sivexcy80_18	80	41.80	49.44	47.46		0.087	477.917	1.702	0.867
	sivexcy80_19	80	43.30	49.58	47.69		0.089	488.919	1.984	1.010
	sivexcy80_20	80	48.90	49.76	48.65		0.092	528.656	2.643	1.346
	sivexcy80_21	80	43.30	49.80	47.76		0.089	485.333	0.901	0.459
	sivexcy80_22	80	40.50	50.00	47.63		0.089	454.605	1.229	0.626
Average			45.92	49.60	48.01		0.090	511.130	2.048	1.043
standard deviation								31.525		0.296
Max. value			51.30	50.00	48.95		0.094	565.648	3.018	1.537
Min. value			40.50	49.35	47.31		0.087	454.605	0.901	0.459
Max. Min. difference			10.800	0.650	1.640		0.007	111.043	2.117	1.078

Sivex cubic:

navn på filter			g	mm	mm	mm	dm3	kg/m3	kN	MPa
produsent	sys navn	ppi	Weight	Height	lengde	Width	volume	density	max force	Crushing strength
Sivex (kvadrat)	sivexsq30_1	30	49.9	50.26	50.82	48.84	0.125	400.007	4.143	2.110
	sivexsq30_2	30	44.8	50.25	48.96	48.86	0.120	372.689	3.017	1.537
	sivexsq30_3	30	46.0	50.29	49.38	49.49	0.123	374.290	3.211	1.635
	sivexsq30_4	30	44.9	50.31	51.14	49.15	0.126	355.065	2.851	1.452
	sivexsq30_5	30	50.7	50.37	49.24	50.62	0.126	403.827	3.646	1.857
	sivexsq30_6	30	44.6	50.22	48.95	50.32	0.124	360.549	3.210	1.635
	sivexsq30_7	30	44.9	50.23	49.37	48.97	0.121	369.734	3.018	1.537
	sivexsq30_8	30	45.3	50.28	49.02	50.42	0.124	364.525	3.031	1.544
	sivexsq30_9	30	47.5	50.44	50.26	49.04	0.124	382.072	3.772	1.921
	sivexsq30_10	30	48.4	50.41	49.87	50.48	0.127	381.391	3.772	1.921
	sivexsq30_11	30	37.7	50.74	49.20	48.25	0.120	312.989	1.702	0.867
	sivexsq30_12	30	49.2	50.23	49.52	50.02	0.124	395.437	4.340	2.210
	sivexsq30_13	30	38.5	50.82	49.41	49.21	0.124	311.572	1.608	0.819
	sivexsq30_14	30	50.0	50.42	50.57	49.37	0.126	397.361	3.626	1.847
	sivexsq30_15	30	44.9	50.34	49.79	48.87	0.122	366.563	3.959	2.016
	sivexsq30_16	30	47.4	50.34	49.31	49.27	0.122	387.568	3.298	1.680
	sivexsq30_17	30	47.2	50.08	49.16	49.76	0.123	385.288	3.585	1.826
	sivexsq30_18	30	43.0	50.39	50.01	48.66	0.123	350.667	3.181	1.620
	sivexsq30_19	30	42.2	50.30	49.64	49.90	0.125	338.698	2.450	1.248
	sivexsq30_20	30	43.6	50.46	49.31	49.59	0.123	353.354	2.514	1.280
	sivexsq30_21	30	48.3	50.23	50.08	49.02	0.123	391.693	4.007	2.041
	sivexsq30_22	30	51.0	49.93	48.67	49.05	0.119	427.866	4.339	2.210
Average			45.9	50.33	49.62	49.42	0.123	371.964	3.285	1.673
standard deviation								27.525		0.373
Max. value			51.0	50.82	51.14	50.62	0.127	427.866	4.340	2.210
Min. value			37.7	49.93	48.67	48.25	0.119	311.572	1.608	0.819
Max. Min. Difference			13.3	0.89	2.47	2.37	0.008	116.295	2.732	1.391

navn på filter			g	mm	mm	mm	dm3	kg/m3	kN	MPa
produsent	sys navn	ppi	Weight	Height	lengde	Width	volume	density	max force	Crushing strength
	sivexsq65_01		67.6	50.38	50.55	50.69	0.129	523.655	6.873	
	sivexsq65_02		68.7	50.44	50.78	50.60	0.130	530.076	6.413	3.266
	sivexsq65_03		61.7	50.66	50.16	50.93	0.129	476.748	2.895	1.474
	sivexsq65_04		64.9	50.99	50.26	49.74	0.127	509.133	5.017	2.555
	sivexsq65_05		56.7	50.92	50.51	50.42	0.130	437.235	2.947	1.501
	sivexsq65_06		66.2	50.53	50.87	51.03	0.131	504.686	5.492	2.797
	sivexsq65_07		65.9	50.69	50.31	50.86	0.130	508.080	5.191	2.644
	sivexsq65_08		66.3	50.94	50.99	50.66	0.132	503.854	4.673	2.380
	sivexsq65_09		69.1	50.67	50.72	50.96	0.131	527.617	8.344	4.250
	sivexsq65_10		67.0	50.82	50.94	50.55	0.131	511.988	5.198	2.647
	sivexsq65_11		64.1	50.76	50.60	50.76	0.130	491.659	4.358	2.220
	sivexsq65_12		65.9	50.76	49.44	50.94	0.128	515.497	4.782	2.435
	sivexsq65_13		70.0	50.74	50.65	51.04	0.131	533.651	6.901	3.515
	sivexsq65_14		62.5	50.92	50.80	49.85	0.129	484.689	4.030	2.052
	sivexsq65_15		62.8	50.39	51.13	50.86	0.131	479.251	4.829	2.459
	sivexsq65_16		55.7	50.98	50.26	51.14	0.131	425.081	3.323	1.692
	sivexsq65_17		60.0	50.90	51.06	50.97	0.132	452.937	2.755	1.403
	sivexsq65_18		66.9	50.55	50.93	51.02	0.131	509.320	5.094	2.594
	sivexsq65_19		66.3	51.07	50.71	51.20	0.133	500.016	5.553	2.828
	sivexsq65_20		57.7	50.83	50.91	50.28	0.130	443.463	2.562	1.305
	sivexsq65_21		69.0	50.99	50.83	51.24	0.133	519.559	5.785	2.946
	sivexsq65_22		62.8	50.93	50.08	51.35	0.131	479.492	4.164	2.121
Average			64.4	50.77	50.61	50.78	0.130	493.986	4.872	2.433
standard deviation			3.971	0.202	0.389	0.404	0.001	30.348	1.444	0.717
Max. value			70.0	51.07	51.13	51.35	0.133	533.651	8.344	4.250
Min. value			55.7	50.38	49.44	49.74	0.127	425.081	2.562	1.305
Max. Min. Difference			14.3	0.69	1.69	1.61	0.005	108.570	5.782	2.945

navn på filter			g	mm	mm	mm	dm3	kg/m3	kN	MPa
produsent	sys navn	ppi	Weight	Height	lengde	Width	volume	density	max force	Crushing strength
Sivex (kvadrat)	sivexsq80_1		59.0	50.82	49.66	50.72	0.128	460.926	3.959	2.016
nummer forskjøvet	sivexsq80_2	80	55.1	45.85	44.97	46.23	0.095	578.050	3.017	1.537
på kompressjonstest	sivexsq80_3	80	53.2	50.11	49.43	49.75	0.123	431.721	3.917	1.995
	sivexsq80_4	80	54.4	50.02	49.57	50.06	0.124	438.274	4.434	2.258
	sivexsq80_5	80	53.8	50.42	49.51	49.96	0.125	431.384	3.958	2.016
	sivexsq80_6	80	53.7	50.48	49.80	49.47	0.124	431.801	3.585	1.826
	sivexsq80_7	80	55.0	50.34	50.01	49.36	0.124	442.606	3.772	1.921
	sivexsq80_8	80	54.6	50.48	49.58	50.15	0.126	435.007	3.871	1.971
	sivexsq80_9	80	54.3	50.35	50.31	50.03	0.127	428.465	2.954	1.504
	sivexsq80_10	80	52.9	50.62	50.26	49.26	0.125	422.101	3.209	1.634
	sivexsq80_11	80	54.6	50.53	49.81	50.24	0.126	431.795	3.678	1.873
	sivexsq80_12	80	53.2	50.63	49.66	49.65	0.125	426.165	3.520	1.793
true number	sivexsq80_13	80	55.4	50.75	50.56	49.68	0.127	434.595	3.492	1.778
	sivexsq80_14	80	54.3	50.99	49.36	49.75	0.125	433.657	4.130	2.103
	sivexsq80_15	80	55.0	50.74	50.58	49.10	0.126	436.467	2.736	1.393
	sivexsq80_16	80	54.0	50.54	50.97	49.75	0.128	421.358	1.873	0.954
	sivexsq80_17	80	55.6	51.00	50.56	49.80	0.128	432.980	3.398	1.731
	sivexsq80_18	80	53.9	50.90	50.44	49.67	0.128	422.670	3.300	1.681
	sivexsq80_19	80	52.8	50.42	50.24	49.66	0.126	419.735	1.635	0.833
	sivexsq80_20	80	55.9	50.40	49.92	49.49	0.125	448.941	4.692	2.390
	sivexsq80_21	80	57.9	50.50	49.56	49.86	0.125	463.985	4.102	2.089
	sivexsq80_22	80	56.7	50.90	49.06	50.65	0.126	448.289	4.050	2.063
Average			54.8	50.35	49.72	49.65	0.124	441.862	3.513	1.789
standard deviation								31.830		0.369
Max. value			59.0	51.00	50.97	50.72	0.128	578.050	4.692	2.390
Min. value			52.8	45.85	44.97	46.23	0.095	419.735	1.635	0.833
Max. Min. Difference			6.2	5.15	6.00	4.49	0.033	158.316	3.057	1.557

Sivex NP:

navn på filter producent	sys navn	ppi	g Weight	mm Height	mm Lengde	mm Width	dm3 volume	kg/m3 density	kN max force	MPa Crushing strength
	SivexNP30_01	30	39.5	50.29		51.15	0.103	382.238	3.699	1.884
	SivexNP30_02	30	41.2	51.25		51.07	0.105	392.448	4.073	2.074
	SivexNP30_03	30	41.9	50.37		50.85	0.102	409.61	4.263	2.171
	SivexNP30_04	30	41.7	50.5		50.84	0.103	406.765	4.034	2.054
	SivexNP30_05	30	36.9	50.56		50.92	0.103	358.387	3.229	1.645
	SivexNP30_06	30	42.2	50.58		50.83	0.103	411.153	4.872	2.481
	SivexNP30_07	30	38.7	50.57		50.87	0.103	376.534	3.855	1.963
	SivexNP30_08	30	40.3	50.35		50.84	0.102	394.28	3.883	1.978
	SivexNP30_09	30	39.9	50.72		50.9	0.103	386.606	4.07	2.073
	SivexNP30_10	30	40.4	50.47		50.89	0.103	393.544	4.269	2.174
	SivexNP30_11	30	40.6	50.63		50.86	0.103	394.708	3.883	1.978
	SivexNP30_12	30	40.6	50.77		50.87	0.103	393.464	4.451	2.267
	SivexNP30_13	30	40.2	50.42		50.89	0.103	391.984	3.883	1.978
	SivexNP30_14	30	40.1	50.37		50.86	0.102	391.859	3.985	2.03
	SivexNP30_15	30	40.5	50.52		50.74	0.102	396.461	4.264	2.172
	SivexNP30_16	30	41.6	50.43		50.86	0.102	406.033	4.545	2.315
	SivexNP30_17	30	38.8	50.51		50.75	0.102	379.745	4.358	2.22
	SivexNP30_18	30	40.3	50.62		50.8	0.103	392.795	4.36	2.221
	SivexNP30_19	30	40.4	50.67		50.82	0.103	393.071	3.883	1.978
	SivexNP30_20	30	39.3	50.51		50.75	0.102	384.639	3.859	1.965
	SivexNP30_21	30	40.8	50.87		50.85	0.103	394.936	4.451	2.267
	SivexNP30_22	30	39.9	50.45		50.82	0.102	389.899	4.07	2.073
Average			40.3	50.57		50.87	0.103	391.871	4.102	2.089
standard deviation								11.36442		0.171712048
Max. value			42.2	51.25		51.15	0.105	411.153	4.872	2.481
Min. value			36.9	50.29		50.74	0.102	358.387	3.229	1.645
Max. Min. Difference			5.3	0.96		0.41	0.003	52.766	1.643	0.837

Drache:

navn på filter producent	sys navn	ppi	g Weight	mm Height	mm Lengde	mm Width	dm3 volume	kg/m3 density	kN max force	MPa Crushing strength
	drachecy30_01	30	39.4	48.76		50.92	0.099	396.795	2.755	1.403
	drachecy30_02	30	39.8	48.60		50.45	0.097	409.670	2.755	1.403
	drachecy30_03	30	41.0	48.71		50.91	0.099	413.494	2.754	1.403
	drachecy30_04	30	41.6	48.82		50.86	0.099	419.424	2.948	1.501
	drachecy30_05	30	42.7	48.67		50.98	0.099	429.810	3.129	1.594
	drachecy30_06	30	42.1	48.63		50.91	0.099	425.287	3.230	1.645
	drachecy30_07	30	40.5	48.69		50.79	0.099	410.553	2.988	1.522
	drachecy30_08	30	39.6	48.67		50.76	0.098	402.069	2.474	1.260
	drachecy30_09	30	42.6	48.48		50.73	0.098	434.738	3.149	1.604
	drachecy30_10	30	43.1	48.70		50.58	0.098	440.454	3.362	1.712
	drachecy30_11	30	42.1	48.76		50.66	0.098	428.349	3.515	1.790
	drachecy30_12	30	42.4	48.65		50.63	0.098	432.890	3.269	1.665
	drachecy30_13	30	42.9	48.75		51.04	0.100	430.102	2.562	1.305
	drachecy30_14	30	42.9	48.56		50.74	0.098	436.906	2.233	1.137
	drachecy30_15	30	40.5	48.58		50.87	0.099	410.189	2.190	1.115
	drachecy30_16	30	38.3	48.70		50.44	0.097	393.577	2.771	1.411
	drachecy30_17	30	37.7	48.81		50.73	0.099	382.132	2.647	1.348
	drachecy30_18	30	38.2	48.86		50.67	0.099	387.720	2.764	1.408
	drachecy30_19	30	39.2	48.66		50.85	0.099	396.682	2.755	1.403
	drachecy30_20	30	40.1	48.77		50.86	0.099	404.715	2.176	1.108
	drachecy30_21	30	41.3	48.65		50.86	0.099	417.854	2.490	1.268
	drachecy30_22	30	42.5	48.76		50.81	0.099	429.870	2.755	1.403
Average			40.9	48.69		50.78	0.099	415.149	2.803	1.428
standard deviation								16.671		0.185
Max. value			43.1	48.86		51.04	0.100	440.454	3.515	1.790
Min. value			37.7	48.48		50.44	0.097	382.132	2.176	1.108
Max. Min. Difference			5.4	0.38		0.60	0.003	58.323	1.339	0.682

navn på filter			g	mm	mm	mm	dm3	kg/m3	kN	MPa	
producent	sys navn	ppi	Weight	Height	Lengde	Width	volume	density	max force	Crushing strength	
	Drachecy60_01	60	37.4	47.97	-		48.19	0.087	427.463	2.129	1.084
	Drachecy60_02	60	38.1	48.05	-		47.57	0.085	446.144	2.375	1.210
	Drachecy60_03	60	38.4	47.81	-		48.40	0.088	436.548	2.475	1.261
	Drachecy60_04	60	39.3	48.05	-		47.90	0.087	453.877	2.282	1.162
	Drachecy60_05	60	40.9	47.90	-		48.07	0.087	470.489	2.656	1.353
	Drachecy60_06	60	39.6	47.82	-		47.40	0.084	469.288	2.607	1.328
	Drachecy60_07	60	40.6	47.79	-		48.14	0.087	466.753	2.755	1.403
	Drachecy60_08	60	40.8	47.98	-		47.50	0.085	479.869	2.755	1.403
	Drachecy60_09	60	39.7	48.05	-		47.03	0.083	475.617	2.188	1.114
	Drachecy60_10	60	40.8	48.05	-		48.30	0.088	463.428	2.562	1.305
	Drachecy60_11	60	41.7	47.89	-		48.42	0.088	472.881	2.581	1.314
	Drachecy60_12	60	39.7	47.88	-		48.76	0.089	444.037	2.988	1.522
	Drachecy60_13	60	41.1	47.90	-		48.53	0.089	463.870	3.276	1.668
	Drachecy60_14	60	41.8	47.88	-		47.86	0.086	485.274	3.036	1.546
	Drachecy60_15	60	40.5	47.99	-		47.17	0.084	482.928	2.562	1.305
	Drachecy60_16	60	42.8	48.18	-		48.88	0.090	473.396	1.847	0.941
	Drachecy60_17	60	39.6	48.44	-		49.84	0.095	419.030	2.234	1.138
	Drachecy60_18	60	45.5	48.00	-		50.65	0.097	470.459	2.562	1.305
	Drachecy60_19	60	46.0	47.96	-		50.64	0.097	476.213	3.352	1.707
	Drachecy60_20	60	44.0	47.90	-		50.37	0.095	460.981	3.509	1.787
	Drachecy60_21	60	42.2	47.90	-		50.09	0.094	447.080	3.324	1.693
	Drachecy60_22	60	40.9	48.03	-		49.43	0.092	443.751	2.734	1.392
Average			41.0	47.97			48.60	0.089	460.426	2.672	1.361
standard deviation											0.215
Max. value			46.0	48.44			50.65	0.097	485.274	3.509	1.787
Min. value			37.4	47.79			47.03	0.083	419.030	1.847	0.941
Max. Min. Difference			8.6	0.65			3.62	0.013	66.244	1.662	0.846

Lanik:

navn på filter			g	g	mm	mm	mm	dm3	kg/m3	kN	MPa	
producent	sys navn	ppi	Weight	weight dry	Height	Lengde	Width	volume	density	max force	Crushing strengt	
	lanikcy30_01	30	36.6	36.9	47.68			50.80	0.097	378.728	2.170	1.105
	lanikcy30_02	30	37.8	37.7	47.81			50.30	0.095	397.876	2.486	1.266
	lanikcy30_03	30	38.5	38.3	47.69			50.26	0.095	406.910	2.985	1.520
	lanikcy30_04	30	38.7	38.5	47.63			50.04	0.094	413.148	3.185	1.622
	lanikcy30_05	30	39.1	39.0	47.80			50.82	0.097	403.264	3.044	1.550
	lanikcy30_06	30	38.3	38.3	47.69			50.59	0.096	399.533	2.739	1.395
	lanikcy30_07	30	38.3	37.4	47.61			50.34	0.095	404.189	2.631	1.340
	lanikcy30_08	30	39.9	38.6	47.64			50.50	0.095	418.147	2.189	1.115
	lanikcy30_09	30	38.1	37.5	47.84			50.70	0.097	394.483	2.461	1.253
	lanikcy30_10	30	38.3	37.5	47.86			50.62	0.096	397.642	2.099	1.069
	lanikcy30_11	30	38.8	38.8	47.85			50.26	0.095	408.710	2.315	1.179
	lanikcy30_12	30	37.3	36.6	47.99			50.77	0.097	383.932	2.320	1.182
	lanikcy30_13	30	38.7	38.2	48.01			50.43	0.096	403.563	2.188	1.114
	lanikcy30_14	30	41.6	39.4	47.61			50.77	0.096	431.609	2.651	1.350
	lanikcy30_15	30	38.2	38.0	47.70			50.69	0.096	396.836	2.609	1.329
	lanikcy30_16	30	39.5	38.9	47.64			50.44	0.095	414.940	2.803	1.428
	lanikcy30_17	30	39.7	37.6	47.61			50.31	0.095	419.463	2.562	1.305
	lanikcy30_18	30	38.3	38.2	47.61			50.79	0.096	397.058	2.849	1.451
	lanikcy30_19	30	38.3	38.0	47.70			50.70	0.096	397.717	2.849	1.451
	lanikcy30_20	30	39.8	39.4	47.68			50.72	0.096	413.141	2.655	1.352
	lanikcy30_21	30	39.4	39.0	47.59			50.75	0.096	409.278	2.850	1.451
	lanikcy30_22	30	38.7	38.2	47.88			50.80	0.097	398.786	2.946	1.500
Average			38.7	38.2	47.73			50.56	0.096	404.043	2.618	1.333
standard deviation										11.567		0.154
Max. value			41.6	39.4	48.01			50.82	0.097	431.609	3.185	1.622
Min. value			36.6	36.6	47.59			50.04	0.094	378.728	2.099	1.069
Max. Min. Difference			5.0	2.8	0.42			0.78	0.003	52.881	1.086	0.553

navn på filter			g	g	mm	mm	mm	dm3	kg/m3	kN	MPa	
produsent	sys navn	ppi	Weight	weight dry	Height	Lengde	Width	volume	density	max force	Crushing strengt	
	lanikcy60_01	60	28.7	28.3	47.37			41.46	0.064	448.776	0.394	0.201
	lanikcy60_02	60	30.1	29.9	47.33			43.49	0.070	428.116	0.492	0.251
	lanikcy60_03	60	31.3	29.7	47.02			42.44	0.067	470.567	0.562	0.286
	lanikcy60_04	60	27.0	27.0	47.02			40.00	0.059	456.953	0.669	0.341
wet	lanikcy60_05	60	32.3	29.4	46.88			43.66	0.070	460.212	0.671	0.342
wet	lanikcy60_06	60	29.2	27.9	47.72			42.09	0.066	439.779	0.305	0.155
wet	lanikcy60_07	60	32.2	32.1	47.65			43.37	0.070	457.430	0.650	0.331
wet	lanikcy60_08	60	34.5	34.0	47.66			46.64	0.081	423.700	0.492	0.251
wet	lanikcy60_09	60	31.8	31.7	47.32			44.50	0.074	432.088	0.640	0.326
wet	lanikcy60_10	60	32.7	32.4	47.14			45.46	0.077	427.375	0.362	0.184
	lanikcy60_11	60	27.2	27.1	47.06			44.48	0.073	371.961	0.658	0.335
	lanikcy60_12	60	28.3	28.2	46.99			43.34	0.069	408.238	0.634	0.323
	lanikcy60_13	60	26.5	26.2	46.83			41.12	0.062	426.114	0.493	0.251
	lanikcy60_14	60	26.4	26.2	46.79			43.27	0.069	383.696	0.492	0.251
	lanikcy60_15	60	28.8	28.7	47.05			42.67	0.067	428.053	0.665	0.339
	lanikcy60_16	60	27.0	26.9	46.82			43.16	0.068	394.166	0.535	0.272
	lanikcy60_17	60	26.9	26.7	46.87			43.87	0.071	379.693	0.319	0.162
	lanikcy60_18	60	28.9	28.7	46.93			41.33	0.063	459.015	0.492	0.251
	lanikcy60_19	60	27.8	27.6	47.26			44.23	0.073	382.849	0.656	0.334
	lanikcy60_20	60	28.4	28.3	47.36			43.33	0.070	406.667	0.493	0.251
	lanikcy60_21	60	26.1	26.0	46.82			42.37	0.066	395.369	0.389	0.198
	lanikcy60_22	60	28.9	28.7	47.11			42.58	0.067	430.808	0.492	0.251
Average			29.1		47.14	#DIV/0!		43.13	0.069	423.256	0.525	0.267
standard deviation												0.059
Max. value			34.5		47.72	0.00	46.64	0.081	470.567	0.671	0.342	
Min. value			26.1		46.79	0.00	40.00	0.059	371.961	0.305	0.155	
Max. Min. Difference			8.4		0.93	0.00	6.64	0.022	98.605	0.366	0.186	

Selee:

navn på filter			g	mm	mm	mm	dm3	kg/m3	kN	MPa	
produsent	sys navn	ppi	Weight	Height	Lengde	Width	volume	density	max force	Crushing strength	
	seleecy30_01	30	30	32.3	50.34		50.26	0.100	323.411	1.902	0.969
	seleecy30_02	30	30	34.5	50.24		50.90	0.102	337.477	2.426	1.236
	seleecy30_03	30	30	32.3	50.23		50.82	0.102	317.015	2.391	1.218
	seleecy30_04	30	30	31.6	50.17		50.78	0.102	311.005	2.284	1.163
	seleecy30_05	30	30	30.6	50.07		50.47	0.100	305.483	2.095	1.067
	seleecy30_06	30	30	31.8	50.20		50.76	0.102	313.033	2.321	1.182
	seleecy30_07	30	30	33.2	50.58		50.81	0.103	323.721	2.095	1.067
	seleecy30_08	30	30	33.7	49.82		50.37	0.099	339.463	2.235	1.138
	seleecy30_09	30	30	31.1	49.98		50.62	0.101	309.193	2.282	1.162
	seleecy30_10	30	30	32.0	50.22		50.76	0.102	314.876	1.774	0.903
	seleecy30_11	30	30	33.7	50.15		50.79	0.102	331.675	2.352	1.198
	seleecy30_12	30	30	34.0	50.10		50.92	0.102	333.253	2.930	1.492
	seleecy30_13	30	30	34.1	50.39		50.91	0.103	332.441	2.388	1.216
	seleecy30_14	30	30	34.7	50.48		50.79	0.102	339.284	2.562	1.305
	seleecy30_15	30	30	31.7	50.04		50.82	0.102	312.308	2.295	1.169
	seleecy30_16	30	30	33.5	50.14		50.93	0.102	327.962	2.471	1.258
	seleecy30_17	30	30	33.7	50.34		50.83	0.102	329.903	2.522	1.284
	seleecy30_18	30	30	33.4	50.22		50.92	0.102	326.590	2.001	1.019
	seleecy30_19	30	30	34.5	49.93		50.85	0.101	340.240	2.948	1.501
	seleecy30_20	30	30	32.5	50.26		50.85	0.102	318.412	2.281	1.162
	seleecy30_21	30	30	35.4	50.23		50.82	0.102	347.441	2.682	1.366
	seleecy30_22	30	30	33.8	50.25		50.74	0.102	332.652	2.378	1.211
Average				33.1	50.20		50.76	0.102	325.765	2.346	1.195
standard deviation									11.478	0.279	0.142
Max. value				35.4	50.58		50.93	0.103	347.441	2.948	1.501
Min. value				30.6	49.82		50.26	0.099	305.483	1.774	0.903
Max. Min. Difference				4.8	0.76		0.67	0.003	41.958	1.174	0.598

C Raw data from working temperatures compressive tests

Sivex:

navn på filter		g	g	mm	mm	mm	dm3	kg/m3	kN	MPa	
producent	sys navn	ppi	weight wet	weight dry	height	Lengde	Width	volumee	density	max force	Crushing strength
	sivex30_30	30		41.4	50.36		50.65	0.101	408.005	3.365	1.714
	sivex30_31			41.9	50.33		50.55	0.101	414.815	3.160	1.609
	sivex30_32			43.7	50.36		50.72	0.102	429.484	3.124	1.591
	sivex30_33		41.6	41.5	50.01		50.76	0.101	410.070	3.365	1.714
	sivex30_34		41.6	41.6	49.81		50.72	0.101	413.360	3.141	1.600
	sivex30_35		41.8	41.5	49.94		50.80	0.101	409.998	2.948	1.501
	sivex30_36		41.4	41.4	49.86		50.73	0.101	410.798	3.131	1.595
	sivex30_37		41.9	41.8	49.83		50.34	0.099	421.472	3.230	1.645
	sivex30_38		43.8	43.7	50.09		50.81	0.102	430.271	3.192	1.626
	sivex30_39		41.7	41.6	50.10		50.78	0.101	409.997	3.311	1.686
Average			42.0	42.0	50.07	#DIV/0!	50.69	0.101	415.827	3.197	1.628
standard deviation									7.885		0.062
Max. value			43.8	43.7	50.36	0.00	50.81	0.102	430.271	3.365	1.714
Min. value			41.4	41.4	49.81	0.00	50.34	0.099	408.005	2.948	1.501
Max. Min. Difference			2.4	2.3	0.55	0.00	0.47	0.003	22.266	0.417	0.212
	Sivex30_40	30	39.0	39.0	50.07		50.79	0.101	384.451	2.951	1.503
	sivex30_41		37.4	37.3	50.26		50.65	0.101	369.318	2.561	1.304
	Sivex30_42		37.8	37.5	49.96		50.82	0.101	373.001	2.562	1.305
	Sivex30_43		37.7	37.6	49.95		50.89	0.102	371.066	2.467	1.256
	Sivex30_44		37.9	37.8	50.10		50.57	0.101	376.639	2.584	1.316
	Sivex30_45		38.1	38.1	49.76		50.91	0.101	376.139	2.375	1.210
	Sivex30_46		36.6	36.6	49.94		50.99	0.102	358.899	2.375	1.210
	Sivex30_47		40.1	39.9	50.25		50.83	0.102	393.259	2.938	1.496
	Sivex30_48		42.4	42.2	50.08		51.03	0.102	413.962	3.129	1.594
	Sivex30_49		41.7	41.6	50.21		50.93	0.102	407.670	2.964	1.510
Average			38.9	38.8	50.06	#DIV/0!	50.84	0.102	382.440	2.691	1.370
standard deviation			1.826	1.798	0.151	#DIV/0!	0.136	0.001	16.642	0.263	0.134
Max. value			42.4	42.2	50.26	0.00	51.03	0.102	413.962	3.129	1.594
Min. value			36.6	36.6	49.76	0.00	50.57	0.101	358.899	2.375	1.210
Max. Min. Difference			5.8	5.6	0.50	0.00	0.46	0.002	55.063	0.754	0.384
	sivex30_50		41.3	41.2	50.00		51.01	0.102	404.184	2.730	1.390
	sivex30_51		41.1	40.8	50.12		50.98	0.102	401.736	2.850	1.451
	sivex30_52		40.5	40.1	50.30		51.00	0.103	394.146	2.562	1.305
	sivex30_53		38.2	38.1	49.95		50.75	0.101	378.064	2.562	1.305
	sivex30_54		35.6	35.5	50.08		50.65	0.101	352.807	2.233	1.137
	sivex30_55		39.9	39.5	50.26		50.96	0.103	389.226	3.129	1.594
	sivex30_56		42.9	42.4	50.13		50.97	0.102	419.412	3.322	1.692
	sivex30_57		42.6	42.6	50.18		50.93	0.102	416.717	3.162	1.610
	sivex30_58		43.3	43.3	50.22		50.75	0.102	426.235	2.948	1.501
	sivex30_59		43.7	43.5	50.16		50.72	0.101	431.197	2.849	1.451
Average			40.9		50.14	#DIV/0!	50.87	0.102	401.372	2.835	1.444
standard deviation			2.392	2.387	0.104	#DIV/0!	0.130	0.001	22.756	0.311	0.158
Max. value			43.7		50.30	0.00	51.01	0.103	431.197	3.322	1.692
Min. value			35.6		49.95	0.00	50.65	0.101	352.807	2.233	1.137
Max. Min. Difference			8.1		0.35	0.00	0.36	0.002	78.390	1.089	0.555

SivexNP:

navn på filter produsent	sys navn	ppi	g Weight	mm Height	mm Lengde	mm Width	dm3 volume	kg/m3 density	kN max force	MPa Crushing strength
SivexNP30hot_10m_30	SivexNP30_30	30	38.6	50.58		50.77	0.1024	376.968	3.138	1.601
SivexNP30hot_10m_31	SivexNP30_31	30	37.8	50.55		50.7	0.1021	370.395	3.129	1.596
SivexNP30hot_10m_32	SivexNP30_32	30	39.3	50.18		50.75	0.1015	387.168	2.964	1.512
SivexNP30hot_10m_33	SivexNP30_33	30	35.1	50.45		50.82	0.1023	342.994	2.608	1.331
SivexNP30hot_10m_34	SivexNP30_34	30	36.7	50.51		50.79	0.1023	358.627	2.755	1.406
SivexNP30hot_10m_35	SivexNP30_35	30	37.7	50.37		50.58	0.1012	372.436	2.583	1.318
SivexNP30hot_10m_36	SivexNP30_36	30	37.6	50.48		50.82	0.1024	367.206	2.656	1.355
SivexNP30hot_10m_37	SivexNP30_37	30	36.3	50.77		50.81	0.1029	352.623	2.56	1.306
SivexNP30hot_10m_38	SivexNP30_38	30	36.1	50.95		50.23	0.1010	357.558	2.188	1.116
SivexNP30hot_10m_39	SivexNP30_39	30	35	50.28		50.7	0.1015	344.800	2.095	1.069
Average			37.02	50.512	#DIV/0!	50.697	0.102	363.083	2.668	1.361
standard deviation								13.526		0.170
Max. value			39.3	50.95	0	50.82	0.1029	387.168	3.138	1.601
Min. value			35	50.18	0	50.23	0.101	342.994	2.095	1.069
Max. Min. Difference			4.3	0.77	0	0.59	0.002	44.174	1.043	0.532
SivexNP30hot_1h_40	SivexNP30_40	30	39.4	50.6		50.85	0.103	383.419	3.271	1.666
SivexNP30hot_1h_41	SivexNP30_41	30	39.2	50.48		50.86	0.103	382.229	2.65	1.35
SivexNP30hot_1h_42	SivexNP30_42	30	39.5	50.54		50.91	0.103	383.942	2.282	1.162
SivexNP30hot_1h_43	SivexNP30_43	30	38.3	50.41		50.83	0.102	374.414	2.656	1.353
SivexNP30hot_1h_44	SivexNP30_44	30	39.6	50.75		50.88	0.103	383.774	2.562	1.305
SivexNP30hot_1h_45	SivexNP30_45	30	41.6	50.46		50.83	0.102	406.271	2.849	1.451
SivexNP30hot_1h_46	SivexNP30_46	30	41.3	50.51		50.90	0.103	401.835	3.322	1.692
SivexNP30hot_1h_47	SivexNP30_47	30	41.6	50.38		50.80	0.102	407.397	3.405	1.734
SivexNP30hot_1h_48	SivexNP30_48	30	41	50.53		50.83	0.103	399.383	2.755	1.403
SivexNP30hot_1h_49	SivexNP30_49	30	40.5	50.74		50.88	0.103	392.573	3.129	1.594
Average			40.2	50.546	#DIV/0!	50.857	0.1027	391.524	2.8881	1.471
standard deviation								10.959		0.181
Max. value			41.6	50.75	0	50.91	0.103	407.397	3.405	1.734
Min. value			38.3	50.38	0	50.8	0.102	374.414	2.282	1.162
Max. Min. Difference			3.3	0.37	0	0.11	0.001	32.983	1.123	0.572
SivexNP30hot_2h_50	SivexNP30_50	30	40.0	50.57		50.65	0.1019	392.571	2.948	1.504
SivexNP30hot_2h_51	SivexNP30_51	30	39.5	50.62		50.67	0.1021	386.975	2.947	1.504
SivexNP30hot_2h_52	SivexNP30_52	30	40.6	50.64		50.76	0.1025	396.186	2.582	1.317
SivexNP30hot_2h_53	SivexNP30_53	30	39.5	50.80		50.64	0.1023	386.061	1.968	1.004
SivexNP30hot_2h_54	SivexNP30_54	30	40.5	50.72		50.67	0.1023	395.990	2.914	1.487
SivexNP30hot_2h_55	SivexNP30_55	30	39.7	50.60		50.65	0.1020	389.396	2.755	1.406
SivexNP30hot_2h_56	SivexNP30_56	30	40.4	50.62		50.81	0.1026	393.614	2.475	1.263
SivexNP30hot_2h_57	SivexNP30_57	30	40.0	50.63		50.75	0.1024	390.562	2.379	1.214
SivexNP30hot_2h_58	SivexNP30_58	30	39.9	50.87		50.67	0.1026	388.973	2.125	1.084
SivexNP30hot_2h_59	SivexNP30_59	30	40.2	50.67		50.84	0.1029	390.818	2.282	1.164
Average			40.03	50.674	#DIV/0!	50.711	0.102	391.115	2.538	1.295
standard deviation								3.293	0.334	0.170
Max. value			40.6	50.87	0	50.84	0.103	396.186	2.948	1.504
Min. value			39.5	50.57	0	50.64	0.102	386.061	1.968	1.004
Max. Min. Difference			1.1	0.3	0	0.2	0.001	10.125	0.980	0.500

Drache:

navn på filter		g	mm	mm	mm	dm3	kg/m3	kN	MPa		
produsent	sys navn	Weight	Height	Lengde	Width	volume	density	max force	Crushing strength		
Drachehot30_10min_01	drachecy30_3	11	41.4	48.74		50.72	0.098	354.398	2.849	1.451	
Drachehot30_10min_02	drachecy30_3	12	40.7	48.85		50.72	0.099	357.653	2.763	1.407	
Drachehot30_10min_03	drachecy30_3	13	41.3	48.69		50.87	0.099	385.010	2.948	1.501	
Drachehot30_10min_04	drachecy30_3	14	41.4	48.86		50.55	0.098	358.969	2.374	1.209	
Drachehot30_10min_05	drachecy30_3	15	39.0	48.89		50.79	0.099	388.682	2.531	1.289	
Drachehot30_10min_06	drachecy30_3	16	42.0	48.62		50.59	0.098	388.821	2.752	1.402	
Drachehot30_10min_07	drachecy30_3	17	40.6	48.68		50.78	0.099	392.541	2.562	1.305	
Drachehot30_10min_08	drachecy30_3	18	35.3	49.08		50.44	0.098	408.884	1.725	0.879	
Drachehot30_10min_09	drachecy30_3	19	37.3	48.99		50.92	0.100	397.939	2.021	1.029	
Drachehot30_10min_10	drachecy30_3	20	38.9	48.95		50.88	0.100	402.910	2.337	1.190	
Average		39.8	48.8	#DIV/0!		50.7	0.1	383.581	2.486	1.266	
standard deviation								18.669	0.365	0.186	
Max. value			42.0	49.1	0.0	50.9	0.1	408.884	2.948	1.501	
Min. value			35.3	48.6	0.0	50.4	0.1	354.398	1.725	0.879	
Max. Min. Difference			6.7	0.46	0.00	0.48	0.002	54.485	1.223	0.623	
Drachehot30_1h_30	drachecy30_40		43.0	48.66		50.84	0.099	435.307	2.188	1.114	
Drachehot30_1h_31	drachecy30_41		42.8	48.67		50.83	0.099	433.363	2.547	1.297	
Drachehot30_1h_32	drachecy30_42		43.2	48.65		50.64	0.098	440.883	3.065	1.561	
Drachehot30_1h_33	drachecy30_43		42.8	48.58		50.70	0.098	436.396	2.754	1.403	
Drachehot30_1h_34	drachecy30_44		42.4	48.70		50.88	0.099	428.206	2.562	1.305	
Drachehot30_1h_35	drachecy30_45		41.4	48.66		50.62	0.098	422.760	1.903	0.969	
Drachehot30_1h_36	drachecy30_46		40.5	48.61		50.86	0.099	410.097	2.307	1.175	
Drachehot30_1h_37	drachecy30_47		40.4	48.64		50.83	0.099	409.315	2.362	1.203	
Drachehot30_1h_38	drachecy30_48		41.4	48.58		50.83	0.099	419.965	2.687	1.368	
Drachehot30_1h_39	drachecy30_49		39.1	48.78		50.75	0.099	396.253	2.562	1.305	
Average			41.7	48.7	#DIV/0!		50.8	0.1	423.255	2.494	1.270
standard deviation								13.649	0.306	0.156	
Max. value			43.2	48.8	0.0	50.9	0.1	440.883	3.065	1.561	
Min. value			39.1	48.6	0.0	50.6	0.1	396.253	1.903	0.969	
Max. Min. Difference			4.1	0.20	0.00	0.26	0.001	44.630	1.162	0.592	
Drachehot30_2h_1	drachecy30_5	1	34.9	48.97		50.64	0.099	419.752	1.932	0.984	
Drachehot30_2h_2	drachecy30_5	2	35.3	48.97		50.84	0.099	409.415	2.188	1.114	
Drachehot30_2h_3	drachecy30_5	3	38.1	48.80		50.76	0.099	418.213	2.096	1.067	
Drachehot30_2h_4	drachecy30_5	4	35.2	49.06		50.84	0.100	415.692	1.720	0.876	
Drachehot30_2h_5	drachecy30_5	5	38.5	48.63		50.69	0.098	397.398	1.998	1.018	
Drachehot30_2h_6	drachecy30_5	6	38.0	48.67		50.57	0.098	429.647	2.001	1.019	
Drachehot30_10m_01	drachecy30_5	7	38.7	48.77		50.48	0.098	415.953	2.353	1.198	
Drachehot30_10m_02	drachecy30_5	8	40.1	48.68		50.67	0.098	359.611	2.719	1.385	
Drachehot30_10m_03	drachecy30_5	9	39.7	48.73		50.56	0.098	381.249	2.721	1.386	
Drachehot30_10m_04	drachecy30_5	10	40.1	48.61		50.91	0.099	393.123	2.479	1.263	
Average			37.9	48.8	#DIV/0!		50.7	0.1	404.005	2.221	1.131
standard deviation								20.166	0.321	0.164	
Max. value			40.1	49.1	0.0	50.9	0.1	429.647	2.721	1.386	
Min. value			35.3	48.6	0.0	50.5	0.1	359.611	1.720	0.876	
Max. Min. Difference			4.8	0.45	0.00	0.43	0.002	70.037	1.001	0.510	

Lanik:

navn på filter produsent	sys navn	ppi	g Weight	mm Height	mm Lengde	mm Width	dm3 volume	kg/m3 density	kN max force	MPa Crushing strength
Lanik30_10m_30	Seleecy30_3	30	35.5	48.04		47.14	0.084	423.405	1.053	0.536
Lanik30_10m_31	Seleecy30_3	30	33.4	47.78		48.81	0.089	373.588	0.967	0.492
Lanik30_10m_32	Seleecy30_3	30	33.7	47.75		47.26	0.084	402.327	1.071	0.545
Lanik30_10m_33	Seleecy30_3	30	33.1	47.67		47.26	0.084	395.827	1.434	0.730
Lanik30_10m_34	Seleecy30_3	30	31.5	47.91		47.02	0.083	378.642	0.708	0.361
Lanik30_10m_35	Seleecy30_3	30	32.9	48.20		48.47	0.089	369.924	1.147	0.584
Lanik30_10m_36	Seleecy30_3	30	34.9	48.01		49.93	0.094	371.262	1.237	0.630
Lanik30_10m_37	Seleecy30_3	30	31.6	47.85		45.99	0.079	397.547	1.073	0.546
Lanik30_10m_38	Seleecy30_3	30	32.7	47.77		47.15	0.083	392.048	1.053	0.536
Lanik30_10m_39	Seleecy30_3	30	35.6	48.00		48.09	0.087	408.328	1.280	0.652
Average			33.5	47.9	#DIV/0!	47.7	0.1	391.290	1.102	0.561
standard deviation								16.837	0.185	0.094
Max. value			35.6	48.2	0.0	49.9	0.1	423.405	1.434	0.730
Min. value			31.5	47.7	0.0	46.0	0.1	369.924	0.708	0.361
Max. Min. Difference			4.1	0.53	0.00	3.94	0.015	53.481	0.726	0.370
Lanikhot30_1h_30	Ianikocy30_3f	30	39.3	47.78		50.81	0.097	405.656	1.902	0.969
Lanikhot30_1h_31	Ianikocy30_3f	30	37.8	47.69		50.86	0.097	390.141	1.816	0.925
Lanikhot30_1h_32	Ianikocy30_3f	30	37.7	47.40		50.72	0.096	393.654	1.621	0.826
Lanikhot30_1h_33	Ianikocy30_3f	30	38.1	47.68		50.55	0.096	398.159	2.375	1.210
Lanikhot30_1h_34	Ianikocy30_3f	30	39.3	47.76		50.20	0.095	415.749	1.975	1.006
Lanikhot30_1h_35	Ianikocy30_3f	30	38.9	47.93		50.70	0.097	402.010	2.356	1.200
Lanikhot30_1h_36	Ianikocy30_3f	30	37.0	47.77		50.79	0.097	382.296	1.983	1.010
Lanikhot30_1h_37	Ianikocy30_3f	30	37.6	47.99		50.61	0.097	389.470	2.010	1.024
Lanikhot30_1h_38	Ianikocy30_3f	30	37.5	47.96		50.71	0.097	387.146	2.148	1.094
Lanikhot30_1h_39	Ianikocy30_3f	30	38.7	47.68		50.92	0.097	398.573	2.375	1.210
Average			38.2	47.8	#DIV/0!	50.7	0.1	396.29	2.1	1.047
standard deviation								9.37		0.123
Max. value			39.3	48.0	0.0	50.9	0.1	415.7	2.4	1.210
Min. value			37.0	47.4	0.0	50.2	0.1	382.3	1.6	0.826
Max. Min. Difference			2.3	0.59	0.00	0.72	0.003	33.452	0.754	0.384
Lanik30_2h_50	Seleecy30_5	30	34.1	47.48		49.65	0.092	370.950	1.053	0.536
Lanik30_2h_51	Seleecy30_5	30	31.8	47.48		50.69	0.096	331.881	1.387	0.706
Lanik30_2h_52	Seleecy30_5	30	33.7	47.90		48.53	0.089	380.350	1.434	0.730
Lanik30_2h_53	Seleecy30_5	30	32.2	47.91		50.83	0.097	331.207	1.182	0.602
Lanik30_2h_54	Seleecy30_5	30	34.2	47.75		50.56	0.096	356.737	1.246	0.635
Lanik30_2h_55	Seleecy30_5	30	37.9	47.83		50.89	0.097	389.569	2.284	1.163
Lanik30_2h_56	Seleecy30_5	30	34.0	47.72		50.70	0.096	352.917	1.053	0.536
Lanik30_2h_57	Seleecy30_5	30	36.1	47.55		50.07	0.094	385.577	1.100	0.560
Lanik30_2h_58	Seleecy30_5	30	34.7	47.85		49.15	0.091	382.218	1.225	0.624
Lanik30_2h_59	Seleecy30_5	30	32.8	47.82		43.18	0.070	468.392	1.147	0.584
Average			34.2	47.7	#DIV/0!	49.4	0.1	374.980	1.311	0.668
standard deviation								37.070	0.346	0.176
Max. value			37.9	47.9	0.0	50.9	0.1	468.392	2.284	1.163
Min. value			31.8	47.5	0.0	43.2	0.1	331.207	1.053	0.536
Max. Min. Difference			6.1	0.43	0.00	7.71	0.027	137.185	1.231	0.627

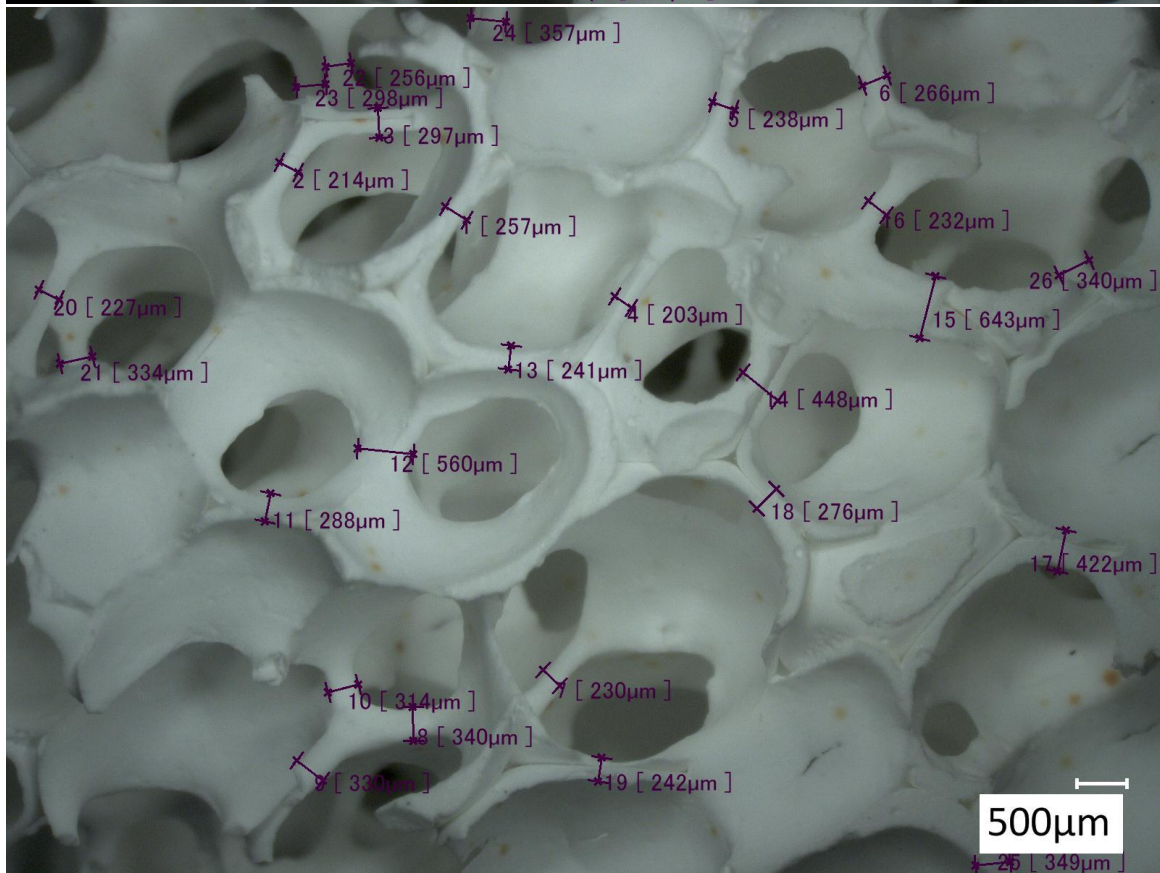
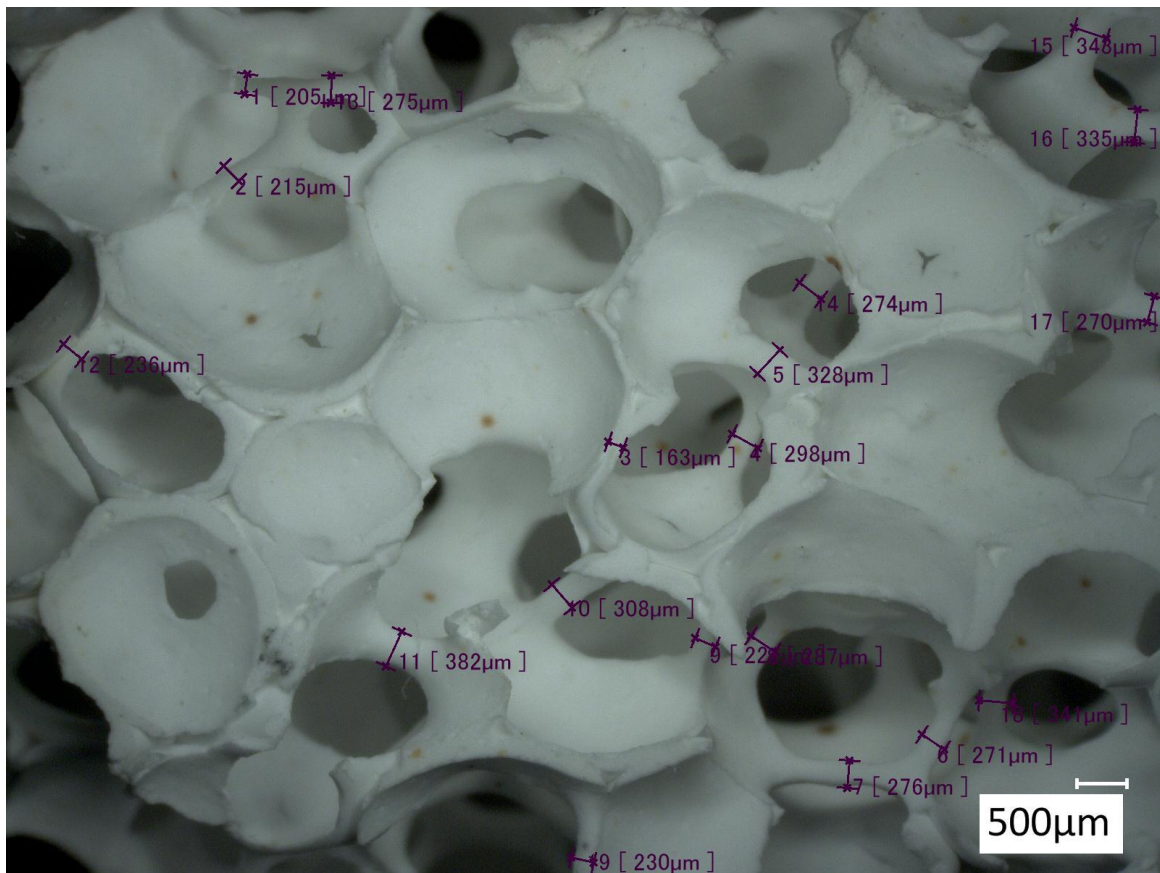
Selee:

navn på filter		g	mm	mm	mm	dm3	kg/m3	kN	MPa	
produsent	sys navn	Weight	Height	Lengde	Width	volume	density	max force	Crushing strength	
Seleehot30_10m_30		30	35.7	50.92		50.75	0.103	346.591	2.280	1.161
Seleehot30_10m_31		30	36.0	51.05		50.96	0.104	345.747	2.478	1.262
Seleehot30_10m_32		30	34.5	50.85		50.61	0.102	337.261	2.139	1.089
Seleehot30_10m_33		30	35.0	50.77		50.43	0.101	345.138	2.001	1.019
Seleehot30_10m_34		30	35.0	50.63		50.74	0.102	341.877	1.983	1.010
Seleehot30_10m_35		30	34.0	50.83		50.78	0.103	330.281	2.233	1.137
Seleehot30_10m_36		30	35.5	50.87		50.76	0.103	344.853	2.001	1.019
Seleehot30_10m_37		30	35.4	50.66		50.62	0.102	347.219	2.002	1.020
Seleehot30_10m_38		30	35.4	50.71		50.70	0.102	345.783	2.001	1.019
Seleehot30_10m_39		30	36.4	50.63		50.74	0.102	355.552	2.285	1.164
Average			35.3	50.8	#DIV/0!	50.7	0.1	344.030	2.140	1.090
standard deviation								6.300	0.163	0.083
Max. value			36.4	51.1	0.0	51.0	0.1	355.552	2.478	1.262
Min. value			34.0	50.6	0.0	50.4	0.1	330.281	1.983	1.010
Max. Min. Difference			2.4	0.42	0.00	0.53	0.003	25.271	0.495	0.252
Seleehot30_1h_30	seleecy30_30	30	31.3	49.82		50.78	0.101	310.217	1.475	0.751
Seleehot30_1h_31	seleecy30_31	30	32.8	50.24		50.84	0.102	321.605	1.220	0.621
Seleehot30_1h_32	seleecy30_32	30	34.2	50.21		50.84	0.102	335.533	2.118	1.079
Seleehot30_1h_33	seleecy30_33	30	34.9	50.42		50.82	0.102	341.243	1.620	0.825
Seleehot30_1h_34	seleecy30_34	30	34.1	50.55		50.90	0.103	331.519	2.000	1.019
Seleehot30_1h_35	seleecy30_35	30	31.3	50.12		50.76	0.101	308.603	1.780	0.907
Seleehot30_1h_36	seleecy30_36	30	31.7	50.20		50.87	0.102	310.701	1.621	0.826
Seleehot30_1h_37	seleecy30_37	30	32.1	50.11		50.78	0.101	316.304	1.813	0.923
Seleehot30_1h_38	seleecy30_38	30	32.3	50.15		50.73	0.101	318.649	1.839	0.937
Seleehot30_1h_39	seleecy30_39	30	31.6	50.07		50.93	0.102	309.793	1.813	0.923
Average			32.6	50.2	#DIV/0!	50.8	0.1	320.417	1.730	0.881
standard deviation								11.215		0.125
Max. value			34.9	50.6	0.0	50.9	0.1	341.243	2.118	1.079
Min. value			31.3	49.8	0.0	50.7	0.1	308.603	1.220	0.621
Max. Min. Difference			3.6	0.73	0.00	0.20	0.002	32.640	0.898	0.457
Seleehot30_2h_50		30	36.1	50.91		50.78	0.103	350.130	2.375	1.210
Seleehot30_2h_51		30	36.3	50.77		50.66	0.102	354.715	2.376	1.210
Seleehot30_2h_52		30	34.9	50.70		50.80	0.103	339.625	1.902	0.969
Seleehot30_2h_53		30	33.9	50.57		50.82	0.103	330.482	2.095	1.067
Seleehot30_2h_54		30	33.4	50.65		50.68	0.102	326.892	2.188	1.114
Seleehot30_2h_55		30	34.3	50.78		50.71	0.103	334.445	2.188	1.114
Seleehot30_2h_56		30	34.6	50.65		50.87	0.103	336.111	2.060	1.049
Seleehot30_2h_57		30	36.1	50.81		50.78	0.103	350.819	2.562	1.305
Seleehot30_2h_58		30	36.4	51.09		50.95	0.104	349.452	2.356	1.200
Seleehot30_2h_59		30	36.0	50.84		50.84	0.103	348.816	2.375	1.210
Average			35.2	50.8	#DIV/0!	50.8	0.1	342.149	2.248	1.145
standard deviation								9.304	0.186	0.095
Max. value			36.4	51.1	0.0	51.0	0.1	354.715	2.562	1.305
Min. value			33.4	50.6	0.0	50.7	0.1	326.892	1.902	0.969
Max. Min. Difference			3.0	0.52	0.00	0.29	0.002	27.823	0.660	0.336

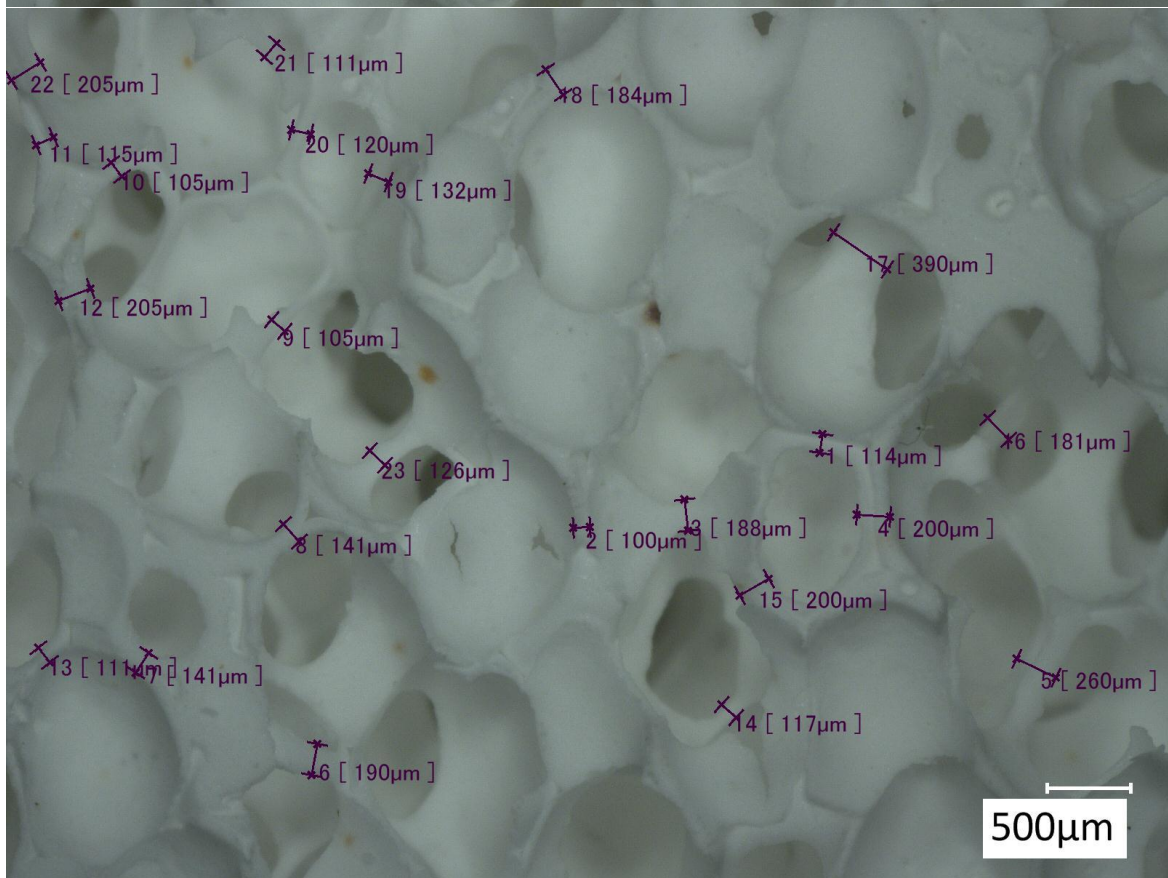
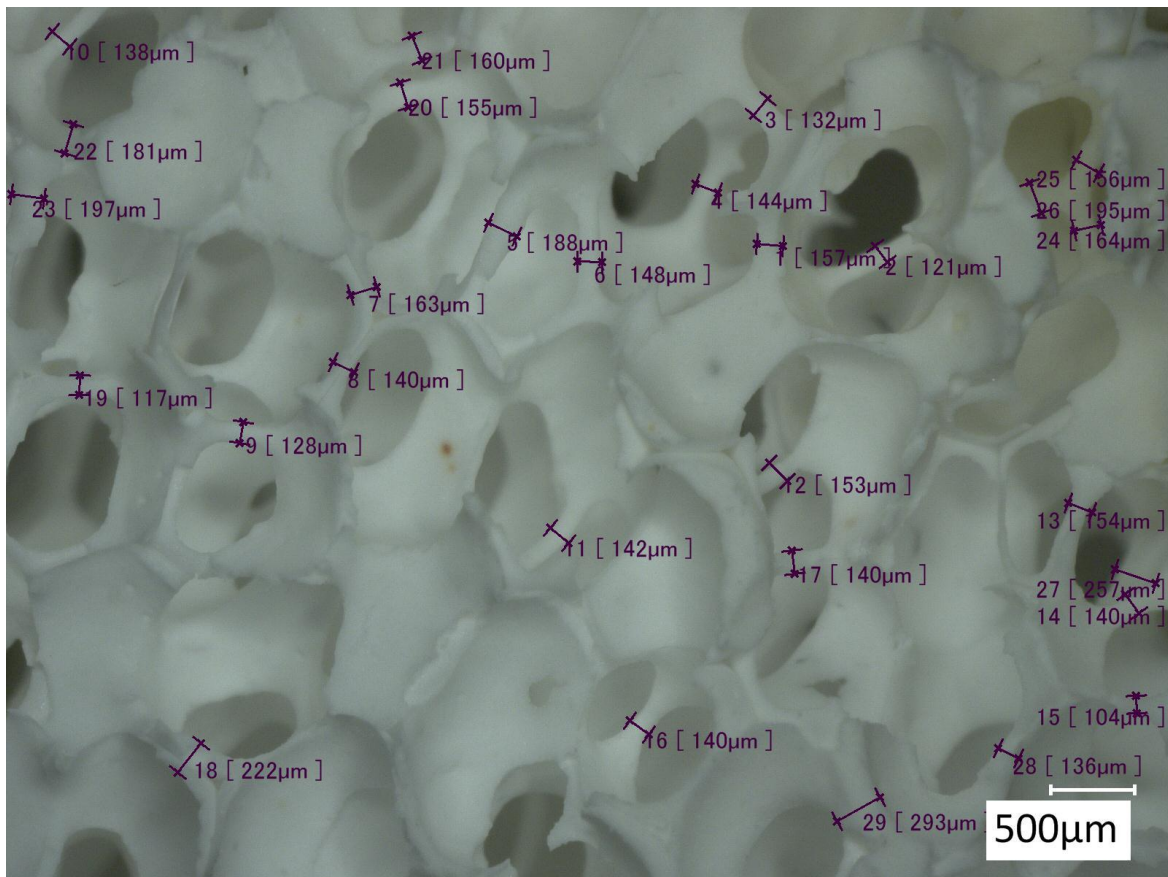
Selee:

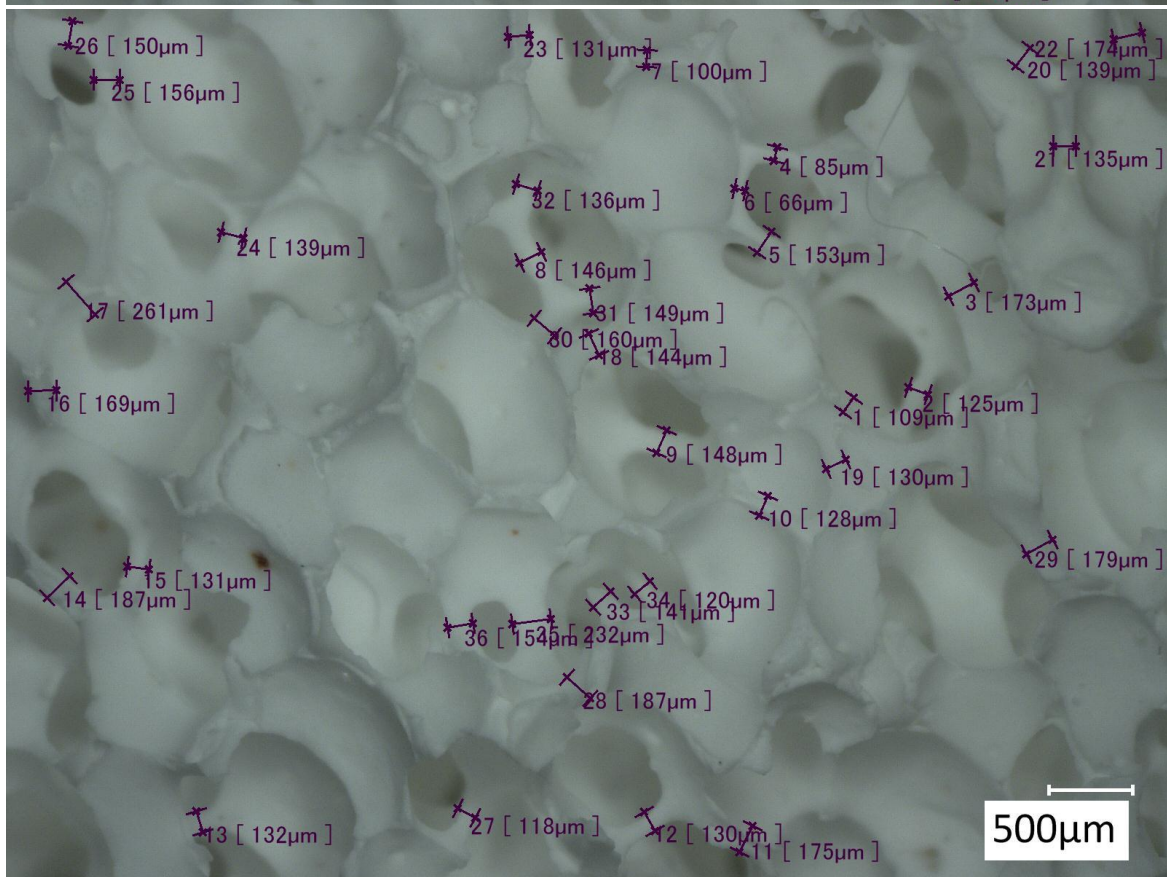
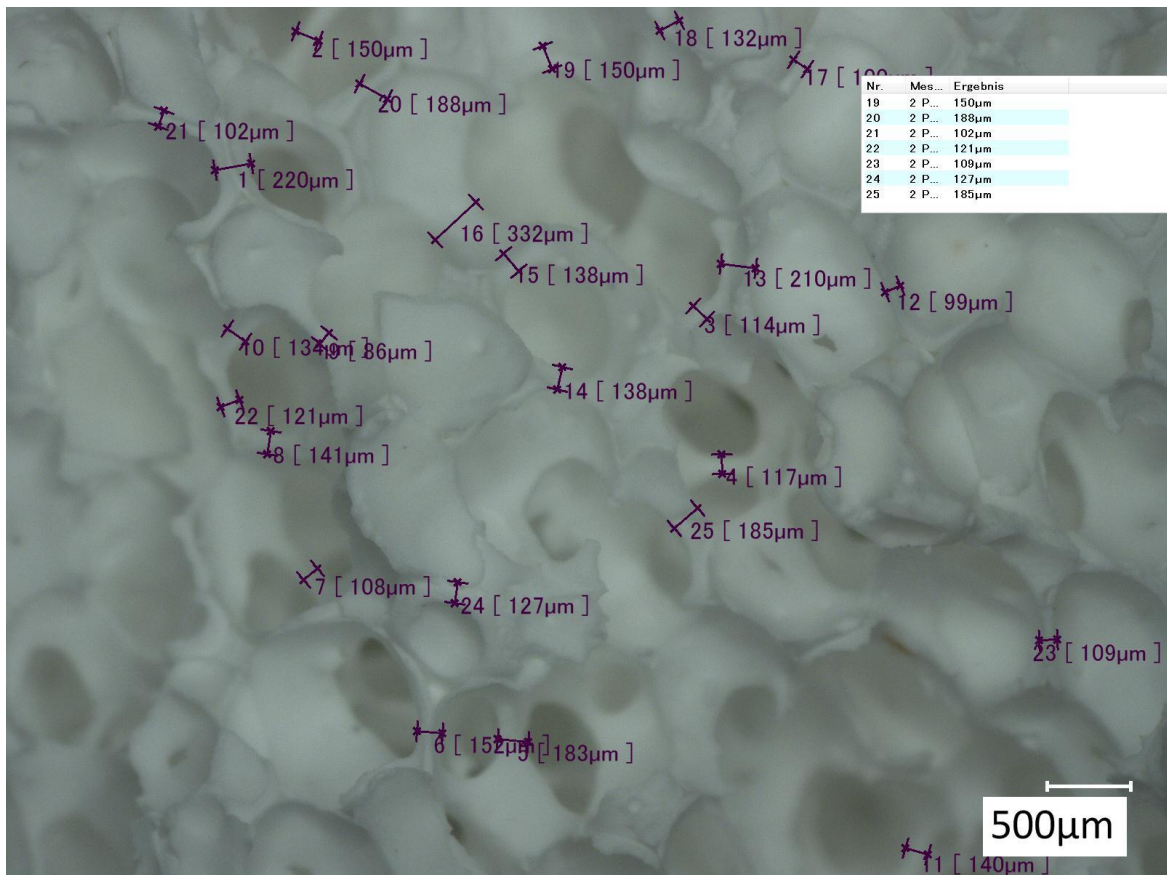
navn på filter produsent	sys navn	ppi	g Weight	mm Height	mm Lengde	mm Width	dm3 volume	kg/m3 density	kN max force	MPa Crushing strength	
Seleehot30_10m_30		11	30	35.7	50.92		50.75	0.103	346.591	2.280	1.161
Seleehot30_10m_31		12	30	36.0	51.05		50.96	0.104	345.747	2.478	1.262
Seleehot30_10m_32		13	30	34.5	50.85		50.61	0.102	337.261	2.139	1.089
Seleehot30_10m_33		14	30	35.0	50.77		50.43	0.101	345.138	2.001	1.019
Seleehot30_10m_34		15	30	35.0	50.63		50.74	0.102	341.877	1.983	1.010
Seleehot30_10m_35		16	30	34.0	50.83		50.78	0.103	330.281	2.233	1.137
Seleehot30_10m_36		17	30	35.5	50.87		50.76	0.103	344.853	2.001	1.019
Seleehot30_10m_37		18	30	35.4	50.66		50.62	0.102	347.219	2.002	1.020
Seleehot30_10m_38		19	30	35.4	50.71		50.70	0.102	345.783	2.001	1.019
Seleehot30_10m_39		20	30	36.4	50.63		50.74	0.102	355.552	2.285	1.164
Average				35.3	50.8	#DIV/0!	50.7	0.1	344.030	2.140	1.090
standard deviation									6.300	0.163	0.083
Max. value				36.4	51.1	0.0	51.0	0.1	355.552	2.478	1.262
Min. value				34.0	50.6	0.0	50.4	0.1	330.281	1.983	1.010
Max. Min. Difference				2.4	0.42	0.00	0.53	0.003	25.271	0.495	0.252
Seleehot30_1h_30	seleecy30_30		30	31.3	49.82		50.78	0.101	310.217	1.475	0.751
Seleehot30_1h_31	seleecy30_31		30	32.8	50.24		50.84	0.102	321.605	1.220	0.621
Seleehot30_1h_32	seleecy30_32		30	34.2	50.21		50.84	0.102	335.533	2.118	1.079
Seleehot30_1h_33	seleecy30_33		30	34.9	50.42		50.82	0.102	341.243	1.620	0.825
Seleehot30_1h_34	seleecy30_34		30	34.1	50.55		50.90	0.103	331.519	2.000	1.019
Seleehot30_1h_35	seleecy30_35		30	31.3	50.12		50.76	0.101	308.603	1.780	0.907
Seleehot30_1h_36	seleecy30_36		30	31.7	50.20		50.87	0.102	310.701	1.621	0.826
Seleehot30_1h_37	seleecy30_37		30	32.1	50.11		50.78	0.101	316.304	1.813	0.923
Seleehot30_1h_38	seleecy30_38		30	32.3	50.15		50.73	0.101	318.649	1.839	0.937
Seleehot30_1h_39	seleecy30_39		30	31.6	50.07		50.93	0.102	309.793	1.813	0.923
Average				32.6	50.2	#DIV/0!	50.8	0.1	320.417	1.730	0.881
standard deviation									11.215		0.125
Max. value				34.9	50.6	0.0	50.9	0.1	341.243	2.118	1.079
Min. value				31.3	49.8	0.0	50.7	0.1	308.603	1.220	0.621
Max. Min. Difference				3.6	0.73	0.00	0.20	0.002	32.640	0.898	0.457
Seleehot30_2h_50		1	30	36.1	50.91		50.78	0.103	350.130	2.375	1.210
Seleehot30_2h_51		2	30	36.3	50.77		50.66	0.102	354.715	2.376	1.210
Seleehot30_2h_52		3	30	34.9	50.70		50.80	0.103	339.625	1.902	0.969
Seleehot30_2h_53		4	30	33.9	50.57		50.82	0.103	330.482	2.095	1.067
Seleehot30_2h_54		5	30	33.4	50.65		50.68	0.102	326.892	2.188	1.114
Seleehot30_2h_55		6	30	34.3	50.78		50.71	0.103	334.445	2.188	1.114
Seleehot30_2h_56		7	30	34.6	50.65		50.87	0.103	336.111	2.060	1.049
Seleehot30_2h_57		8	30	36.1	50.81		50.78	0.103	350.819	2.562	1.305
Seleehot30_2h_58		9	30	36.4	51.09		50.95	0.104	349.452	2.356	1.200
Seleehot30_2h_59		10	30	36.0	50.84		50.84	0.103	348.816	2.375	1.210
Average				35.2	50.8	#DIV/0!	50.8	0.1	342.149	2.248	1.145
standard deviation									9.304	0.186	0.095
Max. value				36.4	51.1	0.0	51.0	0.1	354.715	2.562	1.305
Min. value				33.4	50.6	0.0	50.7	0.1	326.892	1.902	0.969
Max. Min. Difference				3.0	0.52	0.00	0.29	0.002	27.823	0.660	0.336

D Microscopic photos with strut thickness displayed of the filters

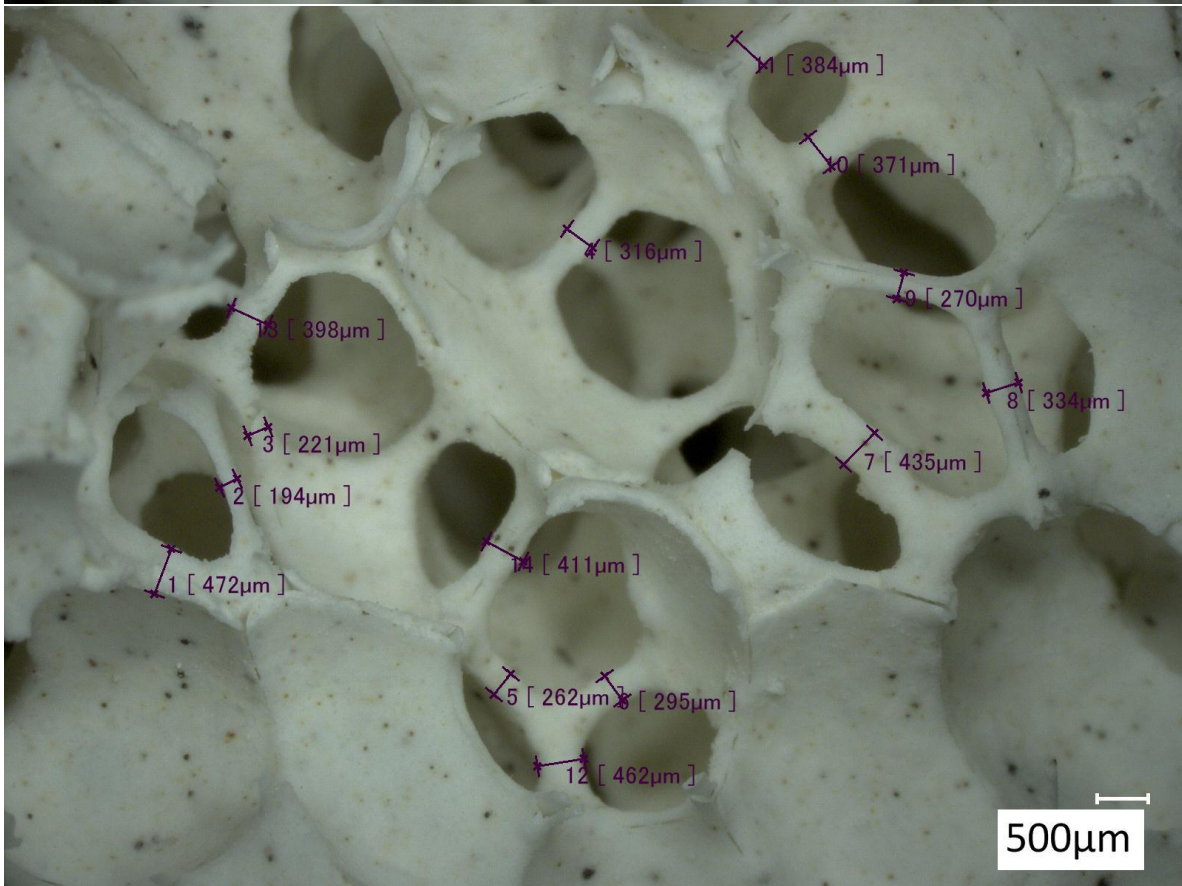
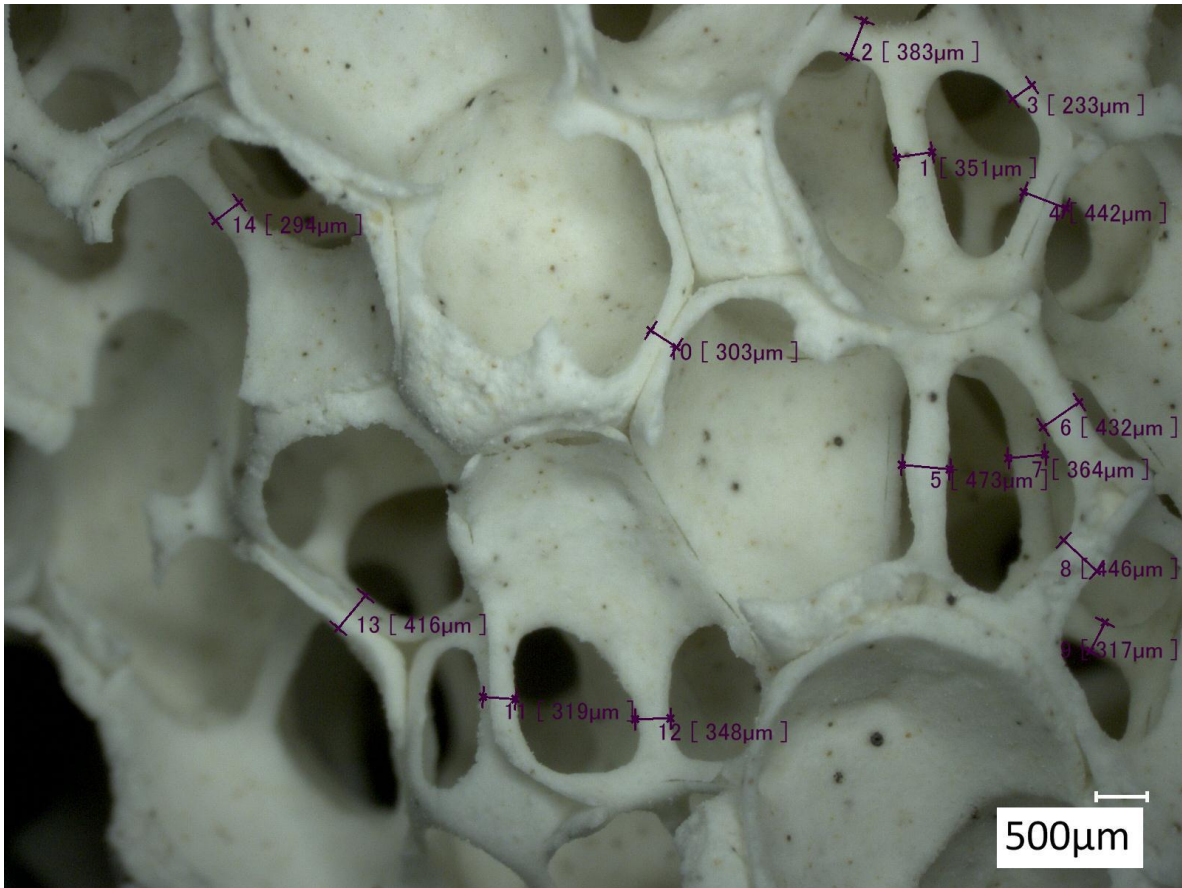


Sivex 65 ppi

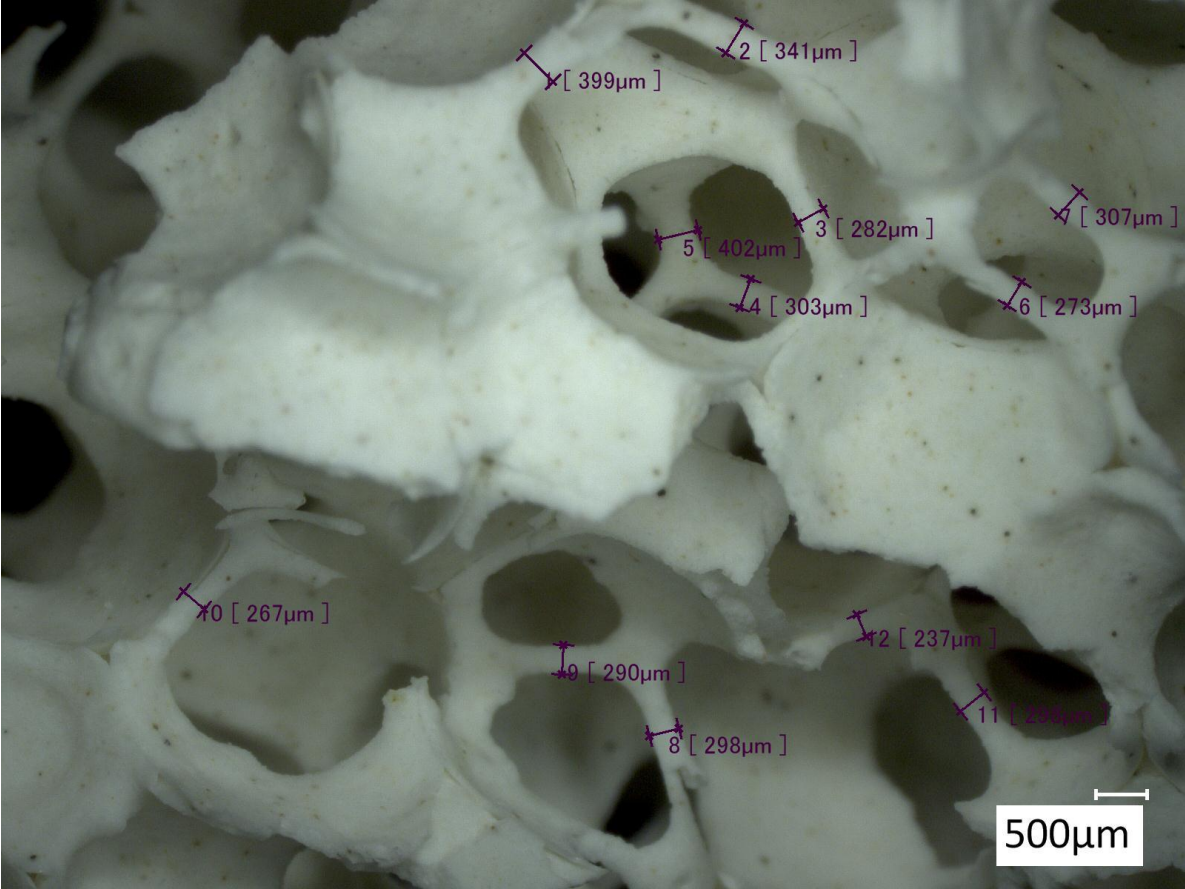




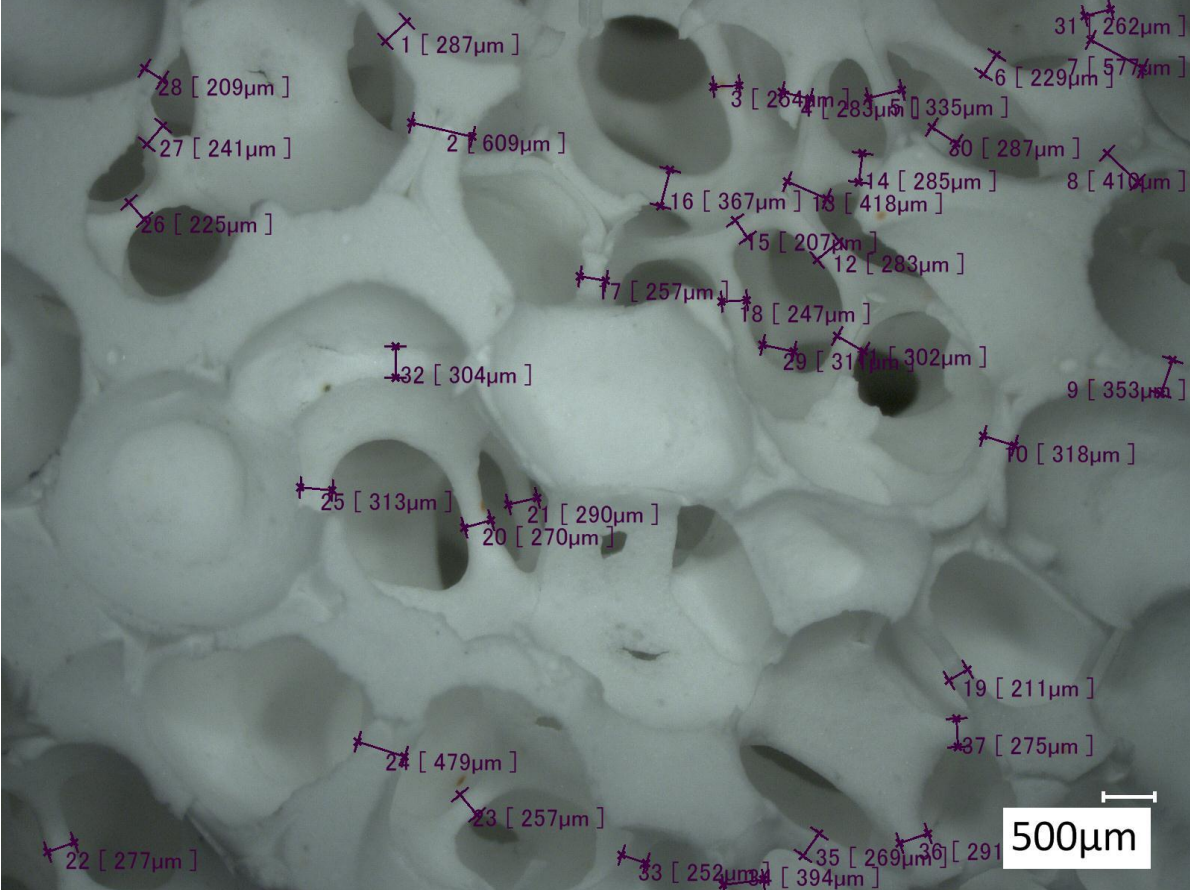
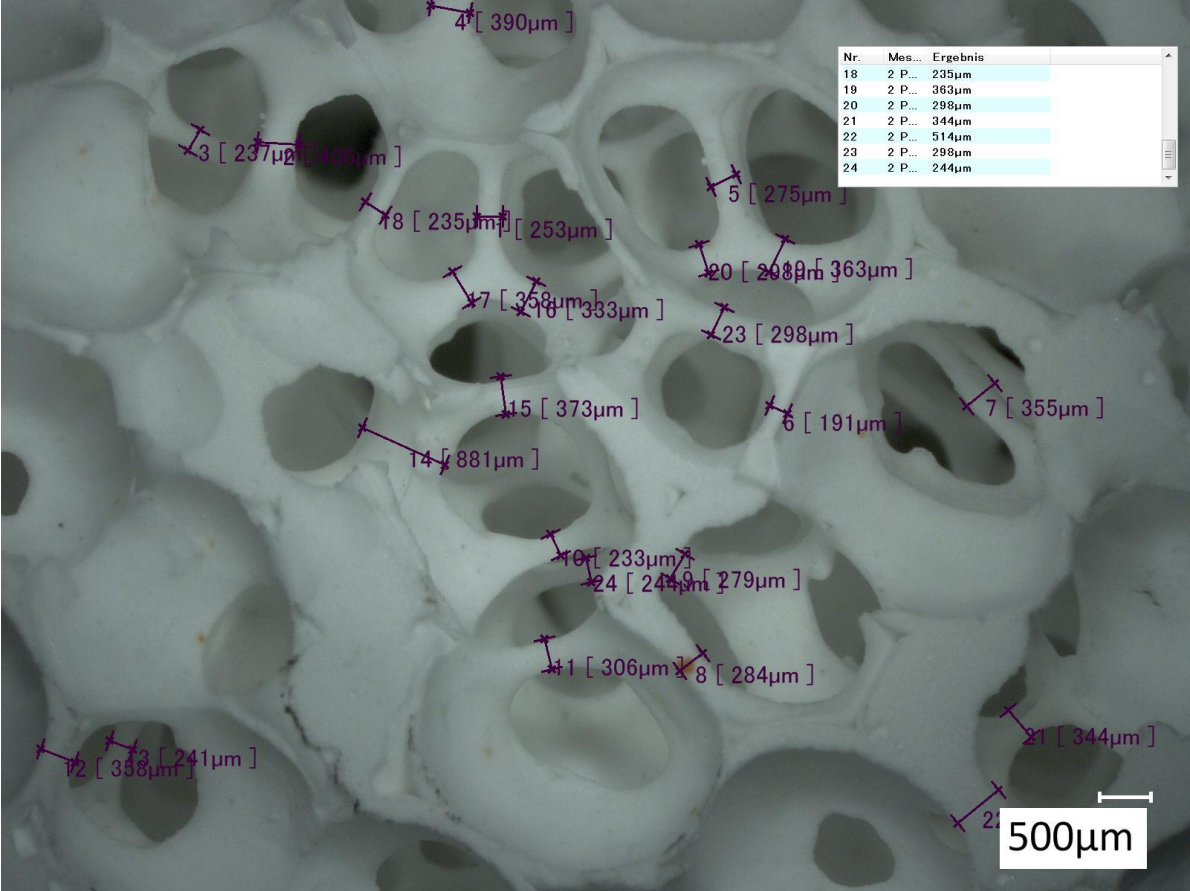
Sivex Non Phosphorus 30 ppi



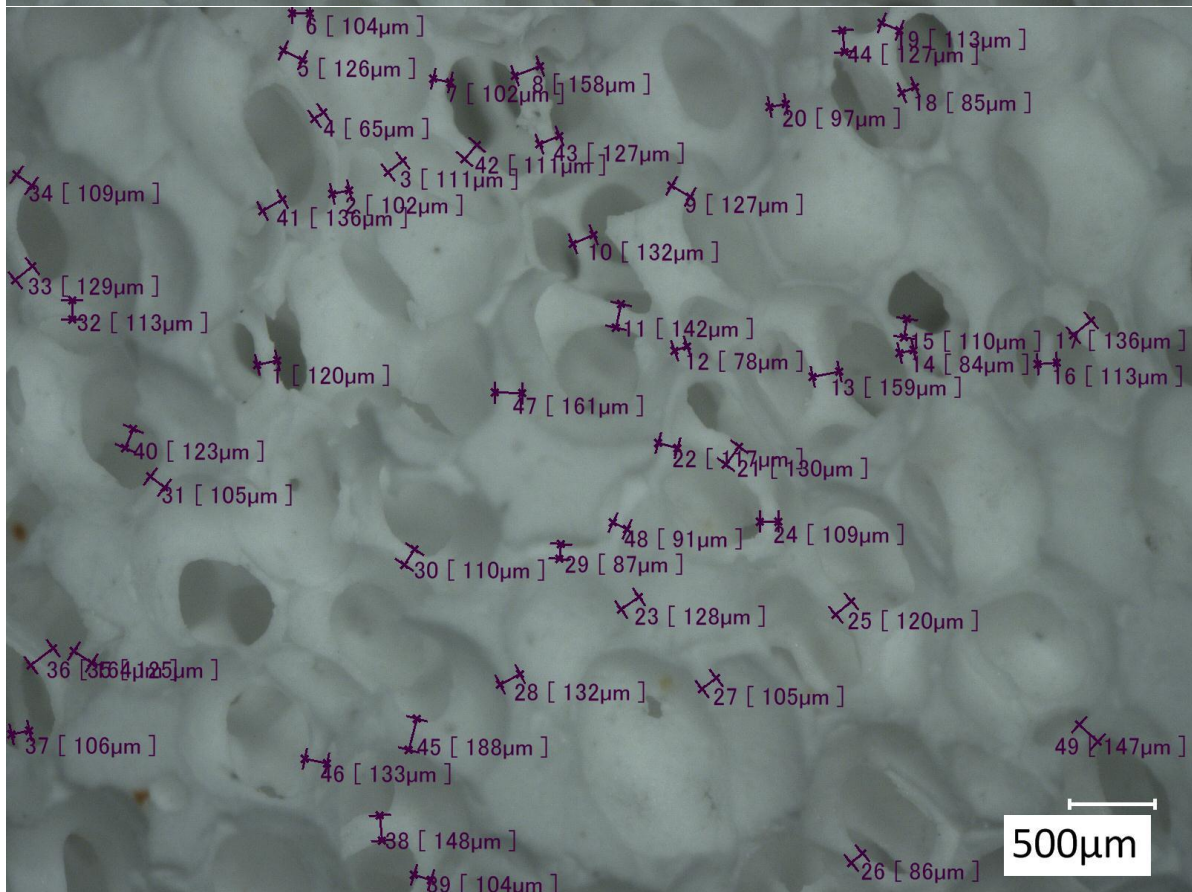
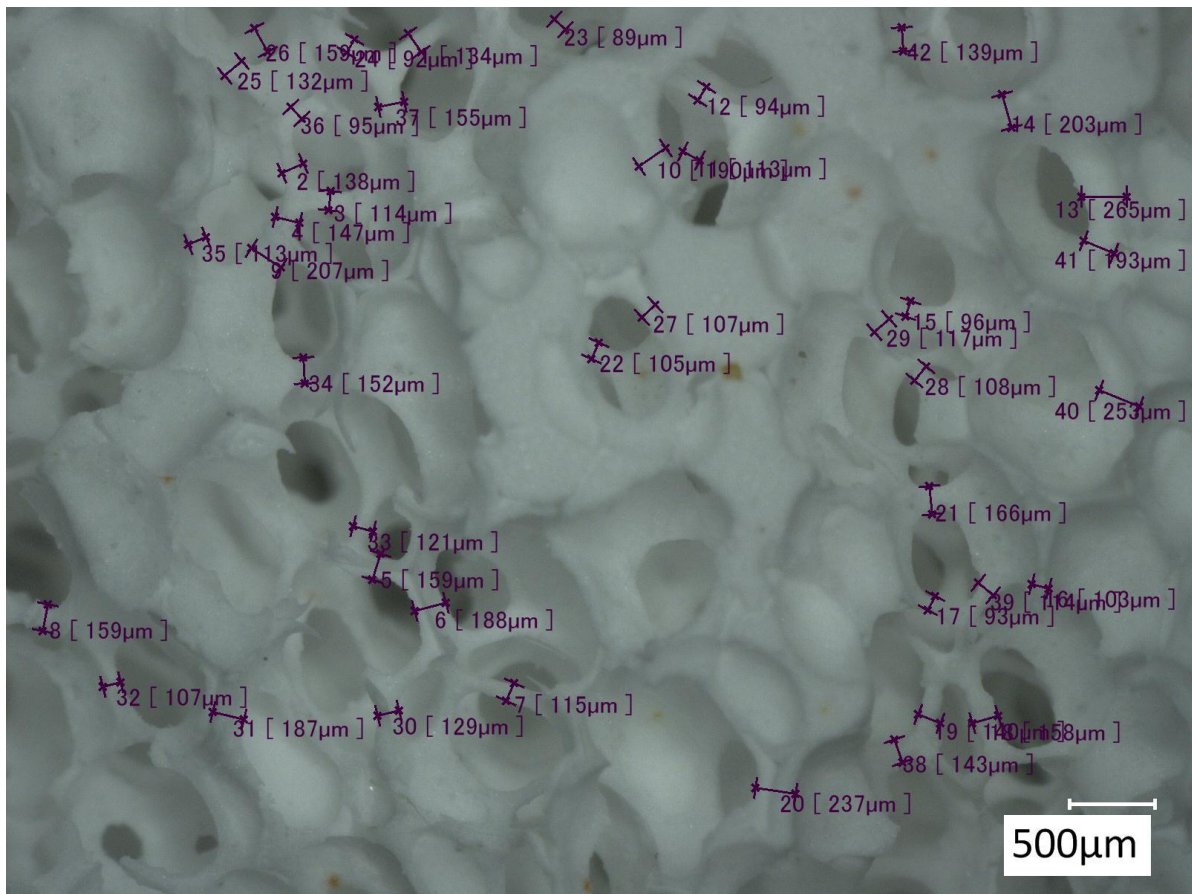
Sivex Non Phosphorus 30 ppi



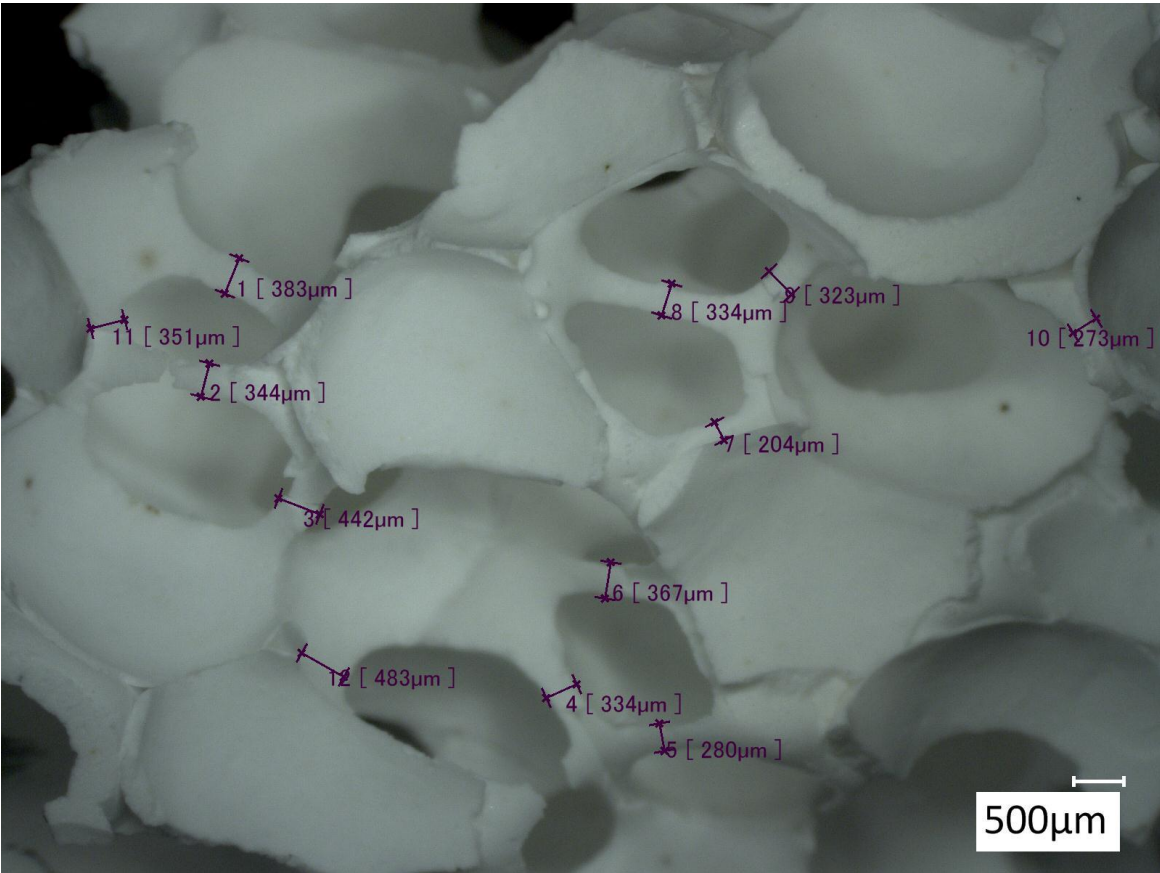
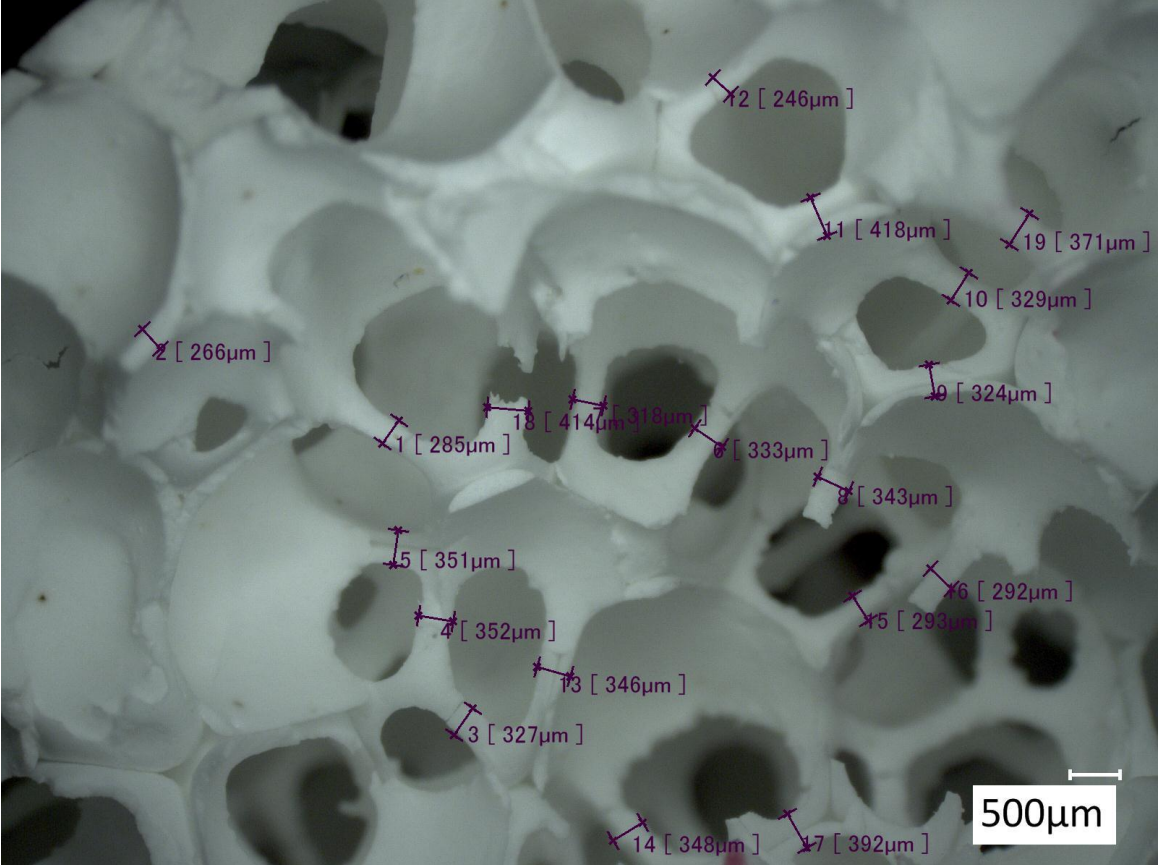
Drache 30 ppi



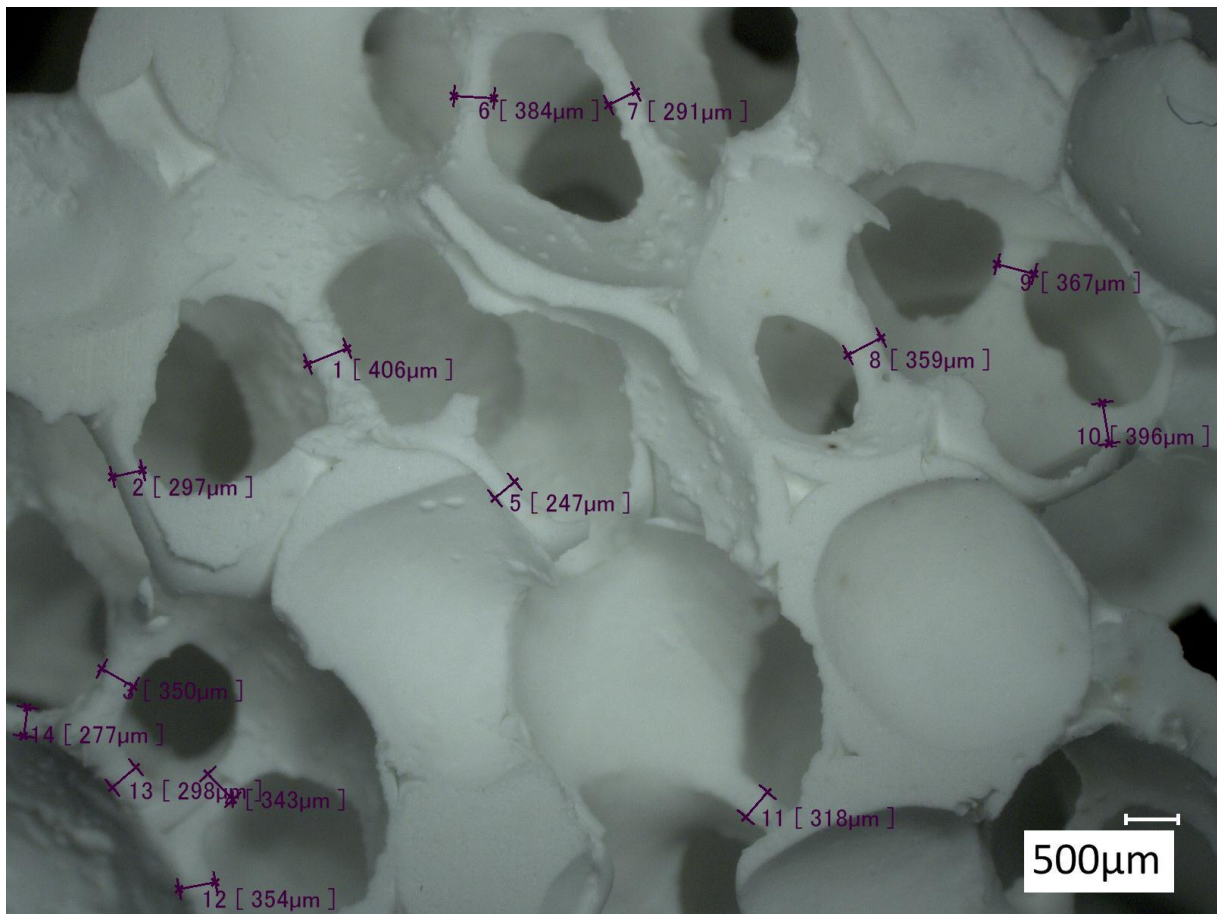
Drache 60 ppi



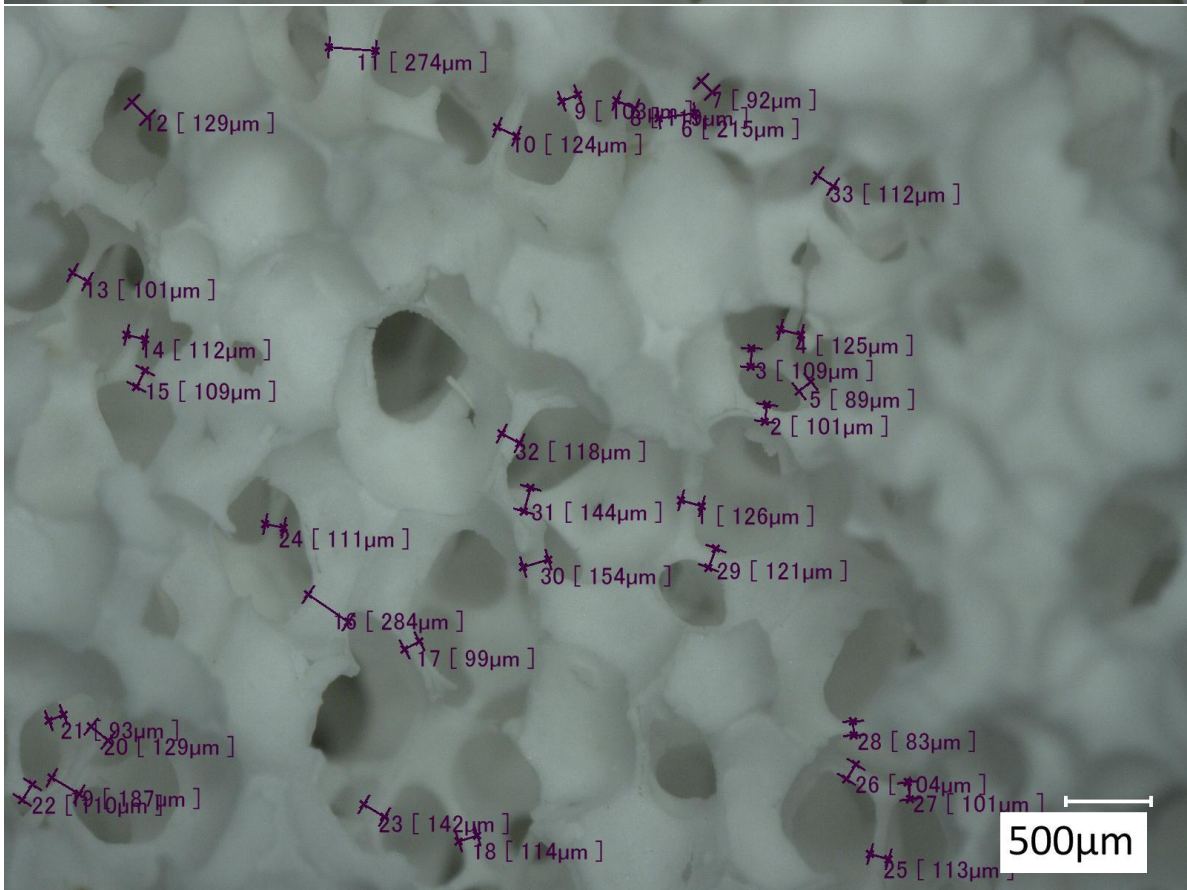
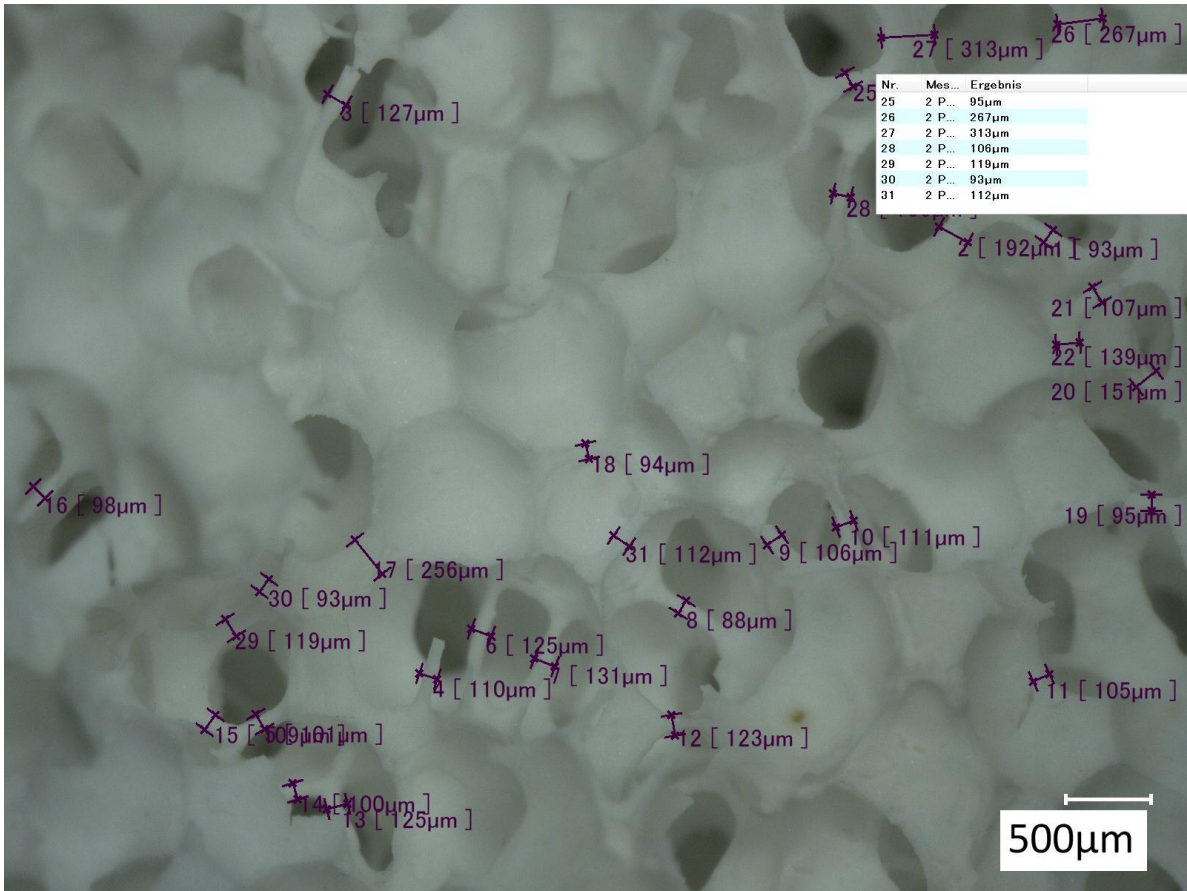
Lanik 30 ppi



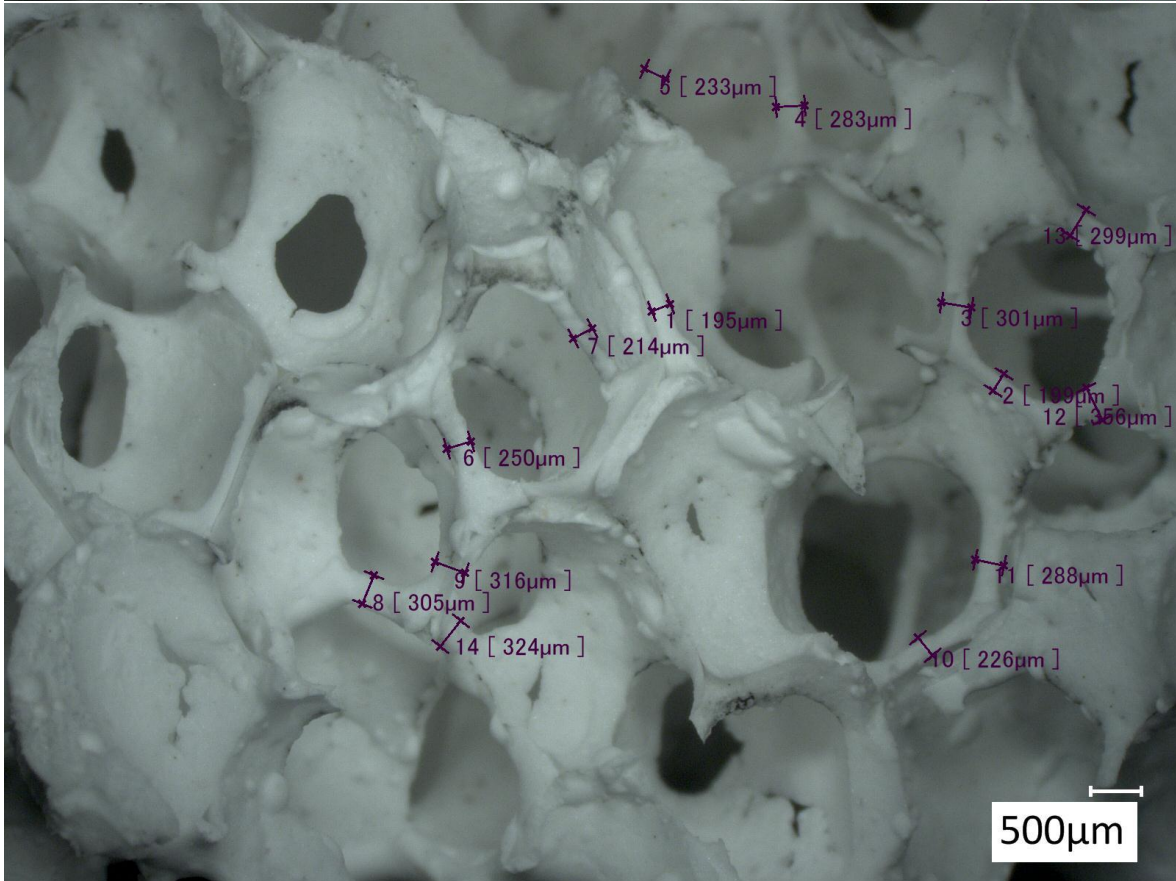
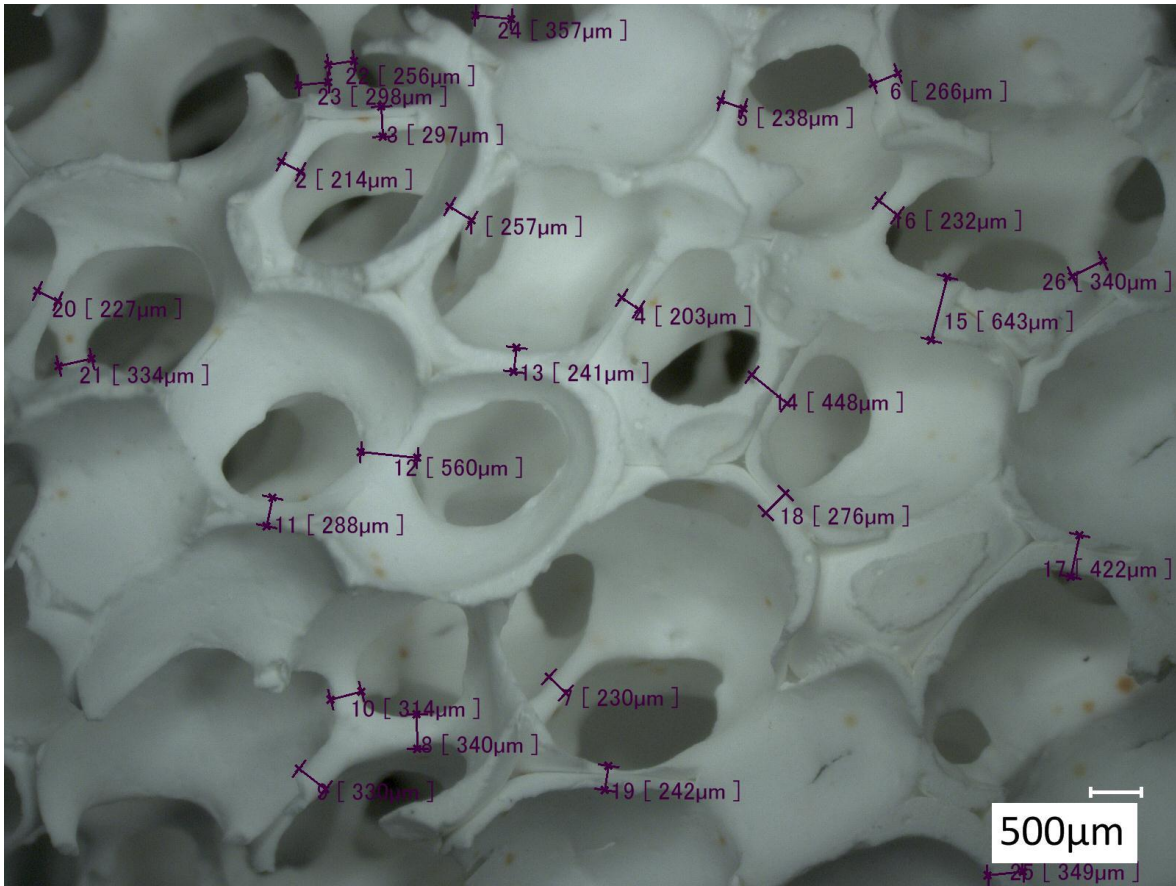
Lanik 30 ppi



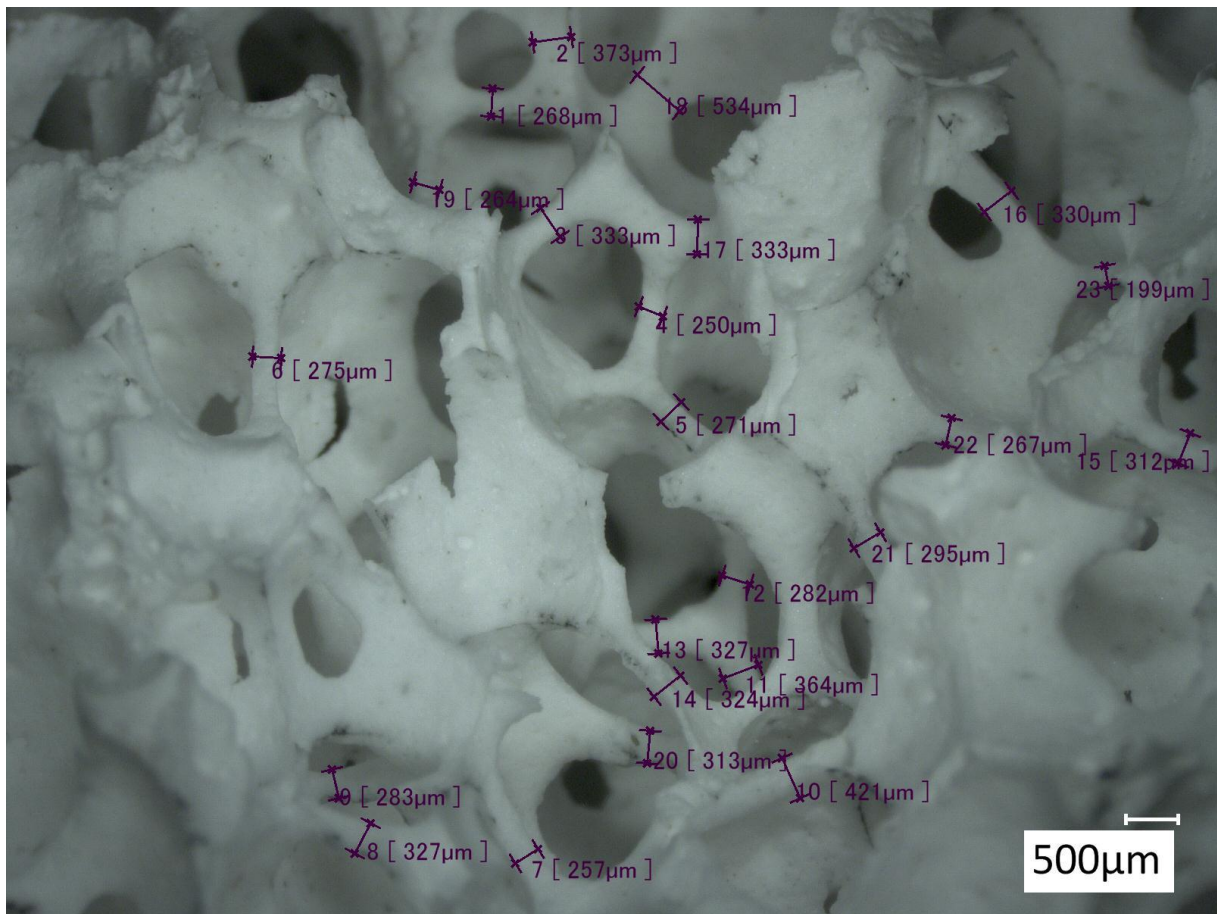
Lanik 60 ppi



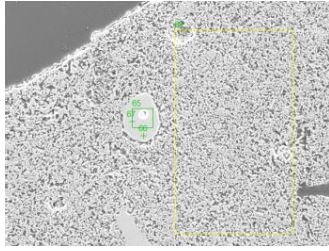
Selee 30 ppi



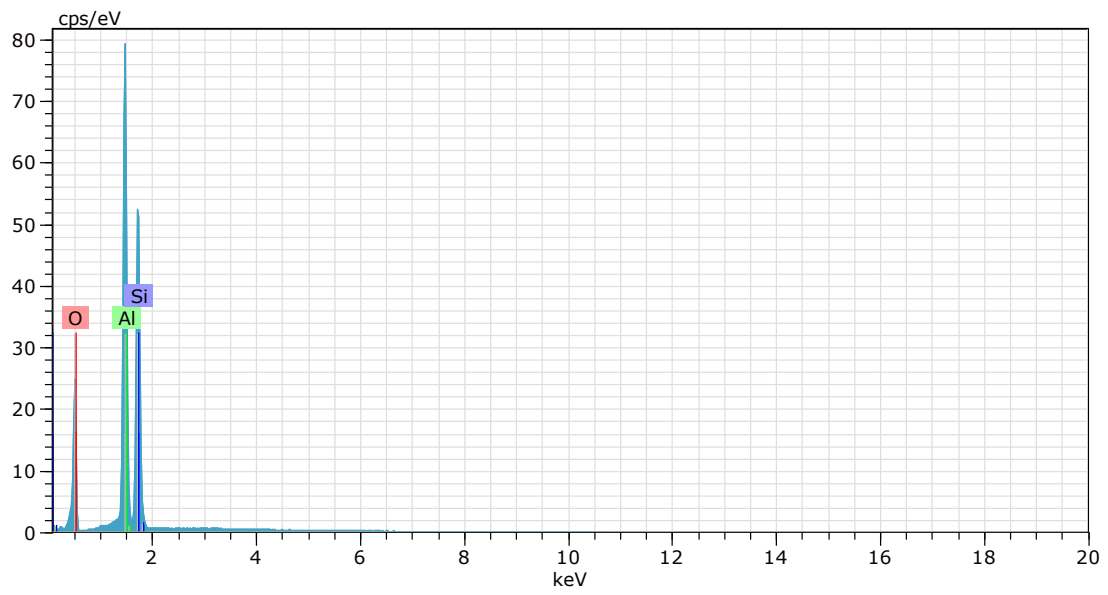
Selee 30 ppi



E EDS RawData Sivex 30

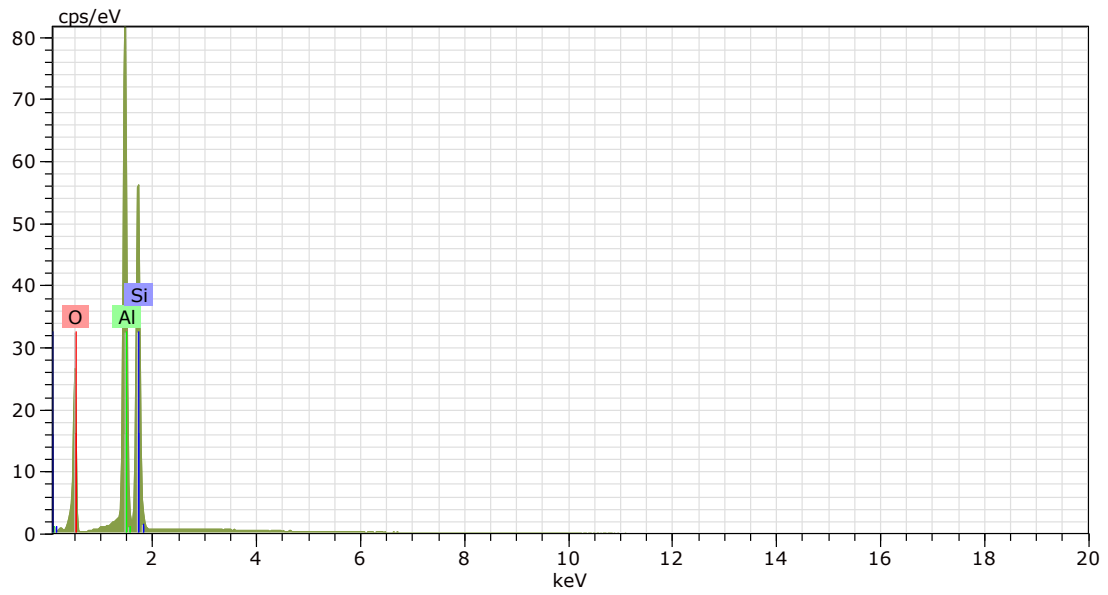


Area1
 Date:4/25/2020 12:47:58 PM
 Image size:1024 x 768
 Mag:600x
 HV:20.0kV



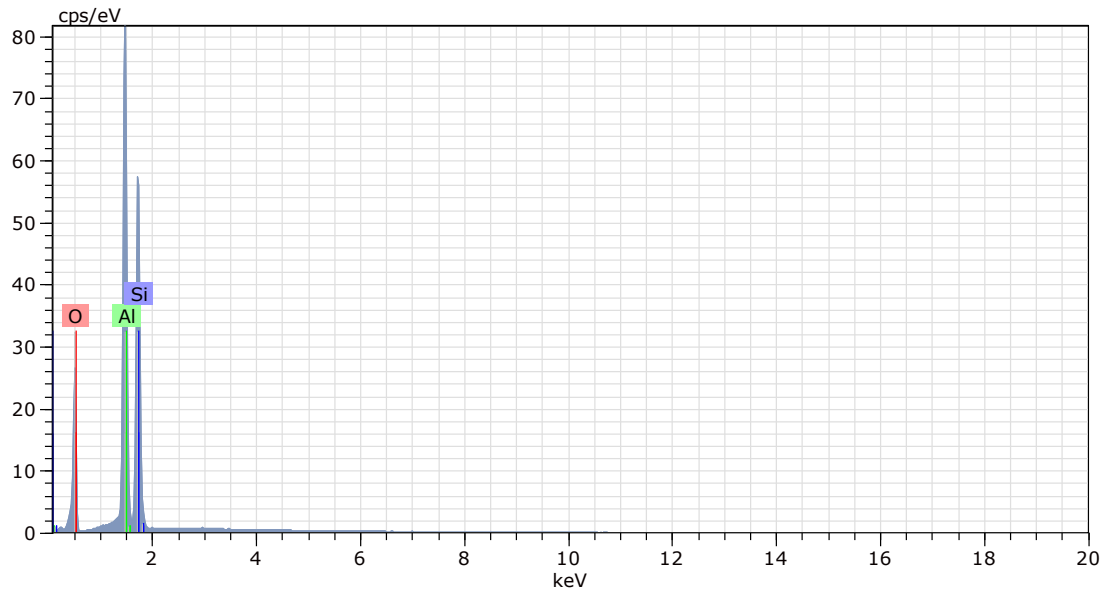
65 Date:4/25/2020 12:50:44 PM HV:20.0kV Puls th.:20.62kcps

El	AN	Series	unn. C [wt.%]	norm. C [wt.%]	Atom. C [at.%]	Error (1 Sigma) [wt.%]
O	8	K-series	24.48	37.99	51.27	2.88
Al	13	K-series	21.49	33.34	26.69	1.05
Si	14	K-series	18.48	28.67	22.05	0.81
Total:			64.44	100.00	100.00	



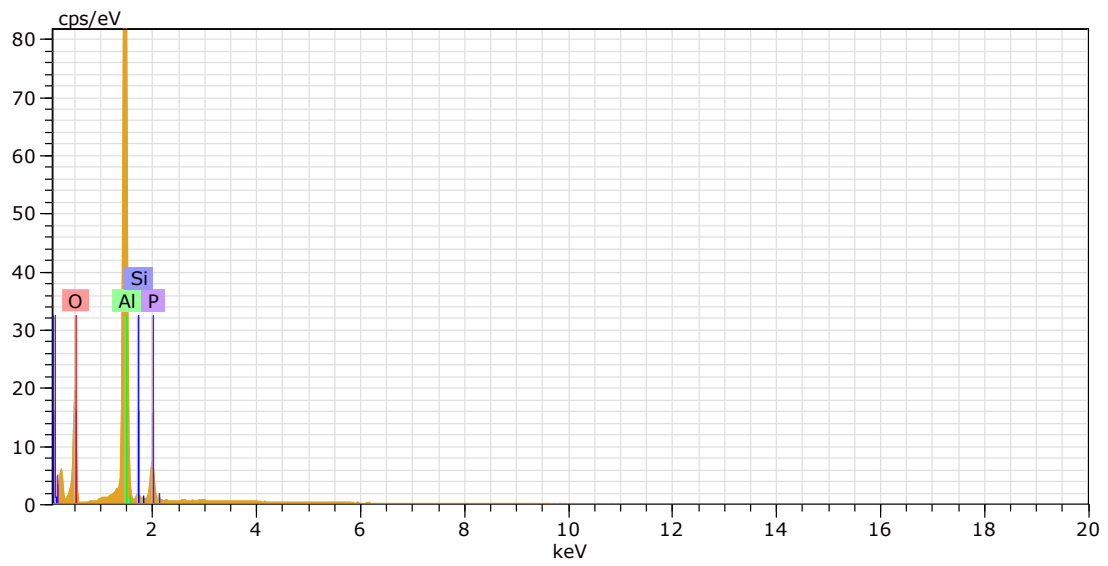
66 Date:4/25/2020 12:51:24 PM HV:20.0kV Puls th.:21.94kcps

El	AN	Series	unn. C [wt.%]	norm. C [wt.%]	Atom. C [at.%]	Error (1 Sigma) [wt.%]
O	8	K-series	19.81	37.97	51.28	2.32
Al	13	K-series	16.27	31.19	24.98	0.80
Si	14	K-series	16.10	30.85	23.74	0.71
Total:			52.18	100.00	100.00	



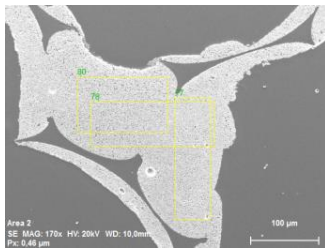
67 Date:4/25/2020 12:52:05 PM HV:20.0kV Puls th.:21.97kcps

El	AN	Series	unn. C [wt.%]	norm. C [wt.%]	Atom. C [at.%]	Error (1 Sigma) [wt.%]
O	8	K-series	19.88	37.91	51.23	2.33
Al	13	K-series	16.41	31.31	25.08	0.81
Si	14	K-series	16.14	30.78	23.69	0.71
Total:			52.43	100.00	100.00	

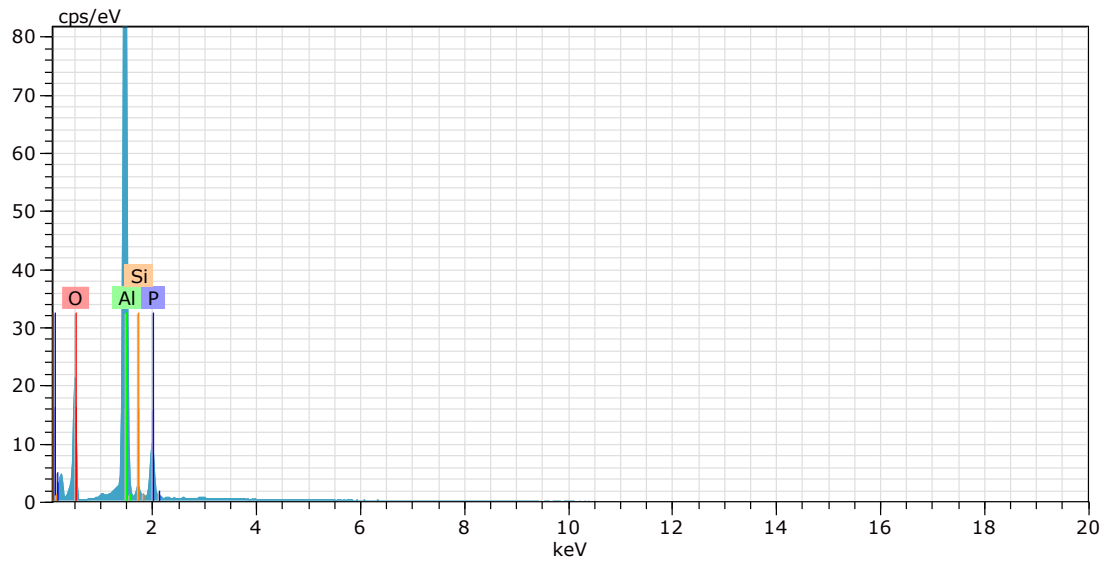


68 Date:4/25/2020 12:52:46 PM HV:20.0kV Puls th.:20.65kcps

El	AN	Series	unn. C [wt.%]	norm. C [wt.%]	Atom. C [at.%]	Error (1 Sigma) [wt.%]
Al	13	K-series	45.59	59.23	48.17	2.20
O	8	K-series	26.54	34.48	47.30	3.17
P	15	K-series	4.01	5.21	3.69	0.18
Si	14	K-series	0.83	1.08	0.84	0.06
Total:			76.96	100.00	100.00	

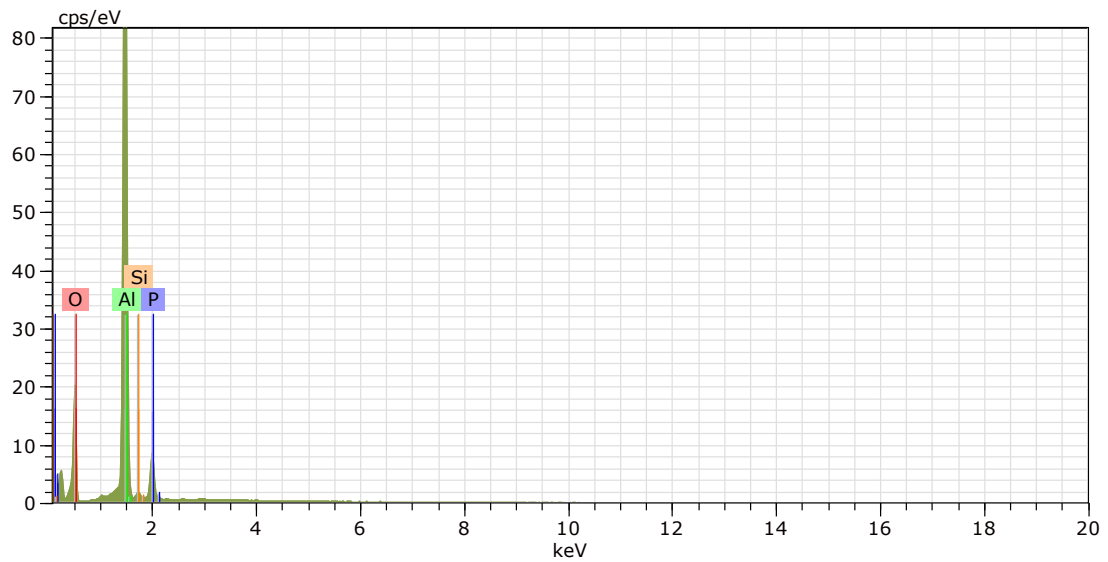


Area 2
 Date:4/25/2020 1:01:14 PM
 Image size:1024 x 768
 Mag:169.812x
 HV:20.0kV



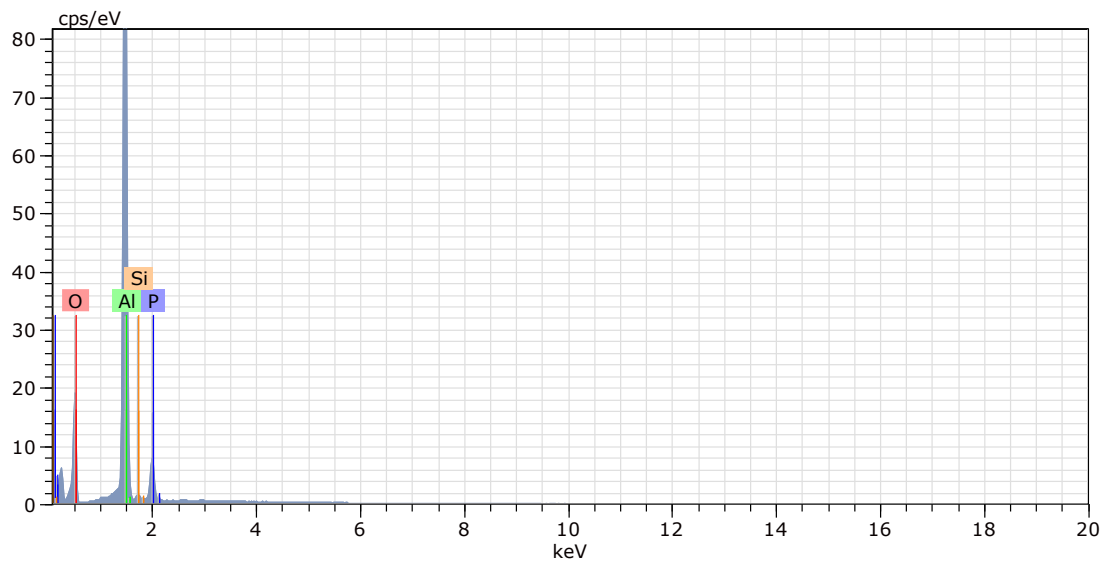
77 Date:4/25/2020 1:04:30 PM HV:20.0kV Puls th.:20.01kcps

El	AN	Series	unn. C [wt.%]	norm. C [wt.%]	Atom. C [at.%]	Error (1 Sigma) [wt.%]
O	8	K-series	27.56	35.80	48.84	3.27
Al	13	K-series	43.00	55.85	45.17	2.08
P	15	K-series	5.24	6.81	4.80	0.23
Si	14	K-series	1.18	1.54	1.19	0.08
Total:			76.99	100.00	100.00	



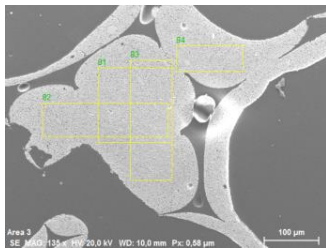
78 Date:4/25/2020 1:05:10 PM HV:20.0kV Puls th.:19.71kcps

El	AN	Series	unn. C [wt.%]	norm. C [wt.%]	Atom. C [at.%]	Error (1 Sigma) [wt.%]
O	8	K-series	27.17	35.25	48.18	3.24
Al	13	K-series	44.45	57.67	46.74	2.15
P	15	K-series	4.65	6.03	4.26	0.21
Si	14	K-series	0.81	1.06	0.82	0.06
Total:			77.08	100.00	100.00	

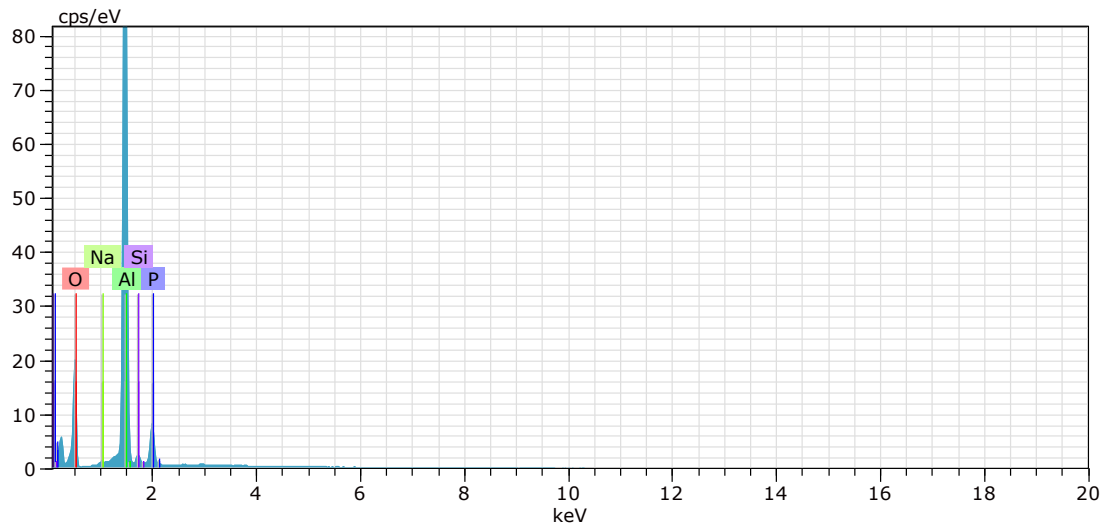


80 Date:4/25/2020 1:05:51 PM HV:20.0kV Puls th.:19.60kcps

El	AN	Series	unn. C [wt.%]	norm. C [wt.%]	Atom. C [at.%]	Error (1 Sigma) [wt.%]
O	8	K-series	25.34	34.74	47.62	3.03
Al	13	K-series	42.61	58.42	47.48	2.06
P	15	K-series	4.30	5.90	4.18	0.20
Si	14	K-series	0.68	0.93	0.73	0.06
Total:			72.94	100.00	100.00	



Area 3
 Date:4/25/2020 1:08:58 PM
 Image size:1024 x 768
 Mag:135.09164x
 HV:20.0kV

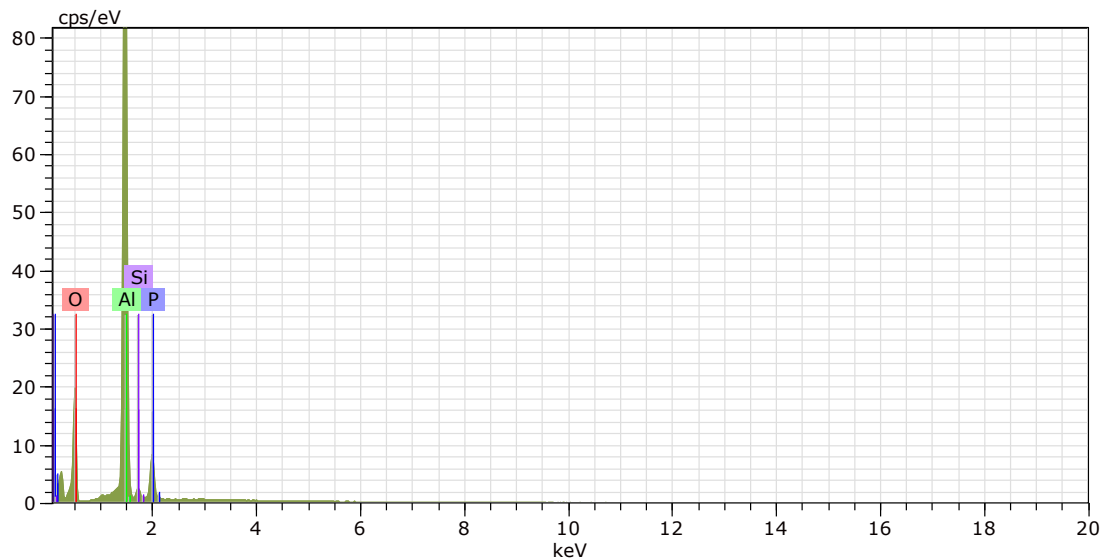


81 Date:4/25/2020 1:10:11 PM HV:20.0kV Puls th.:19.37kcps

El	AN	Series	unn. C [wt.%]	norm. C [wt.%]	Atom. C [at.%]	Error (1 Sigma) [wt.%]
----	----	--------	---------------	----------------	----------------	------------------------

O	8	K-series	13.66	35.09	48.05	1.64
Al	13	K-series	21.60	55.48	45.06	1.06
P	15	K-series	3.00	7.70	5.45	0.14
Si	14	K-series	0.47	1.20	0.94	0.05
Na	11	K-series	0.21	0.53	0.50	0.04

Total: 38.93 100.00 100.00

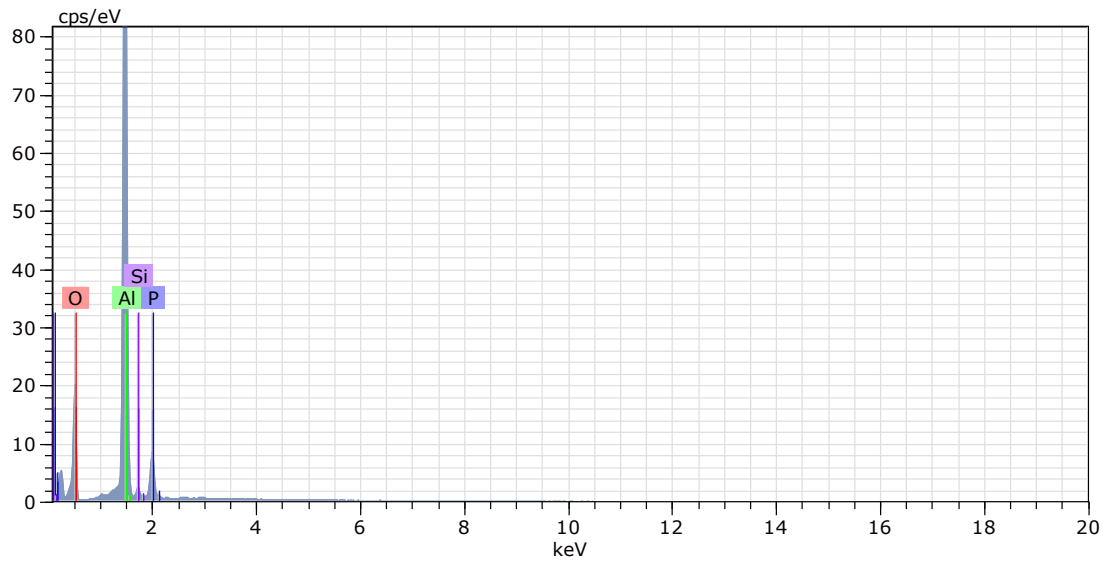


82 Date:4/25/2020 1:10:51 PM HV:20.0kV Puls th.:19.25kcps

El	AN	Series	unn. C [wt.%]	norm. C [wt.%]	Atom. C [at.%]	Error (1 Sigma) [wt.%]
----	----	--------	---------------	----------------	----------------	------------------------

O	8	K-series	22.60	35.06	48.00	2.70
Al	13	K-series	36.77	57.03	46.30	1.78
P	15	K-series	4.12	6.38	4.51	0.19
Si	14	K-series	0.98	1.52	1.18	0.07

Total: 64.46 100.00 100.00

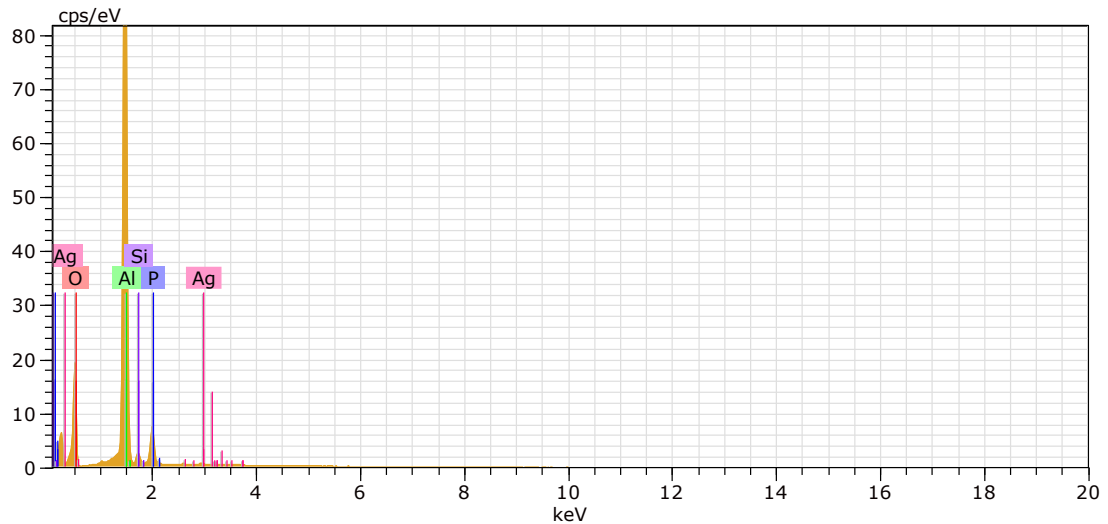


83 Date:4/25/2020 1:11:32 PM HV:20.0kV Puls th.:19.52kcps

El AN Series un. C norm. C Atom. C Error (1 Sigma)
[wt.%) [wt.%) [at.%) [wt.%)

El	AN	Series	un. C [wt.%)	norm. C [wt.%)	Atom. C [at.%)	Error (1 Sigma) [wt.%)
O	8	K-series	25.92	35.20	48.12	3.09
Al	13	K-series	42.42	57.60	46.70	2.05
P	15	K-series	4.31	5.86	4.13	0.20
Si	14	K-series	0.99	1.35	1.05	0.07

Total: 73.65 100.00 100.00



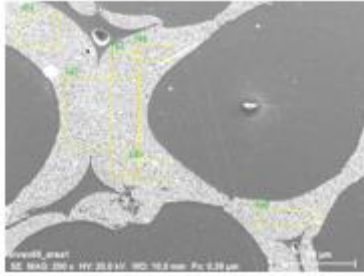
84 Date:4/25/2020 1:12:12 PM HV:20.0kV Puls th.:19.05kcps

El AN Series un. C norm. C Atom. C Error (1 Sigma)
[wt.%) [wt.%) [at.%) [wt.%)

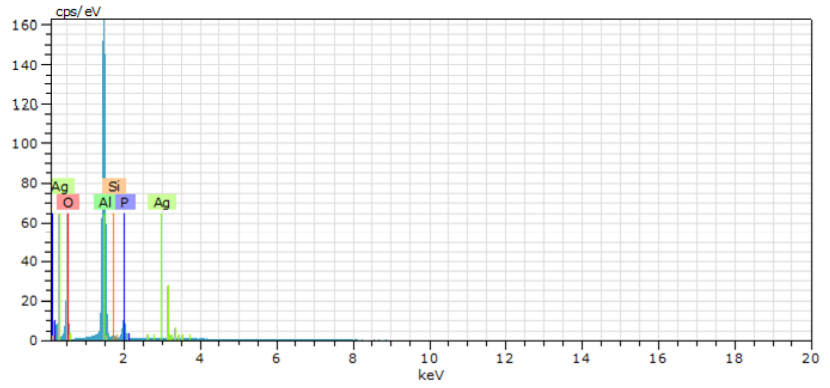
El	AN	Series	un. C [wt.%)	norm. C [wt.%)	Atom. C [at.%)	Error (1 Sigma) [wt.%)
O	8	K-series	13.97	35.15	48.34	1.68
Al	13	K-series	22.13	55.68	45.42	1.08
P	15	K-series	2.82	7.09	5.04	0.14
Si	14	K-series	0.54	1.35	1.06	0.05
Ag	47	L-series	0.29	0.73	0.15	0.04

Total: 39.74 100.00 100.00

F EDS RawData Sivex 65

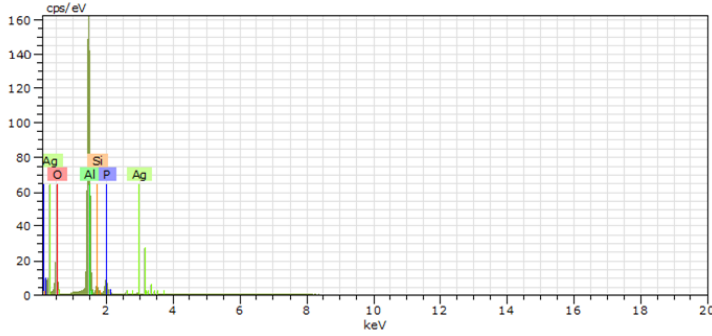


Sivex65_area1
 Date:26.04.2020 11:56:05
 Image size:1024 x 768
 Mag:200x
 HV:20,0kV



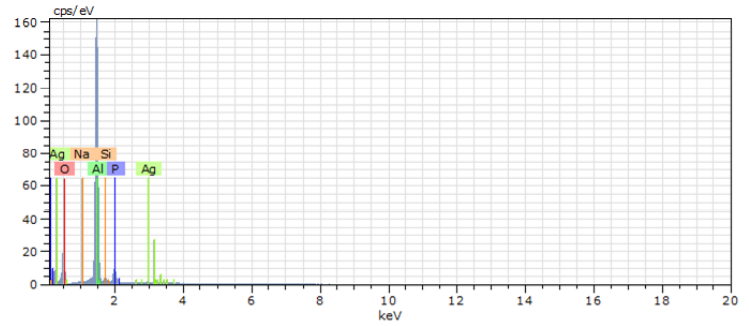
147 Date:26.04.2020 11:57:49 HV:20,0kV Puls th.:26,92kcps

El	AN	Series	unn. C [wt.%]	norm. C [wt.%]	Atom. C [at.%]	Error (1 Sigma) [wt.%]
Al	13	K-series	42,75	58,26	47,57	2,06
O	8	K-series	25,32	34,50	47,51	2,96
P	15	K-series	4,12	5,61	3,99	0,19
Si	14	K-series	0,76	1,04	0,81	0,06
Ag	47	L-series	0,43	0,58	0,12	0,04
Total:			73,37	100,00	100,00	



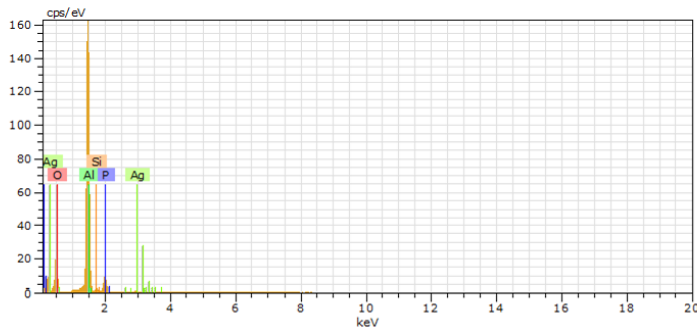
148 Date:26.04.2020 11:58:29 HV:20,0kV Puls th.:26,98kcps

El	AN	Series	unn. C [wt.%]	norm. C [wt.%]	Atom. C [at.%]	Error (1 Sigma) [wt.%]
O	8	K-series	23,63	34,41	47,38	2,77
Al	13	K-series	39,39	57,34	46,82	1,90
P	15	K-series	3,41	4,97	3,53	0,16
Si	14	K-series	1,89	2,75	2,16	0,11
Ag	47	L-series	0,37	0,54	0,11	0,04
Total:			68,69	100,00	100,00	



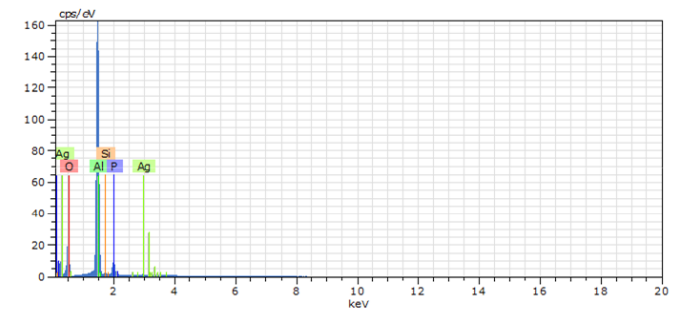
149 Date:26.04.2020 11:59:10 HV:20,0kV Puls th.:26,93kcps

El	AN	Series	unn. C [wt.%]	norm. C [wt.%]	Atom. C [at.%]	Error (1 Sigma) [wt.%]
Al	13	K-series	41,24	58,14	47,50	1,99
O	8	K-series	24,19	34,09	46,98	2,83
P	15	K-series	3,60	5,07	3,61	0,17
Si	14	K-series	1,17	1,65	1,30	0,08
Na	11	K-series	0,37	0,53	0,51	0,05
Ag	47	L-series	0,37	0,52	0,11	0,04
Total:			70,94	100,00	100,00	



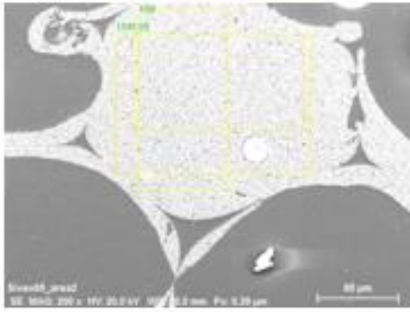
150 Date:26.04.2020 11:59:50 HV:20,0kV Puls th.:26,58kcps

El	AN	Series	unn. C [wt.%]	norm. C [wt.%]	Atom. C [at.%]	Error (1 Sigma) [wt.%]
O	8	K-series	16,19	34,97	48,16	1,90
Al	13	K-series	26,42	57,08	46,61	1,29
P	15	K-series	2,89	6,25	4,44	0,14
Si	14	K-series	0,34	0,74	0,58	0,04
Ag	47	L-series	0,44	0,96	0,20	0,04
Total:			46,28	100,00	100,00	



151 Date:26.04.2020 12:00:31 HV:20,0kV Puls th.:26,52kcps

El	AN	Series	unn. C [wt.%]	norm. C [wt.%]	Atom. C [at.%]	Error (1 Sigma) [wt.%]
Al	13	K-series	41,65	59,03	48,18	2,01
O	8	K-series	24,27	34,41	47,36	2,85
P	15	K-series	3,53	5,00	3,55	0,16
Si	14	K-series	0,72	1,01	0,80	0,06
Ag	47	L-series	0,39	0,55	0,11	0,04
Total:			70,55	100,00	100,00	



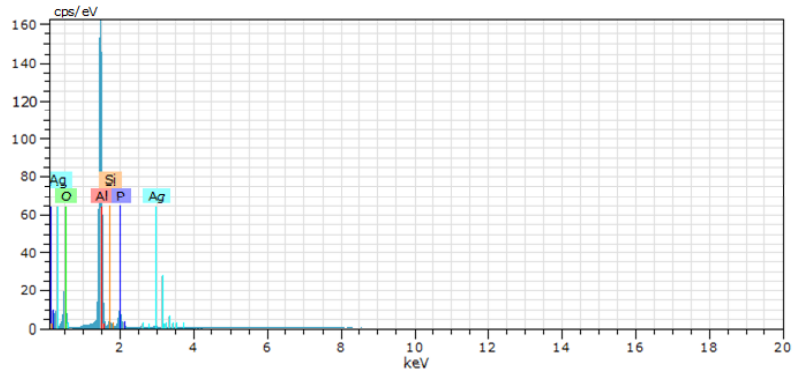
Sivex65_area2

Date:26.04.2020 12:05:00

Image size:1024 x 768

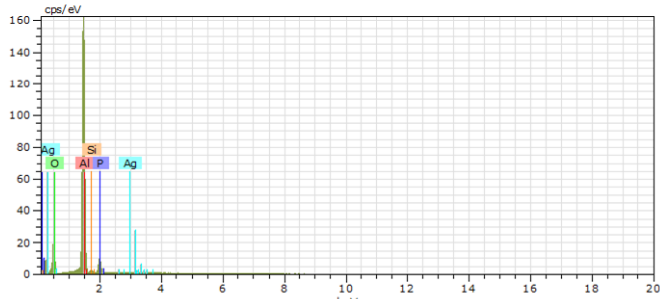
Mag:200x

HV:20,0kV



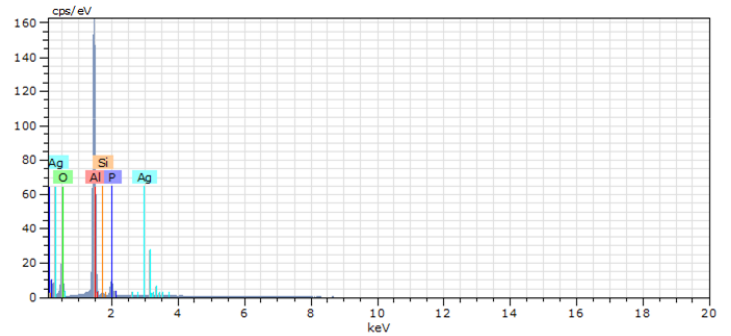
154 Date:26.04.2020 12:05:46 HV:20,0kV Puls th.:27,05kcps

El	AN	Series	unn. C [wt.%]	norm. C [wt.%]	Atom. C [at.%]	Error (1 Sigma) [wt.%]
Al	13	K-series	43,06	58,39	47,67	2,08
O	8	K-series	25,37	34,40	47,36	2,97
P	15	K-series	3,65	4,95	3,52	0,17
Si	14	K-series	1,26	1,71	1,34	0,08
Ag	47	L-series	0,41	0,55	0,11	0,04
Total:			73,76	100,00	100,00	



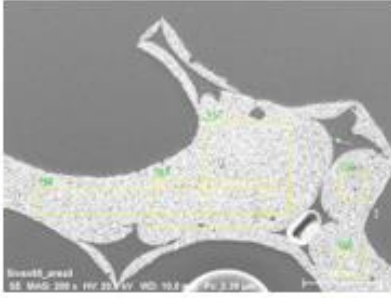
155 Date:26.04.2020 12:06:27 HV:20,0kV Puls th.:27,08kcps

El	AN	Series	unn. C [wt.%]	norm. C [wt.%]	Atom. C [at.%]	Error (1 Sigma) [wt.%]
Al	13	K-series	42,66	58,85	48,02	2,06
O	8	K-series	25,01	34,51	47,48	2,92
P	15	K-series	3,66	5,05	3,59	0,17
Si	14	K-series	0,73	1,01	0,79	0,06
Ag	47	L-series	0,42	0,58	0,12	0,04
Total:			72,49	100,00	100,00	

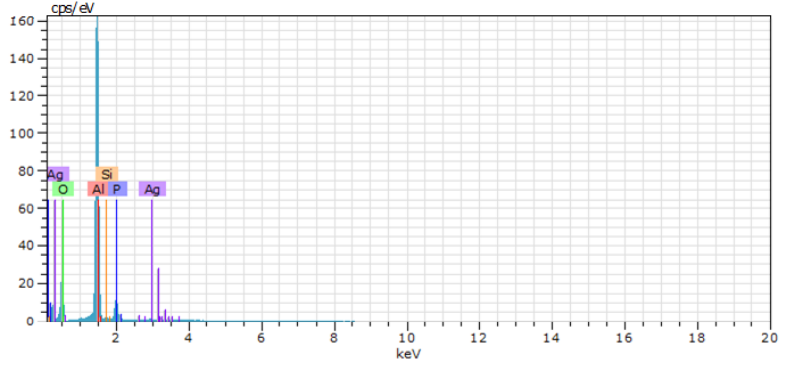


156 Date:26.04.2020 12:07:07 HV:20,0kV Puls th.:27,07kcps

El	AN	Series	unn. C [wt.%]	norm. C [wt.%]	Atom. C [at.%]	Error (1 Sigma) [wt.%]
Al	13	K-series	40,38	58,61	47,77	1,95
O	8	K-series	23,89	34,67	47,65	2,79
P	15	K-series	3,49	5,07	3,60	0,16
Si	14	K-series	0,77	1,11	0,87	0,06
Ag	47	L-series	0,37	0,53	0,11	0,04
Total:			68,89	100,00	100,00	

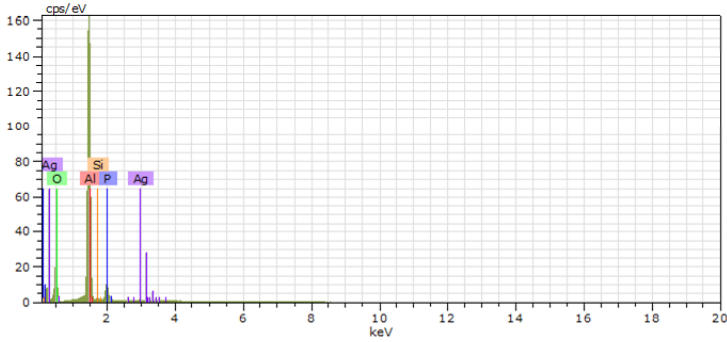


Sivex65_area3
Date:26.04.2020 12:09:37
Image size:1024 x 768
Mag:200x
HV:20,0kV



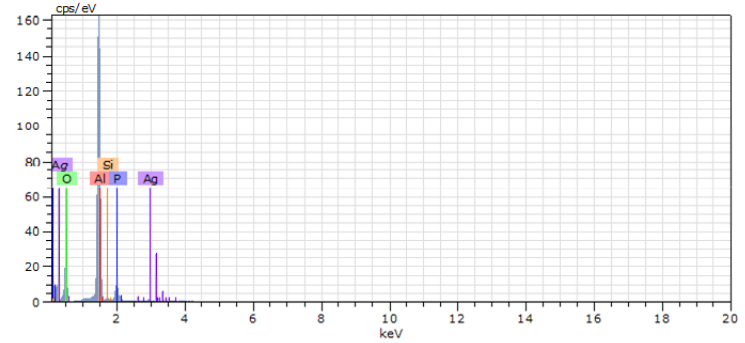
157 Date:26.04.2020 12:10:41 HV:20,0kV Puls th.:27,29kcps

El	AN	Series	unn. C [wt.%]	norm. C [wt.%]	Atom. C [at.%]	Error (1 Sigma) [wt.%]
O	8	K-series	25,60	34,79	47,83	2,98
Al	13	K-series	42,45	57,70	47,03	2,05
P	15	K-series	4,33	5,88	4,17	0,19
Si	14	K-series	0,80	1,09	0,85	0,06
Ag	47	L-series	0,40	0,54	0,11	0,04
Total:			73,58	100,00	100,00	



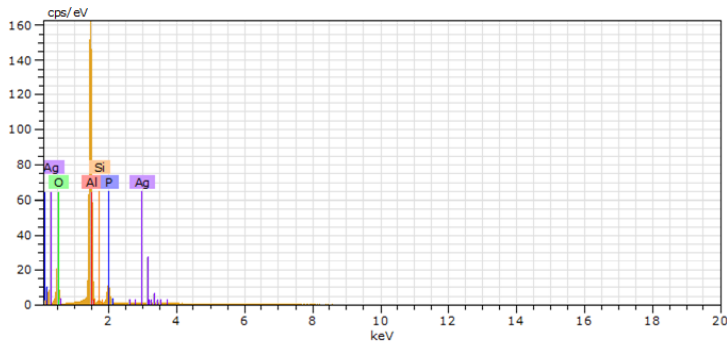
158 Date:26.04.2020 12:11:21 HV:20,0kV Puls th.:26,95kcps

El	AN	Series	unn. C [wt.%]	norm. C [wt.%]	Atom. C [at.%]	Error (1 Sigma) [wt.%]
O	8	K-series	24,78	34,67	47,68	2,89
Al	13	K-series	41,57	58,15	47,42	2,01
P	15	K-series	3,99	5,58	3,96	0,18
Si	14	K-series	0,76	1,06	0,83	0,06
Ag	47	L-series	0,39	0,55	0,11	0,04
Total:			71,49	100,00	100,00	



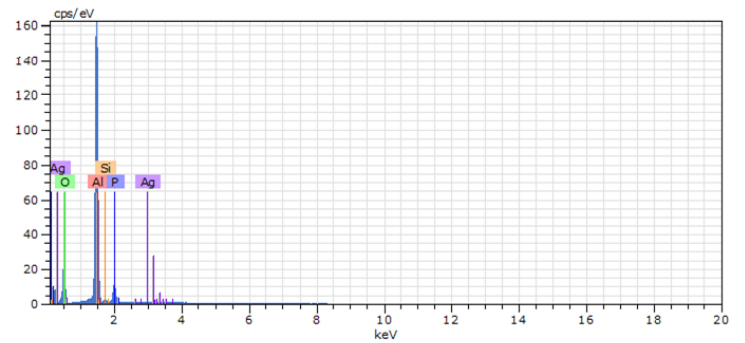
159 Date:26.04.2020 12:12:02 HV:20,0kV Puls th.:26,36kcps

El	AN	Series	unn. C [wt.%]	norm. C [wt.%]	Atom. C [at.%]	Error (1 Sigma) [wt.%]
Al	13	K-series	42,83	58,64	47,78	2,07
O	8	K-series	25,36	34,73	47,72	2,97
P	15	K-series	3,73	5,10	3,62	0,17
Si	14	K-series	0,71	0,97	0,76	0,06
Ag	47	L-series	0,41	0,56	0,12	0,04
Total:			73,04	100,00	100,00	



160 Date:26.04.2020 12:12:43 HV:20,0kV Puls th.:26,74kcps

El	AN	Series	unn. C [wt.%]	norm. C [wt.%]	Atom. C [at.%]	Error (1 Sigma) [wt.%]
O	8	K-series	25,71	34,96	48,02	3,00
Al	13	K-series	42,29	57,51	46,84	2,04
P	15	K-series	4,42	6,00	4,26	0,20
Si	14	K-series	0,73	1,00	0,78	0,06
Ag	47	L-series	0,39	0,53	0,11	0,04
Total:			73,54	100,00	100,00	



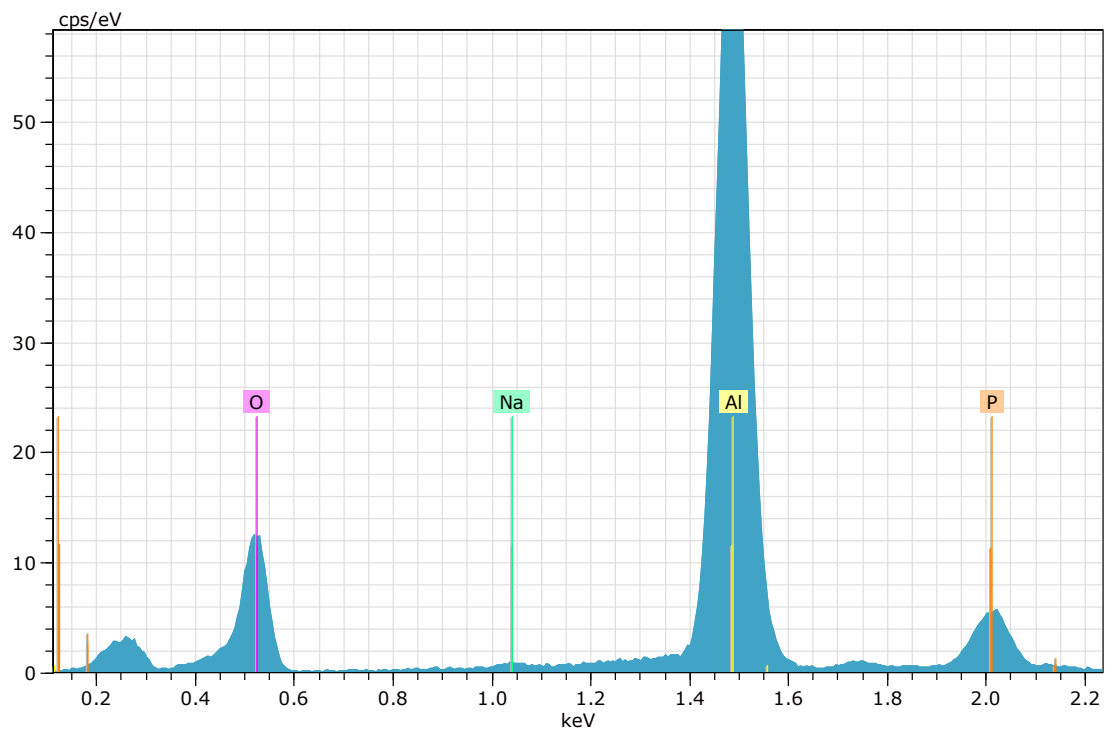
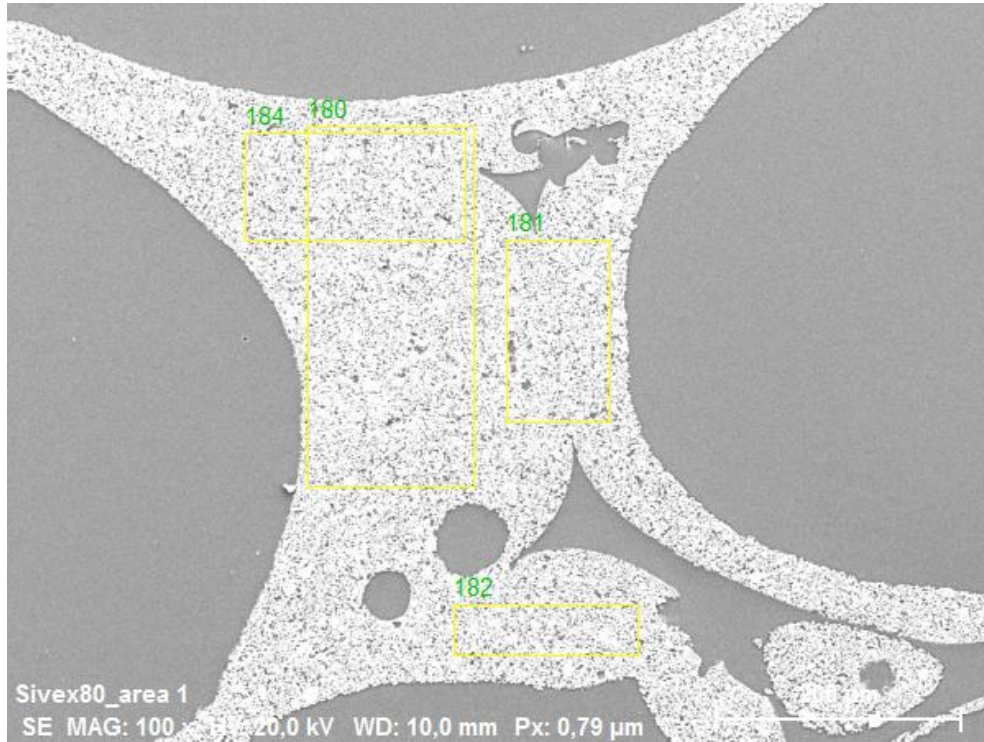
161 Date:26.04.2020 12:13:23 HV:20,0kV Puls th.:26,99kcps

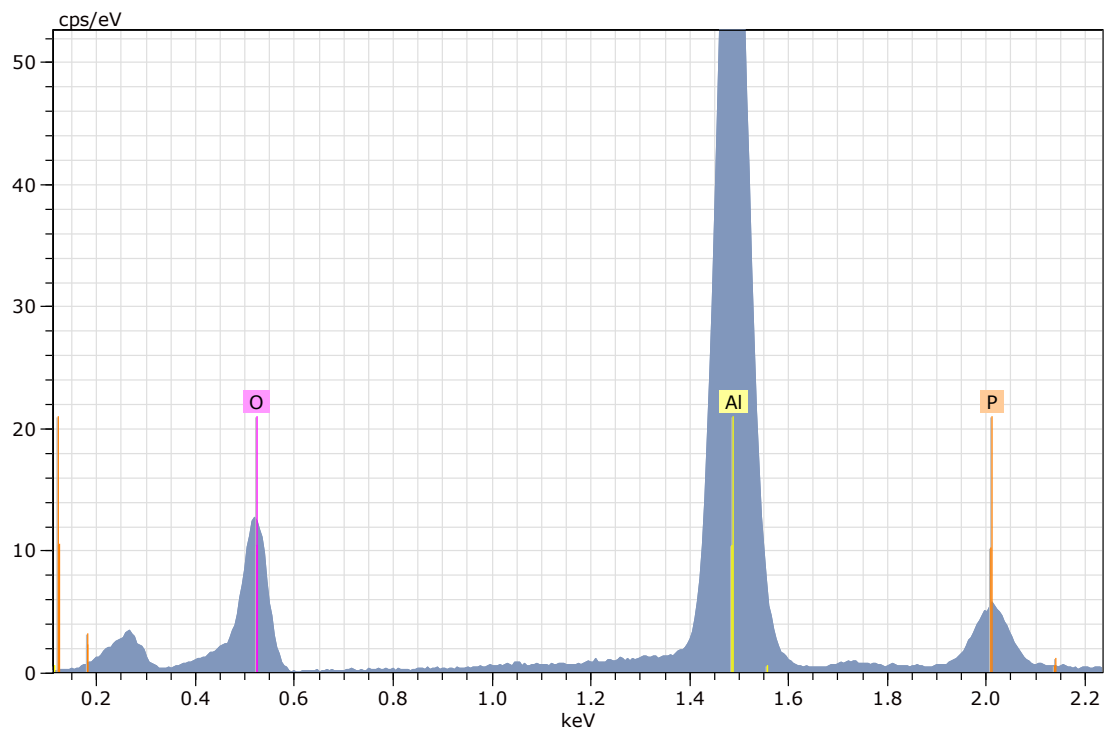
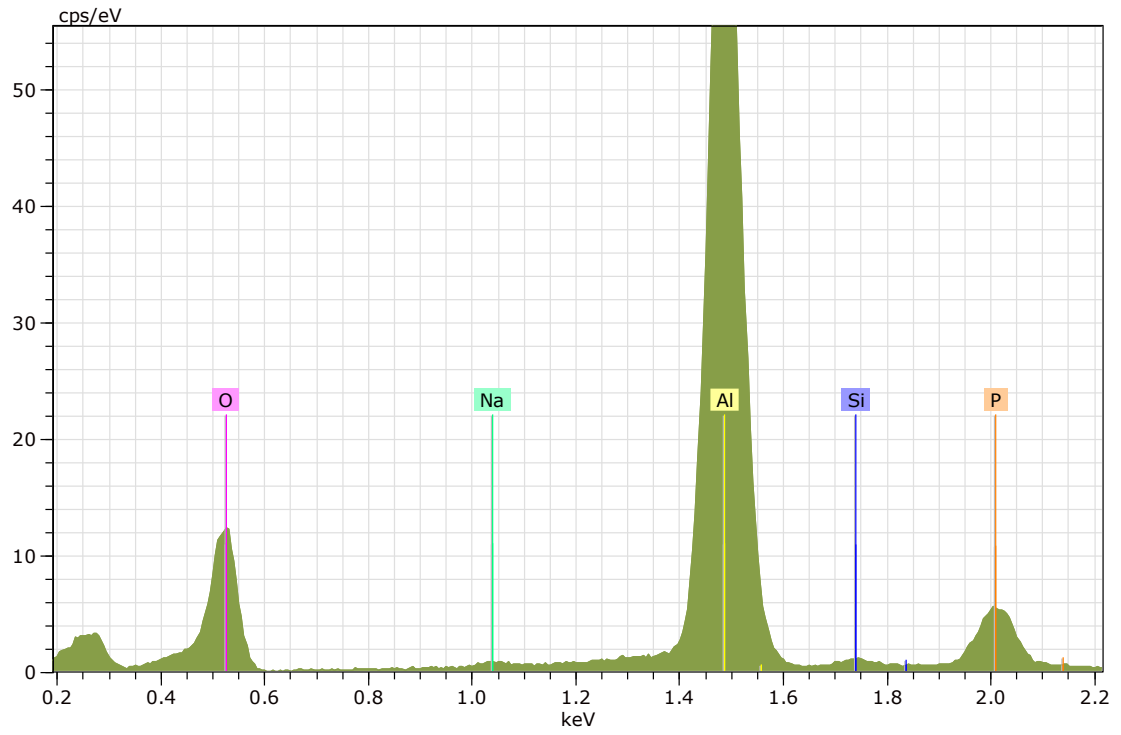
El	AN	Series	unn. C [wt.%]	norm. C [wt.%]	Atom. C [at.%]	Error (1 Sigma) [wt.%]
O	8	K-series	13,78	34,78	48,05	1,62
Al	13	K-series	22,12	55,84	45,75	1,08
P	15	K-series	3,06	7,72	5,51	0,15
Si	14	K-series	0,23	0,58	0,46	0,04
Ag	47	L-series	0,43	1,08	0,22	0,04
Total:			39,62	100,00	100,00	

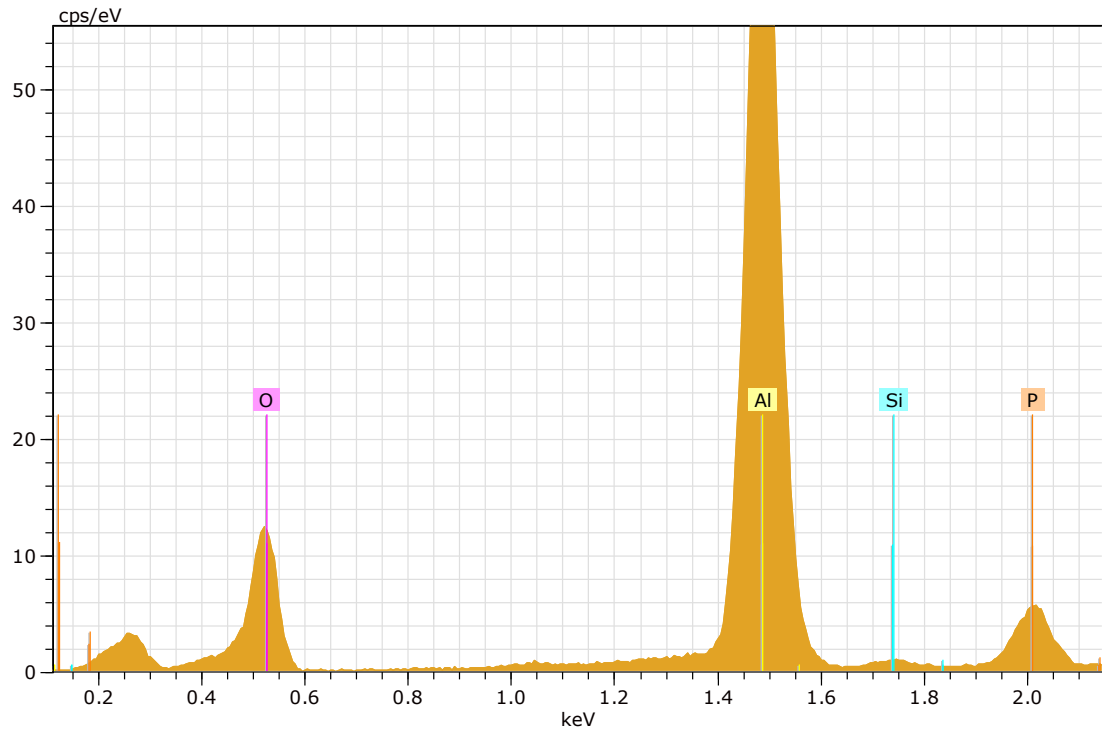
G EDS RawData Sivex 80

Application Note

Company / Department





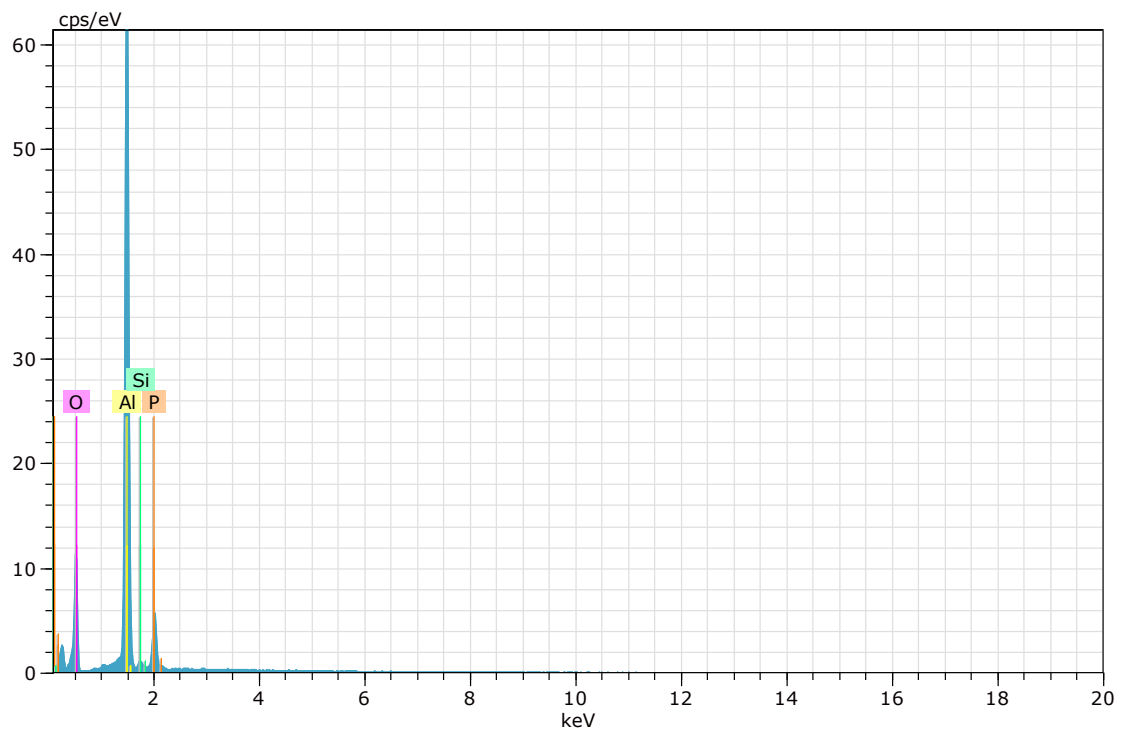
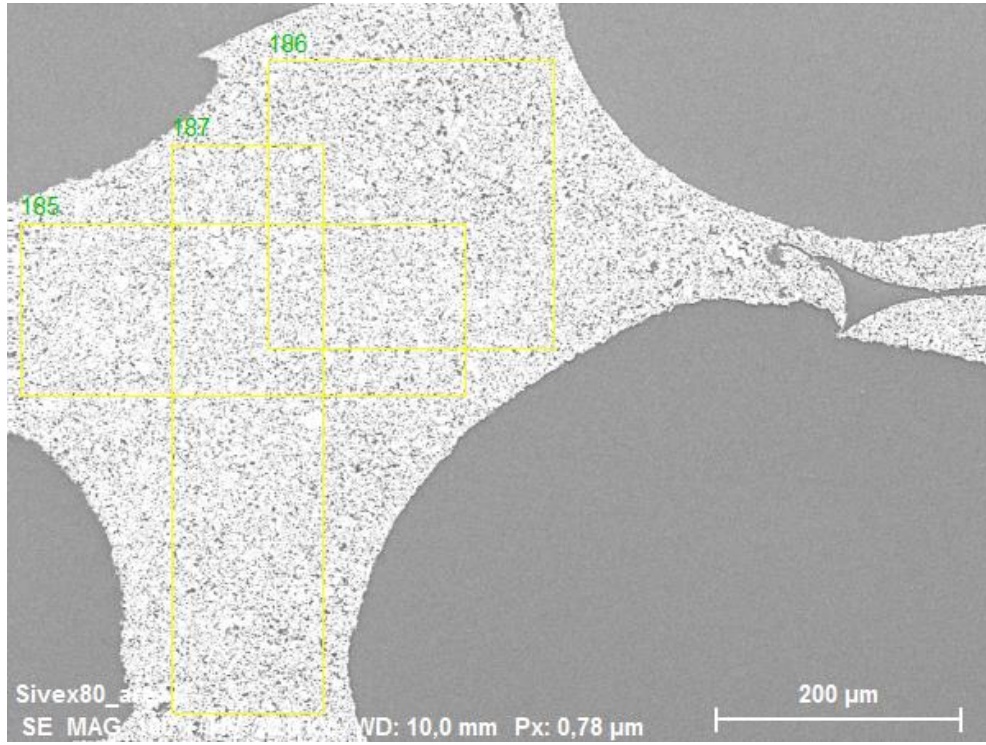


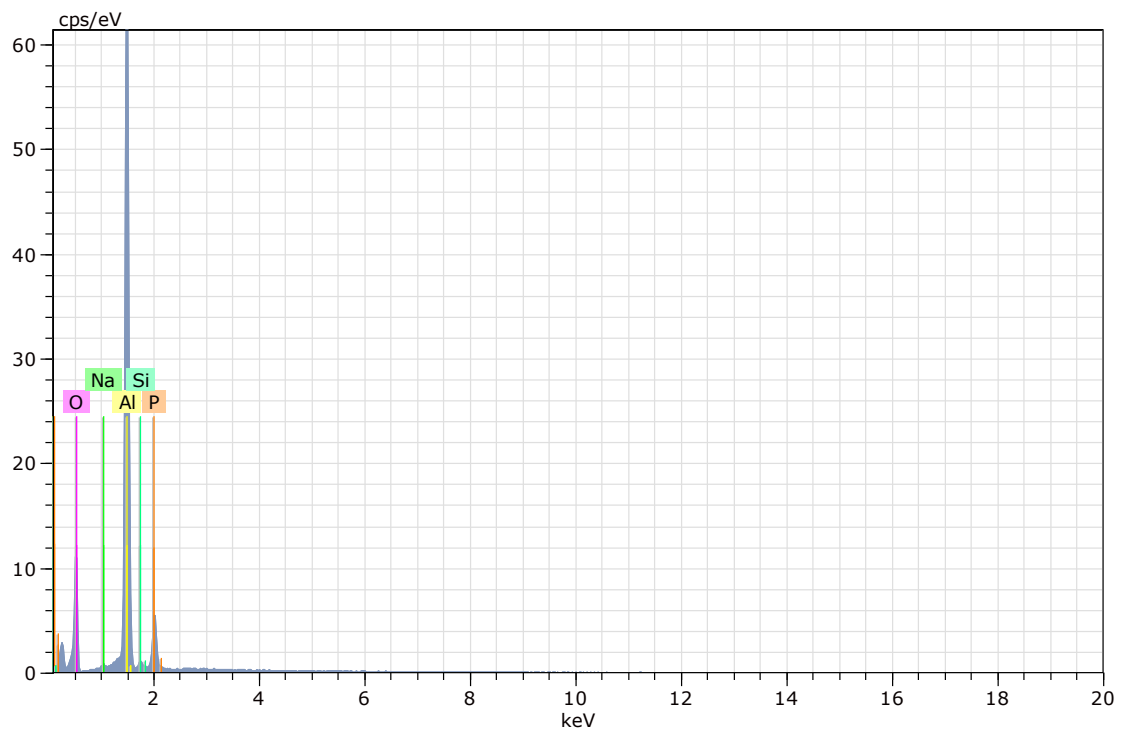
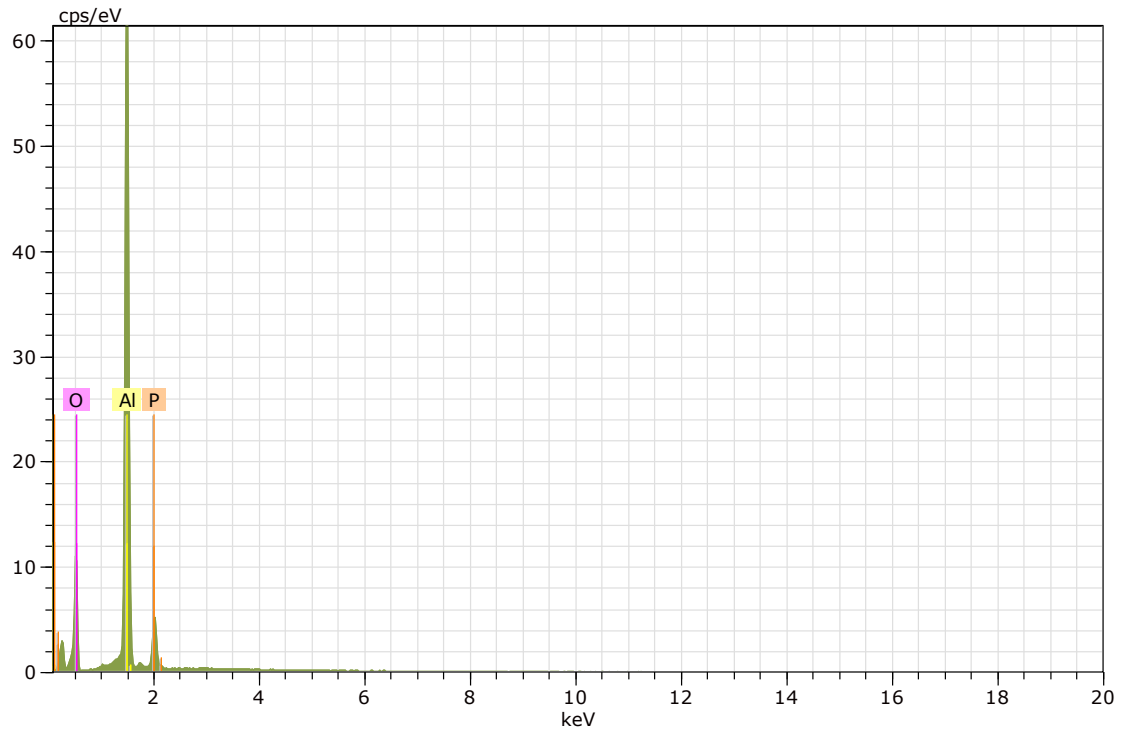
Atomic percent (%)

Spectrum O Na Al Si P

180	49,68	0,52	43,42	-	6,38
181	49,12	0,74	43,25	0,51	6,38
182	49,58	-	44,31	-	6,11
184	49,47	-	43,72	0,43	6,38

Mean value: 49,46 0,63 43,68 0,47 6,31
 Sigma: 0,24 0,15 0,47 0,06 0,13
 Sigma mean: 0,12 0,08 0,23 0,03 0,07



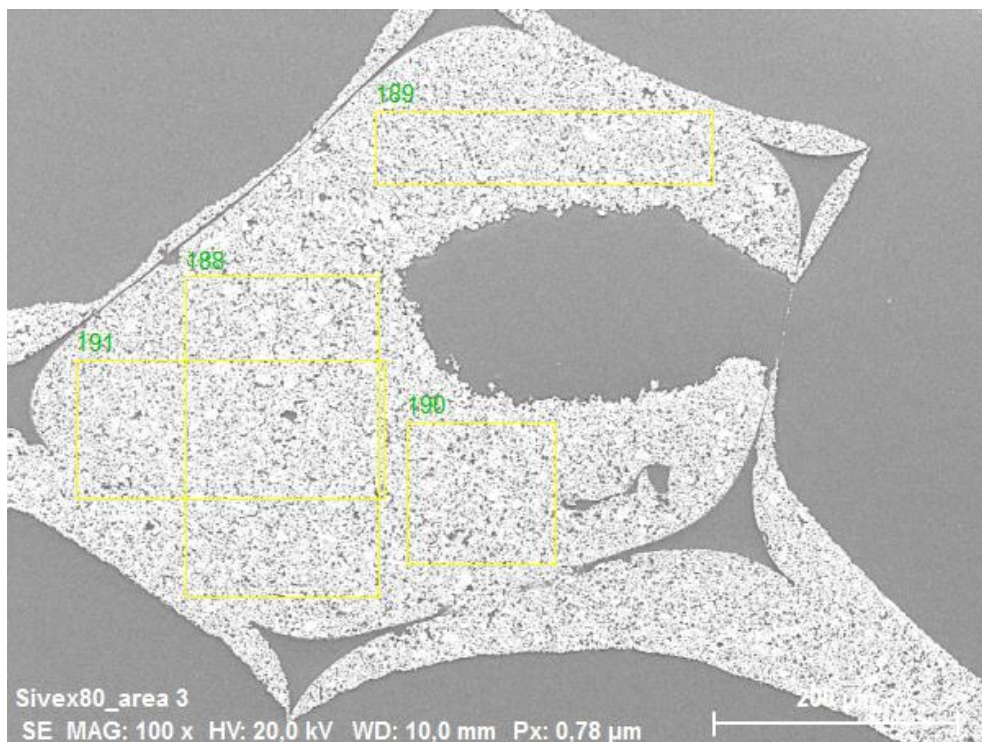


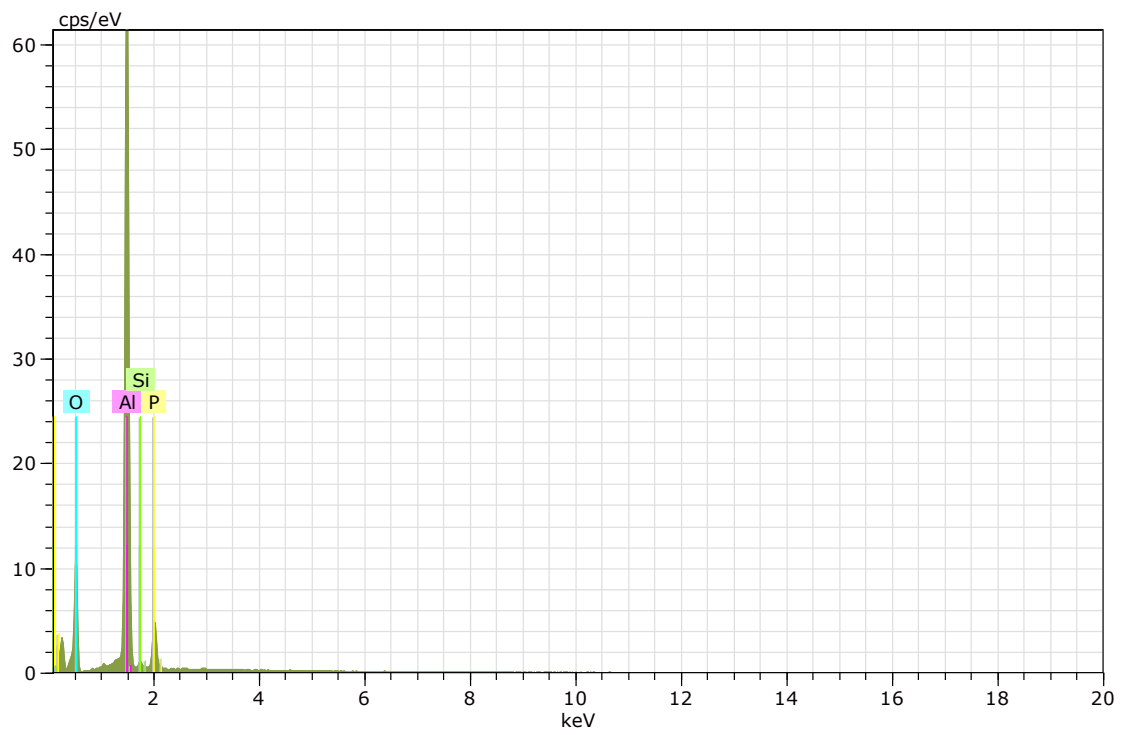
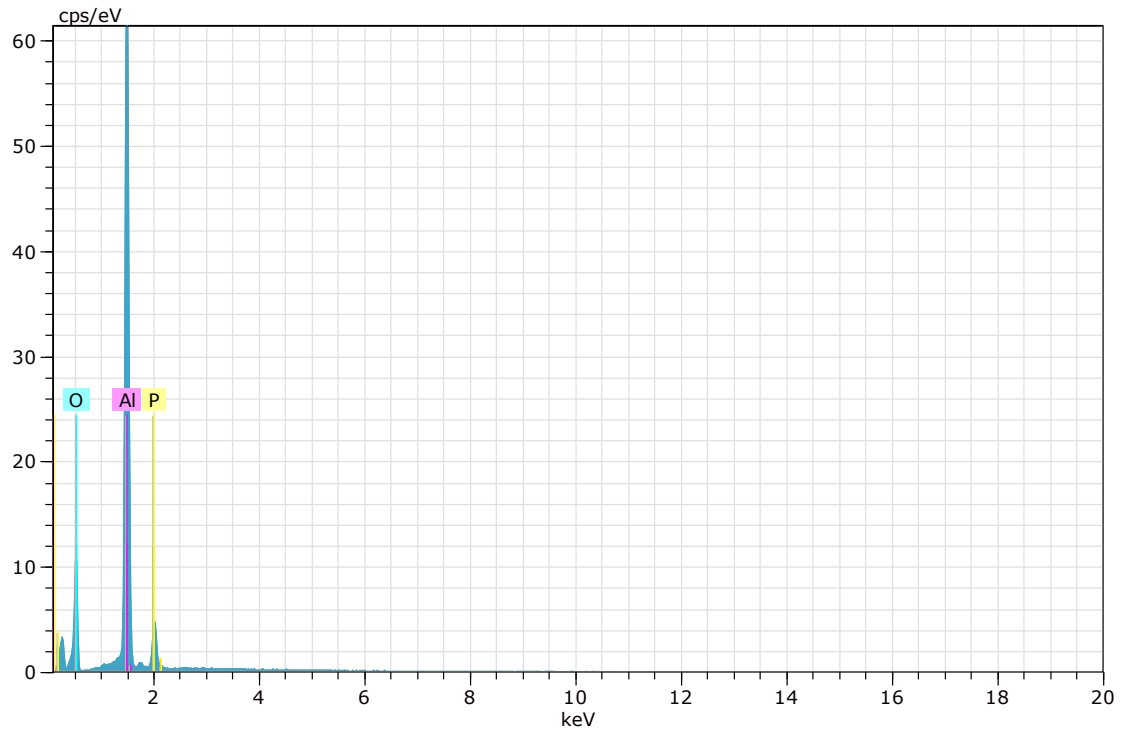
Atomic percent (%)

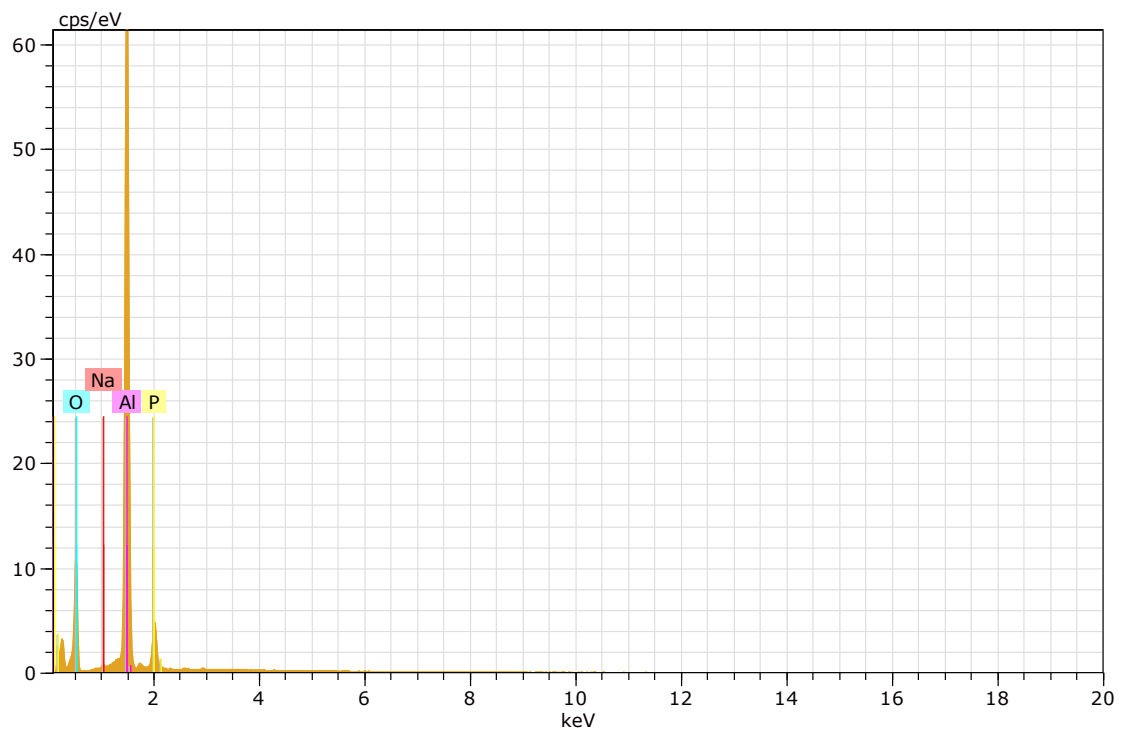
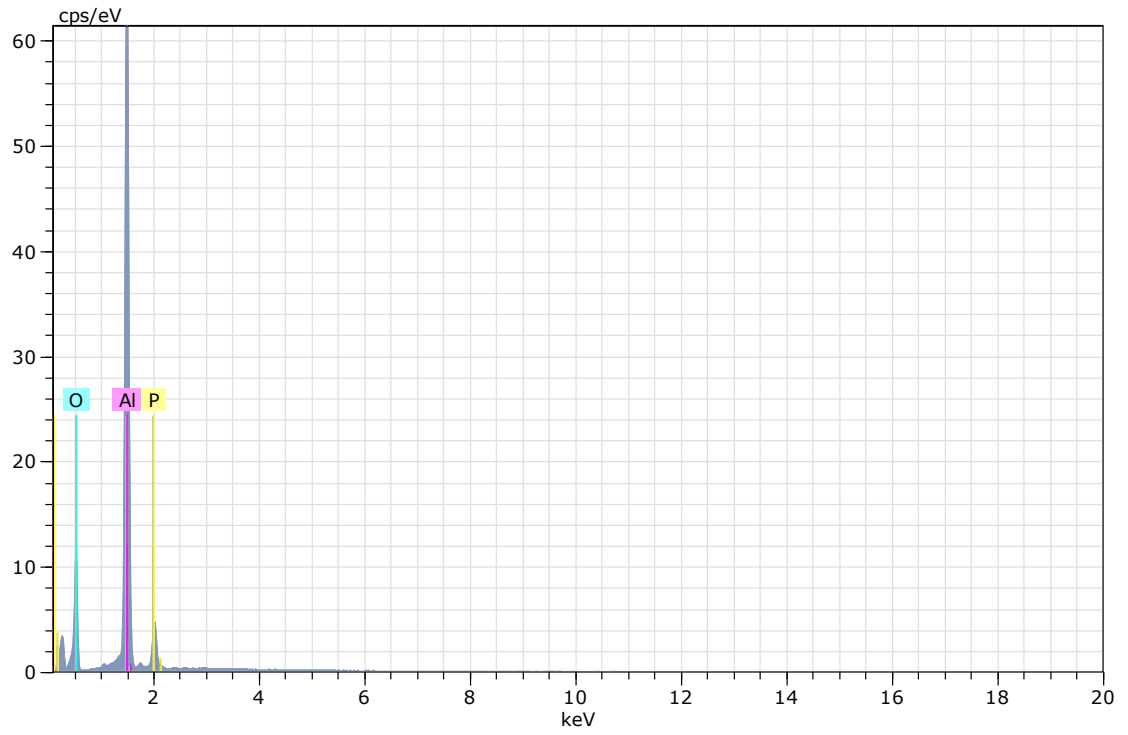
Spectrum O Na Al Si P

 185 49,61 - 43,34 0,59 6,46
 186 49,50 - 44,20 - 6,30
 187 49,50 0,52 42,99 0,50 6,50

Mean value: 49,53 0,52 43,51 0,54 6,42
 Sigma: 0,06 0,00 0,62 0,06 0,10
 Sigma mean: 0,04 0,00 0,36 0,03 0,06









Atomic percent (%)

Spectrum O Na Al Si P

188	49,24	-	44,62	-	6,14
189	48,97	-	44,57	0,49	5,97
190	49,27	-	44,87	-	5,85
191	49,00	0,48	44,53	-	6,00

Mean value: 49,12 0,48 44,65 0,49 5,99

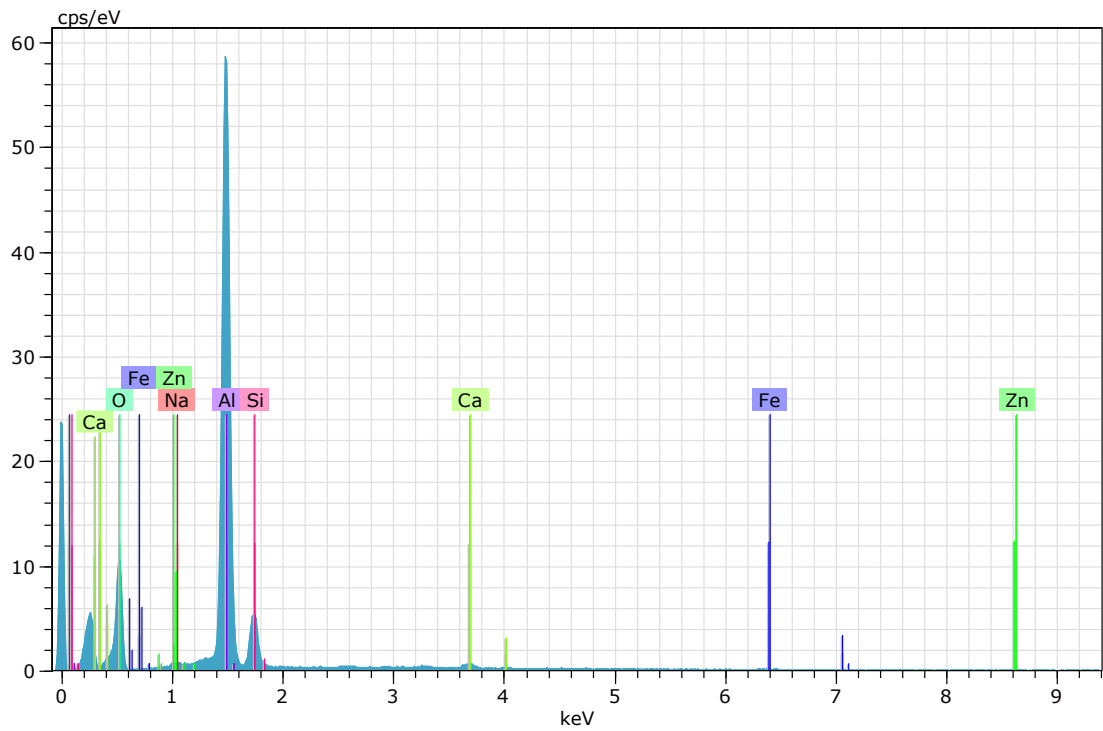
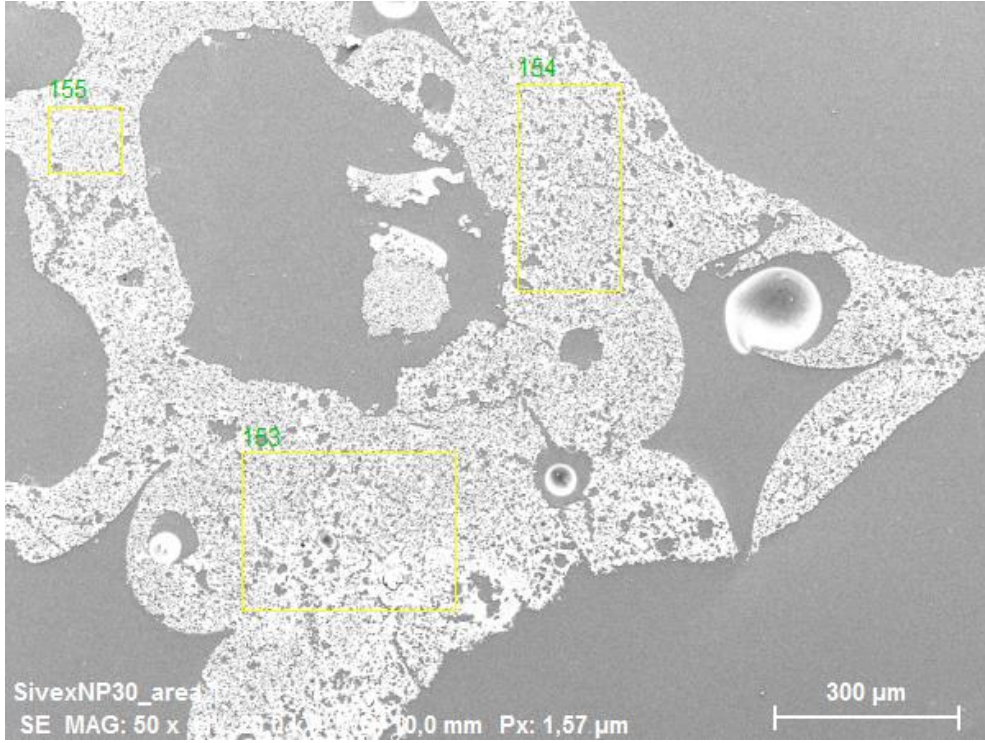
Sigma: 0,16 0,00 0,16 0,00 0,12

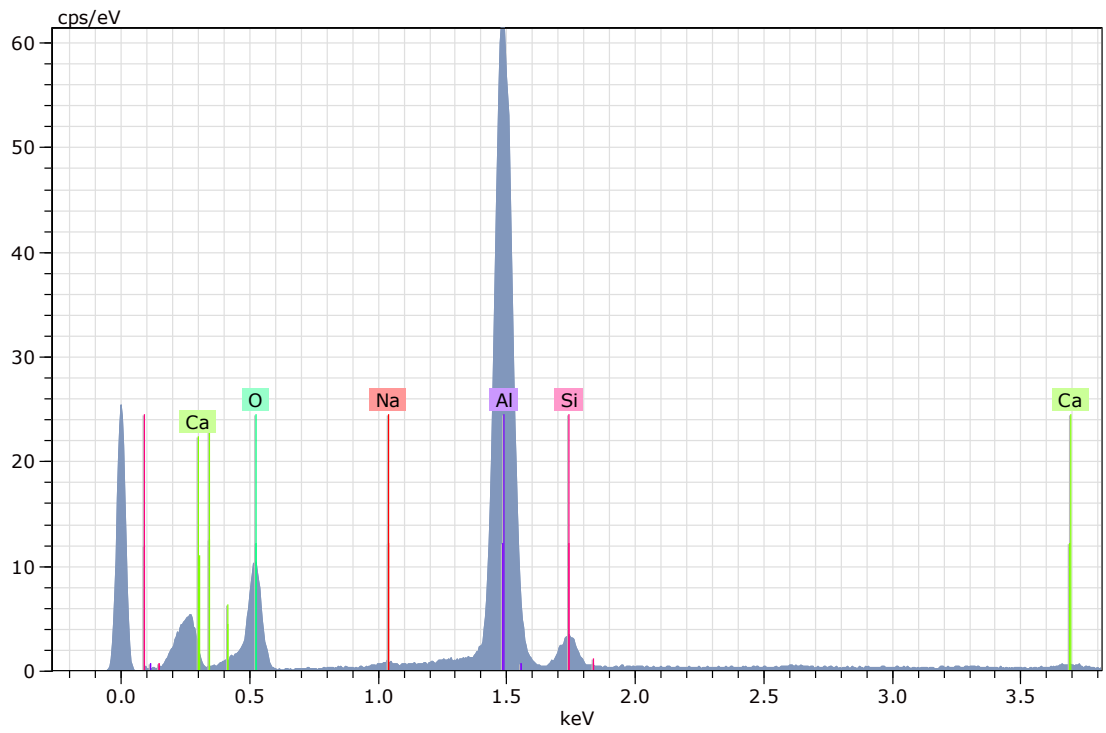
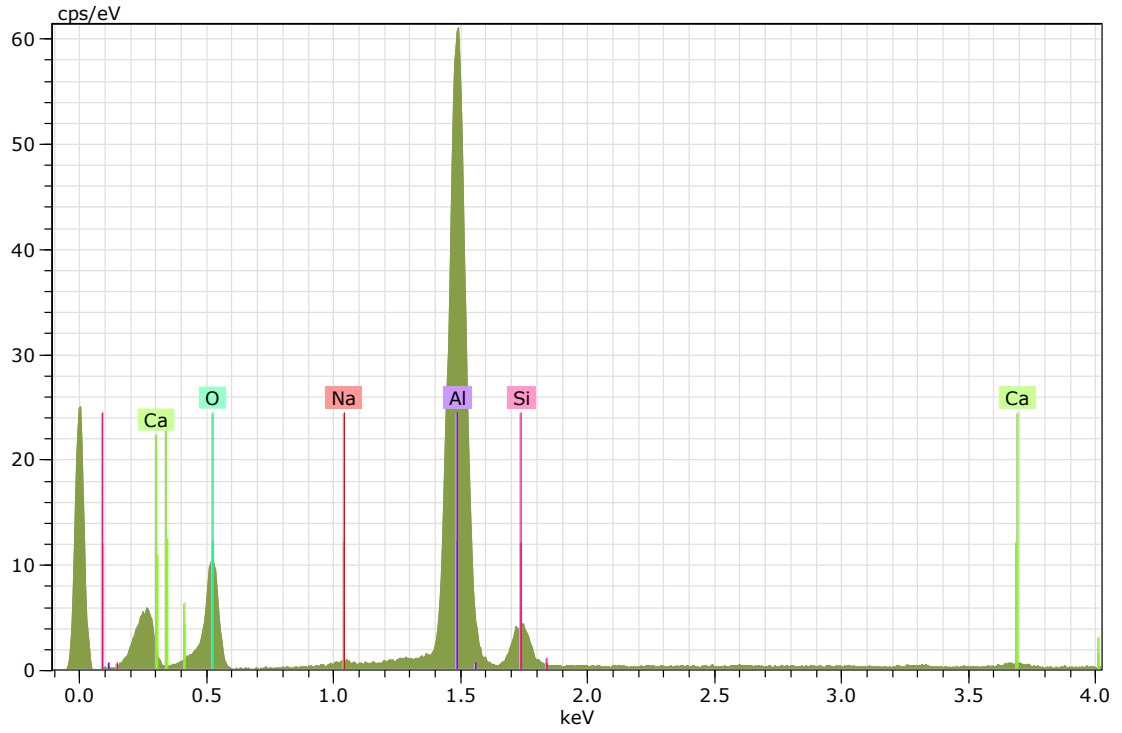
Sigma mean: 0,08 0,00 0,08 0,00 0,06

H EDS RawData SivexNP 30

Application Note

Company / Department



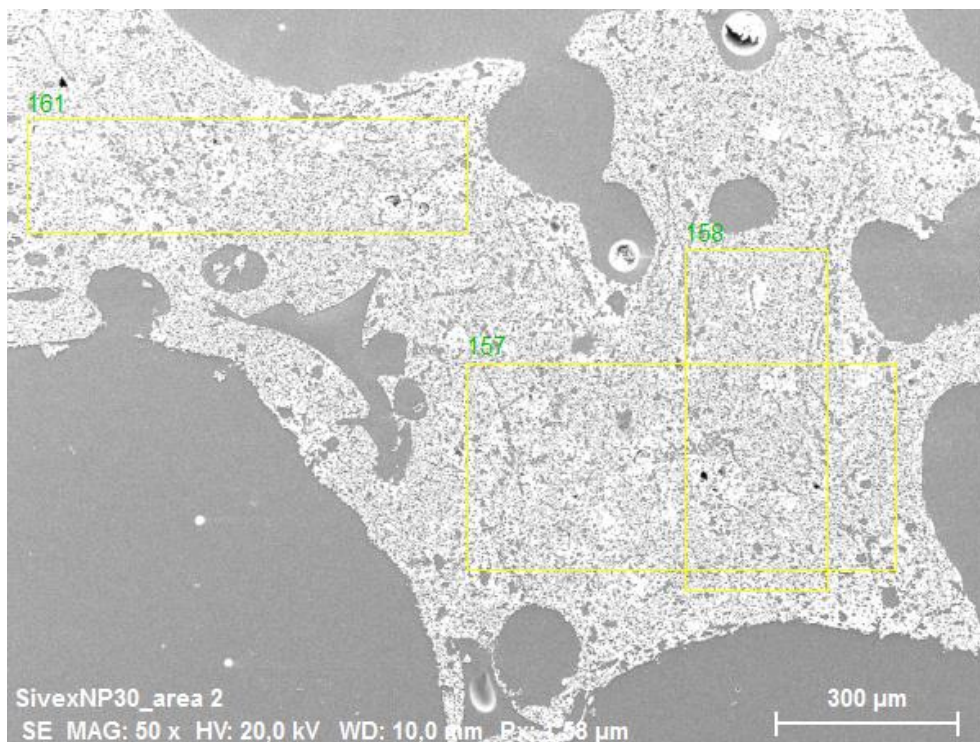


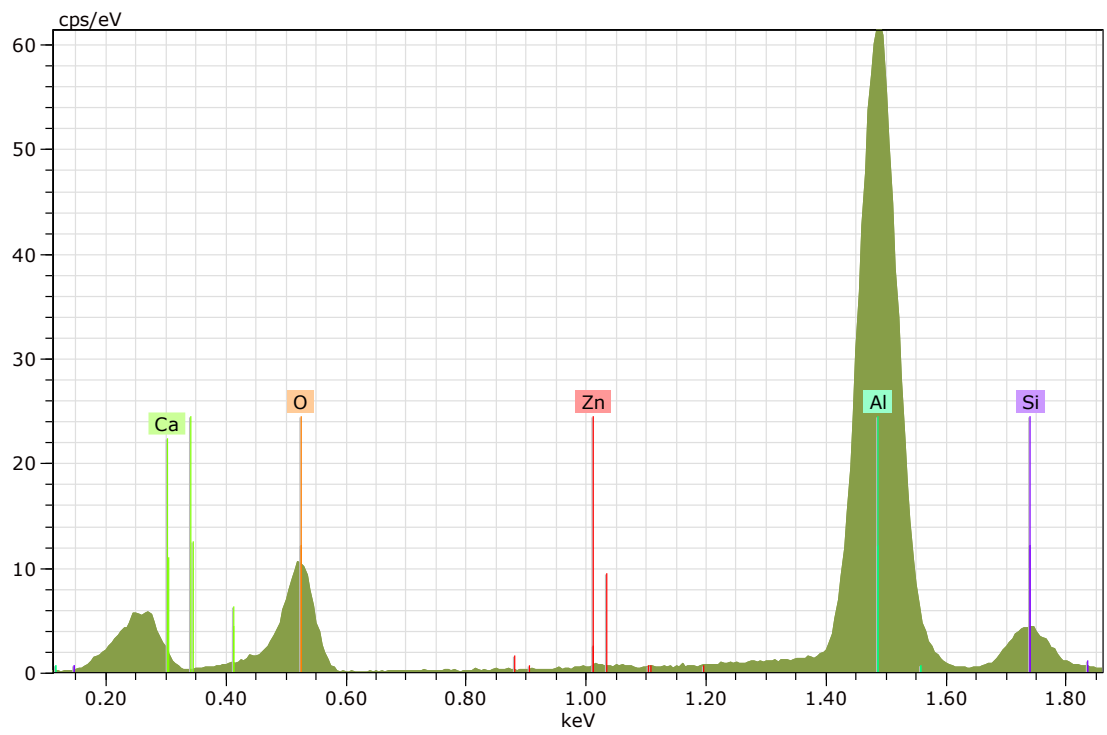
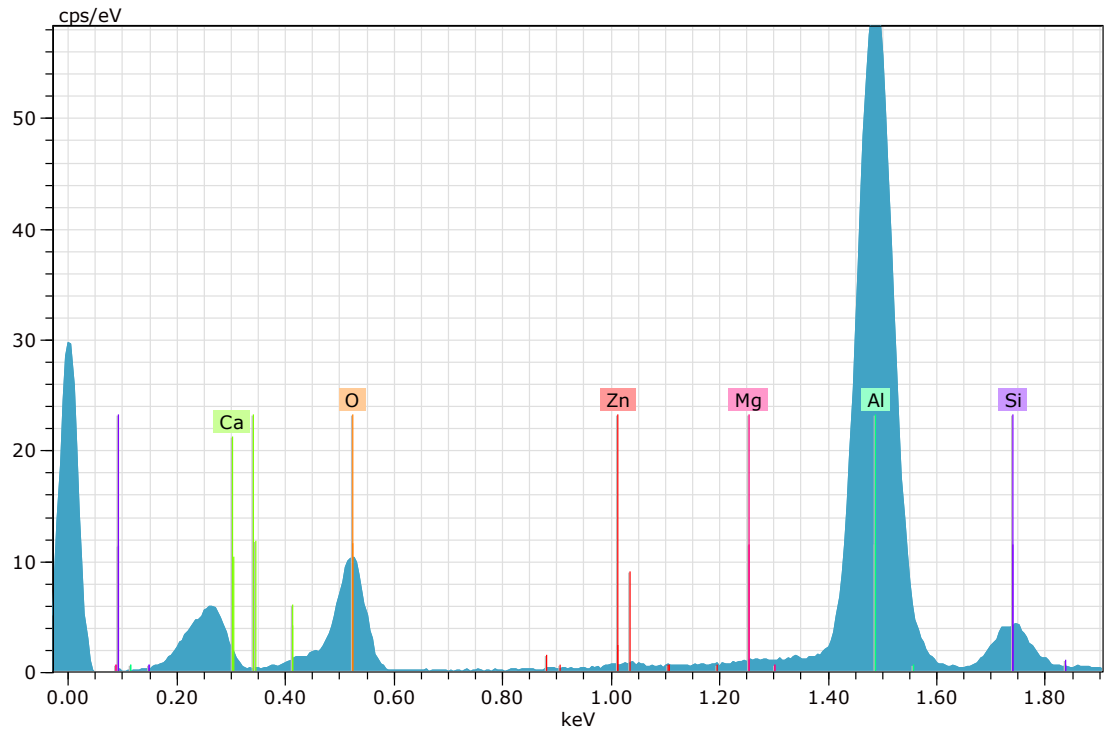
Atomic percent (%)

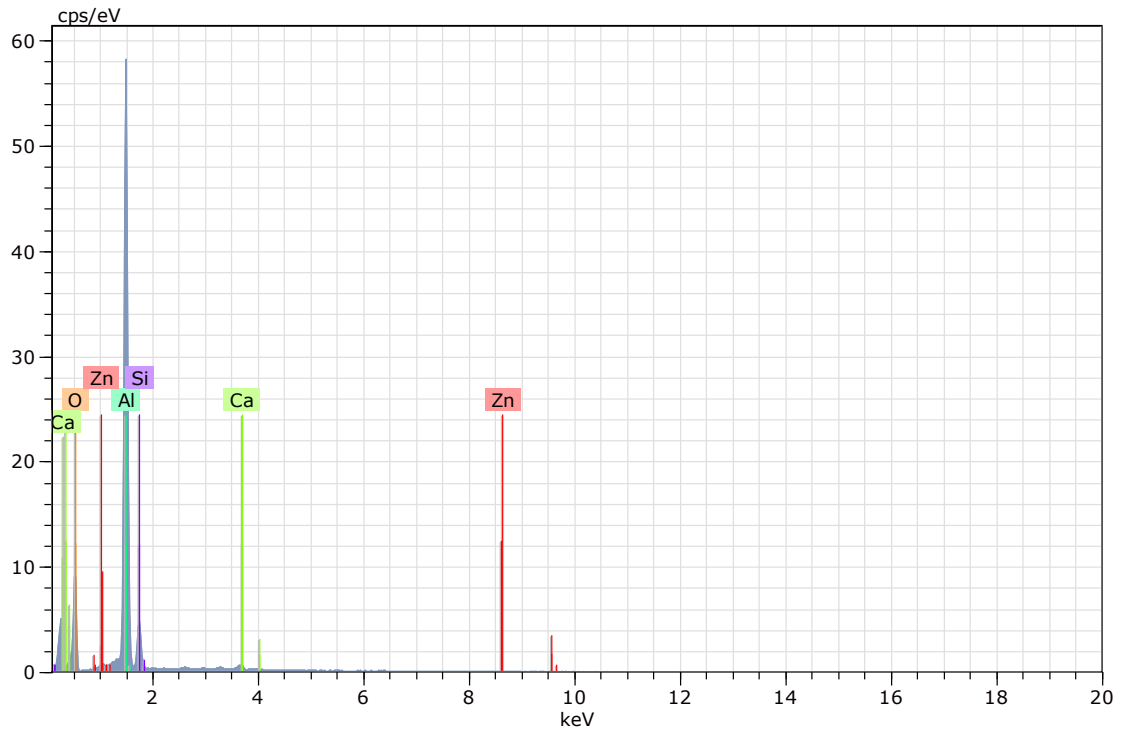
Spectrum O Na Al Si Ca Fe Zn

153	49,52	0,50	42,09	6,62	0,63	0,31	0,34
154	48,80	0,76	45,70	4,31	0,42	-	-
155	48,49	0,65	46,32	3,96	0,59	-	-

Mean value: 48,93 0,64 44,70 4,96 0,54 0,31 0,34
 Sigma: 0,53 0,13 2,29 1,44 0,11 0,00 0,00
 Sigma mean: 0,30 0,07 1,32 0,83 0,06 0,00 0,00



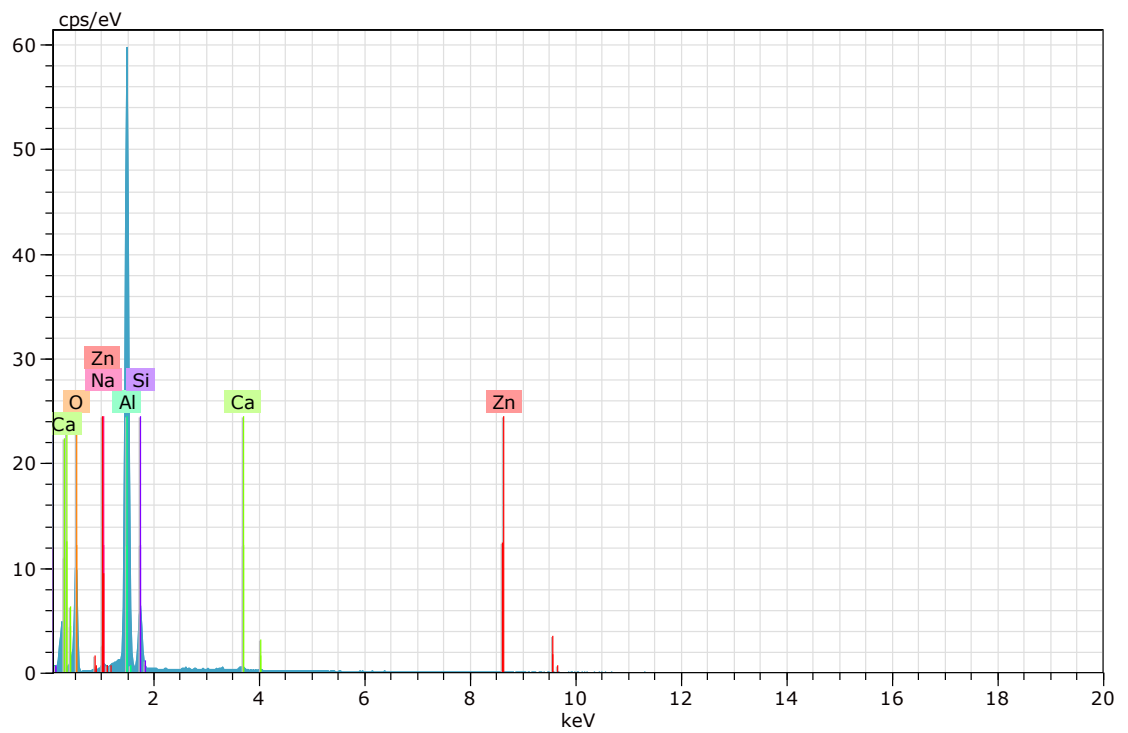
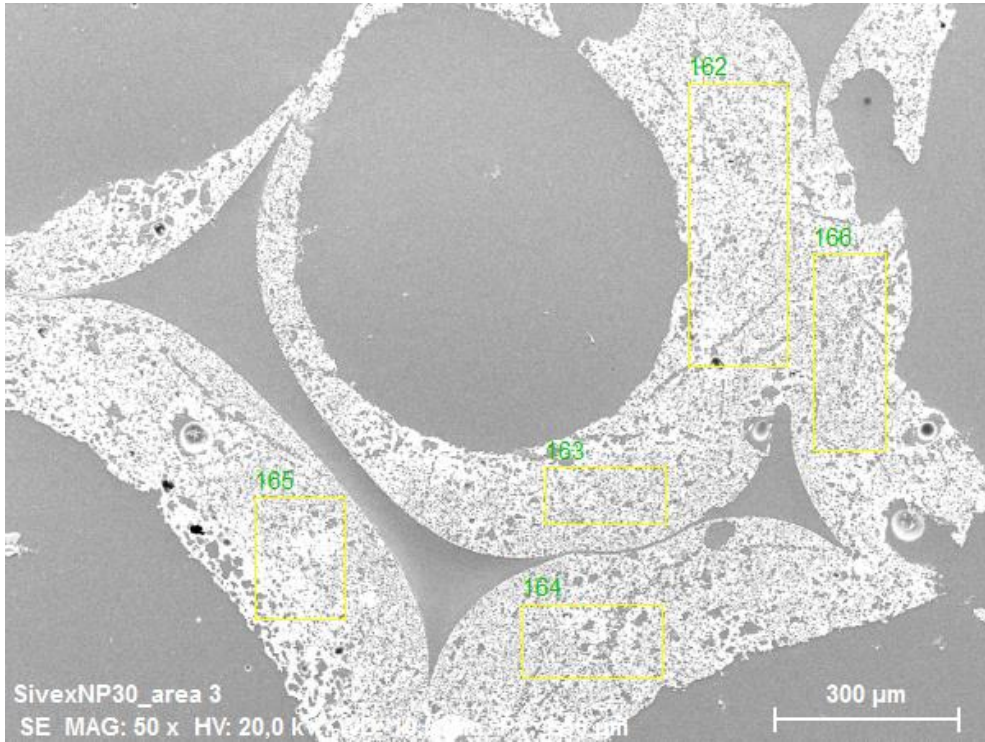


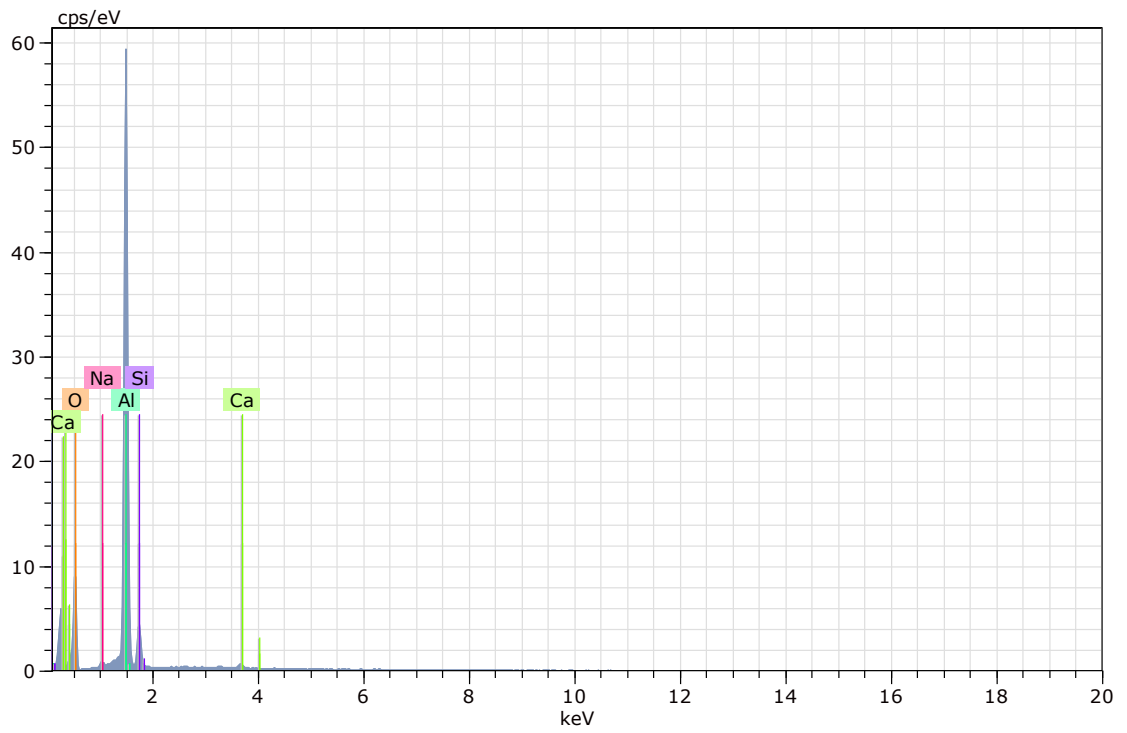
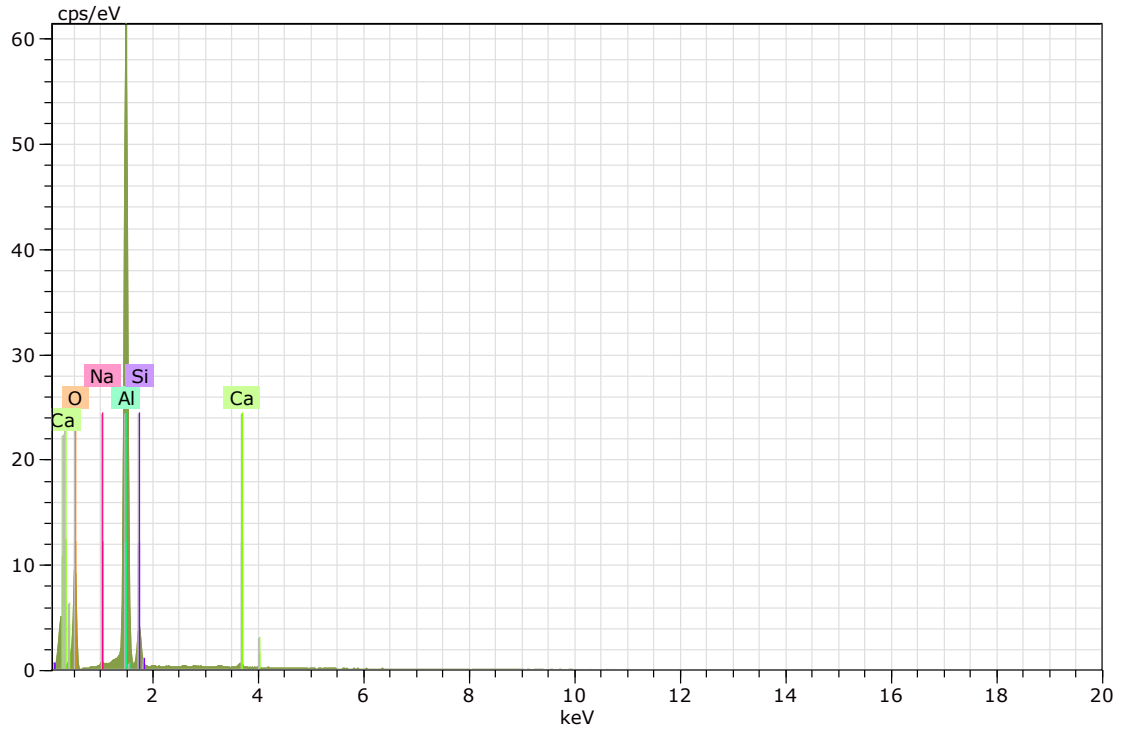


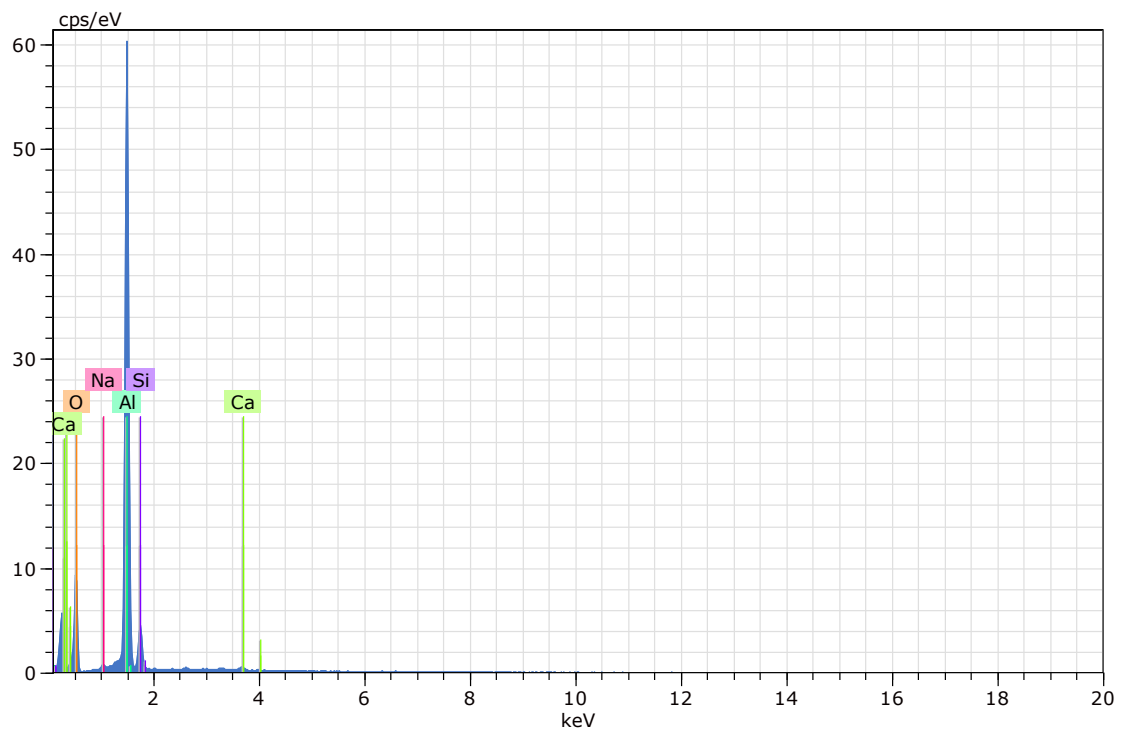
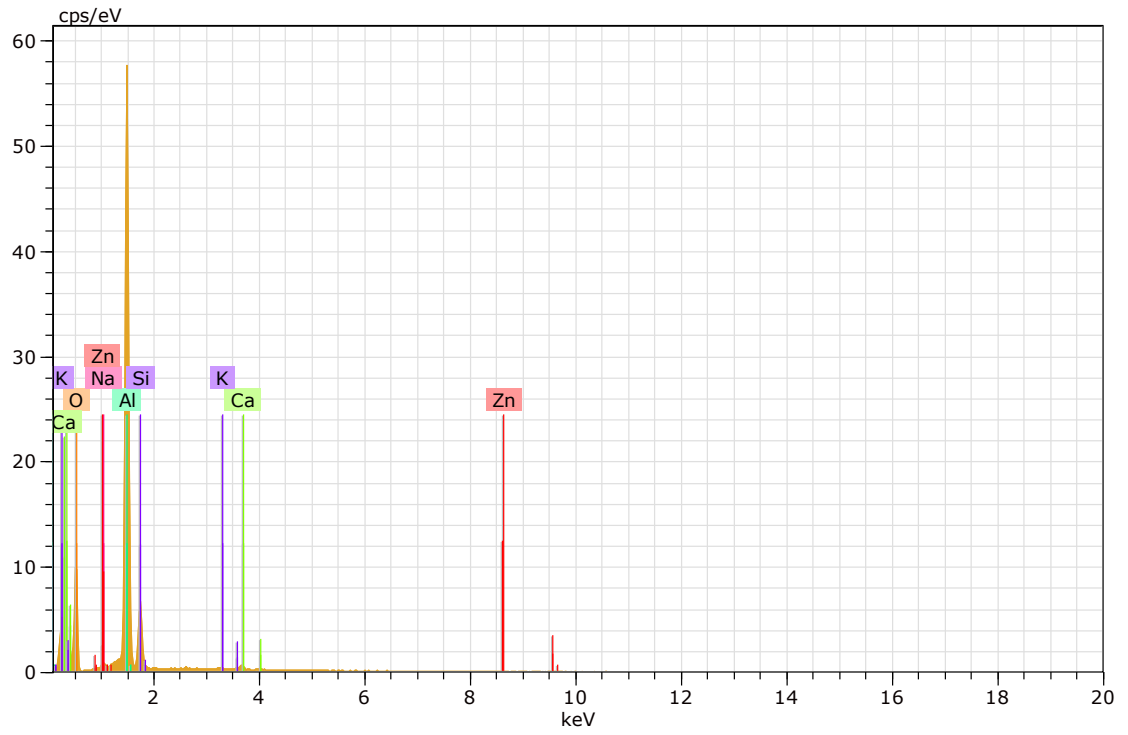
Atomic percent (%)

Spectrum	O	Mg	Al	Si	Ca	Zn
157	47,92	0,65	46,37	4,34	0,44	0,28
158	49,04	-	44,54	5,32	0,68	0,42
161	49,25	-	44,74	5,13	0,57	0,31

Mean value: 48,73 0,65 45,22 4,93 0,57 0,34
 Sigma: 0,72 0,00 1,01 0,52 0,12 0,07
 Sigma mean: 0,41 0,00 0,58 0,30 0,07 0,04









Atomic percent (%)

Spectrum O Na Al Si K Ca Zn

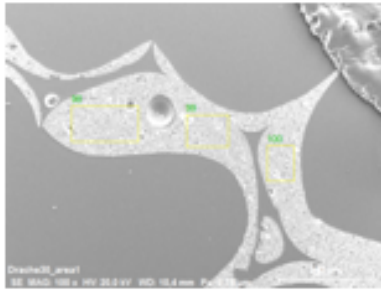
162	49,83	0,69	41,48	6,96	- 0,70	0,34
163	49,28	0,67	44,33	4,91	- 0,82	-
164	49,15	0,80	43,64	5,61	- 0,79	-
165	50,55	0,63	39,91	7,49	0,31	0,78 0,33
166	48,82	0,84	44,11	5,61	- 0,63	-

Mean value: 49,53 0,73 42,69 6,12 0,31 0,74 0,34

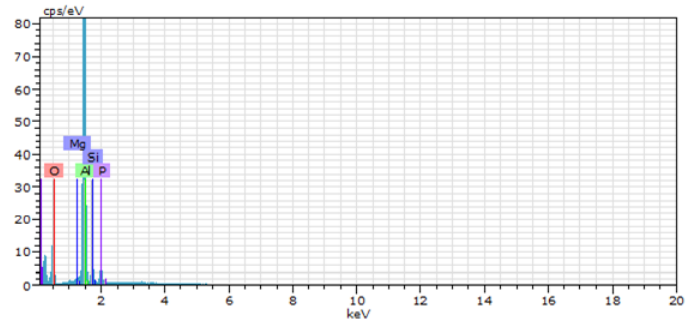
Sigma: 0,68 0,09 1,92 1,07 0,00 0,08 0,01

Sigma mean: 0,30 0,04 0,86 0,48 0,00 0,03 0,00

I EDS RawData Drache 30

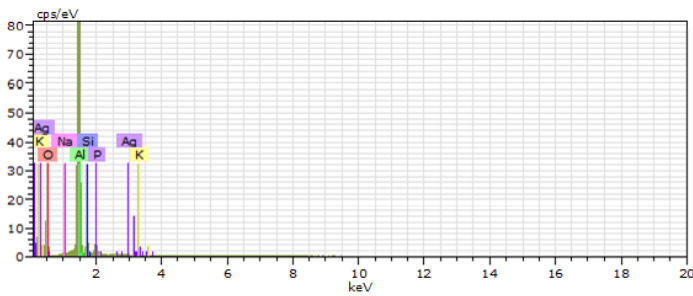


Drache30_area1
 Date:25.04.2020 14:47:21
 Image size:1024 x 768
 Mag:100x
 HV:20,0kV



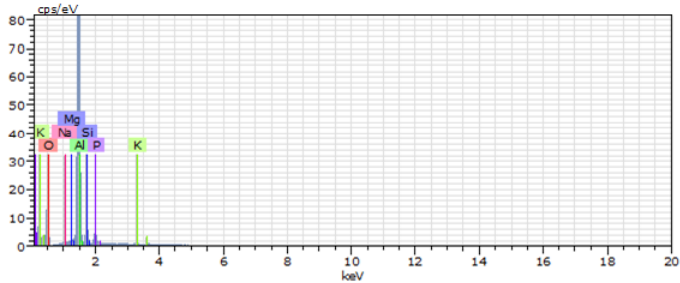
98 Date:25.04.2020 14:48:09 HV:20,0kV Puls th.:18,76kcps

El	AN	Series	unn. C [wt.%]	norm. C [wt.%]	Atom. C [at.%]	Error (1 Sigma) [wt.%]
O	8	K-series	23,64	35,71	48,58	2,83
Al	13	K-series	36,89	55,72	44,95	1,79
Si	14	K-series	2,93	4,42	3,43	0,15
P	15	K-series	2,31	3,49	2,45	0,12
Mg	12	K-series	0,44	0,66	0,59	0,05
Total:			66,21	100,00	100,00	



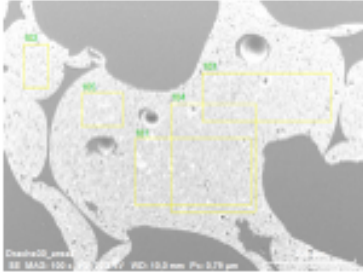
99 Date:25.04.2020 14:48:50 HV:20,0kV Puls th.:19,42kcps

El	AN	Series	unn. C [wt.%]	norm. C [wt.%]	Atom. C [at.%]	Error (1 Sigma) [wt.%]
O	8	K-series	14,46	36,08	49,35	1,73
Al	13	K-series	21,03	52,44	42,54	1,03
Si	14	K-series	1,88	4,69	3,65	0,11
P	15	K-series	1,66	4,14	2,92	0,09
Na	11	K-series	0,31	0,78	0,74	0,05
K	19	K-series	0,45	1,13	0,63	0,04
Ag	47	L-series	0,30	0,74	0,15	0,04
Total:			40,09	100,00	100,00	

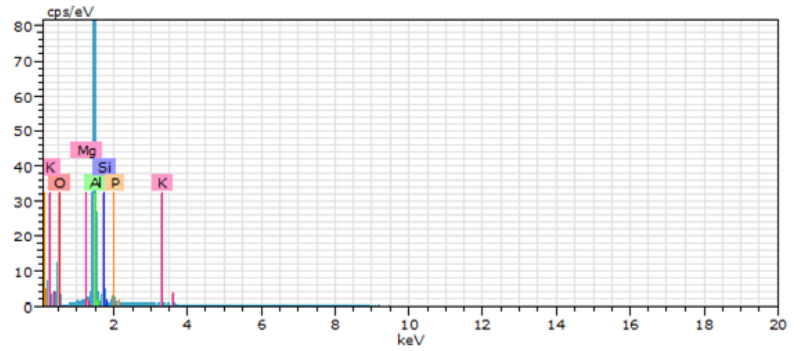


100 Date:25.04.2020 14:49:30 HV:20,0kV Puls th.:19,64kcps

El	AN	Series	unn. C [wt.%]	norm. C [wt.%]	Atom. C [at.%]	Error (1 Sigma) [wt.%]
O	8	K-series	26,34	35,69	48,62	3,13
Al	13	K-series	39,59	53,66	43,34	1,92
Si	14	K-series	3,89	5,27	4,09	0,19
P	15	K-series	2,54	3,44	2,42	0,13
Na	11	K-series	0,46	0,62	0,59	0,06
Mg	12	K-series	0,46	0,62	0,55	0,05
K	19	K-series	0,52	0,71	0,39	0,04
Total:			73,79	100,00	100,00	

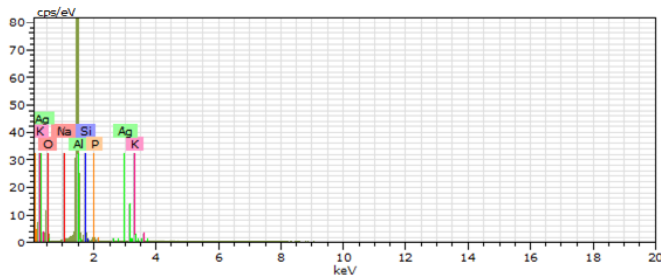


Drache30_area2
 Date:25.04.2020 14:53:31
 Image size:1024 x 768
 Mag:99,92645x
 HV:20,0kV



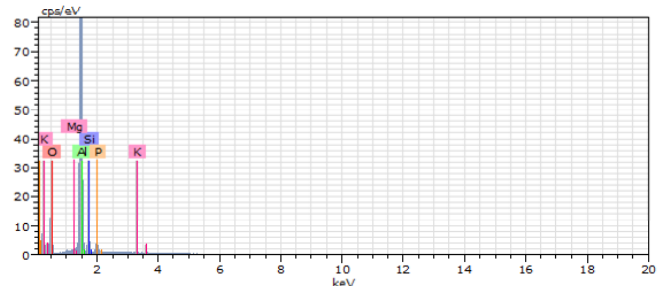
101 Date:25.04.2020 14:54:33 HV:20,0kV Puls th.:20,29kcps

El	AN	Series	unn. [wt.%]	C norm. [wt.%]	C Atom. [at.%]	C Error (1 Sigma) [wt.%]
O	8	K-series	24,68	35,34	48,19	2,94
Al	13	K-series	39,54	56,60	45,77	1,91
Si	14	K-series	3,28	4,70	3,65	0,17
P	15	K-series	1,45	2,08	1,46	0,08
Mg	12	K-series	0,44	0,62	0,56	0,05
K	19	K-series	0,46	0,66	0,37	0,04
Total:			69,85	100,00	100,00	



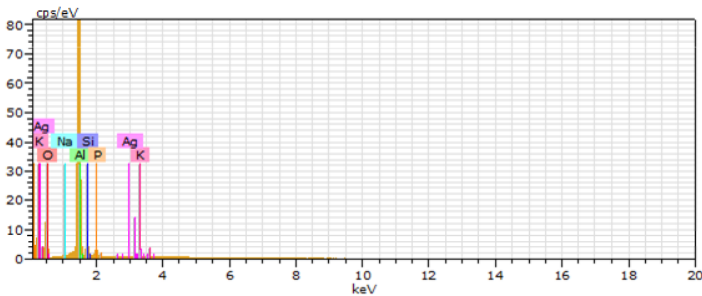
102 Date:25.04.2020 14:55:13 HV:20,0kV Puls th.:19,19kcps

El	AN	Series	unn. [wt.%]	C norm. [wt.%]	C Atom. [at.%]	C Error (1 Sigma) [wt.%]
O	8	K-series	13,43	36,17	49,37	1,62
Al	13	K-series	20,55	55,34	44,80	1,01
Si	14	K-series	1,50	4,03	3,14	0,09
P	15	K-series	0,62	1,68	1,19	0,05
K	19	K-series	0,45	1,22	0,68	0,04
Na	11	K-series	0,25	0,68	0,65	0,04
Ag	47	L-series	0,32	0,87	0,18	0,04
Total:			37,13	100,00	100,00	



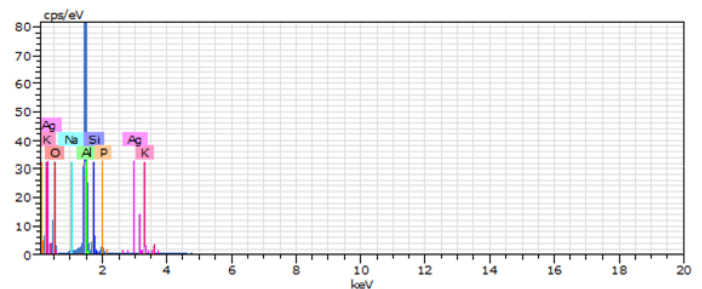
103 Date:25.04.2020 14:55:54 HV:20,0kV Puls th.:19,90kcps

El	AN	Series	unn. [wt.%]	C norm. [wt.%]	C Atom. [at.%]	C Error (1 Sigma) [wt.%]
O	8	K-series	25,44	36,16	49,11	3,03
Al	13	K-series	39,06	55,53	44,72	1,89
Si	14	K-series	3,03	4,31	3,33	0,16
P	15	K-series	2,01	2,86	2,00	0,11
Mg	12	K-series	0,41	0,58	0,52	0,05
K	19	K-series	0,40	0,56	0,31	0,04
Total:			70,34	100,00	100,00	



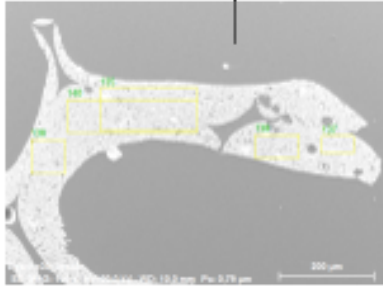
104 Date:25.04.2020 14:56:34 HV:20,0kV Puls th.:20,28kcps

El	AN	Series	unn. [wt.%]	C norm. [wt.%]	C Atom. [at.%]	C Error (1 Sigma) [wt.%]
O	8	K-series	13,91	36,00	49,20	1,67
Al	13	K-series	21,07	54,54	44,21	1,03
Si	14	K-series	1,69	4,37	3,40	0,10
P	15	K-series	1,03	2,65	1,87	0,07
K	19	K-series	0,43	1,11	0,62	0,04
Na	11	K-series	0,22	0,57	0,54	0,04
Ag	47	L-series	0,29	0,75	0,15	0,04
Total:			38,63	100,00	100,00	

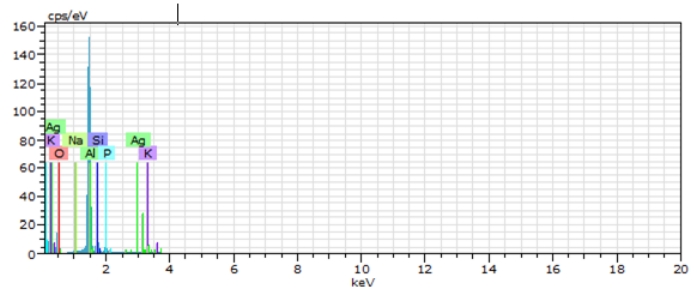


105 Date:25.04.2020 14:57:15 HV:20,0kV Puls th.:19,81kcps

El	AN	Series	unn. [wt.%]	C norm. [wt.%]	C Atom. [at.%]	C Error (1 Sigma) [wt.%]
O	8	K-series	13,72	35,74	49,01	1,65
Al	13	K-series	20,08	52,31	42,53	0,98
Si	14	K-series	2,50	6,50	5,08	0,13
P	15	K-series	0,89	2,32	1,65	0,06
K	19	K-series	0,58	1,50	0,84	0,05
Na	11	K-series	0,29	0,74	0,71	0,05
Ag	47	L-series	0,34	0,88	0,18	0,04
Total:			38,38	100,00	100,00	

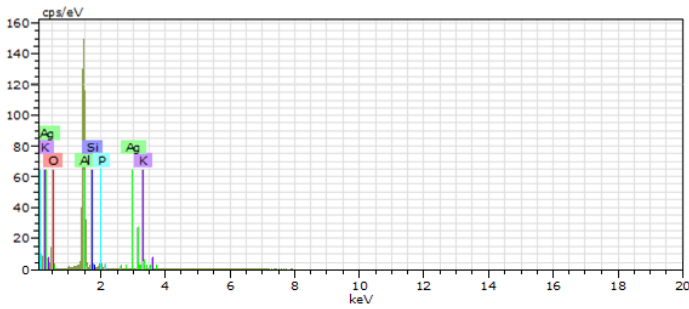


Drache30_area3
 Date:26.04.2020 11:25:17
 Image size:1024 x 768
 Mag:99,92645x
 HV:20,0kV



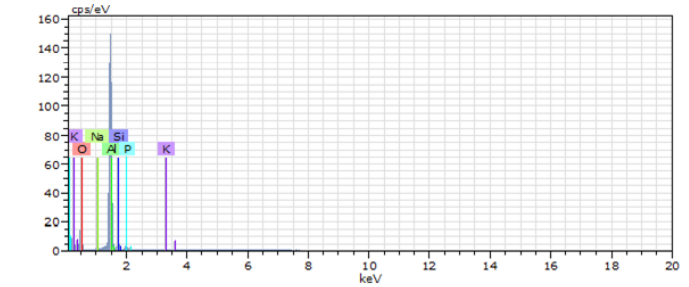
135 Date:26.04.2020 11:27:00 HV:20,0kV Puls th.:25,11kcps

El	AN	Series	unn. C [wt.%]	norm. C [wt.%]	Atom. C [at.%]	Error (1 Sigma) [wt.%]
O	8	K-series	22,95	34,11	47,03	2,70
Al	13	K-series	37,37	55,53	45,40	1,81
Si	14	K-series	3,93	5,84	4,59	0,19
P	15	K-series	1,80	2,68	1,91	0,10
Na	11	K-series	0,41	0,61	0,58	0,05
K	19	K-series	0,44	0,65	0,37	0,04
Ag	47	L-series	0,39	0,58	0,12	0,04
Total:			67,29	100,00	100,00	



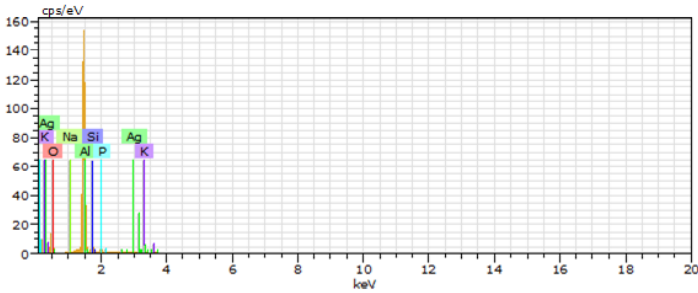
136 Date:26.04.2020 11:27:40 HV:20,0kV Puls th.:23,91kcps

El	AN	Series	unn. C [wt.%]	norm. C [wt.%]	Atom. C [at.%]	Error (1 Sigma) [wt.%]
O	8	K-series	13,26	35,11	48,29	1,58
Al	13	K-series	21,42	56,70	46,25	1,05
Si	14	K-series	1,20	3,19	2,50	0,08
P	15	K-series	1,21	3,21	2,28	0,07
K	19	K-series	0,33	0,88	0,49	0,04
Ag	47	L-series	0,35	0,92	0,19	0,04
Total:			37,78	100,00	100,00	



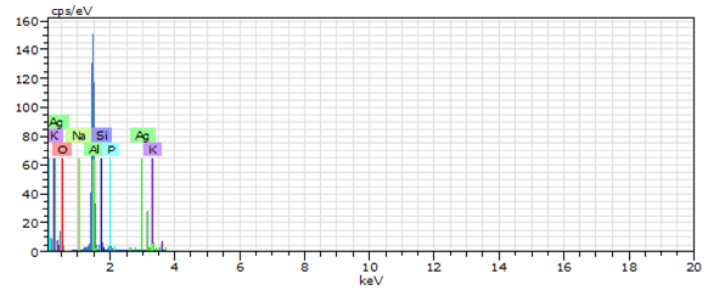
137 Date:26.04.2020 11:28:21 HV:20,0kV Puls th.:23,86kcps

El	AN	Series	unn. C [wt.%]	norm. C [wt.%]	Atom. C [at.%]	Error (1 Sigma) [wt.%]
O	8	K-series	12,56	35,61	48,41	1,49
Al	13	K-series	20,46	58,03	46,78	1,00
Si	14	K-series	1,15	3,27	2,53	0,08
P	15	K-series	0,57	1,60	1,13	0,05
Na	11	K-series	0,28	0,81	0,76	0,05
K	19	K-series	0,24	0,69	0,38	0,03
Total:			35,26	100,00	100,00	



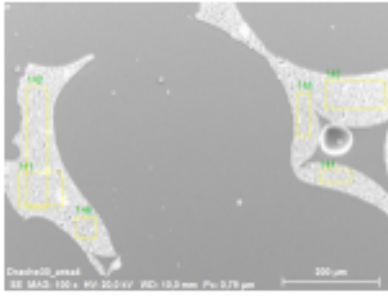
139 Date:26.04.2020 11:29:01 HV:20,0kV Puls th.:24,46kcps

El	AN	Series	unn. C [wt.%]	norm. C [wt.%]	Atom. C [at.%]	Error (1 Sigma) [wt.%]
Al	13	K-series	39,34	58,42	47,59	1,90
O	8	K-series	23,20	34,45	47,33	2,74
Si	14	K-series	2,43	3,61	2,82	0,13
P	15	K-series	1,29	1,91	1,36	0,08
Na	11	K-series	0,34	0,51	0,48	0,05
K	19	K-series	0,37	0,55	0,31	0,04
Ag	47	L-series	0,38	0,56	0,11	0,04
Total:			67,33	100,00	100,00	

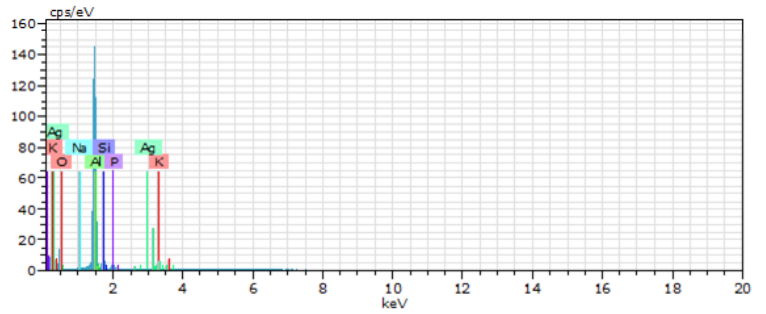


140 Date:26.04.2020 11:29:42 HV:20,0kV Puls th.:24,75kcps

El	AN	Series	unn. C [wt.%]	norm. C [wt.%]	Atom. C [at.%]	Error (1 Sigma) [wt.%]
O	8	K-series	24,08	33,85	46,70	2,84
Al	13	K-series	40,16	56,46	46,18	1,94
Si	14	K-series	3,80	5,34	4,19	0,19
P	15	K-series	1,90	2,67	1,90	0,10
Na	11	K-series	0,44	0,62	0,59	0,06
K	19	K-series	0,40	0,56	0,32	0,04
Ag	47	L-series	0,36	0,50	0,10	0,04
Total:			71,14	100,00	100,00	

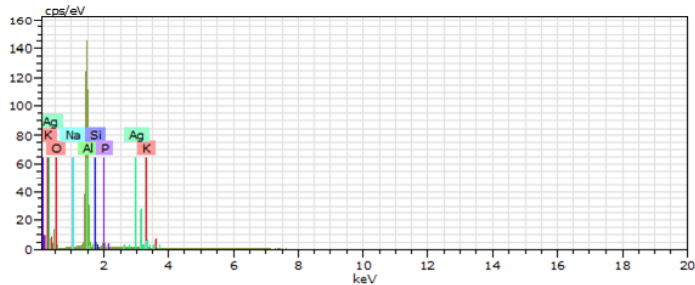


Drache30_area4
 Date:26.04.2020 11:32:57
 Image size:1024 x 768
 Mag:99,92645x
 HV:20,0kV



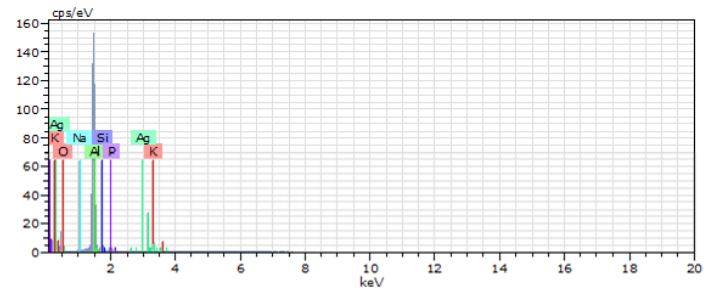
141 Date:26.04.2020 11:33:51 HV:20,0kV Puls th.:23,65kcps

El	AN	Series	unn. C [wt.%]	norm. C [wt.%]	Atom. C [at.%]	Error (1 Sigma) [wt.%]
O	8	K-series	13,48	34,89	48,08	1,60
Al	13	K-series	20,82	53,89	44,03	1,02
Si	14	K-series	1,98	5,11	4,01	0,11
P	15	K-series	1,19	3,08	2,20	0,07
K	19	K-series	0,51	1,32	0,75	0,04
Na	11	K-series	0,30	0,77	0,74	0,05
Ag	47	L-series	0,36	0,92	0,19	0,04
Total:			38,63	100,00	100,00	



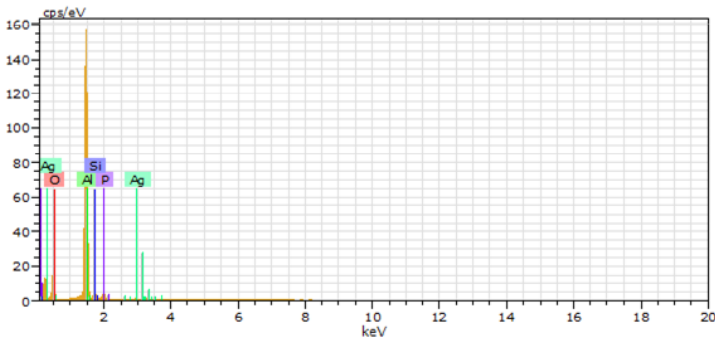
142 Date:26.04.2020 11:34:32 HV:20,0kV Puls th.:23,54kcps

El	AN	Series	unn. C [wt.%]	norm. C [wt.%]	Atom. C [at.%]	Error (1 Sigma) [wt.%]
O	8	K-series	12,87	34,76	47,86	1,54
Al	13	K-series	20,41	55,13	45,01	1,00
Si	14	K-series	1,66	4,48	3,51	0,10
P	15	K-series	1,22	3,29	2,34	0,07
K	19	K-series	0,37	1,01	0,57	0,04
Na	11	K-series	0,21	0,58	0,55	0,04
Ag	47	L-series	0,28	0,75	0,15	0,04
Total:			37,03	100,00	100,00	



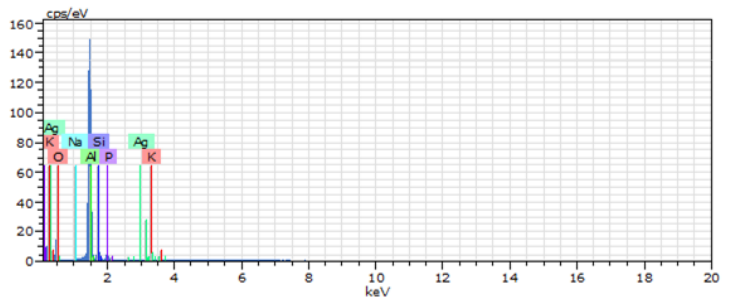
143 Date:26.04.2020 11:35:13 HV:20,0kV Puls th.:24,14kcps

El	AN	Series	unn. C [wt.%]	norm. C [wt.%]	Atom. C [at.%]	Error (1 Sigma) [wt.%]
O	8	K-series	13,91	35,31	48,48	1,65
Al	13	K-series	22,01	55,86	45,48	1,08
Si	14	K-series	1,49	3,77	2,95	0,09
P	15	K-series	1,01	2,55	1,81	0,07
K	19	K-series	0,38	0,96	0,54	0,04
Na	11	K-series	0,22	0,56	0,53	0,04
Ag	47	L-series	0,39	0,99	0,20	0,04
Total:			39,40	100,00	100,00	



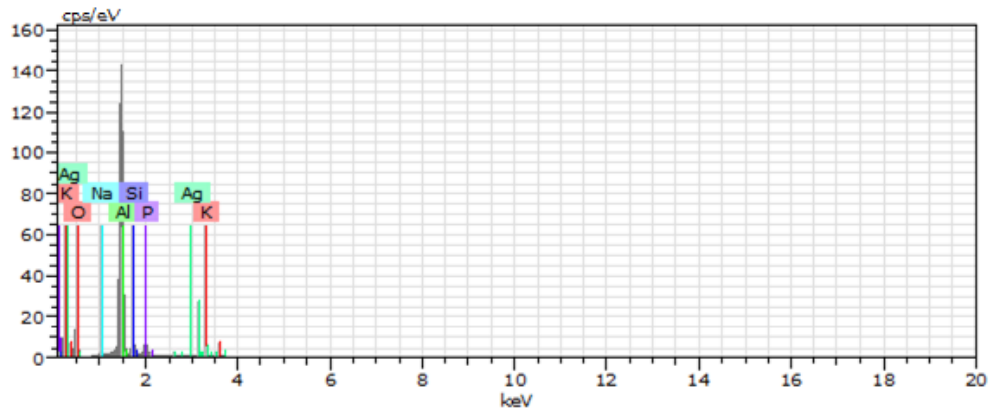
144 Date:26.04.2020 11:35:53 HV:20,0kV Puls th.:24,49kcps

El	AN	Series	unn. C [wt.%]	norm. C [wt.%]	Atom. C [at.%]	Error (1 Sigma) [wt.%]
Al	13	K-series	42,36	59,43	48,40	2,05
O	8	K-series	24,67	34,61	47,53	2,91
Si	14	K-series	1,92	2,70	2,11	0,11
P	15	K-series	1,82	2,55	1,81	0,10
Ag	47	L-series	0,51	0,71	0,14	0,04
Total:			71,28	100,00	100,00	



145 Date:26.04.2020 11:36:34 HV:20,0kV Puls th.:24,29kcps

El	AN	Series	unn. C [wt.%]	norm. C [wt.%]	Atom. C [at.%]	Error (1 Sigma) [wt.%]
O	8	K-series	23,60	34,20	47,10	2,79
Al	13	K-series	39,13	56,72	46,32	1,89
Si	14	K-series	3,34	4,84	3,80	0,17
P	15	K-series	1,74	2,52	1,79	0,09
Na	11	K-series	0,39	0,57	0,55	0,05
K	19	K-series	0,40	0,59	0,33	0,04
Ag	47	L-series	0,39	0,57	0,12	0,04
Total:			68,99	100,00	100,00	



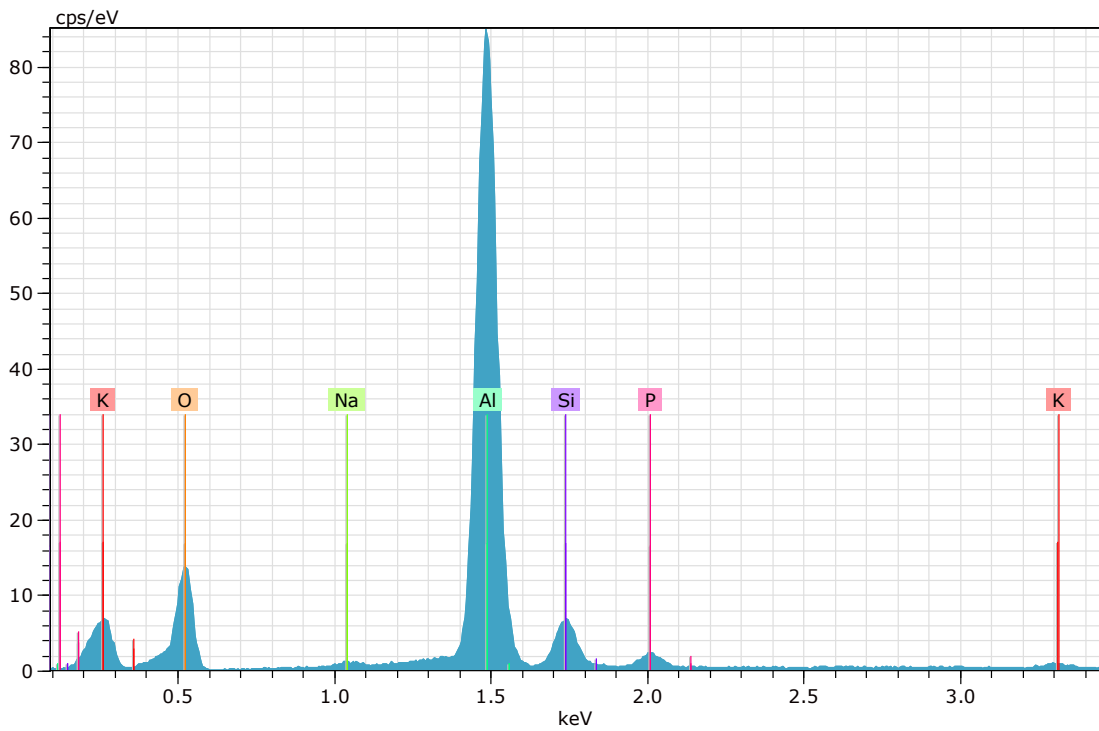
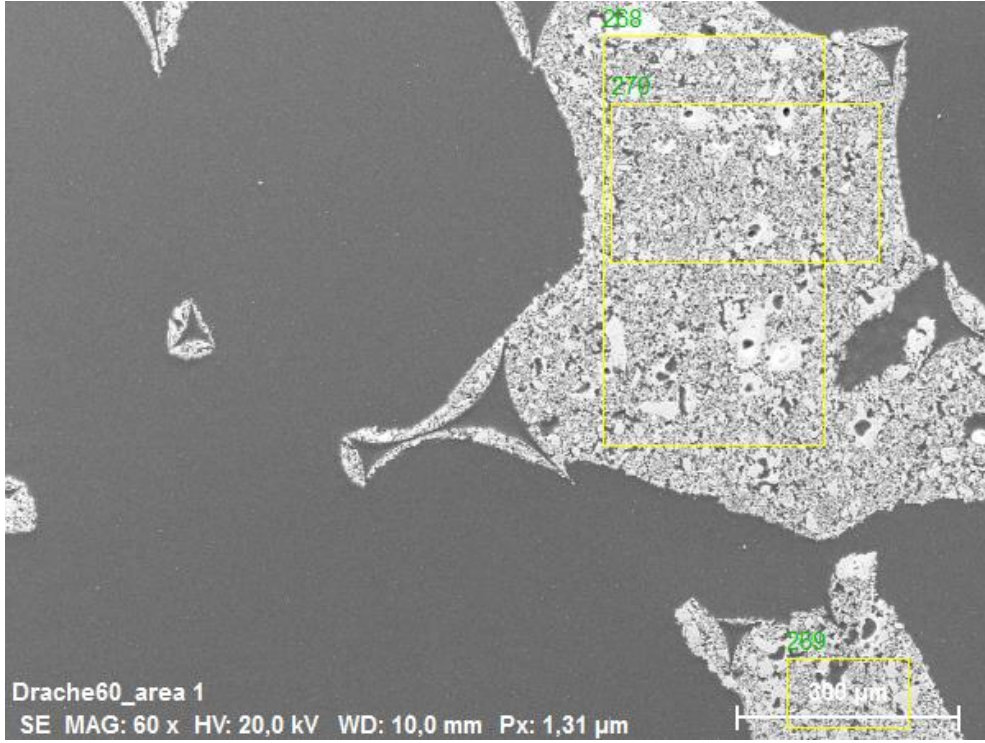
146 Date:26.04.2020 11:37:14 HV:20,0kV Puls th.:24,01kcps

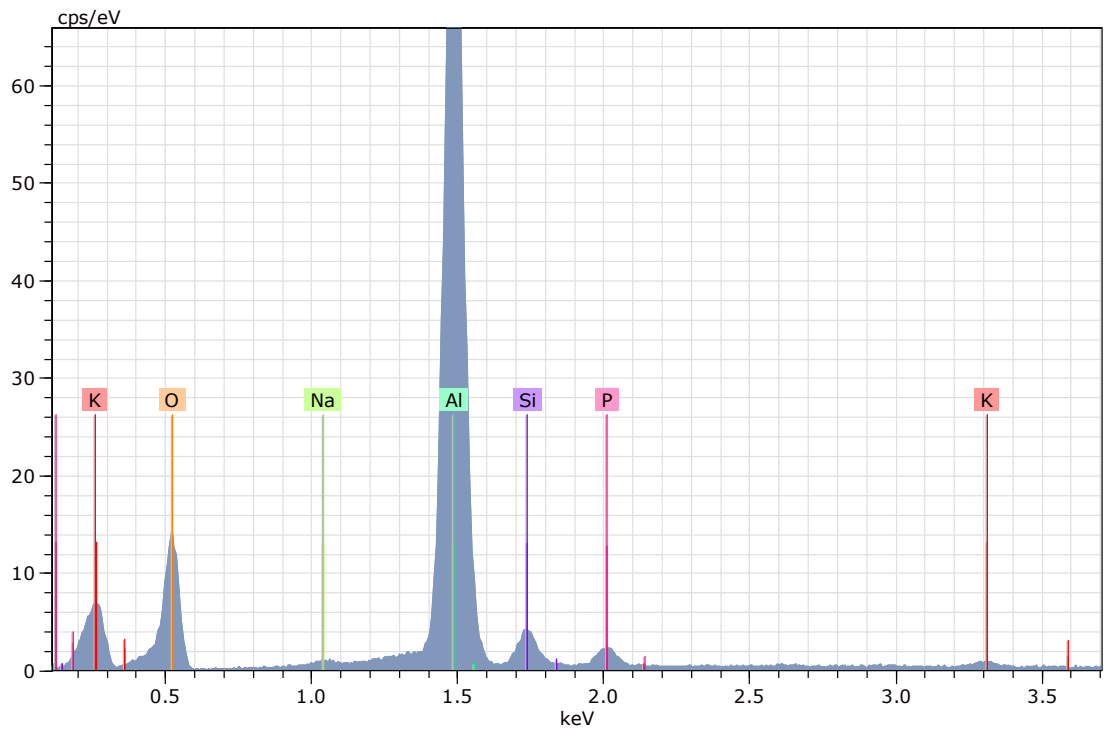
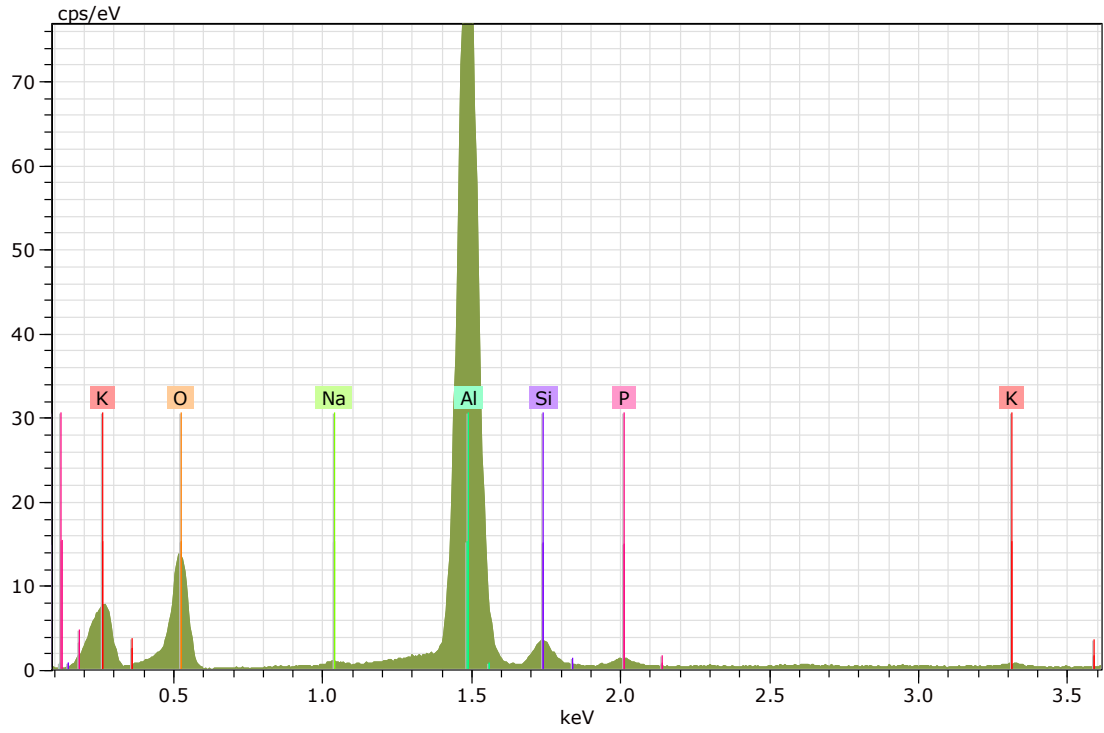
EI	AN	Series	unn. C [wt. %]	norm. C [wt. %]	Atom. C [at. %]	Error (1 Sigma) [wt. %]
O	8	K-series	22,56	34,43	47,43	2,67
Al	13	K-series	35,96	54,86	44,82	1,74
Si	14	K-series	3,10	4,72	3,71	0,16
P	15	K-series	2,82	4,30	3,06	0,14
Na	11	K-series	0,35	0,53	0,51	0,05
K	19	K-series	0,42	0,65	0,36	0,04
Ag	47	L-series	0,34	0,52	0,11	0,04
<u>Total:</u>			65,55	100,00	100,00	

J EDS RawData Drache 60

Application Note

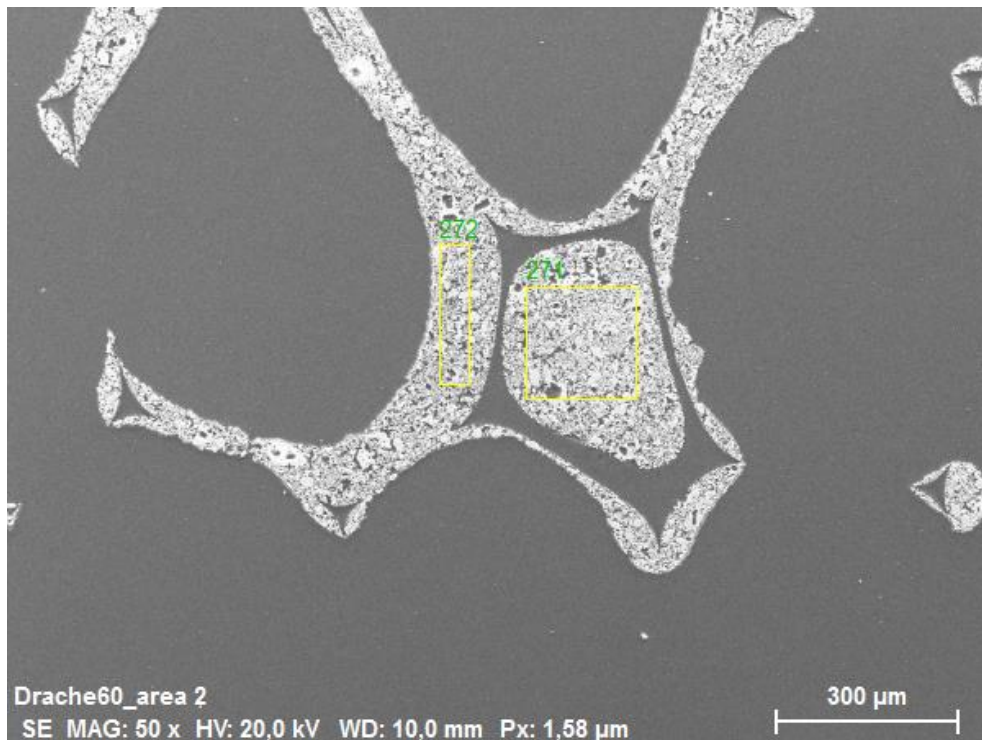
Company / Department

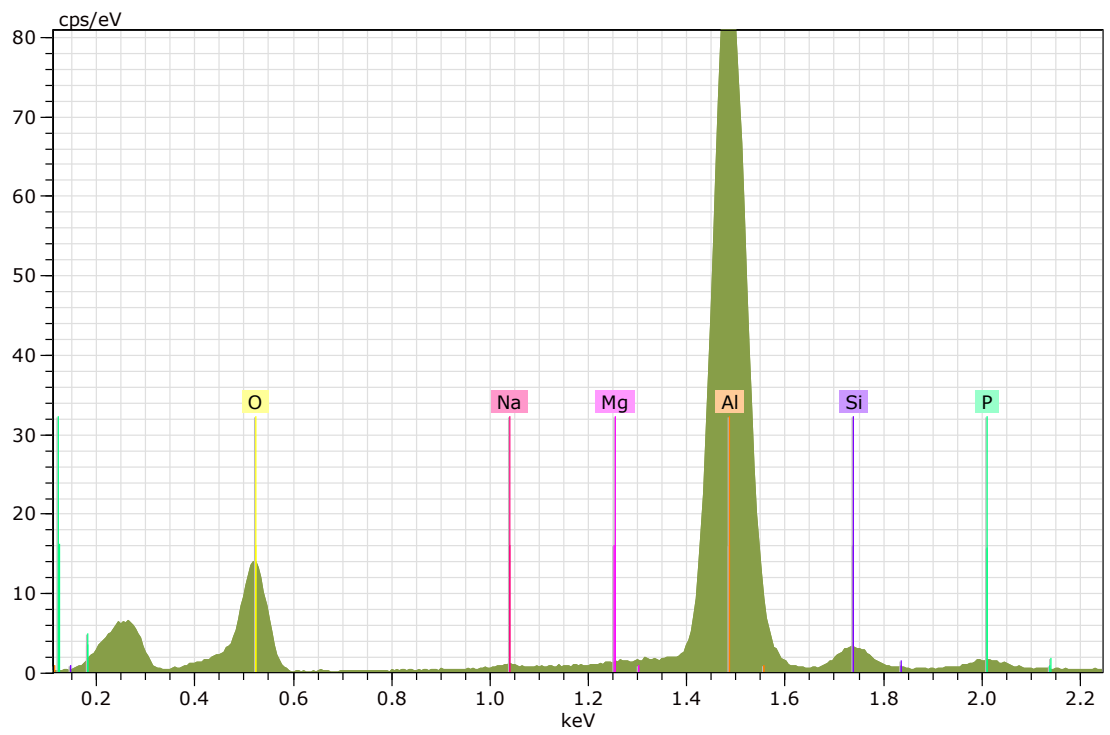
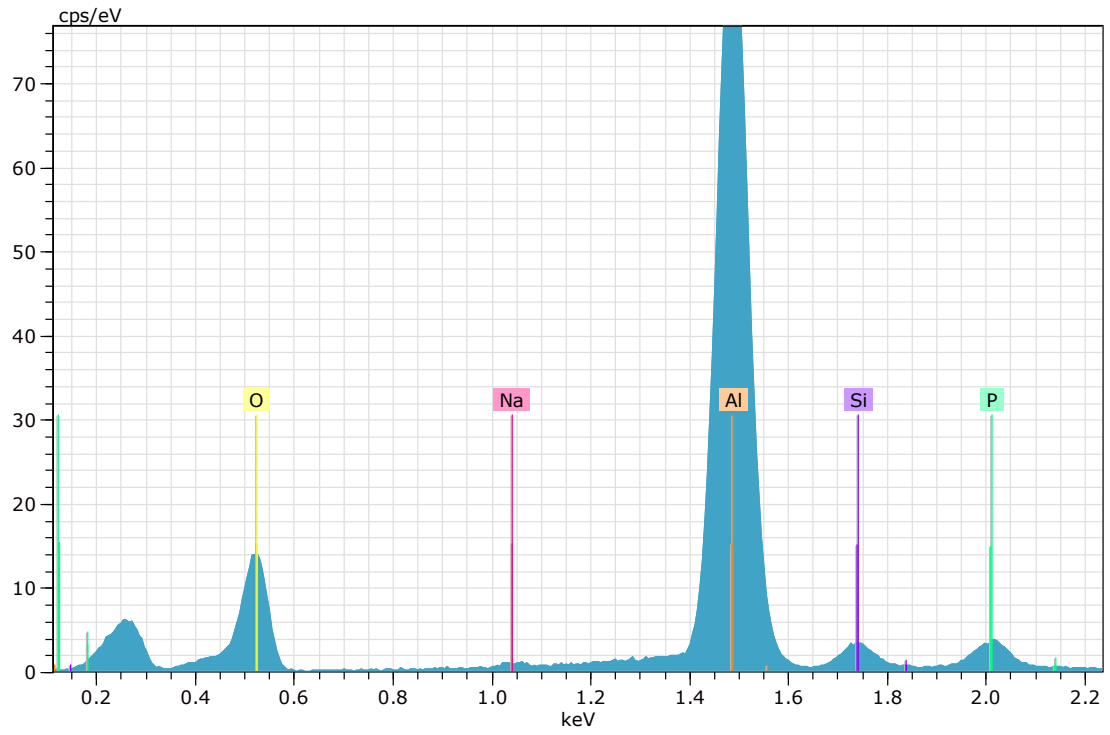




Atomic percent (%)

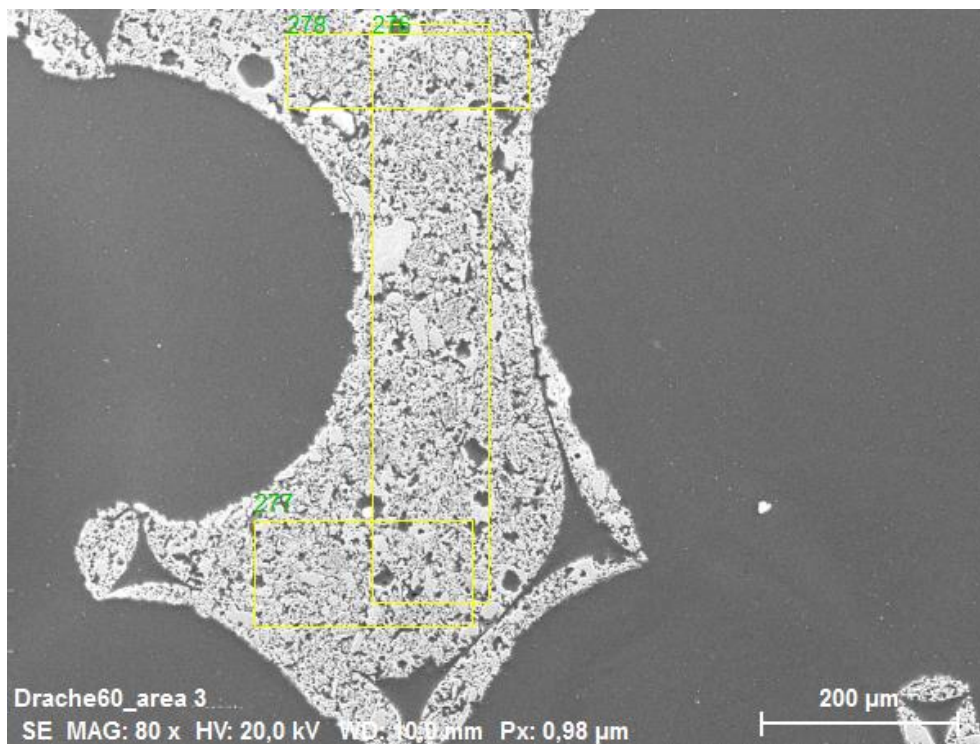
Spectrum	O	Na	Al	Si	P	K
268	47,75	0,78	43,67	5,32	1,85	0,63
269	47,71	0,70	47,80	2,56	0,82	0,41
270	47,94	0,75	45,74	3,06	1,90	0,61
Mean value:	47,80	0,74	45,74	3,65	1,53	0,55
Sigma:	0,12	0,04	2,06	1,47	0,61	0,12
Sigma mean:	0,07	0,02	1,19	0,85	0,35	0,07

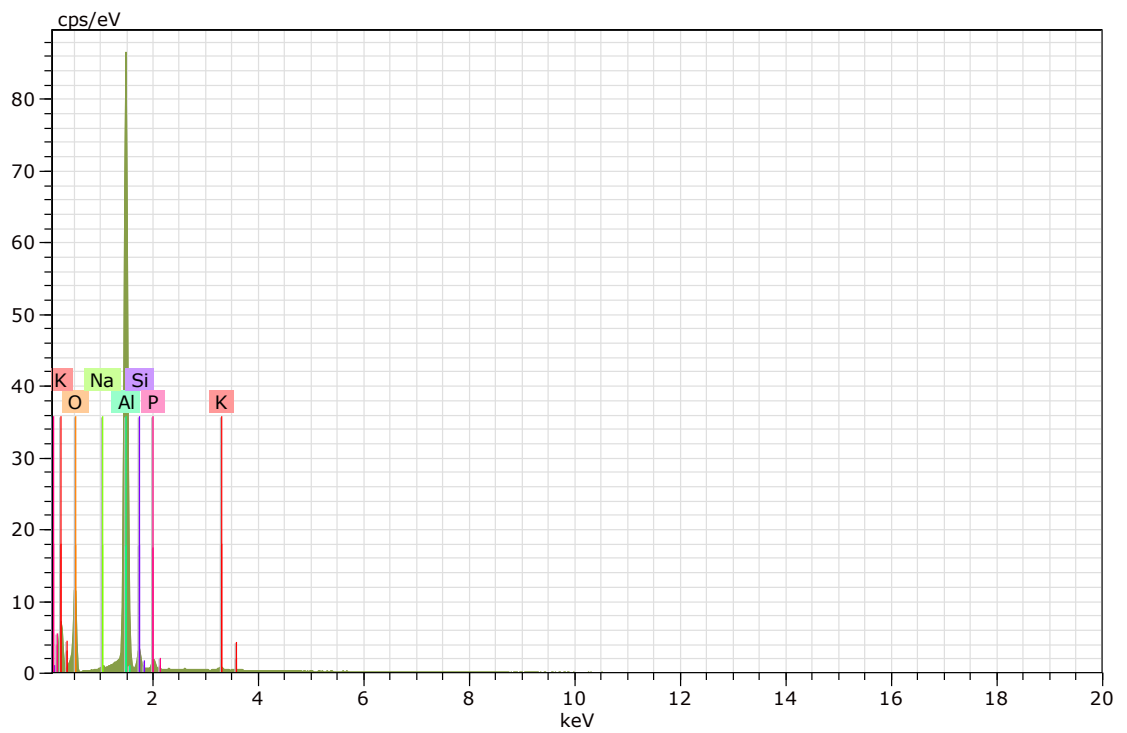
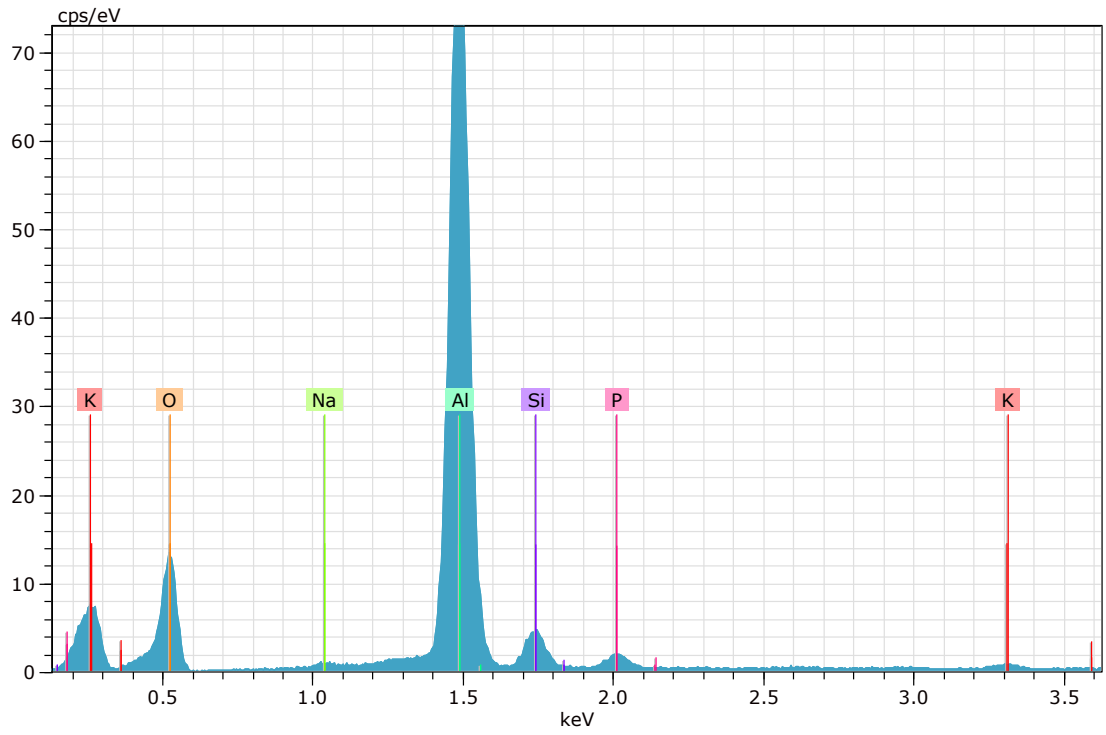


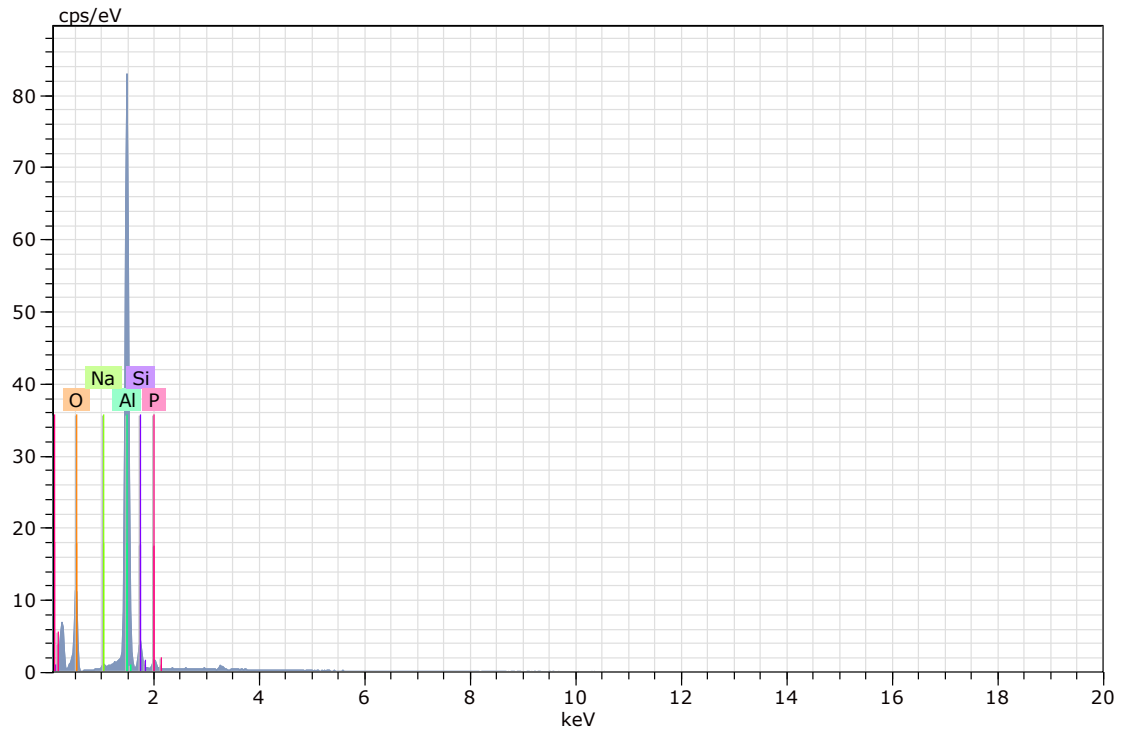


Atomic percent (%)

Spectrum	O	Na	Mg	Al	Si	P
271	47,26	0,56	-	47,36	2,34	2,48
272	46,66	0,57	0,65	48,82	2,34	0,96
Mean value:	46,96	0,57	0,65	48,09	2,34	1,72
Sigma:	0,42	0,01	0,00	1,03	0,00	1,08
Sigma mean:	0,30	0,01	0,00	0,73	0,00	0,76

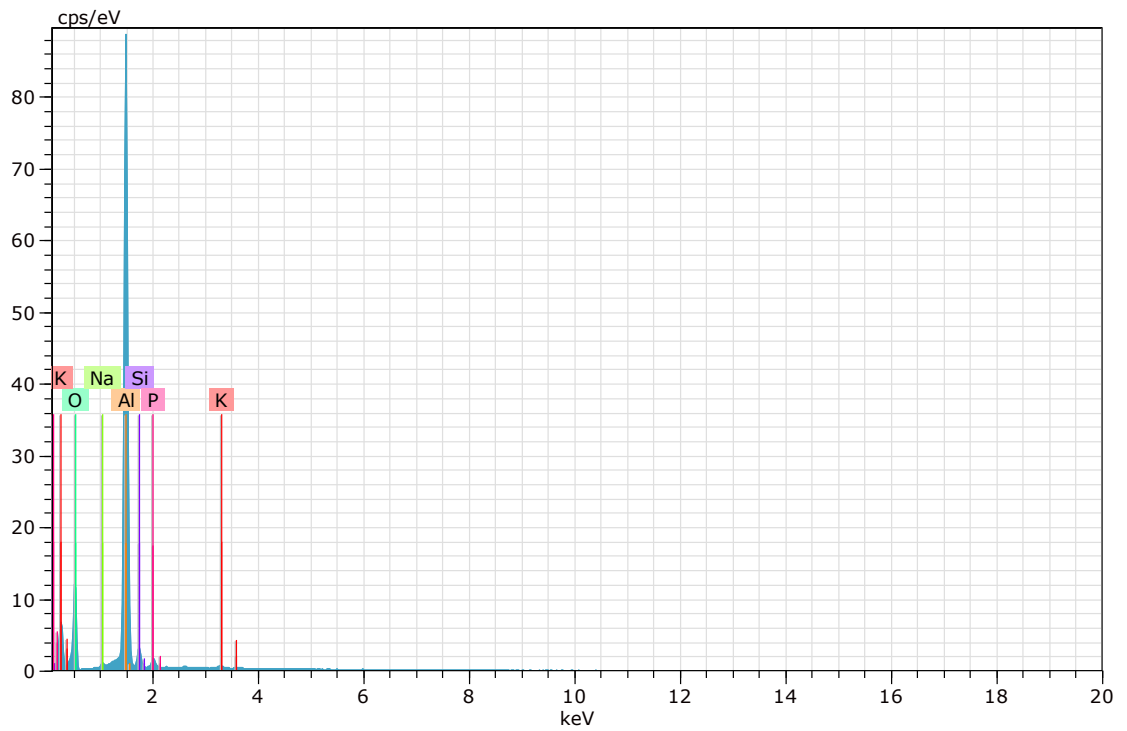
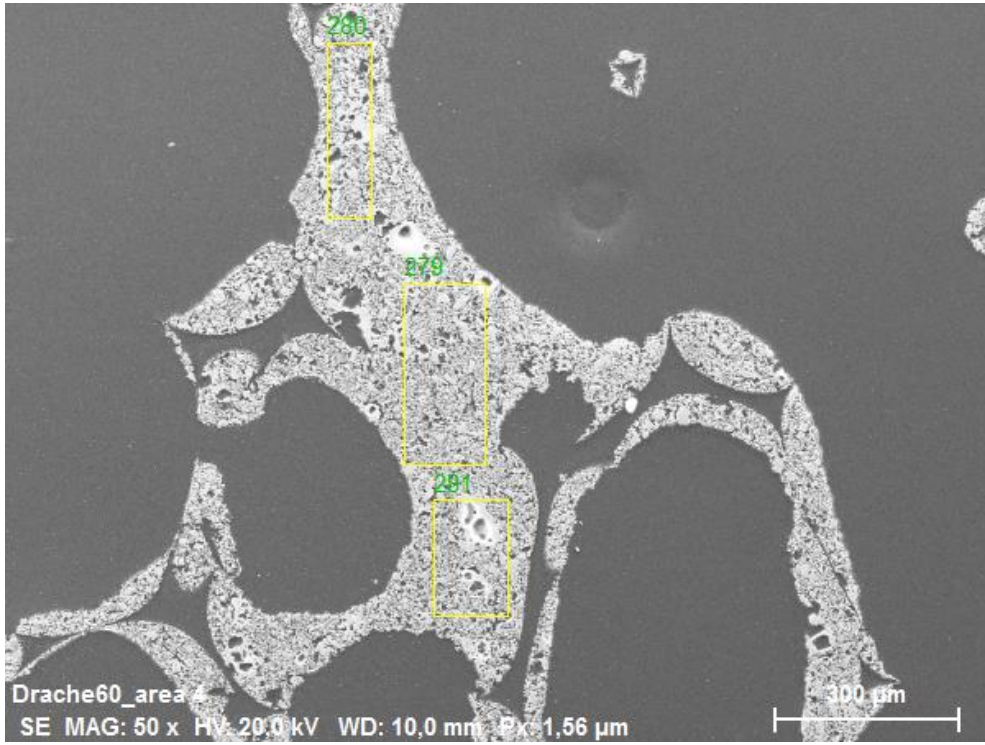


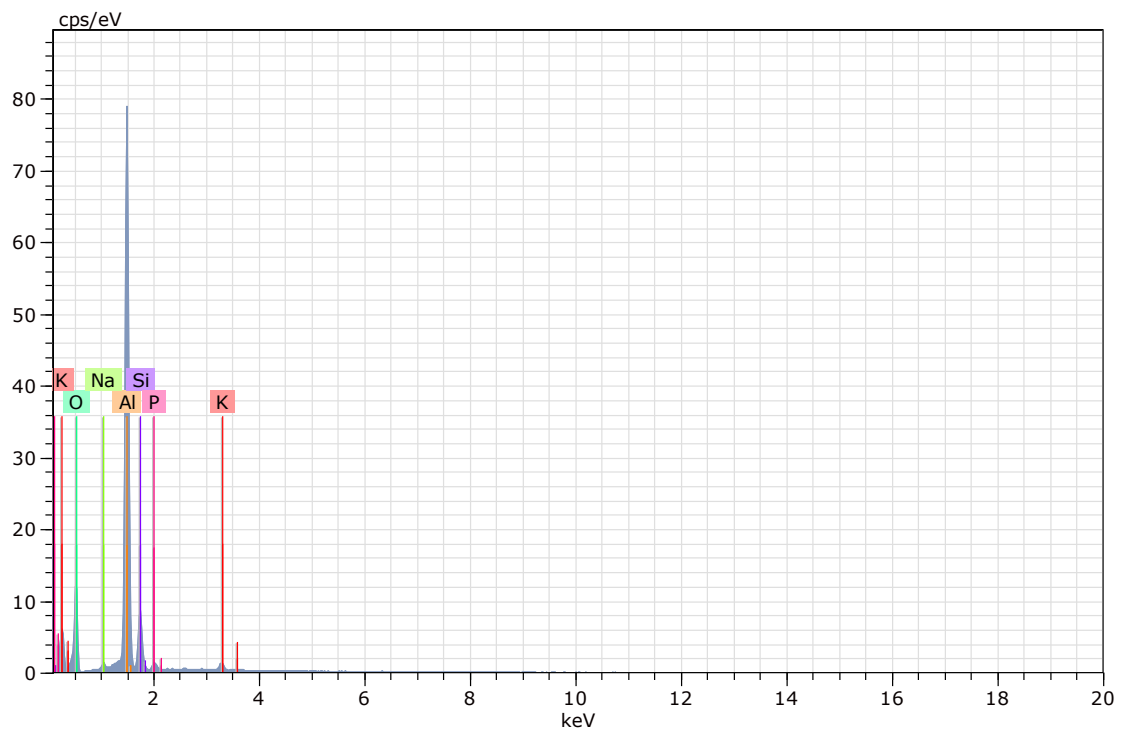
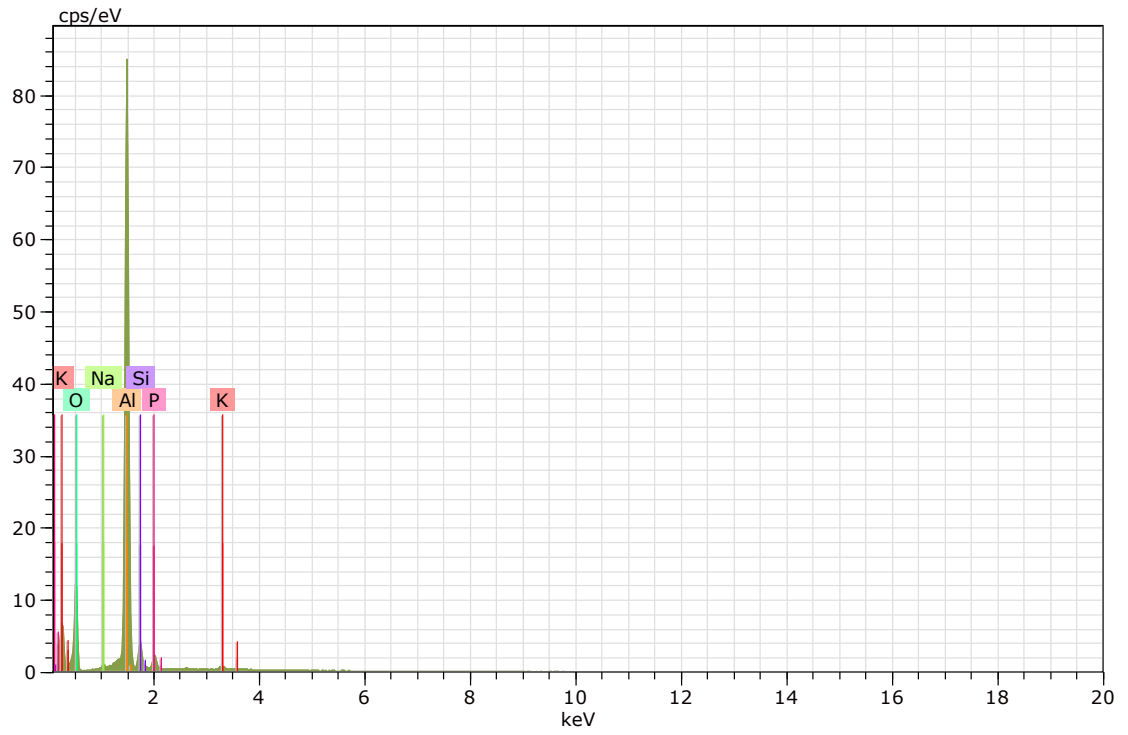




Atomic percent (%)

Spectrum	O	Na	Al	Si	P	K
276	47,66	0,67	45,71	3,72	1,62	0,62
277	47,19	0,52	47,71	2,54	1,53	0,51
278	46,59	0,59	48,41	3,38	1,03	-
Mean value:	47,15	0,59	47,28	3,21	1,39	0,56
Sigma:	0,53	0,08	1,40	0,61	0,32	0,08
Sigma mean:	0,31	0,05	0,81	0,35	0,18	0,04



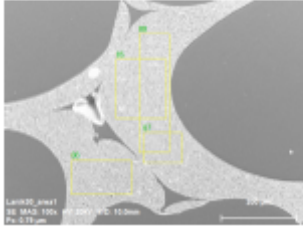




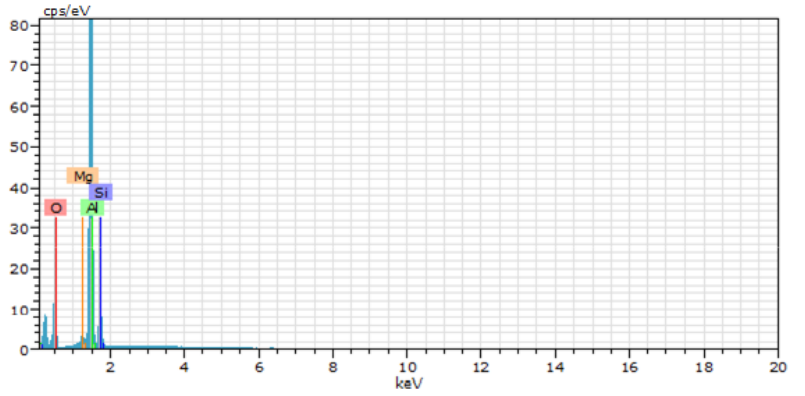
Atomic percent (%)

Spectrum	O	Na	Al	Si	P	K
279	47,32	0,61	48,08	2,36	1,24	0,39
280	47,57	0,59	46,82	3,10	1,55	0,37
281	48,01	1,22	41,68	6,97	0,90	1,23
Mean value:	47,63	0,81	45,52	4,14	1,23	0,66
Sigma:	0,35	0,36	3,39	2,47	0,33	0,49
Sigma mean:	0,20	0,21	1,96	1,43	0,19	0,28

K EDS RawData Lanik 30

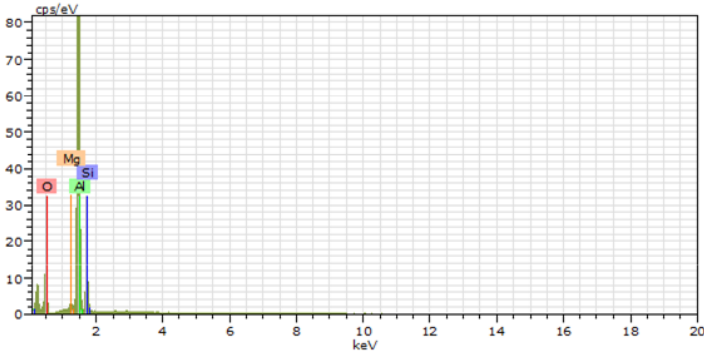


Lanik30_area1
 Date:25.04.2020 13:44:25
 Image size:1024 x 768
 Mag:99,92645x
 HV:20,0kV



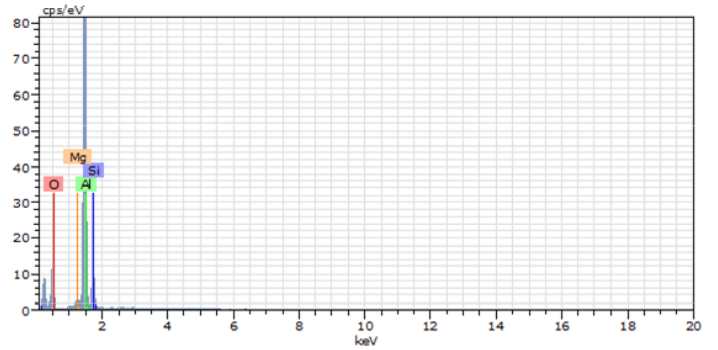
85 Date:25.04.2020 13:45:43 HV:20,0kV Puls th.:18,85kcps

El	AN	Series	unn. C [wt.%]	norm. C [wt.%]	Atom. C [at.%]	Error (1 Sigma) [wt.%]
O	8	K-series	20,55	34,11	46,69	2,47
Al	13	K-series	33,41	55,45	45,01	1,62
Si	14	K-series	5,55	9,21	7,18	0,26
Mg	12	K-series	0,75	1,24	1,12	0,07
Total:			60,26	100,00	100,00	



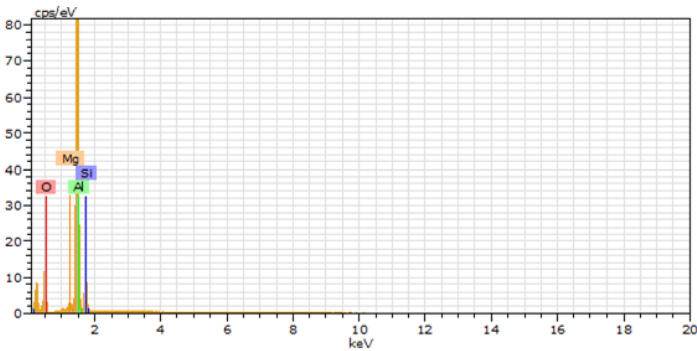
86 Date:25.04.2020 13:46:24 HV:20,0kV Puls th.:18,50kcps

El	AN	Series	unn. C [wt.%]	norm. C [wt.%]	Atom. C [at.%]	Error (1 Sigma) [wt.%]
O	8	K-series	20,24	33,95	46,54	2,44
Al	13	K-series	32,54	54,58	44,36	1,58
Si	14	K-series	6,15	10,31	8,05	0,29
Mg	12	K-series	0,69	1,16	1,04	0,07
Total:			59,61	100,00	100,00	



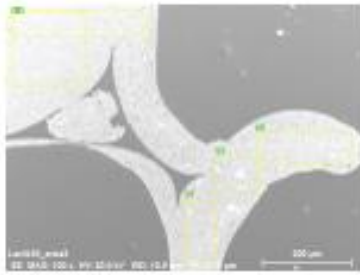
87 Date:25.04.2020 13:47:05 HV:20,0kV Puls th.:18,91kcps

El	AN	Series	unn. C [wt.%]	norm. C [wt.%]	Atom. C [at.%]	Error (1 Sigma) [wt.%]
O	8	K-series	22,89	34,11	46,70	2,75
Al	13	K-series	37,19	55,43	45,00	1,80
Si	14	K-series	6,21	9,25	7,22	0,29
Mg	12	K-series	0,81	1,20	1,09	0,07
Total:			67,09	100,00	100,00	

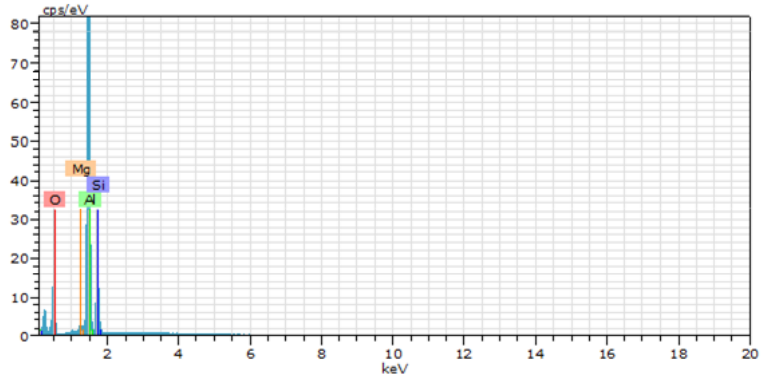


88 Date:25.04.2020 13:47:45 HV:20,0kV Puls th.:18,96kcps

El	AN	Series	unn. C [wt.%]	norm. C [wt.%]	Atom. C [at.%]	Error (1 Sigma) [wt.%]
O	8	K-series	24,15	34,06	46,63	2,90
Al	13	K-series	39,52	55,73	45,25	1,91
Si	14	K-series	6,33	8,92	6,96	0,30
Mg	12	K-series	0,91	1,29	1,16	0,08
Total:			70,91	100,00	100,00	

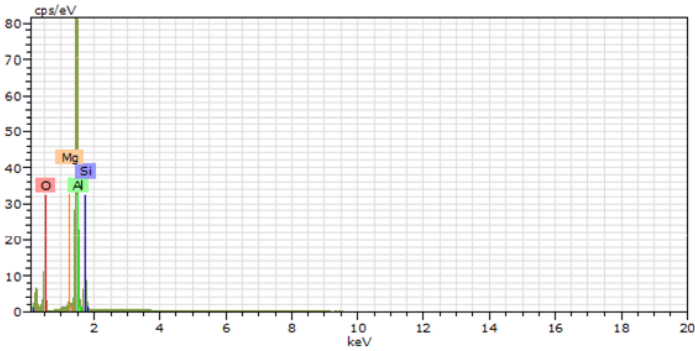


Lanik30_area2
 Date:25.04.2020 13:53:29
 Image size:1024 x 768
 Mag:99,92645x
 HV:20,0kV



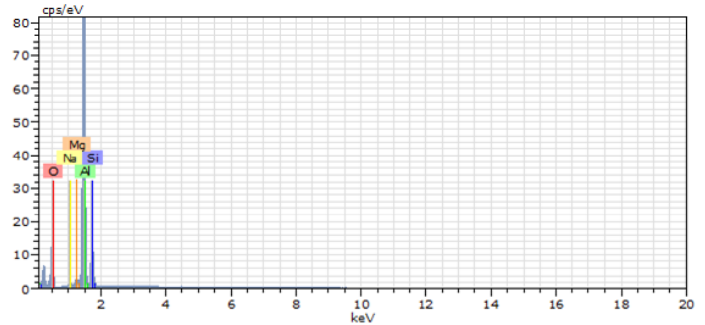
89 Date:25.04.2020 13:54:22 HV:20,0kV Puls th.:18,93kcps

El	AN	Series	unn. C [wt.%]	norm. C [wt.%]	Atom. C [at.%]	Error (1 Sigma) [wt.%]
O	8	K-series	25,58	35,27	48,04	3,05
Al	13	K-series	37,01	51,04	41,22	1,79
Si	14	K-series	9,18	12,66	9,82	0,42
Mg	12	K-series	0,75	1,03	0,92	0,07
Total:			72,51	100,00	100,00	



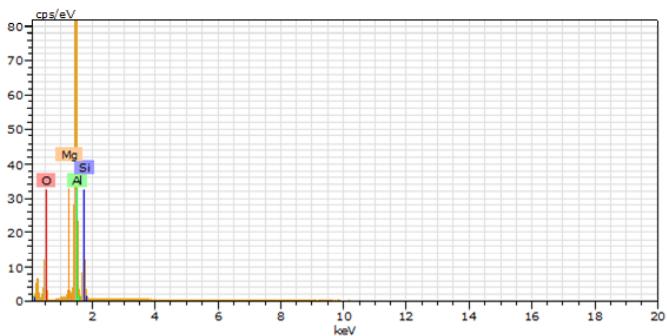
90 Date:25.04.2020 13:55:02 HV:20,0kV Puls th.:18,15kcps

El	AN	Series	unn. C [wt.%]	norm. C [wt.%]	Atom. C [at.%]	Error (1 Sigma) [wt.%]
O	8	K-series	23,73	34,59	47,24	2,85
Al	13	K-series	37,19	54,21	43,89	1,80
Si	14	K-series	6,78	9,89	7,69	0,32
Mg	12	K-series	0,90	1,31	1,18	0,08
Total:			68,60	100,00	100,00	



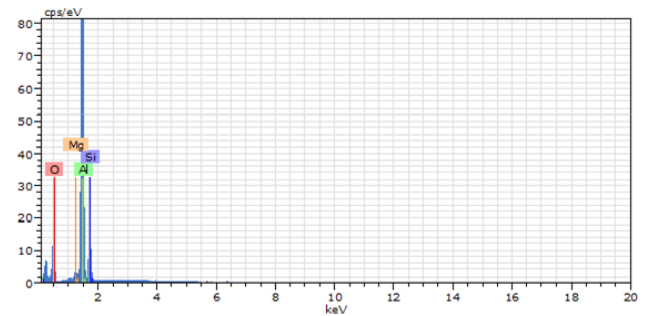
91 Date:25.04.2020 13:55:43 HV:20,0kV Puls th.:19,37kcps

El	AN	Series	unn. C [wt.%]	norm. C [wt.%]	Atom. C [at.%]	Error (1 Sigma) [wt.%]
O	8	K-series	24,76	34,28	46,87	2,96
Al	13	K-series	38,20	52,88	42,88	1,85
Si	14	K-series	7,98	11,04	8,60	0,37
Mg	12	K-series	0,88	1,22	1,10	0,08
Na	11	K-series	0,42	0,58	0,55	0,06
Total:			72,25	100,00	100,00	



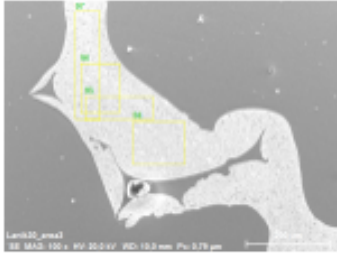
92 Date:25.04.2020 13:56:24 HV:20,0kV Puls th.:18,97kcps

El	AN	Series	unn. C [wt.%]	norm. C [wt.%]	Atom. C [at.%]	Error (1 Sigma) [wt.%]
O	8	K-series	24,81	34,91	47,61	2,96
Al	13	K-series	36,32	51,09	41,33	1,76
Si	14	K-series	8,92	12,54	9,75	0,41
Mg	12	K-series	1,04	1,46	1,31	0,08
Total:			71,09	100,00	100,00	

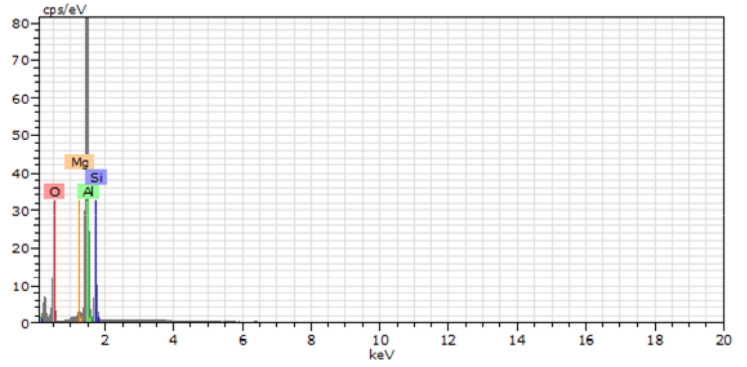


93 Date:25.04.2020 13:57:04 HV:20,0kV Puls th.:18,42kcps

El	AN	Series	unn. C [wt.%]	norm. C [wt.%]	Atom. C [at.%]	Error (1 Sigma) [wt.%]
O	8	K-series	23,47	34,32	46,95	2,82
Al	13	K-series	36,35	53,14	43,11	1,76
Si	14	K-series	7,66	11,19	8,72	0,35
Mg	12	K-series	0,92	1,34	1,21	0,08
Total:			68,39	100,00	100,00	



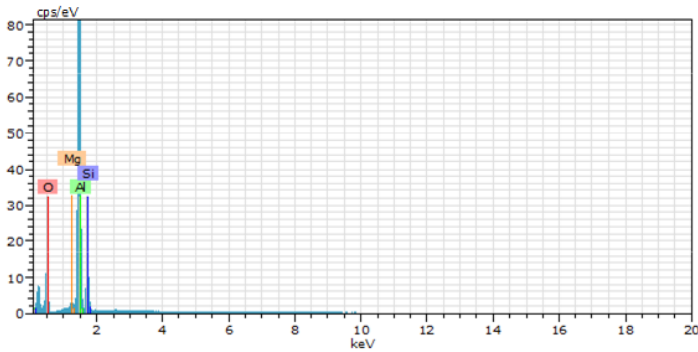
Lanik30_area3
 Date:25.04.2020 14:00:29
 Image size:1024 x 768
 Mag:99,92645x
 HV:20,0kV



94 Date:25.04.2020 14:01:07 HV:20,0kV Puls th.:18,87kcps

El	AN	Series	unn. C [wt.%]	norm. C [wt.%]	Atom. C [at.%]	Error (1 Sigma) [wt.%]
O	8	K-series	23,69	34,59	47,24	2,83
Al	13	K-series	36,92	53,90	43,65	1,79
Si	14	K-series	6,96	10,15	7,90	0,32
Mg	12	K-series	0,93	1,35	1,21	0,08

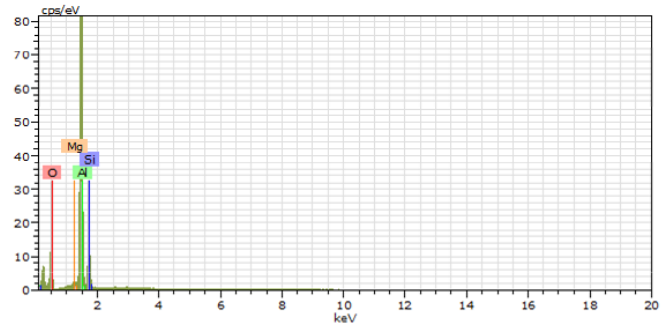
Total: 68,49 100,00 100,00



95 Date:25.04.2020 14:01:48 HV:20,0kV Puls th.:18,35kcps

El	AN	Series	unn. C [wt.%]	norm. C [wt.%]	Atom. C [at.%]	Error (1 Sigma) [wt.%]
O	8	K-series	23,60	34,21	46,83	2,84
Al	13	K-series	37,05	53,70	43,60	1,79
Si	14	K-series	7,52	10,91	8,50	0,35
Mg	12	K-series	0,82	1,18	1,07	0,07

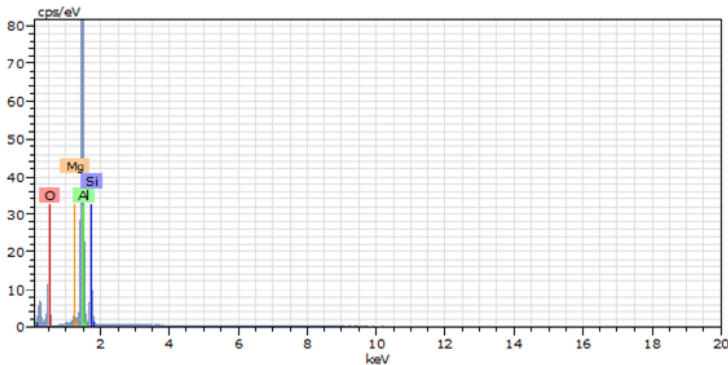
Total: 68,99 100,00 100,00



96 Date:25.04.2020 14:02:28 HV:20,0kV Puls th.:18,27kcps

El	AN	Series	unn. C [wt.%]	norm. C [wt.%]	Atom. C [at.%]	Error (1 Sigma) [wt.%]
O	8	K-series	23,25	34,38	47,03	2,79
Al	13	K-series	36,33	53,73	43,58	1,76
Si	14	K-series	7,32	10,83	8,44	0,34
Mg	12	K-series	0,72	1,06	0,96	0,07

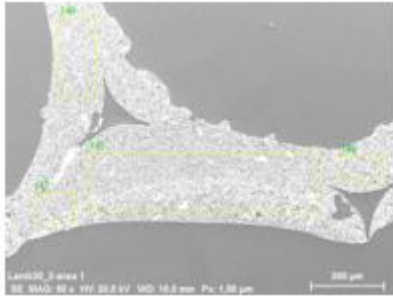
Total: 67,62 100,00 100,00



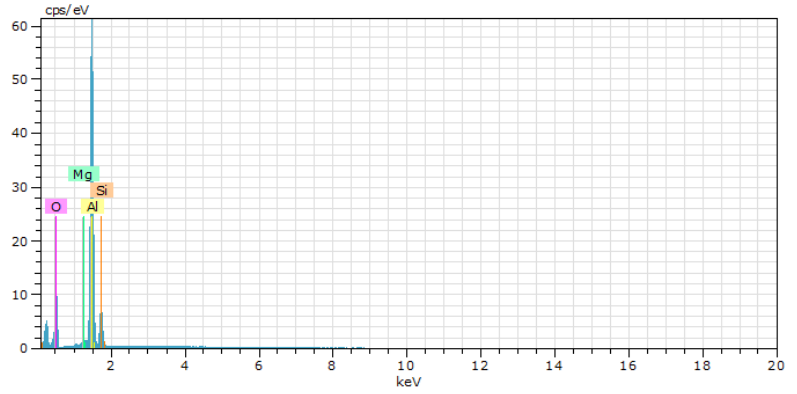
97 Date:25.04.2020 14:03:09 HV:20,0kV Puls th.:18,10kcps

El	AN	Series	unn. C [wt.%]	norm. C [wt.%]	Atom. C [at.%]	Error (1 Sigma) [wt.%]
O	8	K-series	23,45	34,47	47,12	2,82
Al	13	K-series	36,42	53,54	43,40	1,76
Si	14	K-series	7,36	10,82	8,43	0,34
Mg	12	K-series	0,80	1,17	1,06	0,07

Total: 68,02 100,00 100,00



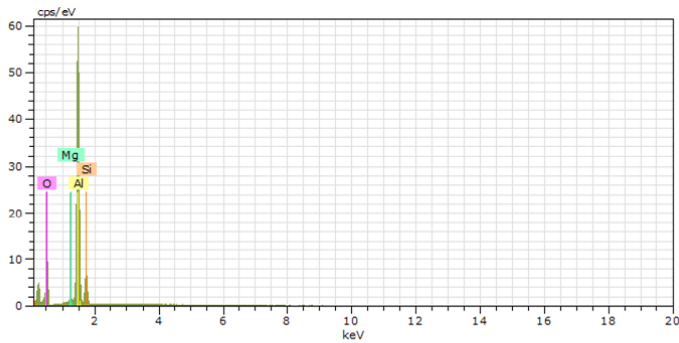
Lanik30_2-area 1
 Date:02.05.2020 10:30:15
 Image size:1024 x 768
 Mag:50,16336x
 HV:20,0kV



145 Date:02.05.2020 10:31:49 HV:20,0kV Puls th.:10,29kcps

El	AN	Series	unn. C [wt.%]	norm. C [wt.%]	Atom. C [at.%]	Error (1 Sigma) [wt.%]
O	8	K-series	25,40	35,47	48,19	3,45
Al	13	K-series	38,88	54,29	43,73	1,89
Si	14	K-series	6,43	8,97	6,94	0,31
Mg	12	K-series	0,91	1,27	1,13	0,08

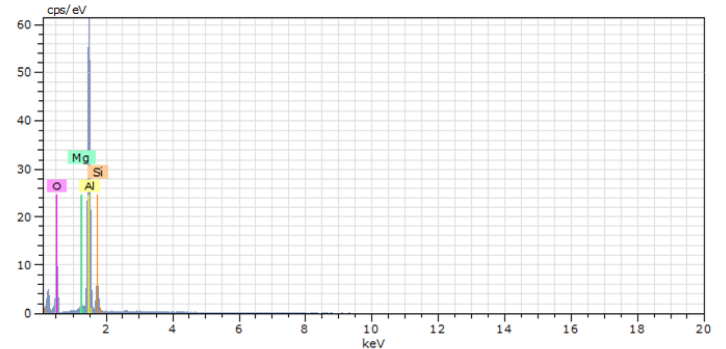
Total: 71,61 100,00 100,00



146 Date:02.05.2020 10:32:10 HV:20,0kV Puls th.:10,05kcps

El	AN	Series	unn. C [wt.%]	norm. C [wt.%]	Atom. C [at.%]	Error (1 Sigma) [wt.%]
O	8	K-series	23,99	35,56	48,28	3,27
Al	13	K-series	36,49	54,08	43,54	1,77
Si	14	K-series	6,04	8,95	6,93	0,29
Mg	12	K-series	0,95	1,40	1,25	0,09

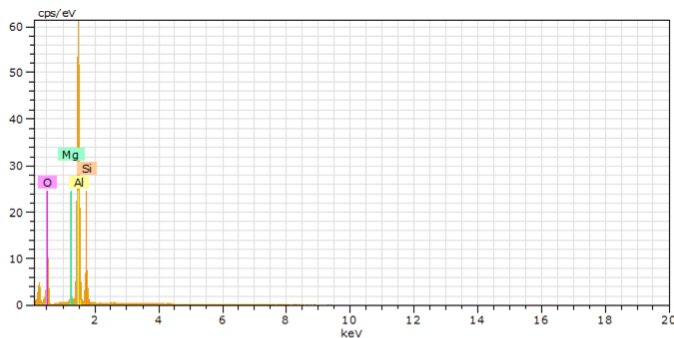
Total: 67,47 100,00 100,00



147 Date:02.05.2020 10:32:30 HV:20,0kV Puls th.:10,26kcps

El	AN	Series	unn. C [wt.%]	norm. C [wt.%]	Atom. C [at.%]	Error (1 Sigma) [wt.%]
O	8	K-series	22,38	35,79	48,54	3,04
Al	13	K-series	34,29	54,84	44,10	1,67
Si	14	K-series	5,22	8,36	6,46	0,26
Mg	12	K-series	0,63	1,01	0,90	0,07

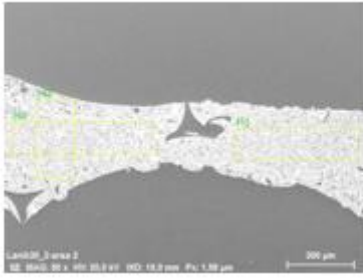
Total: 62,53 100,00 100,00



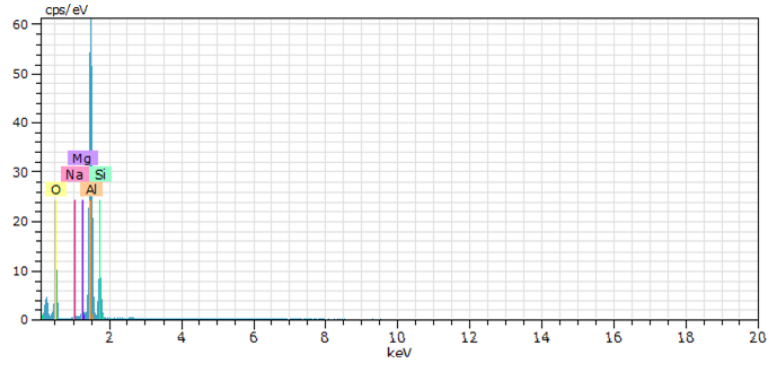
148 Date:02.05.2020 10:32:50 HV:20,0kV Puls th.:10,30kcps

El	AN	Series	unn. C [wt.%]	norm. C [wt.%]	Atom. C [at.%]	Error (1 Sigma) [wt.%]
O	8	K-series	22,00	36,16	48,97	2,97
Al	13	K-series	32,07	52,71	42,33	1,56
Si	14	K-series	6,18	10,15	7,83	0,30
Mg	12	K-series	0,60	0,98	0,88	0,06

Total: 60,84 100,00 100,00



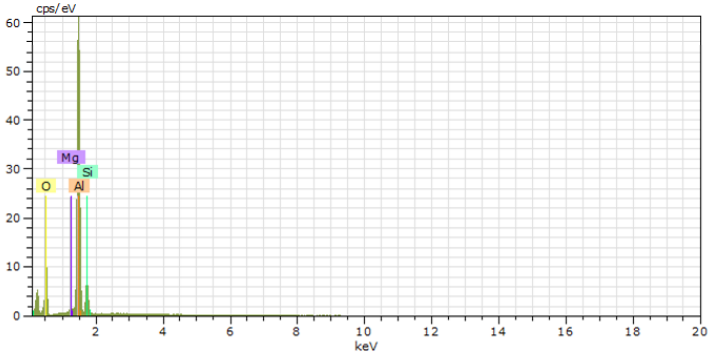
Lanik30_2-area 2
 Date:02.05.2020 10:36:52
 Image size:1024 x 768
 Mag:49,79679x
 HV:20,0kV



150 Date:02.05.2020 10:37:30 HV:20,0kV Puls th.:10,86kcps

El	AN	Series	unn. C [wt.%]	norm. C [wt.%]	Atom. C [at.%]	Error (1 Sigma) [wt.%]
O	8	K-series	25,20	35,30	48,00	3,40
Al	13	K-series	36,99	51,82	41,78	1,80
Si	14	K-series	7,90	11,07	8,57	0,37
Mg	12	K-series	0,91	1,28	1,15	0,08
Na	11	K-series	0,38	0,53	0,50	0,06

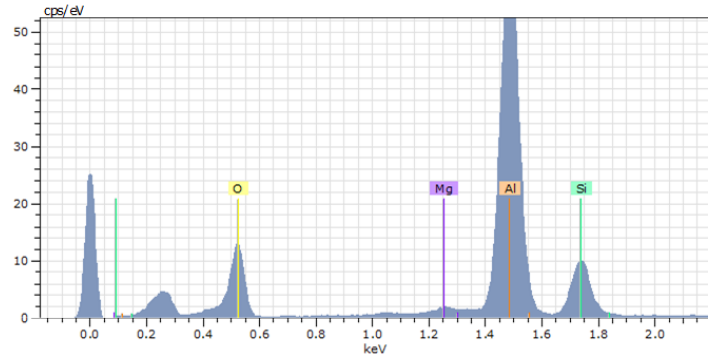
Total: 71,38 100,00 100,00



151 Date:02.05.2020 10:37:51 HV:20,0kV Puls th.:10,84kcps

El	AN	Series	unn. C [wt.%]	norm. C [wt.%]	Atom. C [at.%]	Error (1 Sigma) [wt.%]
O	8	K-series	24,14	35,29	47,98	3,27
Al	13	K-series	37,75	55,19	44,50	1,83
Si	14	K-series	5,72	8,36	6,48	0,28
Mg	12	K-series	0,79	1,16	1,04	0,08

Total: 68,40 100,00 100,00



152 Date:02.05.2020 10:38:12 HV:20,0kV Puls th.:10,90kcps

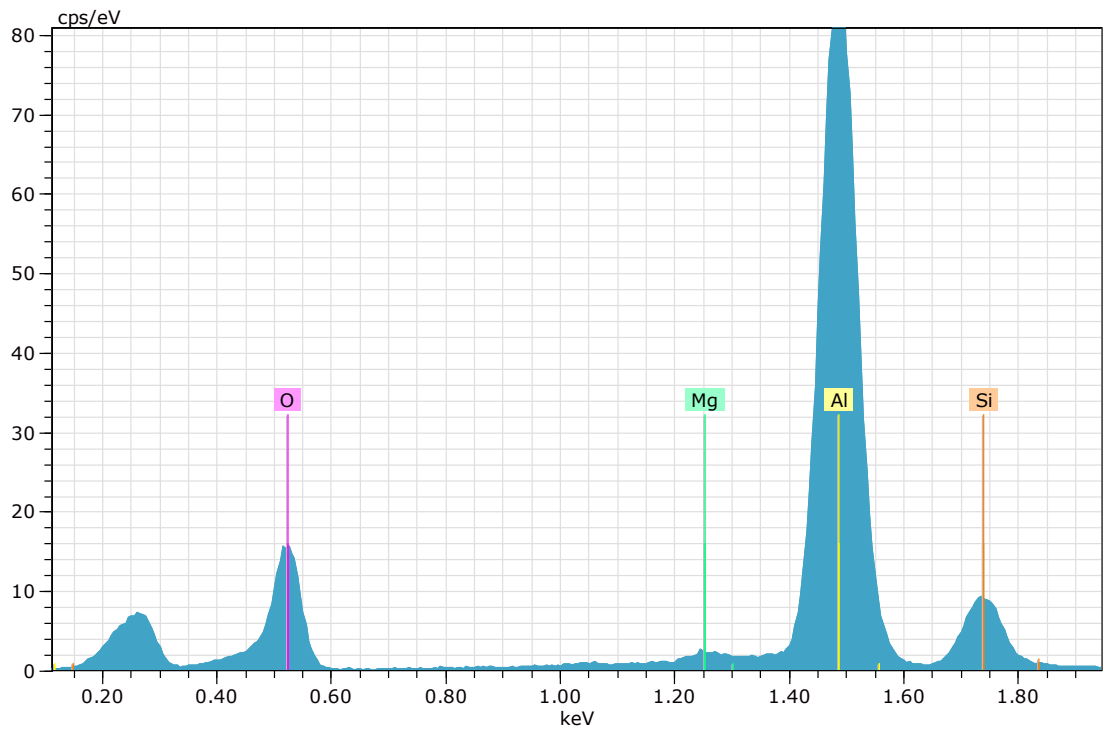
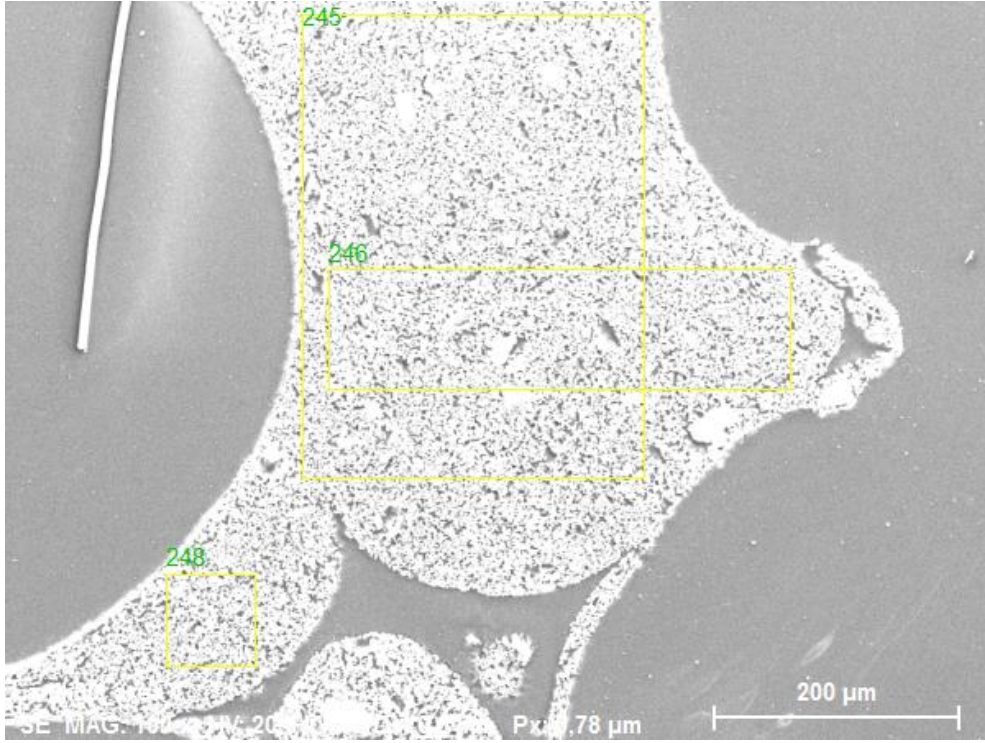
El	AN	Series	unn. C [wt.%]	norm. C [wt.%]	Atom. C [at.%]	Error (1 Sigma) [wt.%]
O	8	K-series	24,58	36,12	48,94	3,30
Al	13	K-series	34,93	51,34	41,24	1,70
Si	14	K-series	7,73	11,37	8,77	0,37
Mg	12	K-series	0,80	1,17	1,05	0,08

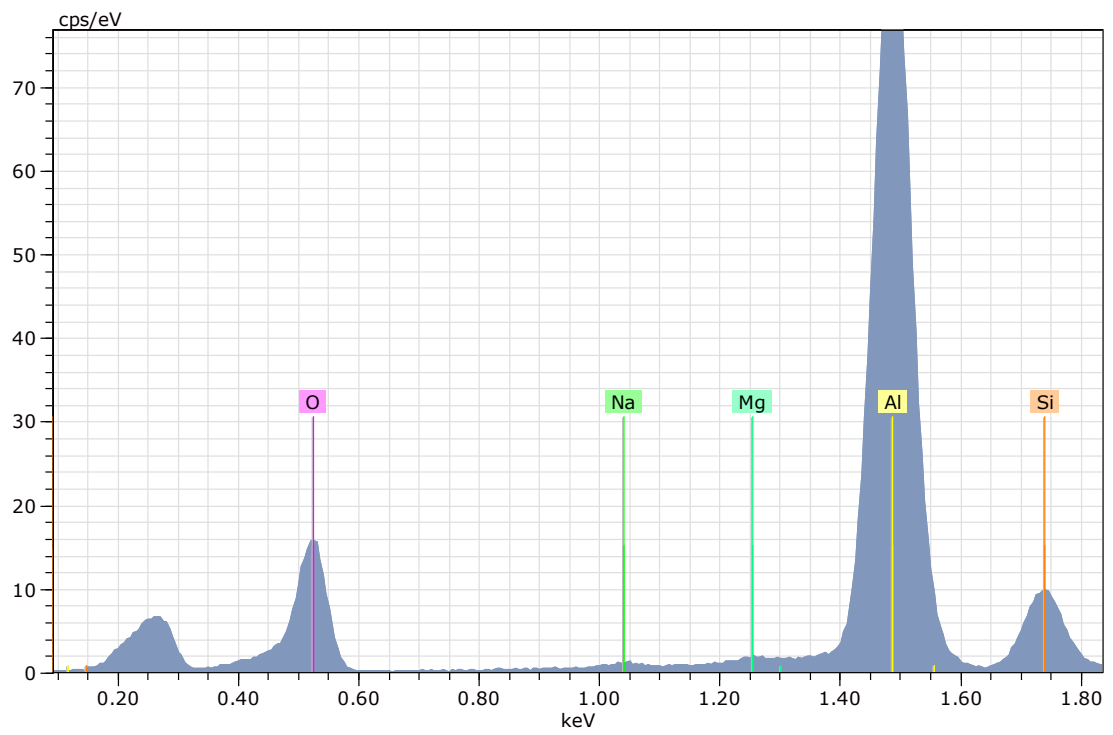
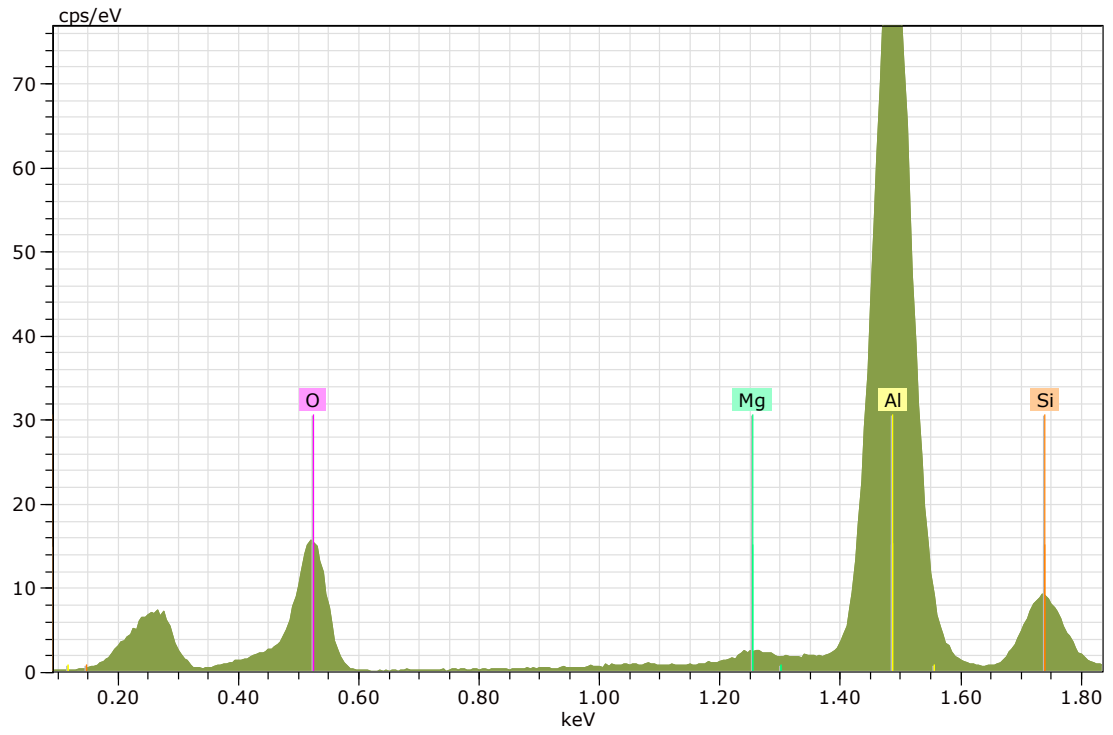
Total: 68,03 100,00 100,00

L EDS RawData Lanik 60

Application Note

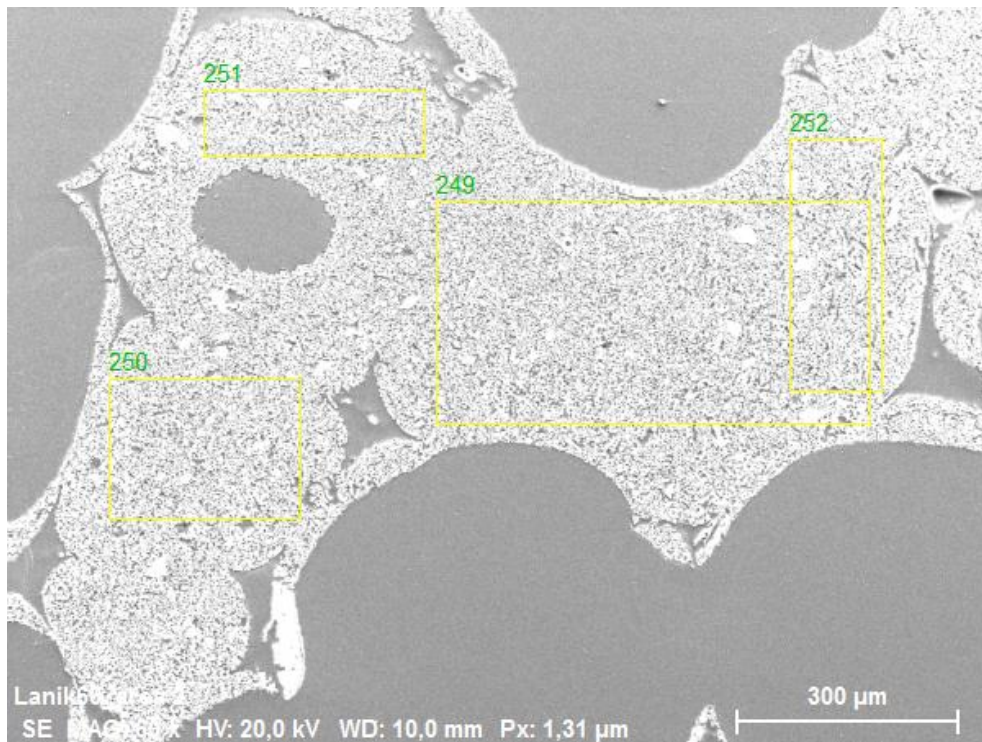
Company / Department

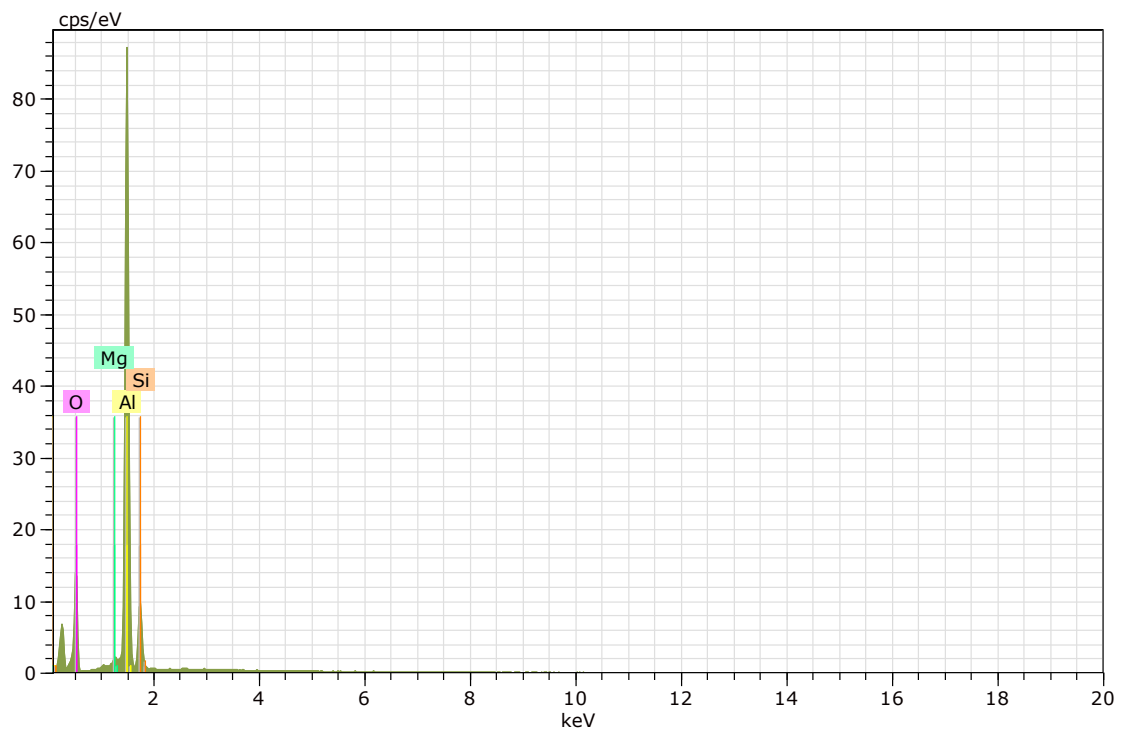
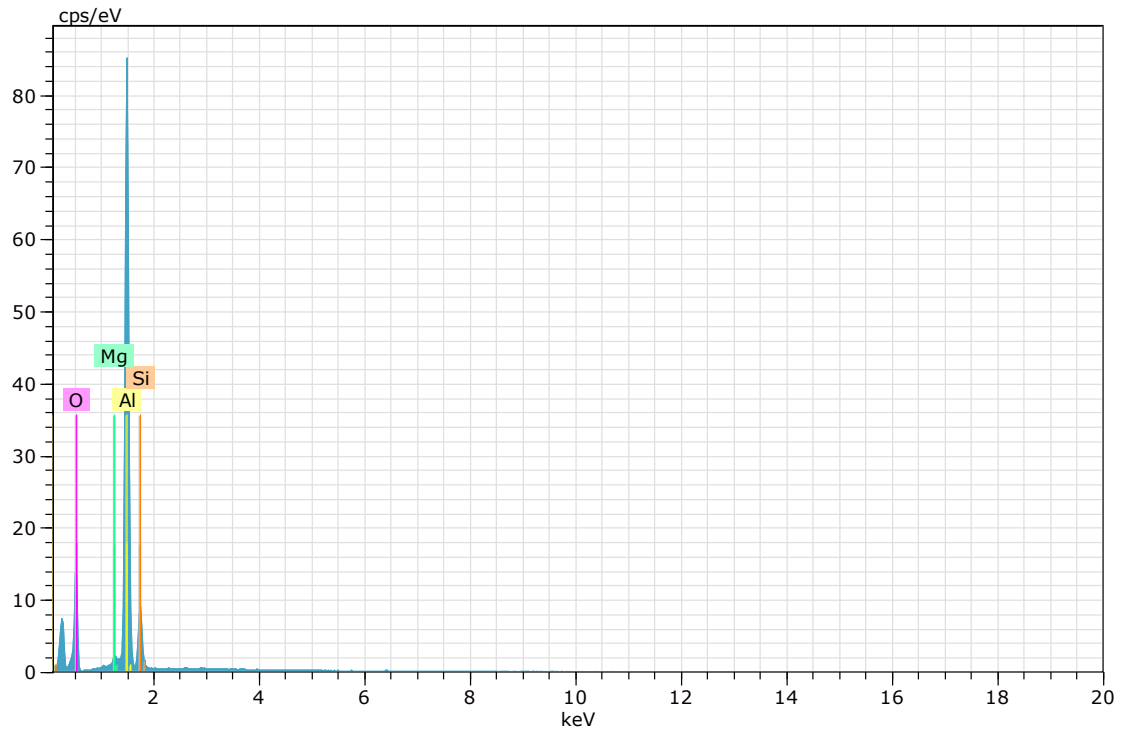


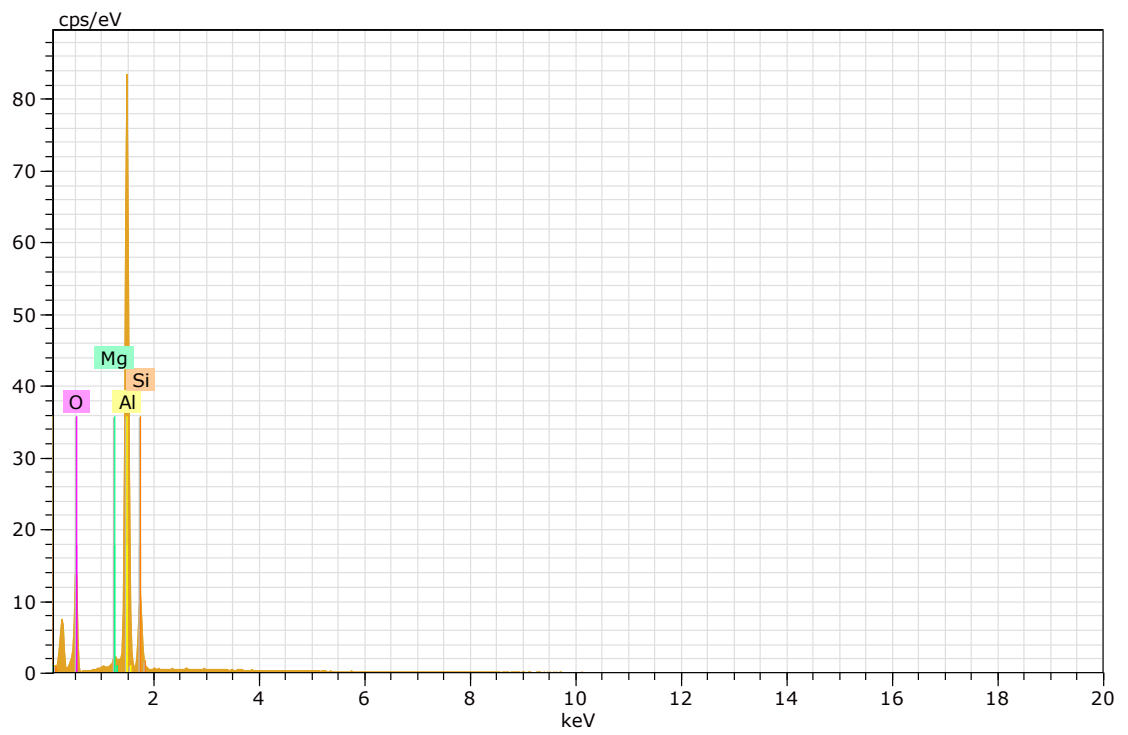
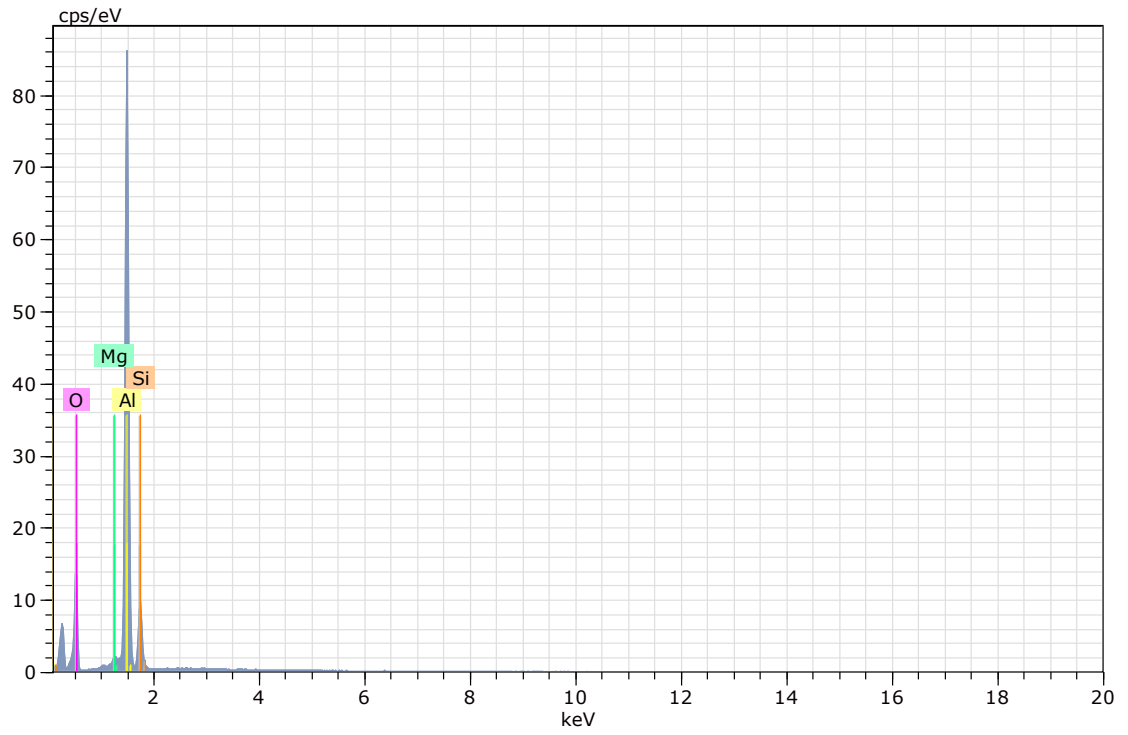


Atomic percent (%)

Spectrum	O	Na	Mg	Al	Si
245	47,98	- 1,11	44,51	6,41	
246	47,84	- 1,25	44,72	6,19	
248	47,44	0,53	0,79	44,63	6,60
Mean value:	47,76	0,53	1,05	44,62	6,40
Sigma:	0,28	0,00	0,23	0,11	0,20
Sigma mean:	0,16	0,00	0,13	0,06	0,12

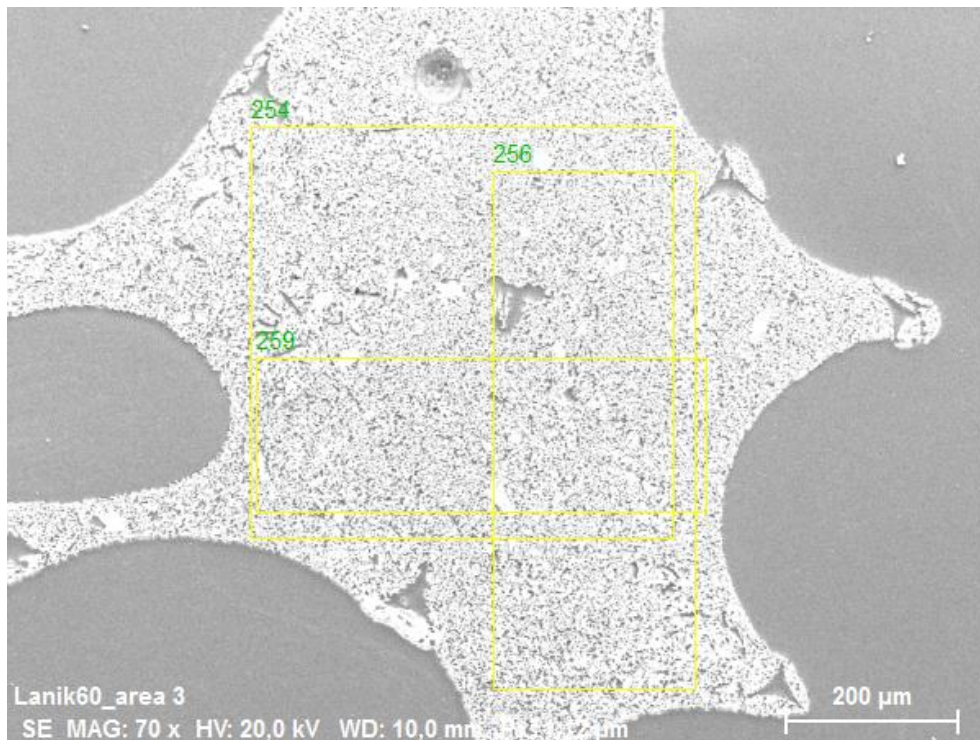


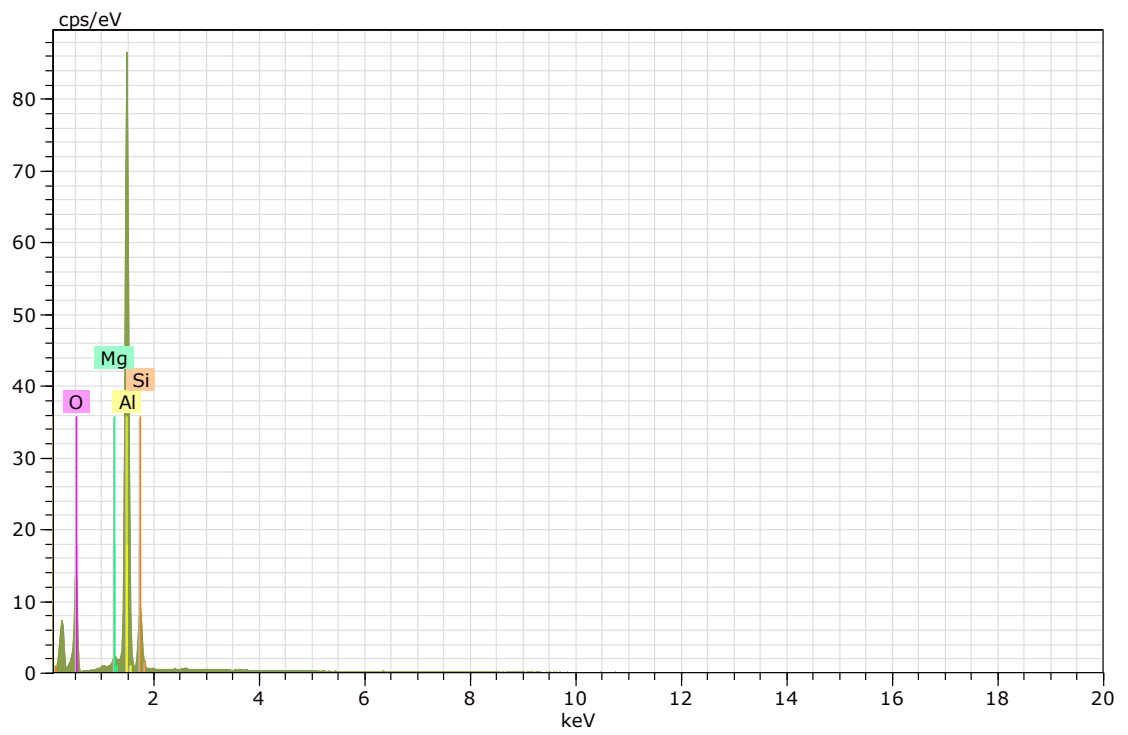
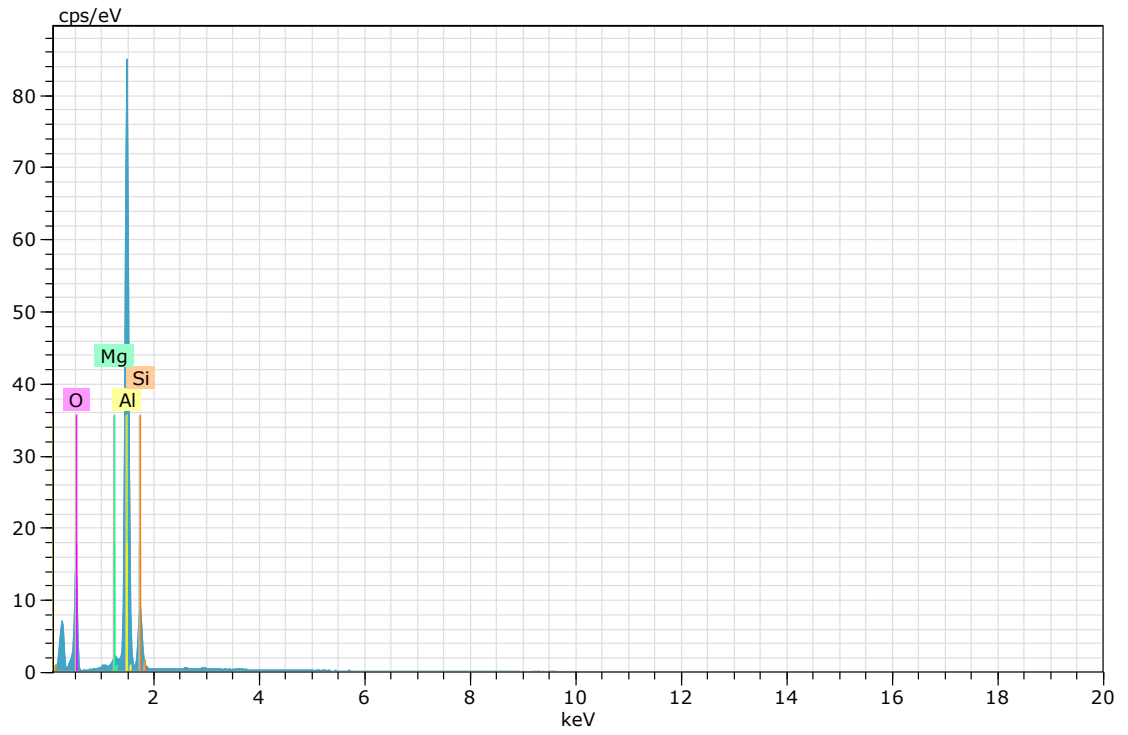


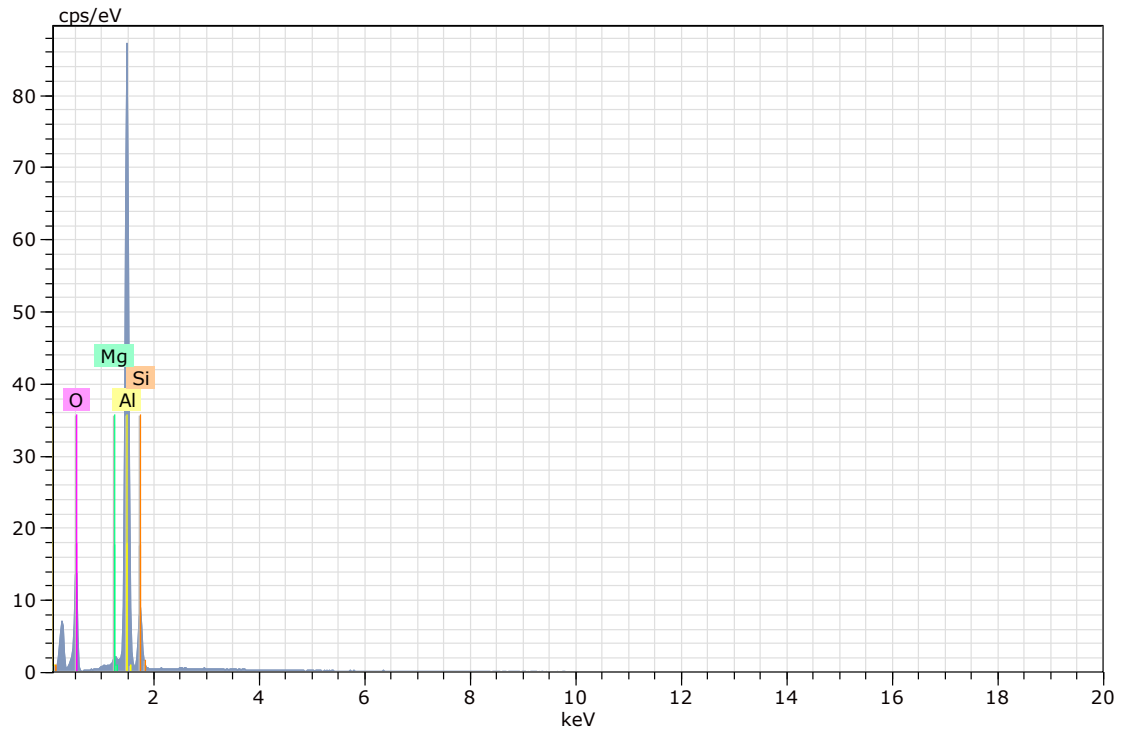


Atomic percent (%)

Spectrum	O	Mg	Al	Si
249	48,08	1,10	44,25	6,56
250	47,72	0,97	44,33	6,98
251	47,78	1,08	44,26	6,88
252	48,23	1,09	43,25	7,42
Mean value:	47,95	1,06	44,03	6,96
Sigma:	0,24	0,06	0,52	0,36
Sigma mean:	0,12	0,03	0,26	0,18







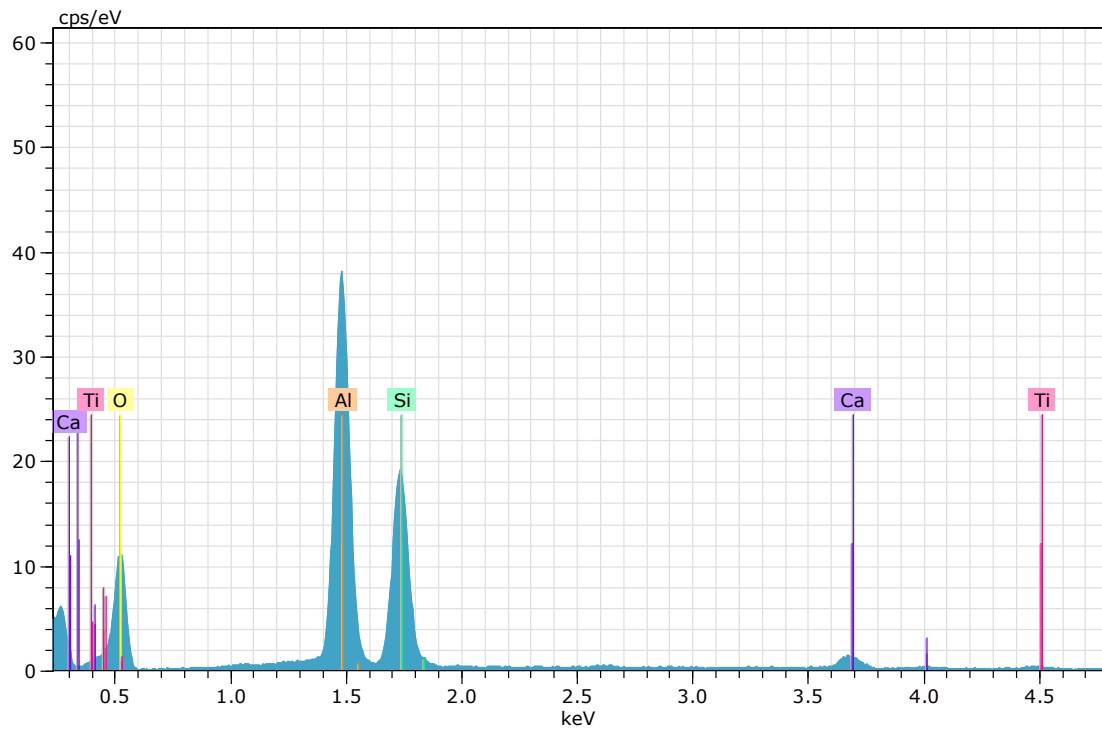
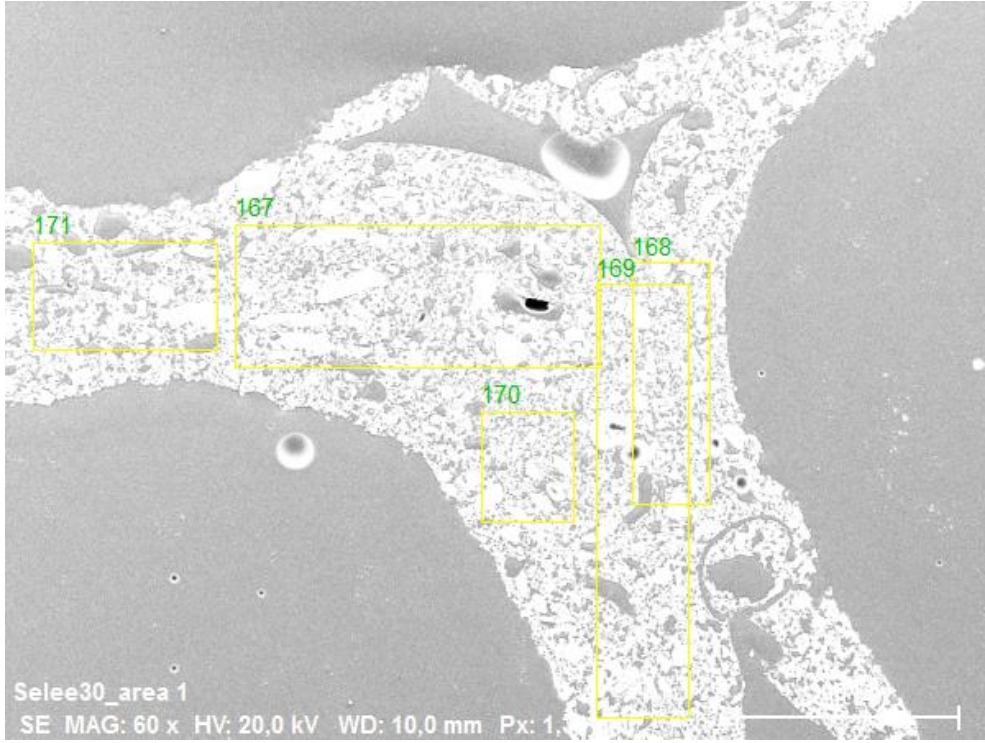
Atomic percent (%)

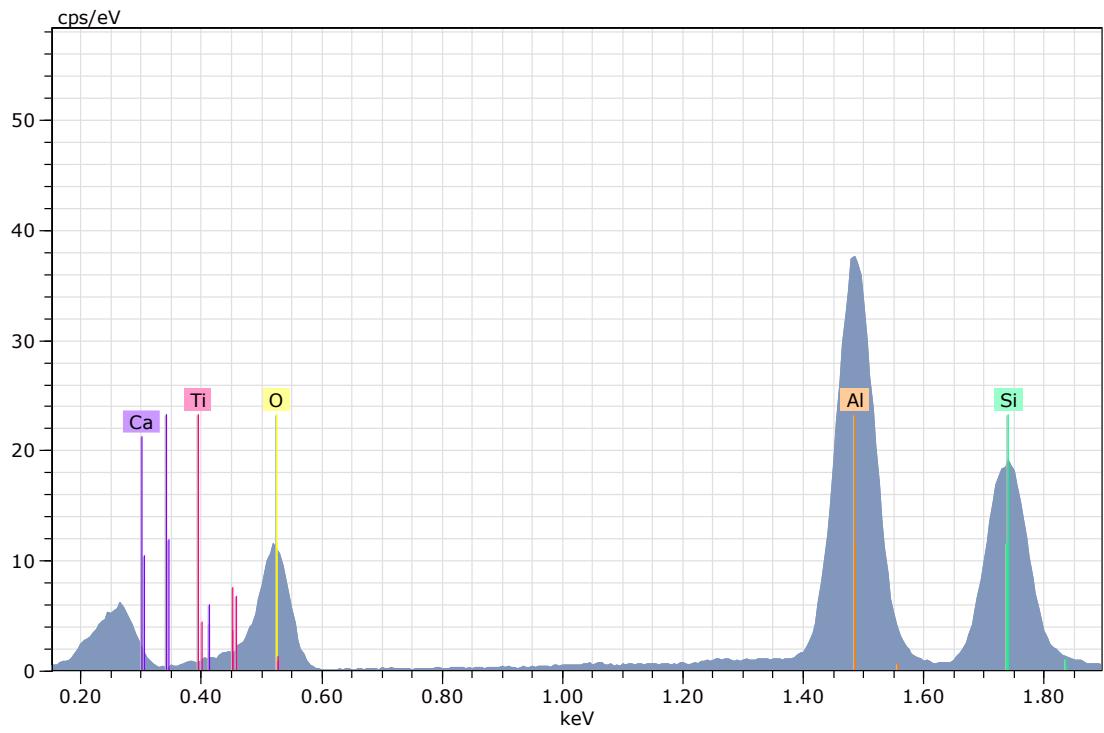
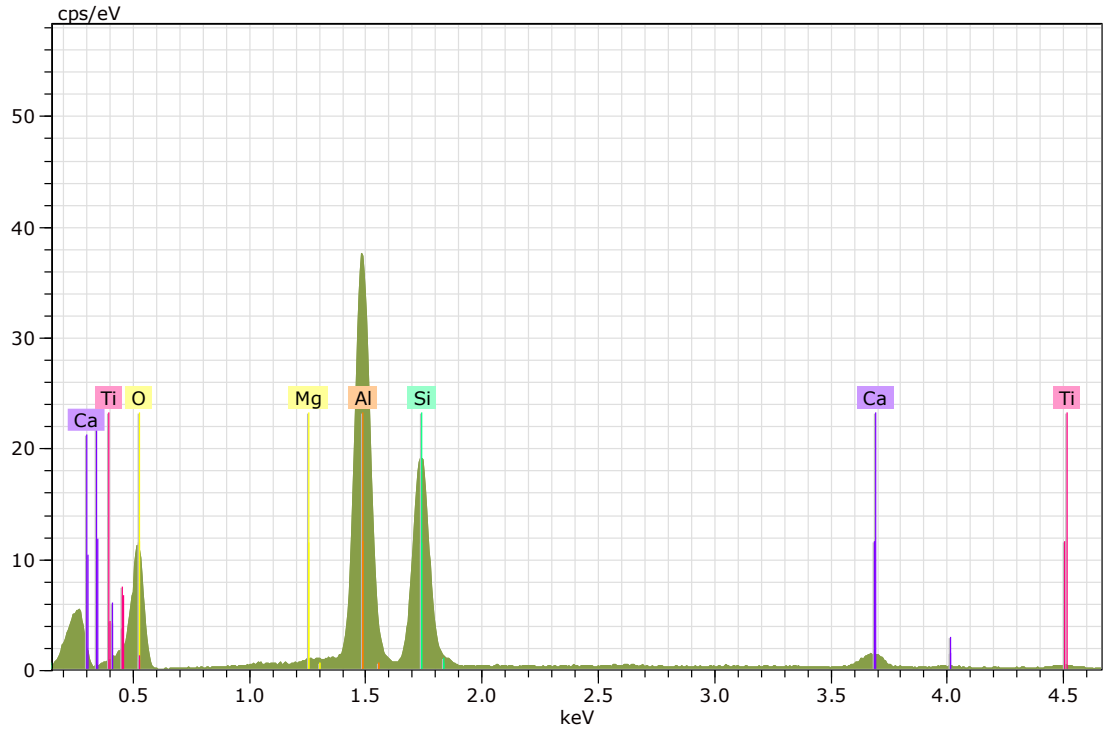
Spectrum	O	Mg	Al	Si
254	48,08	1,13	44,20	6,60
256	47,64	1,12	44,70	6,54
259	47,71	1,02	44,93	6,34
Mean value:	47,81	1,09	44,61	6,49
Sigma:	0,24	0,06	0,38	0,13
Sigma mean:	0,14	0,04	0,22	0,08

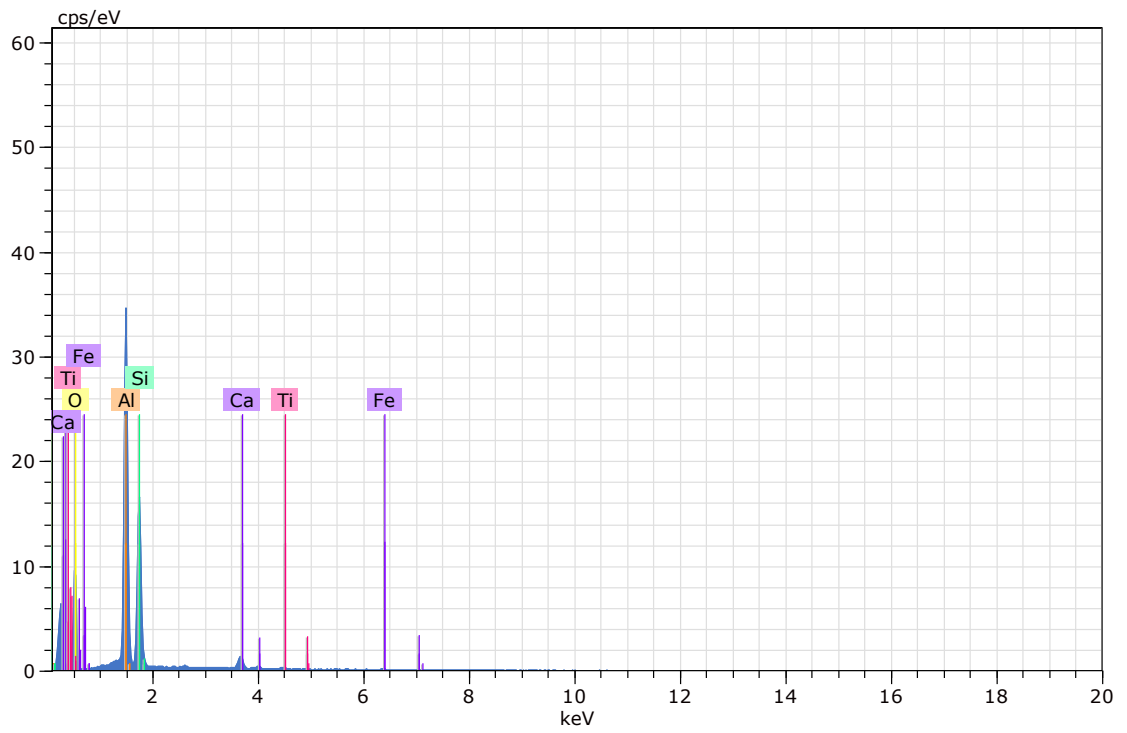
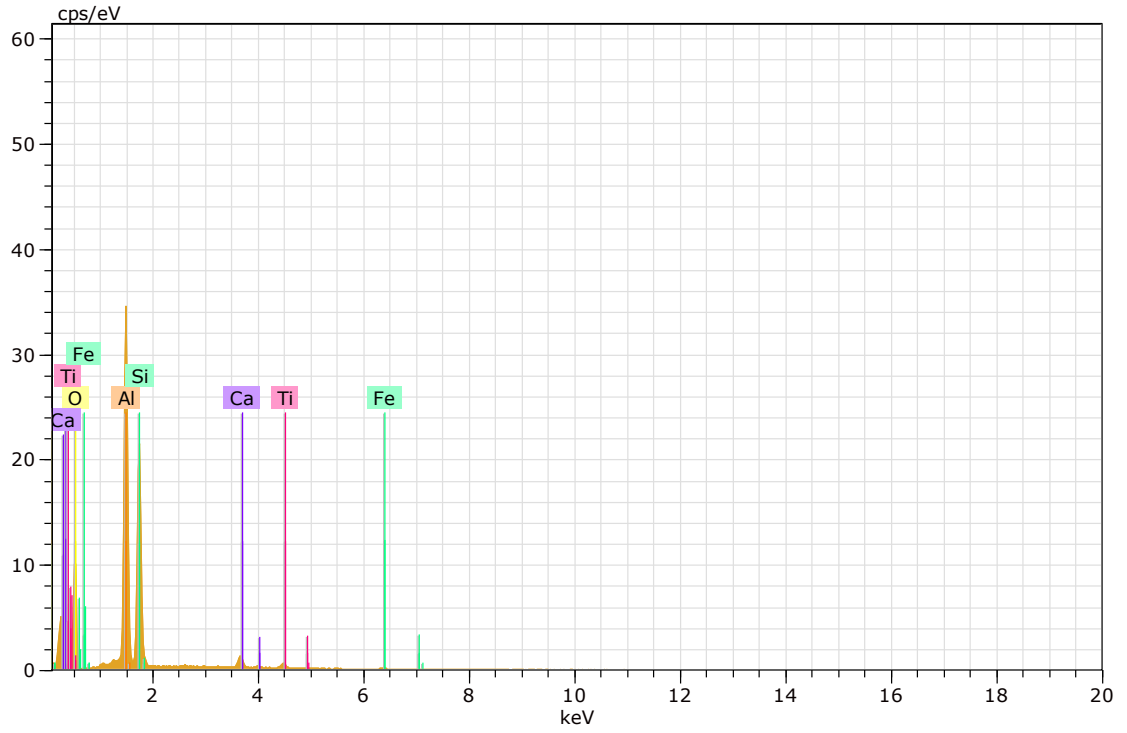
M EDS RawData Selee 30

Application Note

Company / Department







Atomic percent (%)

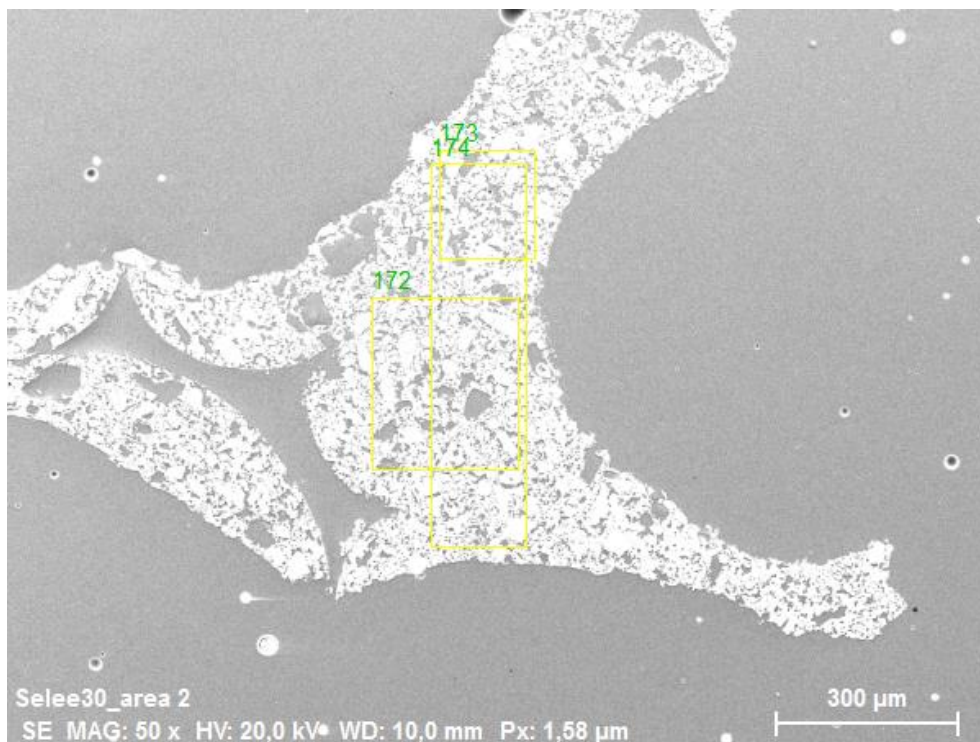
Spectrum O Mg Al Si Ca Ti Fe

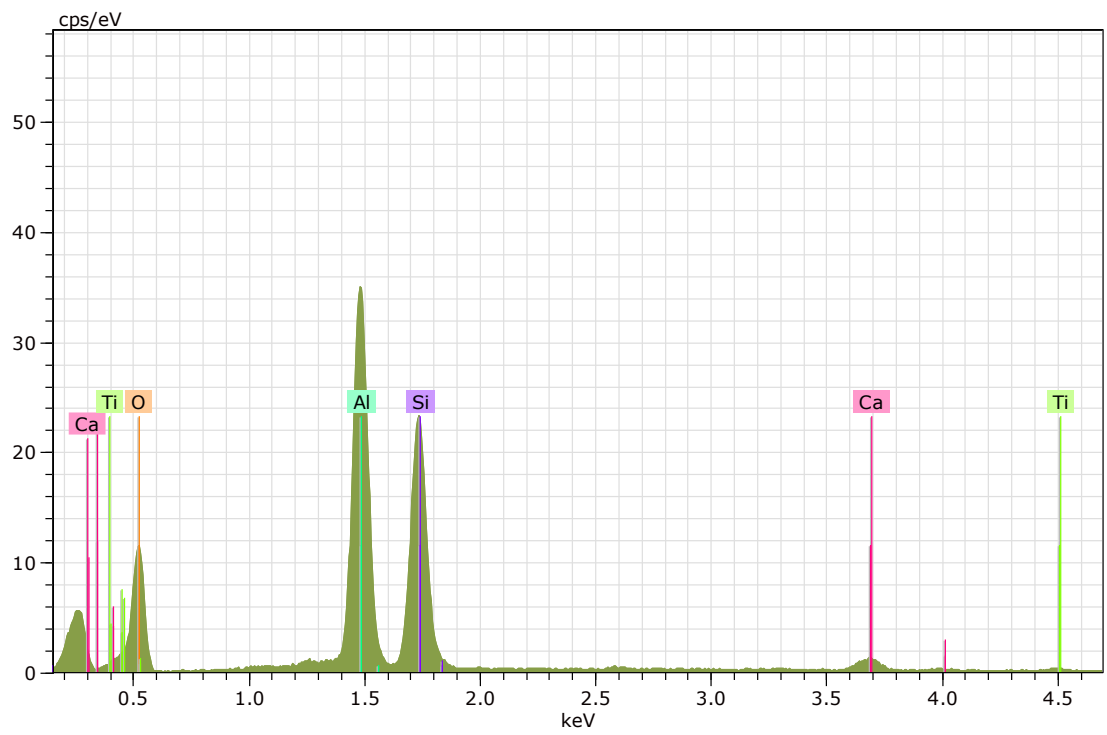
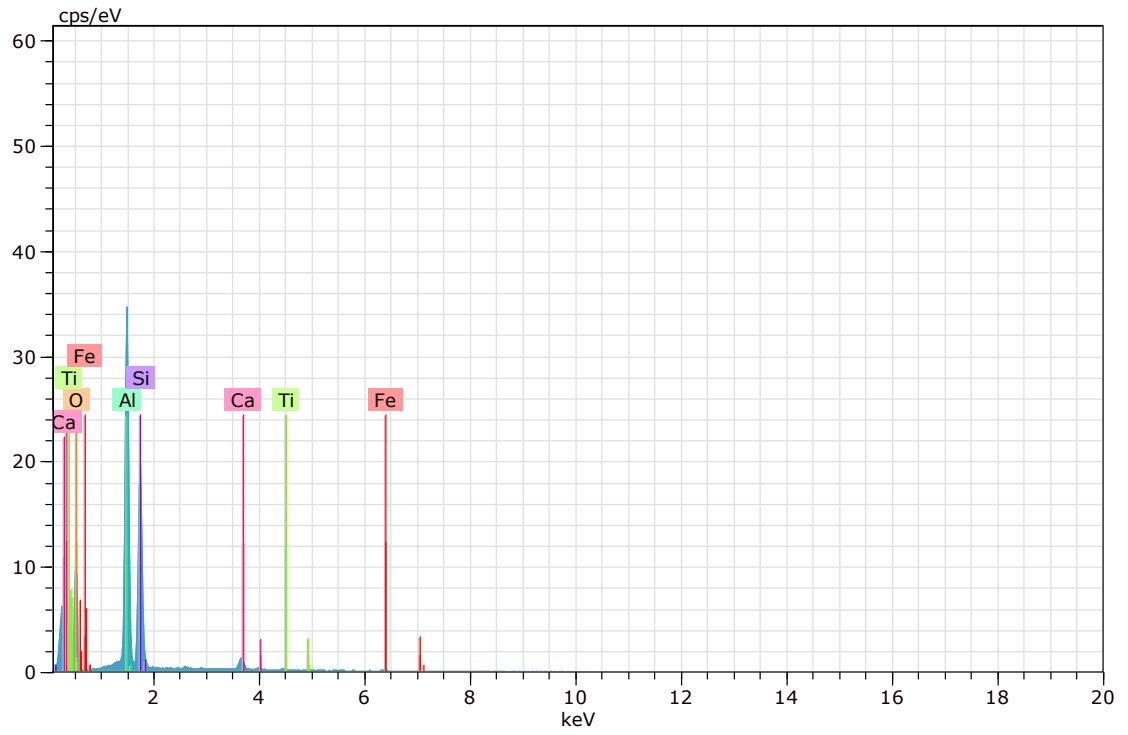
	O	Mg	Al	Si	Ca	Ti	Fe
167	53,51	-	26,89	17,59	1,63	0,38	-
168	52,66	0,51	28,42	16,66	1,40	0,36	-
169	53,11	-	27,78	17,20	1,60	0,30	-
170	53,06	-	25,95	18,86	1,25	0,63	0,25
171	53,87	-	26,19	17,33	2,07	0,32	0,23

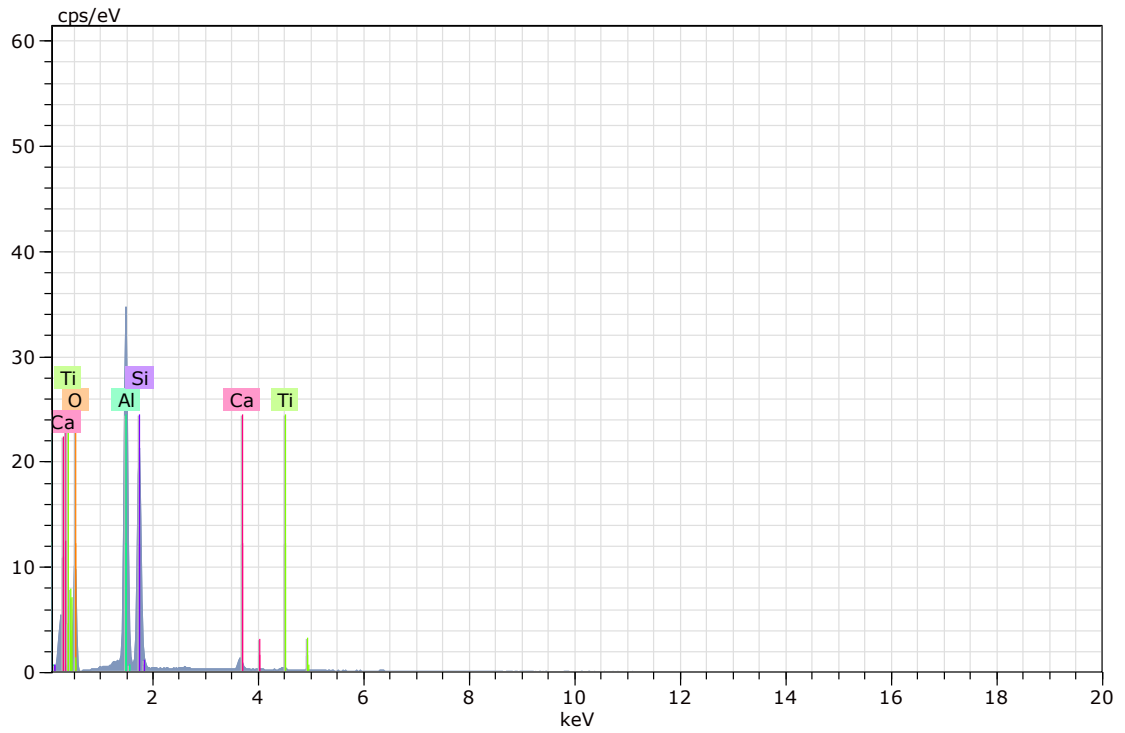
Mean value: 53,24 0,51 27,05 17,53 1,59 0,40 0,24

Sigma: 0,46 0,00 1,05 0,82 0,31 0,13 0,02

Sigma mean: 0,21 0,00 0,47 0,37 0,14 0,06 0,01

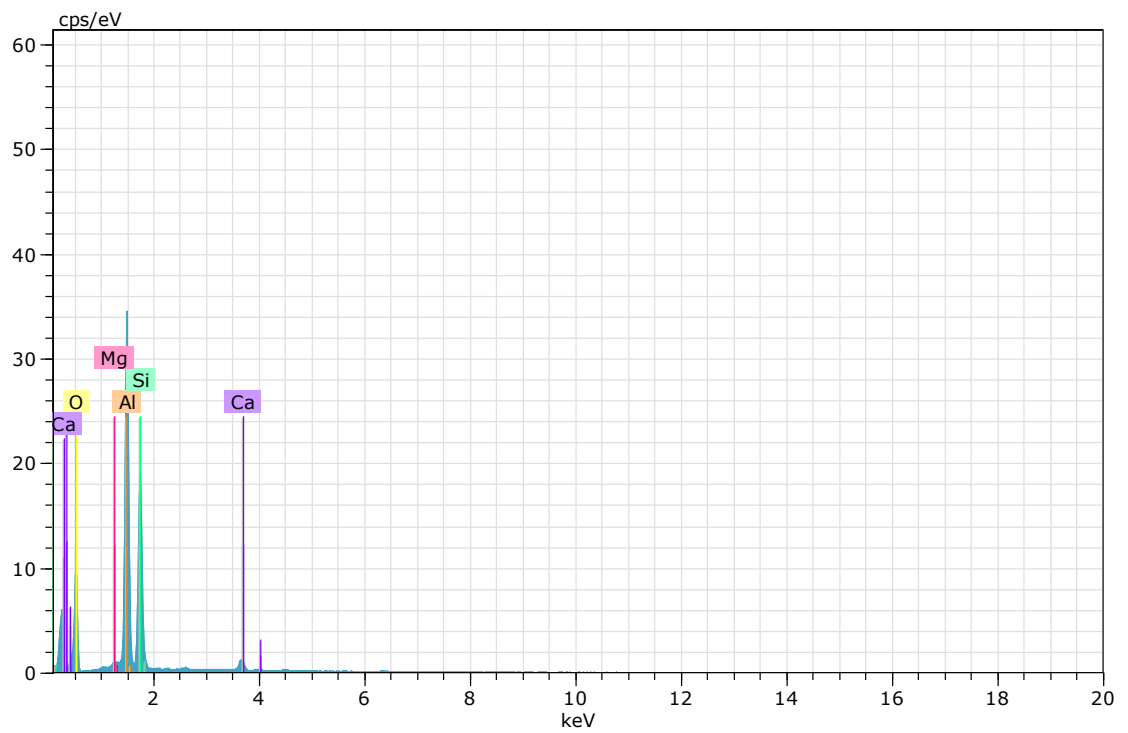
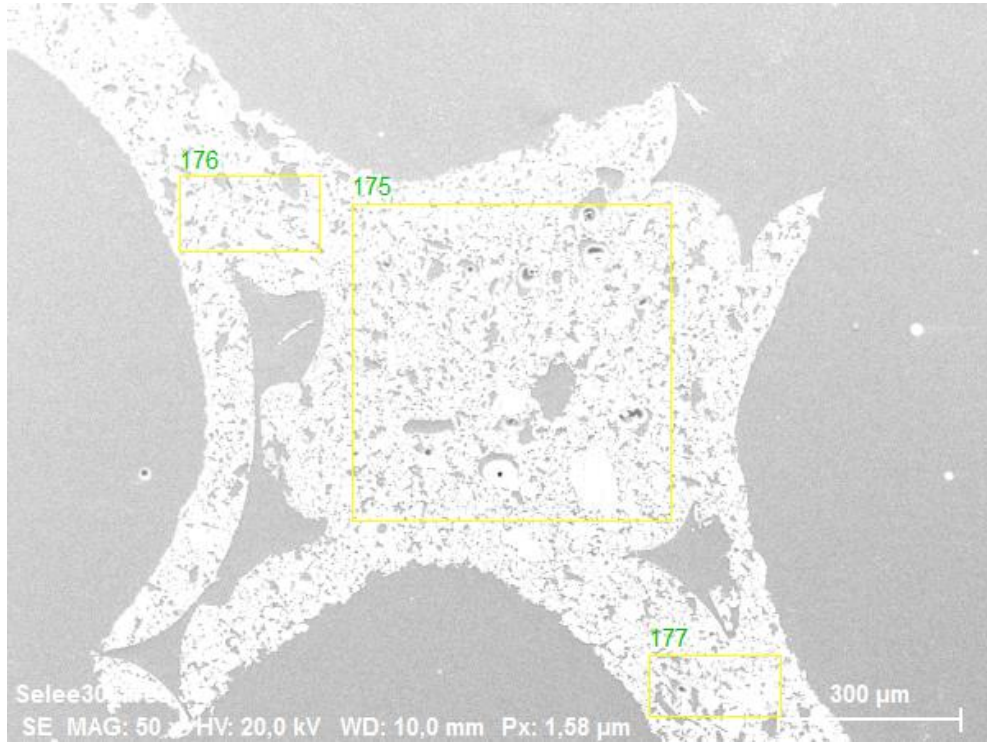


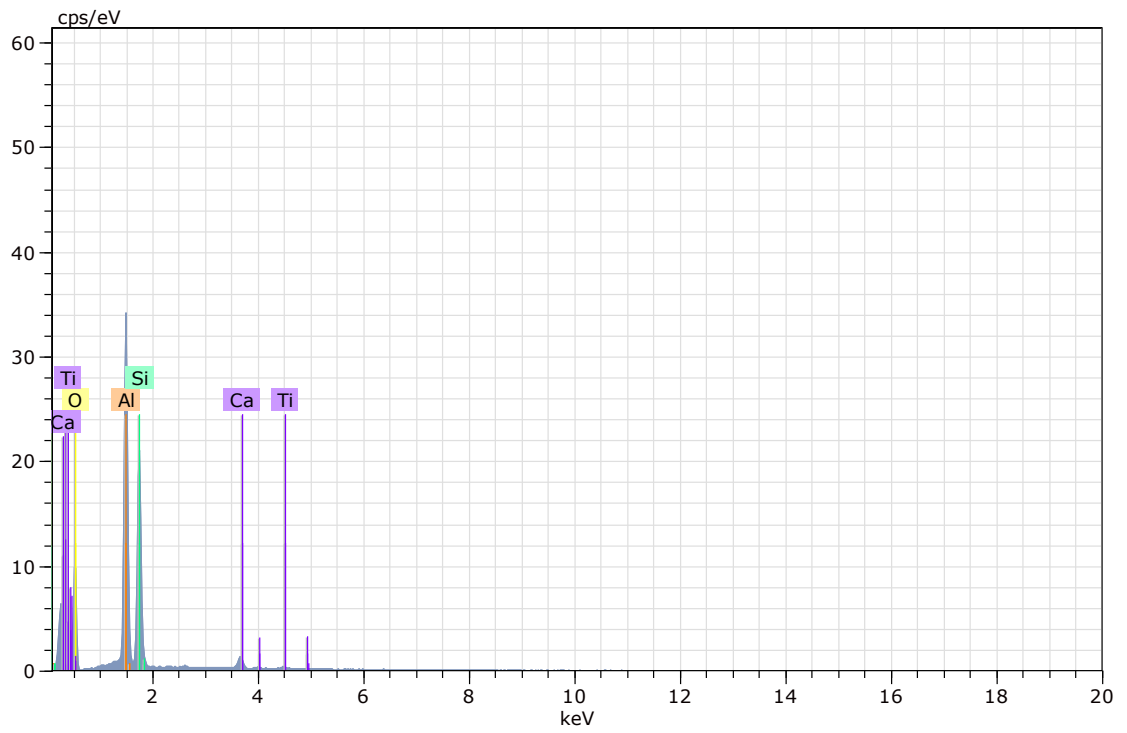
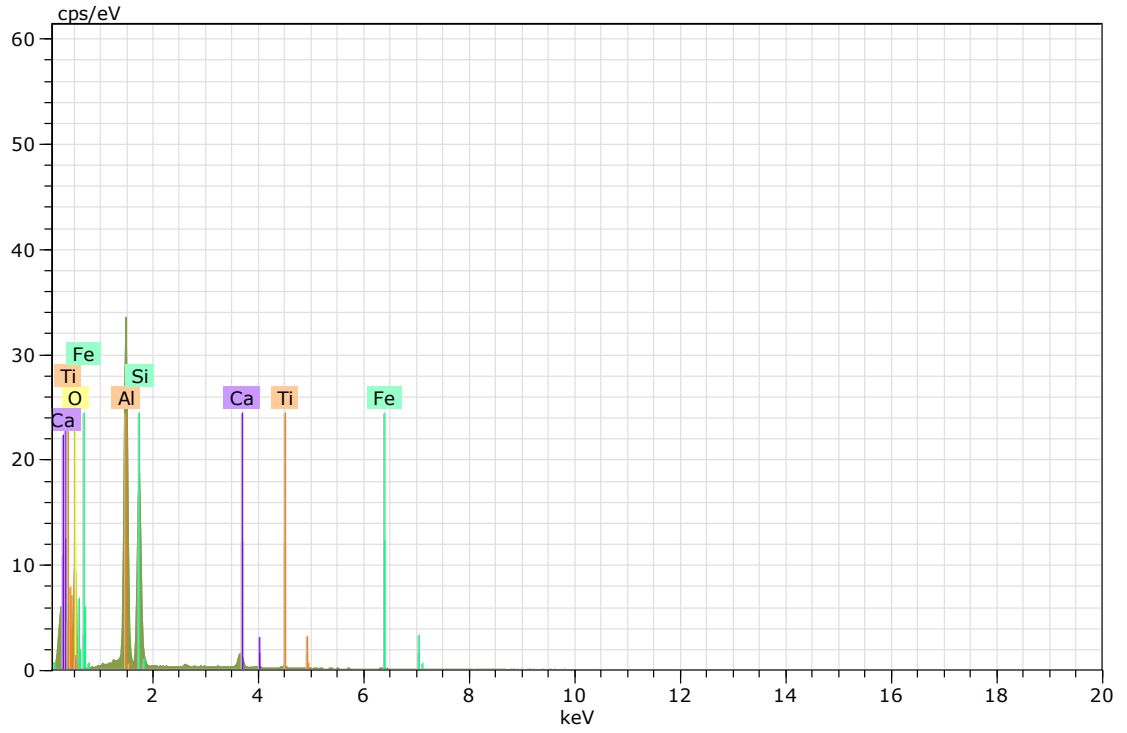




Atomic percent (%)

Spectrum	O	Al	Si	Ca	Ti	Fe
172	53,40	25,50	18,70	1,79	0,34	0,27
173	53,34	25,52	19,45	1,40	0,29	-
174	52,99	26,49	18,85	1,27	0,40	-
Mean value:	53,24	25,84	19,00	1,49	0,34	0,27
Sigma:	0,22	0,56	0,40	0,27	0,05	0,00
Sigma mean:	0,13	0,33	0,23	0,16	0,03	0,00







Atomic percent (%)

Spectrum O Mg Al Si Ca Ti Fe

175 52,65 0,68 27,86 17,49 1,32 - -
176 53,43 - 26,62 17,50 1,84 0,32 0,29
177 53,58 - 24,36 20,04 1,63 0,40 -

Mean value: 53,22 0,68 26,28 18,35 1,60 0,36 0,29

Sigma: 0,50 0,00 1,78 1,47 0,26 0,06 0,00

Sigma mean: 0,29 0,00 1,03 0,85 0,15 0,03 0,00

N Risk Assessment Cold Testing

Hazardous activity identification process



Unit: (Institute) IMA **Date:** 06.02.2020
Line manager: Tor Grande
Participants in the identification process (incl. function): Kristoffer Smedal Olsen, Sara Linnea Larsson Grayston, Are Bergin, Robert Fritzsich
(supervisor, student, co-supervisor, others)
Short description of the main activity/main process: Experimental assessment of the thermal stability of new and innovative ceramic foam filter materials for aluminium melt filtration
Is the project work purely theoretical? (YES/NO) NO
Answer "YES" implies that supervisor is assured that no activities requiring risk assessment are involved in the work. If YES, skip rest of the form.
Will you receive industry samples? (YES/NO) YES
"YES" means that a separate risk assessment of the samples is required
Is the project work safe to perform outside normal work hours (8-17)? (YES/NO) NO
Responsible supervisor: Are Bergin **Student:** Kristoffer Smedal Olsen, Sara Linnea Larsson Grayston

ID nr.	Activity/process	Responsible person	Existing documentation	Existing safety measures	Laws, regulations etc.	Comment
1	Shaping samples	Kristoffer Olsen, Sara Grayston				
	A Using a drill to shape cylindrical samples from a whole filter			Protective equipment: visor, gloves and hearing protection		
	B Drilling samples with phosphate binding after they have been immersed in molten aluminium will produce phosphine			Gas-mask		An additional measure would be better ventilation to disperse the toxic gas
2	Compression testing at room temperature	Kristoffer Olsen, Sara Grayston		Ventilation		
	A Placing the sample in the machine					At all times keep fingers clear of the crushing mechanism, especially when placing and removing the sample.
	B Removing the sample					
	C Cleaning the machine from debris					

NTNU	Risk assessment			Prepared by	Number	Date
				HSE section	HMSRV2603	04.02.2011
HMS /KS				Approved by	Page	Replaces
				The Rector		09.02.2010



Unit: (Institute) IMA **Date:** 06.02.2020
Line manager: Tor Grande
Participants in the identification process (incl. function): Kristoffer Smedal Olsen, Sara Linnea Larsson Grayston, Are Bergin, Robert Fritzsich
(supervisor, student, co-supervisor, others)
Risk assessment of: Experimental assessment of the thermal stability of new and innovative ceramic foam filter materials for aluminium melt filtration
Signatures: Responsible supervisor: Are Bergin **Student:** Kristoffer Smedal Olsen, Sara Linnea Larsson Grayston

ID nr.	Activity from the identification process form	Potential undesirable incident/strain	Likelihood: (1-5)	Consequence:			Risk value (human)	Comments/status Suggested measures
				Human (A-E)	Environment (A-E)	Economy/material (A-E)		
1	Shaping samples							
	A Using a drill to shape cylindrical samples from a whole filter	cuts	2	A			A2	
	B Drilling samples with phosphate binding will produce phosphine	Phosphine poisoning	1	C			C1	
2	Compression testing at room temperature							
	A Placing the sample in the machine	Crushing injuries	1	C			C1	
	B Removing the sample	Crushing injuries	1	C			C1	
	C Cleaning the machine from debris	Crushing injuries	1	C			C1	

Risk value = Likelihood (1, 2 ...) x consequence (A, B ...). Risk value A1 means very low risk. Risk value E5 means very large and serious risk

Likelihood		Consequence				
Value	Criteria	Grading		Human	Environment	Economy/material
1	Minimal: Once every 50 year or less	E	Very critical	May produce fatality/ies	Very prolonged, non-reversible damage	Shutdown of work >1 year.
2	Low: Once every 10 years or less	D	Critical	Permanent injury, may produce serious health damage/sickness	Prolonged damage. Long recovery time.	Shutdown of work 0.5-1 year.
3	Medium: Once a year or less	C	Dangerous	Serious personal injury	Minor damage. Long recovery time	Shutdown of work < 1 month
4	High: Once a month or less	B	Relatively safe	Injury that requires medical treatment	Minor damage. Short recovery time	Shutdown of work < 1week
5	Very high: Once a week	A	Safe	Injury that requires first aid	Insignificant damage. Short recovery time	Shutdown of work < 1day

MATRIX FOR RISK ASSESSMENT

CONSEQUENCE	Very critical	E1	E2	E3	E4	E5
	Critical	D1	D2	D3	D4	D5
	Dangerous	C1	C2	C3	C4	C5
	Relatively safe	B1	B2	B3	B4	B5
	Safe	A1	A2	A3	A4	A5
	Minimal	Low	Medium	High	Very high	
	LIKELIHOOD					

Explanation of the colors used in the risk matrix.

Color	Description
Red	Unacceptable risk. Safety measures must be implemented.
Yellow	Measures to reduce risk shall be considered.
Green	Acceptabel risk.

O Risk Assessment Hot Testing

Unit: *(Institute)* _____ **IMA** _____ **Date:** _____

Line manager: _____ **Tor Grande** _____

Participants in the identification process (incl. function): _____
(supervisor, student, co-supervisor, others) Kristoffer Smedal Olsen, Sara Linnea Larsson Grayston, Are Bergin, Robert Fritsch

Short description of the main activity/main process: _____
 Experimental assessment of the thermal stability of new and innovative ceramic foam filter materials for aluminium melt filtration

Is the project work purely theoretical? (YES/NO) _____
 NO

Answer "YES" implies that supervisor is assured that no activities requiring risk assessment are involved in the work. If YES, skip rest of the form.

Will you receive industry samples? (YES/NO) _____
 YES

"YES" means that a separate risk assessment of the samples is required

Is the project work safe to perform outside normal work hours (8-17)? (YES/NO) _____
 NO

Responsible supervisor: Are Bergin _____ *Student:* Kristoffer Smedal Olsen, Sara Linnea Larsson Grayston

ID nr.	Activity/process	Responsible person	Existing documentation	Existing safety measures	Laws, regulations etc.	Comment
1	Compression testing at high temperatures	Kristoffer Olsen, Sara Grayston				
	A	When transferring the sample from high temperature (up to 900C) oven to crushing strength test machine		Ventilation and protective equipment for high temperatures: heat suit, gloves and visor.	forskrift om utførelse av arbeid. § 5	Keep fingers clear of the crushing mechanism at all times, always wear protective equipment. Avoid dropping the samples or other equipment as this may damage the surroundings. Other people using the lab should be notified and a sign on the door warning of high temperatures. A heat proof bucket is required for disposal of hot waste.
	B	Placing the sample in the test machine				
	C	Removing sample from test machine				
2	Priming the filters	Kristoffer Olsen, Sara Grayston				
	A	Transferring molten metal into priming apparatus		Protective equipment for high temperatures: heat suit, gloves and visor	forskrift om utførelse av arbeid. § 5	Avoid contact with electromagnetic components which have a high current. A heat proof bucket is required for disposal of hot waste.
	B	Actual priming of filter				
C	Cooling					

Unit: (Institute) IMA **Date:** _____
Line manager: Tor Grande

Participants in the identification process (incl. function):
 (supervisor, student, co-supervisor, others) Kristoffer Smedal Olsen, Sara Linnea Larsson Grayston, Are Bergin, Robert Fritzs

Risk assessment of: Experimental assessment of the thermal stability of new and innovative ceramic foam filter materials for aluminium melt filtration

Signatures: Responsible supervisor: Are Bergin Student: Kristoffer Smedal Olsen, Sara Linnea Larsson Grayston

ID nr.	Activity from the identification process form	Potential undesirable incident/strain	Likelihood: (1-5)	Consequence:			Risk value (human)	Comments/status Suggested measures
				Human (A-E)	Environment (A-E)	Economy/material (A-E)		
1	Compression testing at high temperatures							
	A	When transferring the sample from high temperature (up to 900C) oven to crushing strength test machine	Burn-injuries	2	A		A2	
	A		Crushing injuries	1	C		C1	
	B	Placing the sample in the test machine	Burn-injuries	2	A		A2	
	B		Crushing injuries	1	C		C1	
C	Removing sample from test machine	Burn-injuries	2	A		A2		
		Crushing injuries	1	C		C1		
2	Priming the filters							
	A	Transferring molten metal into priming apparatus	Burn-injuries	2	A		A2	
	B	Priming of filter	Burn-injuries	2	A		A2	
	B		Electric shock	1	C		C1	
C	Cooling							
0	C							

Risk value = Likelihood (1, 2 ...) x consequence (A, B ...). Risk value A1 means very low risk. Risk value E5 means very large and serious risk

Likelihood		Consequence				
Value	Criteria	Grading		Human	Environment	Economy/material
1	Minimal: Once every 50 year or less	E	Very critical	May produce fatality/ies	Very prolonged, non-reversible damage	Shutdown of work >1 year.
2	Low: Once every 10 years or less	D	Critical	Permanent injury, may produce serious health damage/sickness	Prolonged damage. Long recovery time.	Shutdown of work 0.5-1 year.
3	Medium: Once a year or less	C	Dangerous	Serious personal injury	Minor damage. Long recovery time	Shutdown of work < 1 month
4	High: Once a month or less	B	Relatively safe	Injury that requires medical treatment	Minor damage. Short recovery time	Shutdown of work < 1week
5	Very high: Once a week	A	Safe	Injury that requires first aid	Insignificant damage. Short recovery time	Shutdown of work < 1day

MATRIX FOR RISK ASSESSMENT

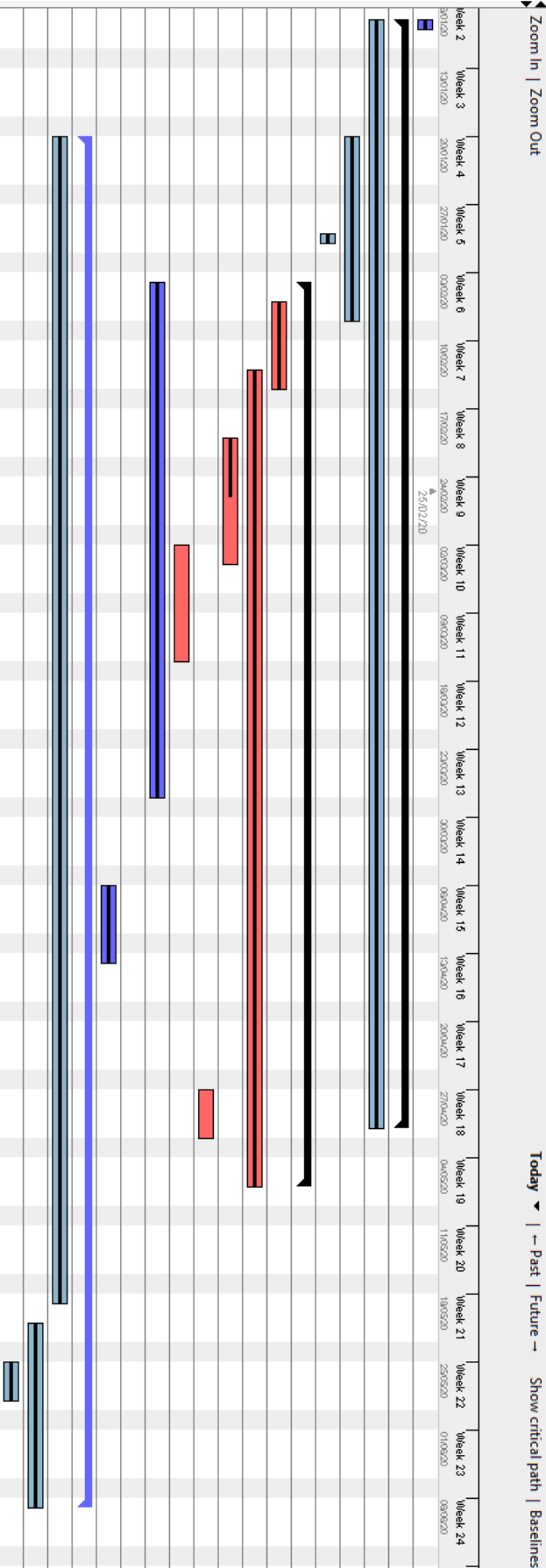
CONSEQUENCE	Very critical	E1	E2	E3	E4	E5
	Critical	D1	D2	D3	D4	D5
	Dangerous	C1	C2	C3	C4	C5
	Relatively safe	B1	B2	B3	B4	B5
	Safe	A1	A2	A3	A4	A5
	Minimal	Low	Medium	High	Very high	
LIKELIHOOD						

Explanation of the colors used in the risk matrix.

Color	Description
Red	Unacceptable risk. Safety measures must be implemented.
Yellow	Measures to reduce risk shall be considered.
Green	Acceptabel risk.

P Project Plan

Name	Begin date	End date
● Startup-Supervisor	08/01/20	08/01/20
● pre-project	08/01/20	30/04/20
● literature	08/01/20	30/04/20
● Risk assessment	20/01/20	07/02/20
● HSE course	30/01/20	30/01/20
● Experimental work	04/02/20	06/05/20
● Effect of shapes	06/02/20	14/02/20
● Preheat and full h...	13/02/20	06/03/20
● Priming filters	20/02/20	03/03/20
● Submerged in liqu...	27/04/20	01/05/20
● Filtration trials?	02/03/20	13/03/20
● Treatment of data	04/02/20	27/03/20
● Final title	04/02/19	04/02/19
● easter	06/04/20	13/04/20
● Rapport	20/01/20	08/06/20
● Draft	20/01/20	18/03/20
● Final rapport	21/05/20	08/06/20
● Presentation	25/05/20	28/05/20



Q Popular Science Article

Ceramic Foam Filters - for Aluminium Melt Filtration

Kristoffer Smedal Olsen and Sara Linnea Larsson Grayston

Norwegian University of Science and Technology

(Dated: May 29, 2020)

When producing and recycling aluminium, ceramic foam filters play an essential part. They filter out unwanted particles resulting in a cleaner, higher grade aluminium alloy with higher mechanical properties.

I. INTRODUCTION

Recycling metal is a sustainable way to make new products, where the need for a more environmental way of getting metal for new products. The molten metal contains non-metallic inclusions which affect adversely the properties of the aluminium, For example, the tensile strength, the elongation at rupture and the surface quality is reduced. These inclusions needs to be removed before the castin step, and one way of doing this is by the use of Ceramic foam filters (CFF) as seen in Figure 1. CFFs is an in-line filtration method which is used as the last step in refining molten metal, and there are different aspects of a CFF that affects the filter, and how effectively it filters the molten metal [1]. Some of these aspects are the composition, density and mechanical properties.



FIG. 1: Illustration of a ceramic foam filter [2].

II. PRODUCTION

A way of making a ceramic foam filter is by using a replication process. This process works by producing a polymer foam with specific pore sizes. When the polymer foam is dry, it is coated with a ceramic slurry composed by a ceramic and different binders. These compositions are more explained in Chapter IV. Then the slurry coating is dried, and the polymer decomposes. Lastly, the ceramic slurry is heated, and the sintering of the ceramic starts.

III. FUNCTIONALITY OFF A CFF

The last step in the refining is the molten metal filtration by using CFFs, due to their ability to withstand temperatures over 1000 degrees. The filter is fitted in the filter bowl, illustrated in Figure 2, and

heated to approximately the working temperature, at 750 °C. Priming is a process where molten metal is pushed through the filter and is done in advance of filtration. This is done to break the surface tensions between the molten aluminium and the filter, allowing the metal to pass through the filter [3]. When the filter is properly primed, the filtration of aluminium starts; with the molten metal coming from the inlet, through the filter and out the outlet to the casting.

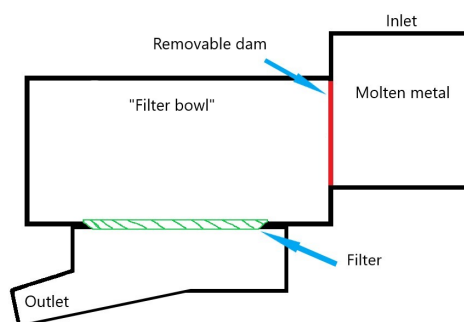


FIG. 2: Illustration of inside the filtration seat in the foundry.

The pores in the filters accumulates the impurities in the molten metal, as illustrated in Figure 3. Here, the molten metal enters the filter from the top and exits through the bottom. The canals through the filters gives it a longer distance rather than straight through, thus making more of the impurities being collected in the filter pores [4].

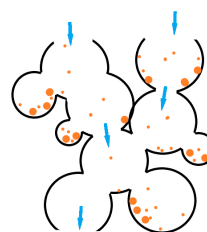


FIG. 3: Structure of a CFF.

IV. COMPOSITIONS

Most CFFs for aluminium filtration consist mainly of alumina, and use binders like phosphate and silica to lower sintering temperature for cheaper use. Phosphate filters are used due to a high bending and compression strength [5], but can be unstable at high temperatures and release phosphine after reacting with aluminium and

in contact with water [6]. Alternative filters often use silica, and negate the health risk of phosphine.

V. DENSITY AND STRUCTURES

The different CFF comes with different densities and pores per inch (ppi). For each manufacturer these may differ. Ceramic foams are often categorized into two groups depending on their structure: open- and closed-cell. While closed-cell foams are used for isolation or structural components, open-celled foams are well suited for filtration. Foams in general are made up of pores, which contain two parts; struts and cell-walls. Struts are the arms that bind the pores together, while cell-walls are thinner walls that can arise when the foam is dense enough. An example of a CFF is shown in 4.

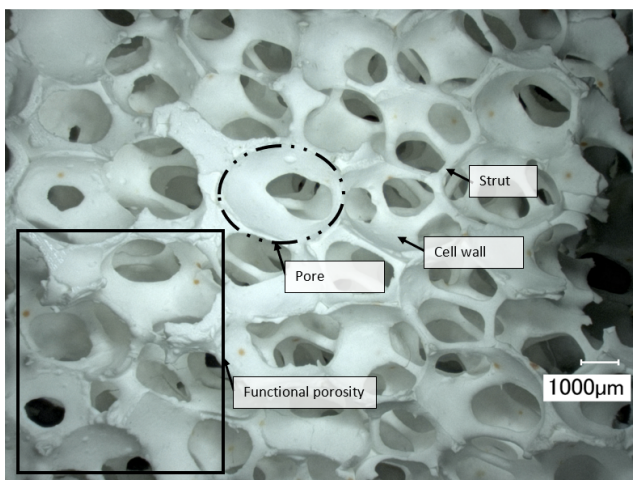


FIG. 4: Illustrative microscope image of a CFF

VI. MECHANICAL PROPERTIES

When categorizing the mechanical properties of ceramic foams, the most used parameter is compressive

strength. The best model for compressive strength, and for the structure of ceramic foams in general, is from Gibson and Ashby [7]. This model details a unit cell as seen in Figure 5 where the struts break from bending, ultimately making the compressive strength of CFFs dependent on the strength of the struts (σ_{fs}) and the ratio between the density of the foam and the density of the material ((ρ^*/ρ_s)), as seen in Equation 1.

$$\sigma_{cr} = C\sigma_{fs}(\rho^*/\rho_s)^{3/2} \quad (1)$$

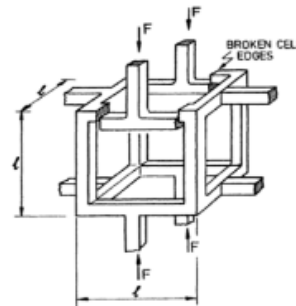


FIG. 5: The unit cell from Gibson and Ashby[7].

The compressive strength of CFFs has been studied well at room temperature, but when increasing the temperature there has been done little research. Our bachelor thesis seeks to establish methods to test the compressive strength at high temperatures. Further focus is on how longer time at the working temperatures of around 730 °C affects the strength of the filters. This could give a picture of how much the filters can handle in the cast house before they break.

ACKNOWLEDGMENTS

The authors would like to express our sincerest thanks to our supervisors Prof. Ragnhild E. Aune, PhD candidate Are Bergin, Dr. Robert Fritsch and Dr.-ing. Claudia Voigt for guidance and assistance through both the theoretical and experimental work.

-
- [1] D. Chesonis, A holistic approach to molten metal cleanliness, *Light Metals* 2017 , 1411 (2017).
 - [2] Foundrymaterial.com, Foundrymaterial.com (2020), retrieved: 28.05.2020.
 - [3] R. Fritsch, M. W. Kennedy, J. A. Bakken, and R. E. Aune, Electromagnetic priming of ceramic foam filters (cff) for liquid aluminum filtration, Sadler B.A. (eds) *Light Metals* 2013. The Minerals, Metals & Materials Series. Springer, Cham , 973 (2016).
 - [4] F. Breton, P. Waite, and P. Robichaud, Advanced compact filtration (acf): an efficient and flexible filtration process, Sadler B.A. (eds) *Light Metals* 2013. The Minerals, Metals & Materials Series. Springer, Cham , 967 (2016).
 - [5] J. A. Fernando and D. D. L. Chung, Improving an alumina fiber filter membrane for hot gas filtration using an acid phosphate binder, *Journal of materials science* **36**, 5079 (2001).
 - [6] L. S. Aubrey, R. Olson, and D. D. Smith, Development of a phosphate-free reticulated foam filter material for aluminium cast houses, *Materials science forum* **630**, 137 (2009).
 - [7] L. J. Gibson and M. F. Ashby, *Cellular Solids: Structure and Properties*, 2nd ed. (Cambridge University Press, 1997).

